



Monitoring, Assessment, Prevention and Mitigation of Rock Burst and Gas Outburst Hazards in Coal Mines **(MAPROC)**

The background of the lower half of the page features a dynamic, abstract design of blue and white wavy lines and circles, suggesting energy or movement.

EUR 30854 EN

**Monitoring, Assessment, Prevention and Mitigation of Rock Burst and Gas Outburst Hazards
in Coal Mines (MAPROC)**

European Commission

Directorate-General for Research and Innovation

Directorate C - Clean Planet

Unit C.3 — Low Emission Future Industries

Contact Andrea Gentili

E-mail RTD-STEEL-COAL@ec.europa.eu

RTD-PUBLICATIONS@ec.europa.eu

European Commission

B-1049 Brussels

Manuscript completed in 2021.

This document has been prepared for the European Commission however it reflects the views only of the authors, and the Commission cannot be held responsible for any use which may be made of the information contained therein.

More information on the European Union is available on the internet (<http://europa.eu>).

Luxembourg: Publications Office of the European Union, 2021

PDF

ISBN 978-92-76-42041-5

ISSN 1831-9424

doi:10.2777/865442

KI-NA-30854-EN-N

© European Union, 2021.

Reuse is authorised provided the source is acknowledged. The reuse policy of European Commission documents is regulated by Decision 2011/833/EU (OJ L 330, 14.12.2011, p. 39).

For any use or reproduction of photos or other material that is not under the EU copyright, permission must be sought directly from the copyright holders.

All pictures, figures and graphs © Imperial College of Science, Technology and Medicine, RFCR-CT-2015-00005 MAPROC

Research Fund for Coal and Steel

Monitoring, Assessment, Prevention and Mitigation of Rock Burst and Gas Outburst Hazards in Coal Mines (MAPROC)

Coordinator:

Prof. Sevket Durucan

Imperial College of Science, Technology and Medicine
Exhibition Road, London, SW7 2AZ, United Kingdom

Prof. Anna Korre, Dr Ji-Quan Shi, Mr Wenzhuo Cao, Dr Wu Cai, Mr Harshit
Agrawal, Dr Zhenggang Nie, Dr Betul Yildirim
Imperial College of Science, Technology and Medicine
Exhibition Road, London, SW7 2AZ, UK

Prof. E. Krause, Prof. Adam Lurka, Dr J. Makowka, Dr J Skiba, Mr B. Jura,
Mr R. Siata, Mr R Hildebrand
Glowny Instytut Gornictwa
Plac Gwarkow 1, Katowice, 40-166, Poland

Dr S. Jamnikar, Dr J. Lazar, Dr J Roser
Premogovnik Velenje, D.D.
3320 Velenje, Slovenia

Mr T Gabzdyl
Jastrzebska Spolka Weglowa SA
Aleja Jana Pawla II 4, 44-330 Jastrzebie-Zdroj, Poland

Dr B.M. Krooss, Dr A. Amann- Hildenbrand, Mr G. Gaus
RWTH Aachen, Lochnerstr
4-20, Haus B, D-52056 Aachen, Germany

Grant Agreement RFCR-CT-2015-00005

1 July 2015 to 30 June 2019

Final Report

TABLE OF CONTENTS

FINAL SUMMARY	5
DETAILED SCIENTIFIC AND TECHNICAL DESCRIPTION OF THE RESULTS	9
INTRODUCTION AND PROJECT OBJECTIVES	9
WORK PACKAGE 1 - LABORATORY AND FIELD CHARACTERISATION OF COAL SEAMS AND SURROUNDING ROCKS AS INDICATORS FOR ROCK BURST AND GAS OUTBURSTS	11
<i>Task 1.1 Laboratory experiments on rock properties and gas emission dynamics in coal mines (led by RWTH, IMPERIAL, GIG, AITEMIN, IMPERIAL, JSW, CM-VELENJE).....</i>	11
<i>Task 1.2 Laboratory investigations into the seismic response of coal and coal measure rocks under stress (IMPERIAL)</i>	15
<i>Task 1.3 Assessment of in situ stress states and stresses induced around production areas in partner mines (led by IMPERIAL, GIG, CM-VELENJE, JSW, AITEMIN)</i>	21
WORK PACKAGE 2 - DEVELOPMENT AND FIELD TESTING OF TECHNOLOGIES FOR THE PREVENTION OF ROCK BURSTS AND GAS OUTBURSTS	27
<i>Task 2.1 Field experiments, monitoring and interpretation of the use of large diameter boreholes and blasting for stress relief to prevent rock bursts (led by CM-VELENJE, GIG, IMPERIAL, JSW)</i>	27
<i>Task 2.2 Field experiments, monitoring and interpretation of the use of water injection for gas pressure relief to prevent gas outbursts (led by GIG, AITEMIN, CM-VELENJE, JSW, IMPERIAL)</i>	35
<i>Task 2.3 Field experiments, monitoring and interpretation of the use of mechanical and/or high pressure slot cutting and hydrofracturing for stress and gas pressure relief to prevent rock bursts and gas outbursts (led by GIG, CM-VELENJE, JSW, IMPERIAL)</i>	36
<i>Task 2.4 Measurement while drilling to characterise coal and rock parameters which influence gas outbursts and rock bursts (led by CM-VELENJE, IMPERIAL, JSW, GIG)</i>	39
WORK PACKAGE 3 - MICROSEISMIC MONITORING AND DEVELOPMENT OF TECHNOLOGIES FOR SHORT-TERM PREDICTION OF ROCK BURSTS AND GAS OUTBURSTS.....	41
<i>Task 3.1 Microseismic monitoring of rock burst and gas outburst indicators at JSW and CM-Velenje (led by GIG, JSW, CM-VELENJE)</i>	41
<i>Task 3.2 Development of Artificial Neural Network (ANN) models for the short-term forecasting of rock bursts and gas outbursts (led by IMPERIAL, GIG, CM-VELENJE, JSW).</i>	49
<i>Task 3.3 Development of Fractal Dimension based models for the short-term forecasting of rock bursts and gas outbursts (led by IMPERIAL, GIG, CM-VELENJE, JSW).</i>	53
WORK PACKAGE 4 - NUMERICAL MODELLING OF PERFORMANCE OF ROCK BURST AND GAS OUTBURST PREVENTION METHODS FOR RISK EVALUATION	61
<i>Task 4.1 Numerical modelling of rock burst and gas outburst prevention techniques using field tested borehole stress and gas pressure relief methods (led by IMPERIAL, GIG, JSW, CM-VELENJE)</i>	61
<i>Task 4.2 Numerical modelling of rock burst and gas outburst prevention techniques using stress control mining (led by IMPERIAL, GIG, JSW, CM-VELENJE)</i>	69
<i>Task 4.3 Numerical modelling of rock burst and gas outburst prevention techniques using protective mining (led by IMPERIAL, GIG, JSW, CM-VELENJE)</i>	75
WORK PACKAGE 5 - DEVELOPMENT AND VALIDATION OF A GENERIC METHODOLOGY FOR THE ASSESSMENT AND MITIGATION OF RISK FROM ROCK BURSTS AND GAS OUTBURSTS	81
<i>Task 5.1 Development of a generic risk assessment methodology for rock bursts and gas outbursts (led by IMPERIAL, GIG, RWTH, CM-VELENJE, JSW)</i>	81
Implementation of the criterion for coal and gas outbursts	87
Fracture mechanics-based gas outburst model	88
A DFN-based microseismicity model	89
<i>Task 5.2 Testing and validation of the developed generic risk assessment methodology at partner mines using the field and laboratory data collected (led by IMPERIAL, CM-VELENJE, JSW)</i>	91
<i>Task 5.3 Modelling and probabilistic assessment of risk for rock bursts and gas outburst in coal mines (led by IMPERIAL, JSW, CM-VELENJE)</i>	105
WORK PACKAGE 6 - CONCLUSIONS, RECOMMENDATIONS AND DISSEMINATION	113
<i>Task 6.1 Dissemination Workshop (led by GIG, ALL PARTNERS)</i>	113

<i>Task 6.2 Lessons learnt document (led by IMPERIAL, ALL PARTNERS)</i>	113
<i>Task 6.3 Scientific journal and conference publications (led by RWTH, ALL PARTNERS)</i>	115
EXPLOITATION AND IMPACT OF THE RESEARCH FINDINGS	117
<i>Actual Applications</i>	117
TECHNICAL AND ECONOMIC POTENTIAL, POSSIBLE APPLICATION AT OTHER COALFIELDS 119	
OTHER ASPECTS CONCERNING THE DISSEMINATION OF RESULTS.....	121
PATENTS 123	
LIST OF ACRONYMS AND ABBREVIATIONS	125
REFERENCES.....	127
BIBLIOGRAPHY	129
LIST OF FIGURES	131
LIST OF TABLES	139

FINAL SUMMARY

Work package 1: Laboratory and Field Characterisation of Coal Seams and Surrounding Rocks as Indicators for Rock Burst and Gas Outbursts

Task 1.1 Laboratory experiments on rock properties and gas emission dynamics in coal mines (led by RWTH, IMPERIAL, GIG, AITEMIN until their withdrawal from the project, IMPERIAL, JSW, CM-VELENJE)

Work towards Task 1.1 was completed during the 1st Annual reporting period and the findings were reported in the Deliverable D1.1 report.

Task 1.2 Laboratory investigations into the seismic response of coal and coal measure rocks under stress (IMPERIAL)

IMPERIAL carried out laboratory research to characterise the seismic response of coal and coal measure rock samples using 300 mm cube samples under true-triaxial loading conditions and carried out acoustic measurements to determine the effect of stress and fracturing on acoustic velocities as baseline and during hydrofracturing.

Analysis of the fluid injection data over the hydraulic fracturing process suggested that a comparatively higher fluid pressure was required for HF initiation in homogenous rock block-1 when compared with that for naturally fractured rock block-2. Visualisation of split post-fractured rock blocks and their corresponding computed tomography analyses provided further information on spatial and geometrical properties of NFs, HFs, and possible NF/HF networks created during fracturing. The true-triaxial testing of large, naturally fractured coal and coal measures rock samples and comparing their seismic response to stress and fracturing helped characterise the seismic wave velocities in different geological media under different mining environments and aided the analysis of underground microseismic monitoring data.

A revised Deliverable D1.2 report was completed and submitted at the time of 3rd Annual Report with the results from both coal and rock samples.

Task 1.3 Assessment of in situ stress states and stresses induced around production areas in partner mines (led by IMPERIAL, GIG, CM-VELENJE, JSW, AITEMIN until their withdrawal from the project)

Work towards Task 1.3 was completed during the 1st Annual reporting period and the findings were reported in the Deliverable D1.1 report.

Work package 2: Development and Field Testing of Technologies for the Prevention of Rock Bursts and Gas Outbursts

Task 2.1 Field experiments, monitoring and interpretation of the use of large diameter boreholes and blasting for stress relief to prevent rock bursts (led by CM-VELENJE, GIG, IMPERIAL, JSW).

Large diameter stress relief boreholes were widely tested at Coal Mine Velenje throughout the project and seven barrier pillars (B k.-80, C k.-80, D k.-80, CD3g, C k.-95, D k.-95 and E k.-95) in levels -80 and -95m of the mine were used to test the effectiveness of 11 groups of several 160mm diameter and up to 80m long boreholes for this purpose. Due to the observed effectiveness of large diameter borehole drilling in the barrier pillars, this technique was extended as use in development headings where two significant rock bursts had occurred in 2018. The technique was documented and recorded by the National Mining Authorities in Slovenia. Coal Mine Velenje's systematic procedure which has now entered in their statutes and will be implemented at all development sites as best-practice through the experience gained in the MapROC project. The Deliverable D2.1 report was completed and submitted at the time of 3rd Annual Report in 2019.

Task 2.2 Field experiments, monitoring and interpretation of the use of water injection for stress and gas pressure relief to prevent gas outbursts (led by GIG, CM-VELENJE, JSW, IMPERIAL)

Work towards Task 2.2 was completed during the 2nd Annual reporting period. It was found that high pressure water injection was not as effective against gas outbursts as drilling and blasting as found out in Task 2.1. The main findings were reported in the 2nd Annual Report. Deliverable D2.2 report was completed and submitted at the time of 3rd Annual Report in 2019.

Task 2.3 Field experiments, monitoring and interpretation of the use of mechanical and/or high pressure slot cutting and hydrofracturing for stress and gas pressure relief to prevent rock bursts and gas outbursts (led by GIG, CM-VELENJE, JSW, IMPERIAL).

The large diameter borehole slotting trials were delayed due to two rock bursts at the planned LTCC panel Dk.-95 site in March and April 2018, and the work was postponed from May 2018 to October

2018. The slotting trials were completed in October 2019 after the repair of damaged roadways and preparation of the site for the work. Deliverable D2.3 report was submitted after the analysis and interpretation of the results at the time of 3rd Annual Report in 2019.

Task 2.4 Measurement while drilling to characterise coal and rock parameters which influence gas outbursts and rock bursts (led by CM-VELENJE, IMPERIAL, JSW, GIG)

Measurement While Drilling development and testing in Task 2.4 was completed while drilling the large diameter boreholes at LTCC panel Ck.-95 in December 2018. Deliverable D2.4 report was submitted after the analysis and interpretation of the results at the time of 3rd Annual Report in 2019.

Work package 3: Microseismic Monitoring and Development of Technologies for Short-term Prediction of Rock Bursts and Gas Outbursts

Task 3.1 Microseismic monitoring of rock burst and gas outburst indicators at JSW and CM-Velenje (led by GIG, JSW, CM-VELENJE)

The microseismic monitoring at Coal Mine Velenje and JSW Pniowek Colliery, which was later transferred to Budryk Colliery, ran through 2016 - 2018. The monitored data from these mines were continuously processed by GIG and forwarded to IMPERIAL for their work in Tasks 3.2 and 3.3. As planned, work by GIG was completed and Deliverable D3.1 Report was submitted after the analysis and interpretation of the results.

It was decided that IMPERIAL takes over the monitoring and assessment of the data from Velenje until the end of the project voluntarily and at its own cost. Therefore, the system was left to continue operational at CM-Velenje.

Task 3.2 Development of Artificial Neural Network (ANN) models for the short term prediction of rock bursts and gas outbursts (led by IMPERIAL, GIG, CM-VELENJE, JSW).

In Task 3.2 IMPERIAL developed and tested the Artificial Neural Network models using the long-term historical micro-seismic monitoring data from the Budryk Colliery of JSW and Coal Mine Velenje. The final Deliverable D3.2 Report was submitted after the analysis and interpretation of all the results at the time of 3rd Annual Report in 2019.

Task 3.3 Development of Fractal Dimension based models for the short term prediction of rock bursts and gas outbursts (led by IMPERIAL, GIG, CM-VELENJE, JSW).

In task 3.3 IMPERIAL developed and tested the Fractal Dimension based models for the short-term forecasting of potential gas outburst and rock burst events using the long-term historical micro-seismic monitoring data from Coal Mine Velenje and the Budryk Colliery of JSW. The final Deliverable D3.3 Report was submitted after the analysis and interpretation of all the results at the time of 3rd Annual Report in 2019.

Work package 4: Numerical modelling of rock burst and gas outburst prevention techniques using field tested borehole stress and gas pressure relief method

Task 4.1 Numerical modelling of rock burst and gas outburst prevention techniques using field tested borehole stress and gas pressure relief methods (led by IMPERIAL, GIG, JSW, CM-VELENJE)

Numerical modelling of unslotted and slotted boreholes using an example Velenje site layout was completed during the 2nd Annual reporting period. After the completion of the slotting experiments and analysis of the field data the Deliverable D4.1 report was submitted at the time of 3rd Annual Report in 2019. Blasting modelling of boreholes was integrated into the D4.1 Deliverable Report as well.

Task 4.2 Numerical modelling of rock burst and gas outburst prevention techniques using stress control mining (led by IMPERIAL, GIG, JSW, CM-VELENJE)

IMPERIAL developed and implemented numerical models to designed mining layouts using sacrificial roadways and/or pillars for stress/gas pressure relief and gas outbursts/rock burst control in coal mining and assessed their performance and evaluate risk. Design of eccentric mine layout in multi-seam workings were also modelled to strategically locate the roadways to mitigate against rock burst risks. Parametric modelling work under Task 4.2 has shown that a width to height ratio of less than 2 will make an ideal yield pillar. The results of eight different mining layouts have shown that symmetrical mining layouts for 2-entry or 3-entry yield pillar systems are best for rock

burst control. In case of multi-seam workings, the roadways in the lower seam should be shifted laterally by around half of the width of the longwall panel to minimise the effect of vertical stress and elastic strain energy accumulation in the lower seams. Deliverable D4.2 report was submitted at the time of 3rd Annual Report in 2019.

Task 4.3 Numerical modelling of rock burst and gas outburst prevention techniques using protective mining (led by IMPERIAL, GIG, JSW, CM-VELENJE).

Numerical modelling of protective mining using the Pniowek Colliery layout as example was completed during the 2nd Annual reporting period. During 2018-19 a generic protective mining model for depths down to 1,200 m depth with different seam and rock properties was developed and integrated in the Deliverable D4.3 report and submitted at the time of 3rd Annual Report in 2019. These data were used in Task 5.3 parametric and probabilistic risk assessment model applications.

Work package 5: Development and validation of a generic methodology for the assessment and mitigation of risk from rock bursts and gas outbursts

Task 5.1 Development of a generic risk assessment methodology for rock bursts and gas outbursts (led by IMPERIAL, GIG, RWTH, CM-VELENJE, JSW)

Work towards Task 5.1 was completed during the 2nd Annual reporting period and the generic risk assessment methodology was developed as reported in the Deliverable D5.1 report at the time of 2nd Annual Report in 2018.

Task 5.2 Testing and validation of the developed generic risk assessment methodology at partner mines using the field and laboratory data collected (led by IMPERIAL, GIG, CM-VELENJE, JSW, RWTH)

The generic risk assessment methodology developed in Task 5.1 was tested and validated using microseismic monitoring data collected from the Budryk Colliery and Coal Mine Velenje. Numerical models developed based on fracture mechanics and DFN-based microseismicity modelling were also tested and validated using field data from partner industries. The Deliverable D5.2 report was submitted at the time of 3rd Annual Report in 2019.

Task 5.3 Modelling and probabilistic assessment of risk for rock bursts and gas outburst in coal mines (led by, JSW, CM-VELENJE)

Work in this Task on parametric analysis and risk assessment developed a risk matrix and populated it with data and layouts and started the modelling work in 2018. Parametric analysis using the layouts developed in WP4 have been used to carry out risk assessment following the matrix. A probabilistic risk assessment methodology was developed and implemented using the lithological heterogeneity data first measured through active and passive seismic monitoring in the field at Coal Mine Velenje during CoGasOUT. This proved a very effective methodology to assess the impact of uncertainty in the measured and monitored field data. This work was completed during the six months of the project and the Deliverable D5.2 report prepared and submitted together with the Final Report.

Work package 6: Conclusions, Recommendations and Dissemination

Task 6.1 Dissemination Workshop (led by GIG, ALL PARTNERS)

The Workshop was held on 30th May 2019 in Katowice with 37 attendees joining the Workshop.

Task 6.2 Lessons learnt document (led by IMPERIAL, ALL PARTNERS)

After completion of all the project WPs and Tasks, the Lessons Learnt document was prepared as a State-of-the-Art best practice document based on the findings of the work under different WPs. The Deliverable D6.2 report prepared and submitted together with the Final Report.

Task 6.3 Scientific journal and conference publications (RWTH, ALL PARTNERS)

Nine conference proceedings and seven journal publications were prepared and submitted during the project. A few other publications from the final years' work are also being written up for further publications

DETAILED SCIENTIFIC AND TECHNICAL DESCRIPTION OF THE RESULTS

Introduction and Project objectives

Coal mining in Europe is extending to deeper and deeper levels, facing ever increasing stress, gas pressure and gas content conditions in production districts. Mining induced high stress and gas pressure concentrations often result in rock bursts and coal/gas outbursts. These events not only form a serious safety risk, but also represent a problem for coal production. Rock bursts and gas outbursts are currently the main hazards experienced by the industry partners Coal Mine Velenje and JSW, but are also applicable to many other mines in Europe.

One common drawback of the current rock burst and gas outburst assessment and prevention methods referred to in the previous section is that their applications mostly depend on site-specific field experience, rather than sound theoretical studies. The CoGasOUT project, which was completed in June 2013 demonstrated that continuous microseismic monitoring is a promising technology to detect areas of high gas pressure and stress concentrations around production faces. However, current microseismic data processing and further analysis methods used involve several weeks, if not months, to finalise, which would be inadequate as a predictive method. Therefore, the main objectives of MapROC were:

- to develop and field test rock burst and gas outburst prevention techniques based on the use of large diameter boreholes with alternative stress and gas pressure relief techniques such as blasting, slotting and/or high pressure water injection.
- to formulate a methodology coupling the near-real time processing of the continuously monitored microseismic data with Artificial Intelligence and Fractal Dimension analysis techniques to develop a short-term forecasting method for rock bursts and gas outbursts. As the project progressed it has been decided to extend these analyses to include the use of numerical modelling techniques as forecasting methods as well.
- to numerically model the field application of the borehole stress/gas pressure relief methods as well as modelling stress control and protective mining options in different mine layouts relevant to common coal mining methods implemented in Europe.
- to demonstrate the use of these short term forecasting methods as a tool for early risk assessment, prevention, and mitigation of rock bursts and gas outbursts.
- to develop and validate a generic risk assessment methodology for the prevention and mitigation of rock bursts and gas outbursts

The application of the developed prediction and prevention techniques, therefore, will be applicable to other mines as well as being available for technology transfer to countries with large coal deposits of similar seam structures, gas contents and rock burst/outburst risks, such as China and India.

WORK PACKAGE 1 - LABORATORY AND FIELD CHARACTERISATION OF COAL SEAMS AND SURROUNDING ROCKS AS INDICATORS FOR ROCK BURST AND GAS OUTBURSTS

Task 1.1 Laboratory experiments on rock properties and gas emission dynamics in coal mines (led by RWTH, IMPERIAL, GIG, AITEMIN, IMPERIAL, JSW, CM-VELENJE)

The two main objectives of this Tasks were:

- (1) to review and make available to the project the coal properties determined in previous and current projects relevant (CoGasOUT and GasDRAIN) in the partner industries, namely JSW and Coal Mine Velenje and then fill in the gaps specific to MapROC with further laboratory experiments and
- (2) to compile a coal property database with additional data from the archives of the industry and RTD partners on coals of different rank and gas contents from the UK, Germany, Poland and Spain, which are particularly relevant to WP5 generic risk assessment model development.

Characterisation of coals from the Pniowek Colliery

Within the context of the MapROC project, very large blocks of coal (Figure 1.1) were collected from underground by JSW Pniowek Colliery and GIG, and taken to London and Aachen for further testing of this second JSW coal seam (Seam 404/1) where the seismic monitoring sensors were first installed.



Figure 1.1 Large (600x600x400 mm) coal sample from the Pniowek Colliery Seam 404/1 and the 38mm diameter core samples prepared for testing.

Table 1.1 He-Pycnometry results on dry coal from the Pniowek Colliery.

Sample	Mass [g]	Bulk volume [cm ³]	Skeletal Volume [cm ³]	Pore volume [cm ³]	Bulk density [g/ cm ³]	Skeletal density [g/ cm ³]	Porosity [%]	Permeability coefficient [m ²]
Pniowek 1	39.03	32.89	30.07	2.82	1.19	1.30	8.57	1.42×10^{-17}
Pniowek 7	60.49	52.35	47.79	4.57	1.16	1.27	8.72	2.05×10^{-17}

Table 1.2 Gas slippage factors and intrinsic permeabilities at 30 MPa confining pressure for constant downstream and uptake experiments for samples from the Pniowek Colliery.

Sample	Intrinsic permeability [m ²]		Gas slippage factor [MPa]		Confining pressure [MPa]
	Constant downstream	Uptake	Constant downstream	Uptake	
Pniowek 1	1.94×10^{-20}	1.12×10^{-20}	0.28	0.44	30

RWTH prepared core plugs to carry out proximate analysis and vitrinite reflectance. Core plugs were used to perform He-Pycnometry experiments. Different experiments such as steady state, constant downstream or uptake experiments were performed to obtain permeability coefficients. Table 1.1 displays the obtained parameters from He-Pycnometry experiments.

Table 1.2 presents the gas slippage factors and intrinsic permeabilities measured at Aachen.

Stress-Permeability Measurements on Pniowek Coals

At Imperial College, solid cores were extracted from the large coal blocks (Figure 1.1) received from the Pniowek Colliery Seam 404/1 and tested for stress-permeability relationship which yielded elastic properties as well as stress dependent permeability for use in numerical modelling. All the samples tested were solid cores cut to a diameter of 38 mm and a length of 76 mm. Multistage triaxial compression and stress-permeability tests were conducted simultaneously using a four-column 2,000 kN capacity electrohydraulic rock testing unit (Figure 1.2). The tests were conducted for confining stress (σ_3) values of 1.5, 5, 8, 14 and 18 MPa. During the experiments, axial loading is applied through the top platen of the cell at constant strain rate of 10 millistrain per hour. In addition to stress, absolute permeability of the coal samples is also measured using Helium as the pore fluid.

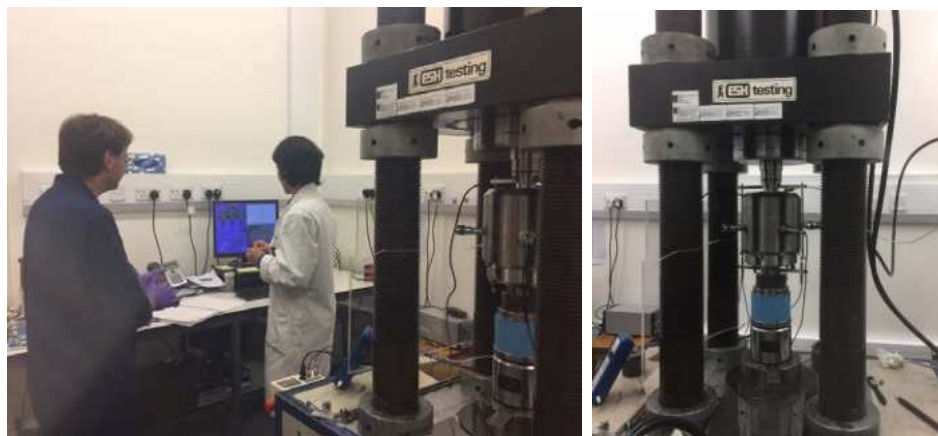


Figure 1.2 External views of the four-column ESH rock testing unit and digital control hardware.

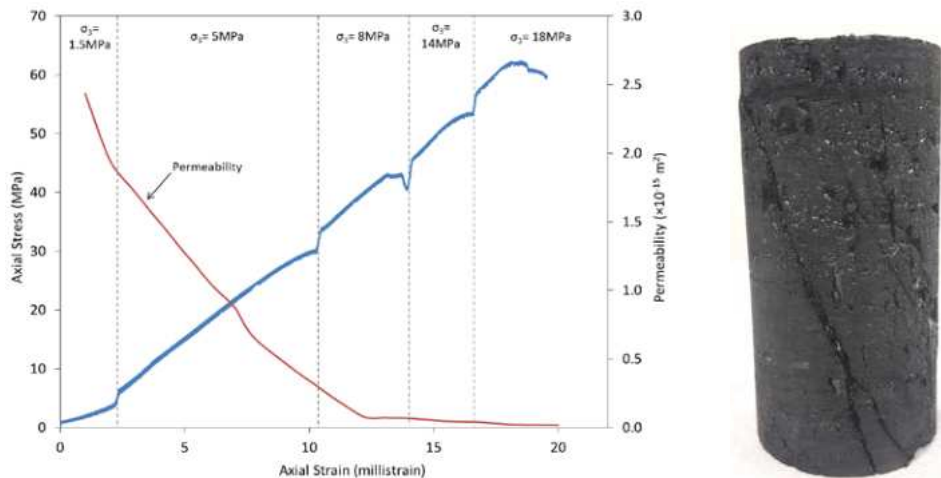


Figure 1.3 Stress-strain and permeability-strain behaviour seam 404/1 coal sample from the Pniowek Colliery.

An example stress-strain and permeability-strain data obtained from the multistage triaxial testing of a Pniowek coal is shown in (Figure 1.3). It can be seen that the permeability of coal gradually decreases with increase in axial strain and appears to stabilise when the shear failure is initiated at each confinement level on the coal sample. The permeability is further reduced when the confining stress is increased and continues to reduce with increase in axial load.

Specific to the Pniówek Colliery, researchers at GIG carried out measurements and coal characterisation work at the mine during roadway development and longwall extraction in Seams 404/1 and 404/2. These included methane content experiments, sorption experiments and coal and gas outburst indexes of the seams (Table 1.3 and Table 1.4).

Table 1.3 Example results of methane content experiments on coal and outburst indexes in the seam 404/1, Zone C at Pniówek Colliery.

#	Date	Methane content $\text{m}^3\text{CH}_4/\text{Mg}_{\text{daf}}$	Desorption intensiveness kPa	Coal conciseness	Coal cuttings production l/running meter of the borehole
<i>Incline C-4 in the seam 404/1</i>					
1.	09.05.2016r	6,81	1,14	0,45	2,6
2.	16.05.2016r	3,50	0,72	0,46	2,5
3.	23.05.2016r	2,49	0,86	0,46	2,5
4.	01.06.2016r	6,20	1,16	0,44	2,7
5.	08.06.2016r	5,60	1,12	0,43	2,7
<i>Incline C-5 in the seam 404/1</i>					
1.	21.07.2016r	7,54	1,36	0,45	2,7
2.	26.07.2016r	5,00	1,52	0,45	2,7
3.	03.08.2016r	7,98	1,42	0,45	2,8
4.	09.08.2016r	8,12	1,40	0,46	2,7
5.	16.08.2016r	6,85	1,36	0,43	2,7
<i>Rise gallery C-5 in the seam 404/1</i>					
1.	24.10.2016r	5,75	1,04	0,42	2,6
2.	04.11.2016r	4,53	1,08	0,45	2,8
3.	14.11.2016r	4,80	0,78	0,45	2,6
4.	22.11.2016r	7,00	1,54	0,41	2,9
5.	25.11.2016r	7,33	1,76	0,39	3,0
<i>Roadway C-5a in the seam 404/1</i>					
1.	12.09.2016r	1,76	0,48	0,44	2,5
2.	23.09.2016r	5,19	0,48	0,44	2,6
3.	30.09.2016r	0,93	0,18	0,43	2,4

Table 1.4 Results of Pniówek Colliery methane sorption experiments.

#	Sample description	Date of analysis	Effective diffusion coefficient $D_e [\text{cm}^2/\text{s}]$	Sorption capacity [cm^3/g]	Sorption capacity with regard to dry ash free coal $a_{\text{cs}} [\text{cm}^3/\text{g}_{\text{cs}}]$
1	Rise gallery C-4c seam 404/1 (KM 64)	16-20.07.2015	$0,107 \times 10^{-8}$	3,366	3,473
2	Rise gallery C-4c seam 403/3	20-24.08.2015	$0,068 \times 10^{-8}$	4,995	5,141
3	Rise gallery Z-VII seam 407/3 (KM 636)	24-27.08.2015	$0,125 \times 10^{-8}$	3,147	3,718
4	Rise gallery Z-VII seam 407/4 KM 718m	10-13.11.2015	$0,088 \times 10^{-8}$	4,546	4,679
5	Roadway C-6 seam 404/1	15-18.12.2015	$0,182 \times 10^{-8}$	4,542	4,729
6	Incline C-1, seam 404/2, 480KM	21-23.12.2015	$0,095 \times 10^{-8}$	4,605	4,692
7	Roadway N-6 seam 404/2 KM-12	28-30.12.2015	$0,128 \times 10^{-8}$	5,047	5,193
8	Roadway PW-1 seam 357/1 20KM	19-22.08.2016	$0,058 \times 10^{-8}$	4,858	5,014
9	Roadway N-5 seam 404/2 445KM	04-07.10.2016	$0,114 \times 10^{-8}$	4,076	4,343
10	Rise gallery K-7 seam 363 KM82	10-13.10.2016	$0,161 \times 10^{-8}$	4,052	4,183
11	Rise gallery N-4 seam 404/2 120KM	28-31.10.2016	$0,108 \times 10^{-8}$	4,694	4,749

Characterisation of coals from Coal Mine Velenje

At Coal Mine Velenje, characteristic geomechanical properties of the lignite coal seam have been determined from core samples taken from exploration boreholes throughout the mine. Table 1.5 list these properties for the coal seam, roof and floor. These provided the fundamental data for the rock burst modelling and risk assessment studies in MapROC. Coal at Velenje has two main lithological

components the geomechanical properties of which were also separately tested and characterised in previous projects by Imperial College and Coal Mine Velenje as presented in Table 1.6 and Table 1.7. Gas contents of Velenje lignite were also determined during CoGasOUT. Furthermore, methane, CO₂ and mixed gas adsorption isotherms of Velenje coals were measured by Imperial College in previous EU funded projects CoGasOUT and GHG2E. The RWTH participated in a European inter-laboratory comparison of high pressure CO₂ sorption experiments using Velenje coal samples (Gensterblum et al., 2010).

Table 1.5 Geomechanical properties of coal and over/underburden at Coal Mine Velenje (Jeromel, 2010).

	Moisture Content W (%)	Unconfined Compressive strength σ_{UCS} (MPa)	Tensile Strength σ_t (MPa)	Young's Modulus E (GPa)	Shear Modulus G (MPa)	Poisson's Ratio v (-)	Cohesion C (MPa)	Internal Friction Angle ϕ (°)
Roof I/II	24.4/32.6	0,85/2.50	0.08/0.23	0.140/0.430	2.0/2.17·10 ⁸	0.35/0.20	0.4/0.7	15/17
Coal (0 - 0.5)	39.0	8.40	0.92	0.480	1.68·10 ⁸	0.25	0.7	30
Coal (0.5 - 1)	35.0	5.40	0.59	0.480	1.68·10 ⁸	0.30	0.7	30
High ash coal	25.6	1.60	0.17	0.375	-	0.35	-	-
Floor	10.0	4.90	0.44	2,917	2.00·10 ⁸	0.30	1.4	21
Broken coal	-	-	0.17	0.352	1.30·10 ⁸	0.35	0.1	25
Caved overburden	-	-	0.03	0.460	1.60·10 ⁸	0.35	0.5	10

Table 1.6 Uniaxial compression test results for lithologies from Coal Mine Velenje.

Borehole and Core number	Lithology	Bulk density (kN/m ³)	P-wave velocity (km/s)	Young's Modulus (GPa)	Bulk Modulus (GPa)	Poisson's ratio	UCS (MPa)	Strain Energy W _z (KJ/m ³)
J.V.1061-3b-GM/06	Fine Detrite	13.65	1.06	0.79	0.68	0.45	9.23	180.35
J.V.1042-3-T	Detrite, gelified	12.44	0.57	0.74	0.51	0.35	14.65	265.80
J.V.3300-2b-GM/05	Fine Detrite	12.48	1.36	0.97	0.84	0.48	11.22	287.34
J.V.1040-1-K	Xylo Detrite	12.42	1.18	0.75	0.59	0.45	7.92	186.30
J.V.3298-12-GM/05	Xylo Detrite	12.75	1.68	1.06	0.98	0.41	9.26	117.22
J.V.3297-4-GM/05	Detrite, gelified	12.84	1.56	1.20	1.02	0.47	7.85	107.32
J.V.3302-10d-GM/05	Fine Detrite	12.94	1.29	1.14	0.90	0.45	6.31	63.38
J.V.3298-3a-GM/05	Xylite	14.89	1.27	0.73	0.32	0.41	4.37	176.48
J.V.3297-3-GM/05	Detrite, gelified	12.84	1.29	1.02	0.89	0.39	6.90	94.76
J.V.3298-4-GM/05	Xylo Detrite	12.68	1.47	1.25	1.05	0.46	6.55	83.46

Table 1.7 Triaxial compression test results for lithologies from Coal Mine Velenje.

Borehole and Core number	Lithology	Young's Modulus (GPa)	Poisson's ratio	Cohesion (MPa)	Friction angle (degree)	UCS (MPa)	Tensile strength (MPa)	Hoek-Brown parameter
J.V.3296-6-GM/05	Fine Detrite	1.11	0.36	2.80	26.08	7.41	-1.17	6.16
J.V.3297-7-GM/05	Gelified Detrite,	1.20	0.37	4.57	21.90	13.30	-3.95	3.07
J.V.3298-6b-GM/05	Xylo Detrite	0.70	0.32	2.35	25.20	6.45	-1.12	5.61
J.V.3302-6d-GM/05	Fine Detrite	0.99	0.48	2.92	23.83	8.46	-2.01	3.96
J.V.3302-4d-GM/05	Xylite	4.80	0.50	4.27	23.29	12.56	-3.28	3.57

Database of other European coal seam characteristics

Also of specific interest to MapROC project were the coal seams from Spain. Data on Spanish mines operated by Hunosa and HVL have been collected in current and past projects by the partners (GasDRAIN and CoGasOut as some example). The # 8 Seam at the Sueros Colliery of HUNOSA, which has also been characterised during the GasDrain project. High-pressure methane sorption isotherms

measured on dry coal samples from the HUNOSA Sueros Colliery Seams #8 at 45°C are shown in Figure 1.4.

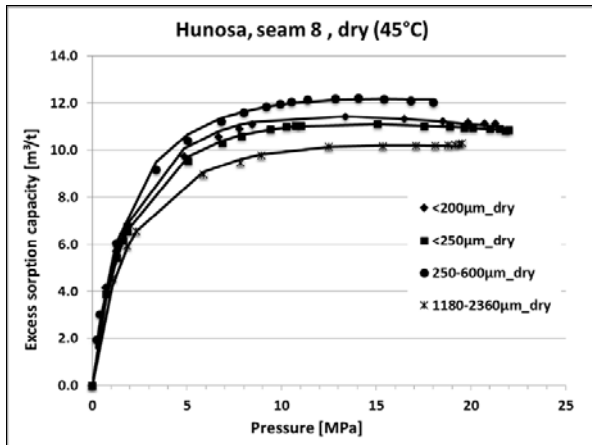


Figure 1.4 High pressure Langmuir isotherms for Seam #8 samples from the HUNOSA Sueros Colliery measured at 45°C.

Data from a large number of coalfields in Germany, UK, Belgium, The Netherlands and Czech Republic were also reported extensively in the project.

Task 1.2 Laboratory investigations into the seismic response of coal and coal measure rocks under stress (IMPERIAL)

The seismic response of coal and coal measures rocks to high stress conditions is crucial in understanding the processes involved in rock bursts and gas outbursts in coal mines. Therefore, the main objective of this task was to carry out acoustic measurements in laboratory and determine the effect of stress and fractures on acoustic velocities, and correlate this with the field measurements taken in WP3 throughout the project. Several large coal and rock blocks were obtained, transported and cut to 300mm cubic samples for the experimental programme. Experiments carried out in the project included two coal and two coal measures rock – shale sandstone – samples.

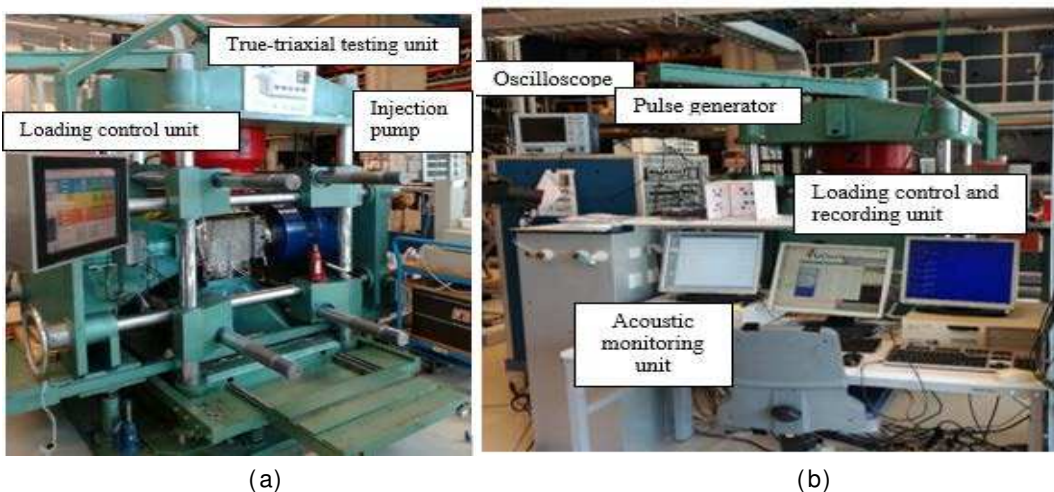


Figure 1.5 (a) True triaxial rock testing set-up equipped with loading, injection and acoustic systems, and (b) experiment control, recording, and monitoring units.

Experimental setup

The experimental apparatus includes a true-triaxial rock testing machine to apply mechanical loads, an injection system for hydraulic fracturing, and an ultrasonic monitoring system with active sources to record seismic response during experiments (Figure 1.5). The large true triaxial cell has large loading plates which are used to apply stress as well as measuring the generated acoustic signals through the transducers inserted in the plates. The injection system allows to inject fluid to a pre-drilled borehole in the sample through an injection tube, which is connected to an injection pump via a valve. The ultrasonic monitoring system is comprised of a pulse generator, and 48 piezoelectric transducers, each functioning in source and receiver modes in a sequence. The transducers are

organised into different source-receiver pairs, which can be categorised into six raypath types: P wave straight transmission (stP), P wave oblique transmission (opt), P wave diffraction (dB), S wave straight transmission (sots), S wave oblique transmission (oats), S wave diffraction (ds').

Sample preparation and testing

Large coal blocks from the partner mines and different seams in Poland (Figure 1.6) have been collected and cut to shape (300mm x 300mm x 300mm cubes), ready for testing. Rock samples representative of coal measures rocks were also collected and prepared as 300 x 300 x 300 mm size cubes. Figure 1.7 presents blocks, one being homogeneous (a) while the other including four visible sets of natural fractures on faces ZC, YD, YC, and XC (b). Outcrop of the main natural fracture on sample-2 (NF1) is found to be starting on the ZC face, and continue on XD face of the block.

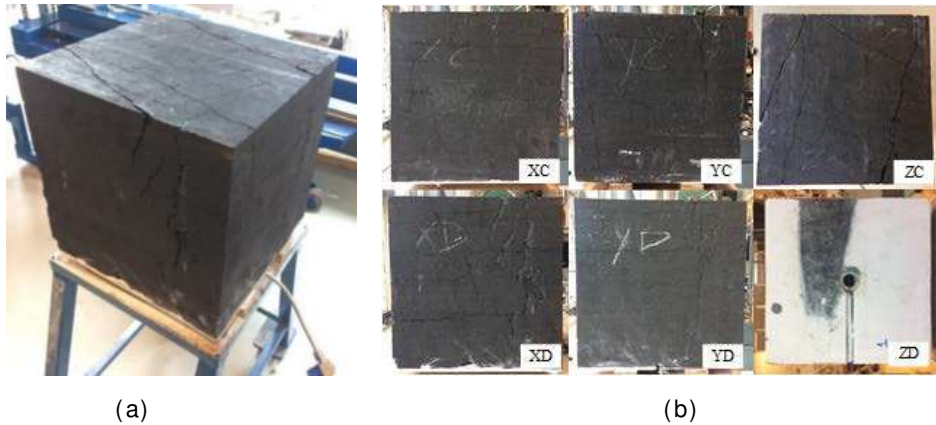


Figure 1.6 (a) Cubic coal block from partner coal mine in Poland, and (b) fracture outcrops on each face of the coal block.

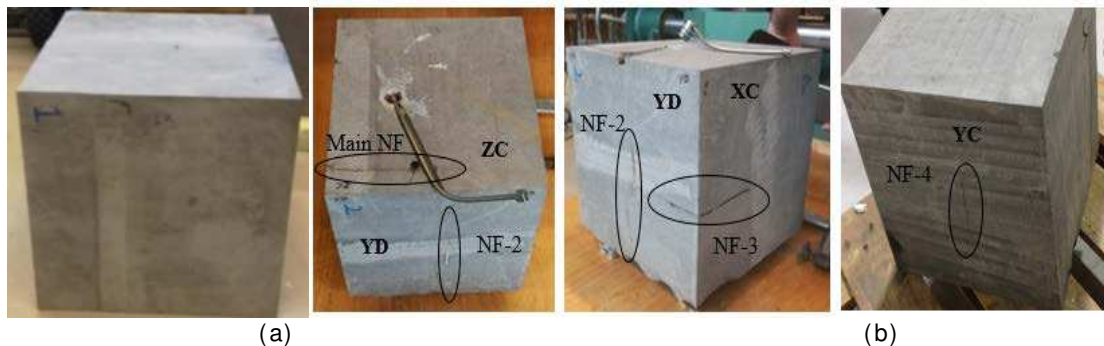


Figure 1.7 (a) Homogeneous rock block-1, and (b) Natural fractures on ZC, YD, YC, and XC surfaces of block-2.

In preparation for the fluid injection experiment to create further fractures and monitor acoustic response, an injection borehole (15 cm in length and 34 mm in diameter) was drilled into the middle of the test blocks. While the rock sample-1 was drilled from the middle of the sample, sample-2 was drilled laterally and 8 cm away from the main natural fracture seen on the surface. For the coal block 2, a short steel casing (4 cm in length and 23 mm in inner diameter) was glued inside the first 4 cm section of the borehole. In the case of rock blocks, 15 cm long casings were used without leaving an open hole section. An injection tube was connected to the steel casing via a connector, and two rubber rings were put between the casing and the connector for sealing purposes. The injection tube was embedded along a pre-drilled groove on the block face to avoid interference with loading platens. The blocks were then placed in the true-triaxial compression machine and loaded at different stress stages and experiments carried out.

To observe the variation in geometry of interior fracture networks formed, computed tomography (CT) scan was performed for the coal measures rock cubes using a medical CT scanner with a maximum resolution of 0.3 mm before and after the experiments. Multiple scanned images were then used to synthesise the cubes in 3D, and both natural and induced fracture traces marked in slice views were used to extract 3D fracture networks. In addition, the cubes were further split for observation of the location and size of natural and induced fractures as well as the fluid-intruded regions. The fractured regions were avoided in splitting to conserve the geometry and size of induced

fractures. Only the procedure, results and analysis of the experiments on one coal and rock block are summarised here.

Results and analysis for coal block 2

Figure 1.8 presents the mechanical behaviour of coal block 2 in response to true triaxial loading and the injection measurements during the hydraulic fracturing process. The displacement of the coal block in each direction is positively correlated with the corresponding stress, showing that the deformation of the coal blocks was mostly within the elastic range. The residual displacement after complete unloading indicates that irreversible plastic deformation also occurred in the coal blocks. In addition, it is obvious that there was anisotropy in displacement in coal block 2, which favours deformation perpendicular to bedding planes (y direction).

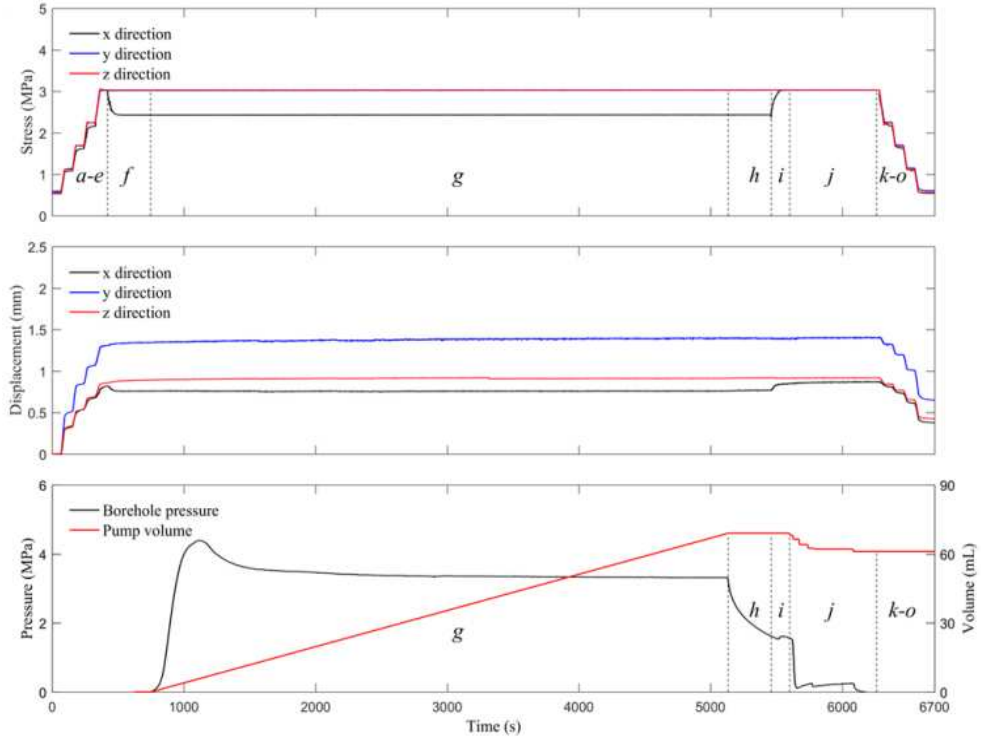


Figure 1.8 Stress, displacement and injection histories for coal block 2 during the true triaxial experiments.

Hydraulic injection at a constant injection rate began at 747 s after the start of the experiments for coal block 2. The borehole pressure increased quickly, and an induced fracture was initiated. Since fractures tend to grow orthogonal to the orientation of the minimum principal stress, the induced fracture was expected to be a vertical fracture running perpendicular to the x direction. Leak-off was believed to have happened when the borehole pressure reached the peak, which was 4.4 MPa at 1,115 s (368 s after the injection) for coal block 2. Afterwards the borehole pressure experienced a gradual decline, which indicates that the induced fracture coalesced with the natural fracture system which provided conduits for the silicon oil. It is noted that the post-peak borehole pressure inside coal block 2 stayed at a plateau of around 3.5 MPa for around 1 hour. A total of 146 acoustic scans were recorded to reveal the evolution of induced fractures.

Figure 1.9 shows the comparison between CT-scanned images before and after the hydraulic fracturing experiment for coal block 2. The post-fracturing CT scan was performed immediately after the experiment, so the injection borehole was filled with injection oil.

Figure 1.10 illustrates the interior natural and hydraulic fracture networks extracted from CT scan images after hydraulic fracturing. A system of microscopic fractures nonuniformly distributed throughout the coal blocks was filtered out, and only main fractures at the block scale are presented. Natural fractures in the coal block are well-connected. Most oil injected in coal block 2 entered natural fractures including three parallel and three perpendicular to bedding planes, rather than to drive the continuous propagation of a hydraulic fracture. After oil leaked into multiple natural fractures and reached the block border, the borehole pressure decreased below what could drive oil to enter natural fractures at the far end, such as NNF 1 in coal block 2, although they intersected with oil-intruded ones. This shows that the interior natural fracture networks of fractured coal blocks, instead of

orientations and patterns of face and butt cleats, dominate hydraulic fracturing behaviour and the associated intrusion of injected oil.

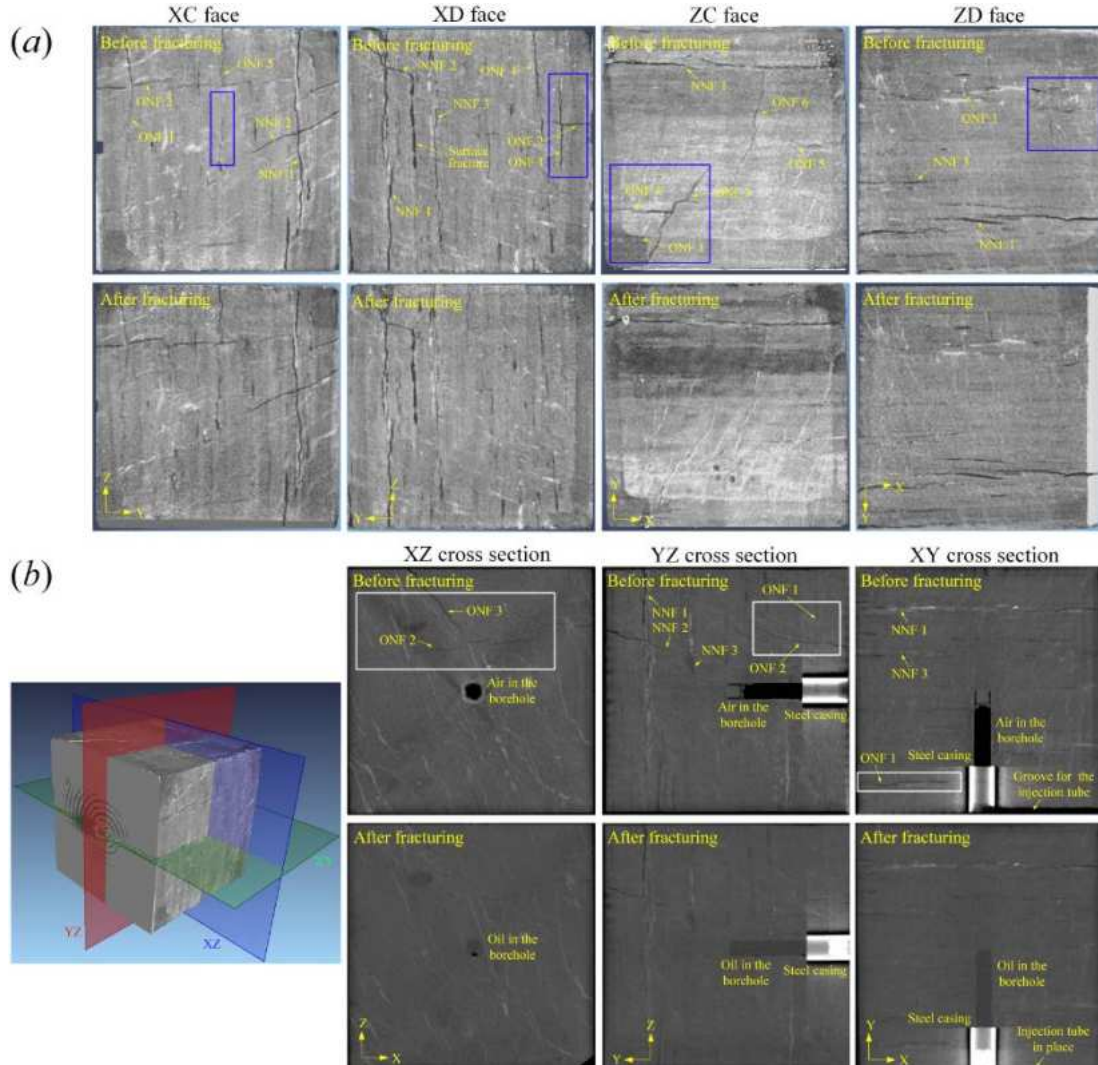


Figure 1.9 CT-scanned images before and after hydraulic fracturing for coal block 2: (a) surfaces, and (b) slice views (ONF: oil-intruded natural fractures; NNF: non-intruded natural fractures).

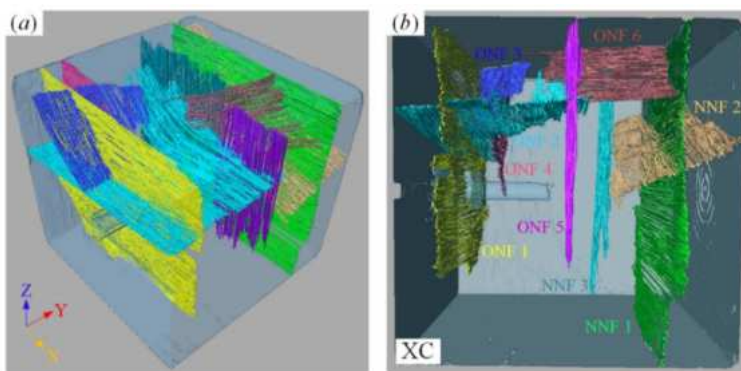


Figure 1.10 Reconstructed natural and hydraulic fracture networks from CT scan images: (a) 3D view for coal block 2, and (b) side view for coal block 2 (HF: hydraulic fractures; ONF: oil-intruded natural fractures; NNF: non-intruded natural fractures).

Figure 1.11 illustrates the velocities of seismic waves relative to hydrostatic confining stresses. The average seismic wave velocity increases with increasing confining stress. Under each confining stress, the scatter plot shows apparent anisotropy in seismic wave velocities: $v_x > v_y \approx v_z$ for coal block 2. On top of the effects of cleat patterns, the low velocity values in the other two directions can be attributed

to the blockage of macroscopic fracture planes perpendicular to these two directions, as observed in fracture outcrops and post-fractured CT images (Figure 1.9). Seismic wave velocities largely disperse in one direction, which indicates the highly heterogeneous distribution of natural fractures in the coal blocks.

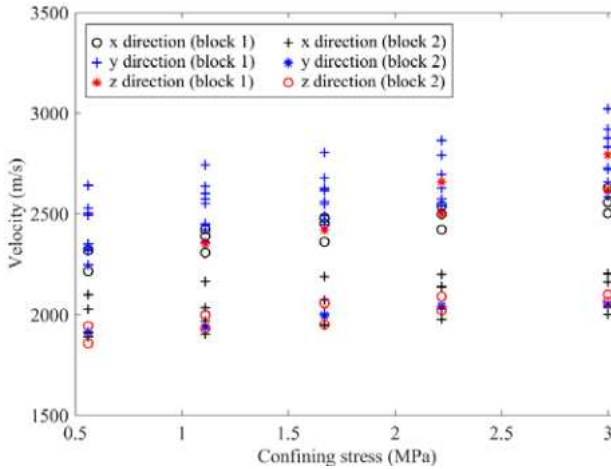


Figure 1.11 S wave velocity as a function of hydrostatic confining stress.

In seismic velocity tomography high-velocity regions represent relatively intact and/or pressurised rock mass, while low-velocity regions are indicative of highly fractured rock mass. A widely used algorithm referred to as the Simultaneous Iterative Reconstructive Technique (SIRT) (Cai *et al.*, 2014; Gilbert, 1972) was adopted for seismic velocity tomography in this work. Seismic velocity tomography calculations were performed before and after hydraulic injection using first arrival times in seismograms recorded from 93 transducer pairs for coal block 2, which are categorised in stS, otS, and dS raypaths.

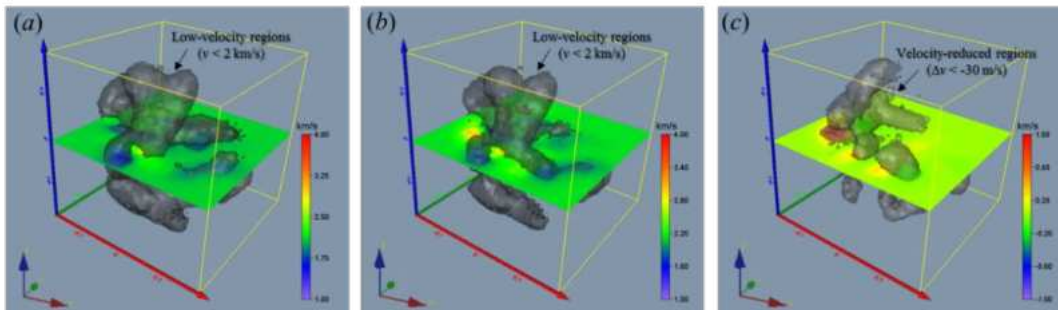


Figure 1.12 S-wave velocity tomograms for coal block 2: (a) before hydraulic fracturing, (b) after hydraulic fracturing, and (c) the difference induced by hydraulic fracturing.

Figure 1.12 illustrates the influence of hydraulic fracturing on the S-wave velocity tomograms. The average S-wave velocities calculated from the tomography for coal block 2 is around 2.1 km/s, which is consistent with that in Figure 1.11 and the low-velocity regions from tomography before injection for coal block 2 correlate well with locations of natural fractures. After the hydraulic injection into coal block 2, the bulk of velocity-reduced regions (Figure 1.12c) overlap with distribution regions of oil-intruded fractures (Figure 1.12b), which indicates that oil intrusion into fractures could increase the damping to seismic wave propagation and thus reduce seismic velocity.

Results and analysis for coal measures rock cube 2

Load, displacement, and pump data were recorded and interpreted to evaluate the fracture initiations in the rock blocks (Figure 1.13). Fractures were believed to be induced when borehole pressures reached their peaks and experienced sudden decrease, which occurred at 22.8 MPa pressure at 650 s after the injection for block-2.

Rock block Sample-2 was split into three smaller blocks after the fracturing experiment (Figure 1.14a). Then, the split block 2 was placed into CT scanner in the same orientation as it was placed into the true-triaxial testing machine, which is presented with its corresponding CT scan analysis in Figure 1.14b. Only the natural fractures, particularly the natural fractures NF1 and NF2, could be visualised with the conducted CT analysis, which is going to be further analysed with the scan results of the split block 3, for a better evaluation of the HF propagation and its interaction with NFs.

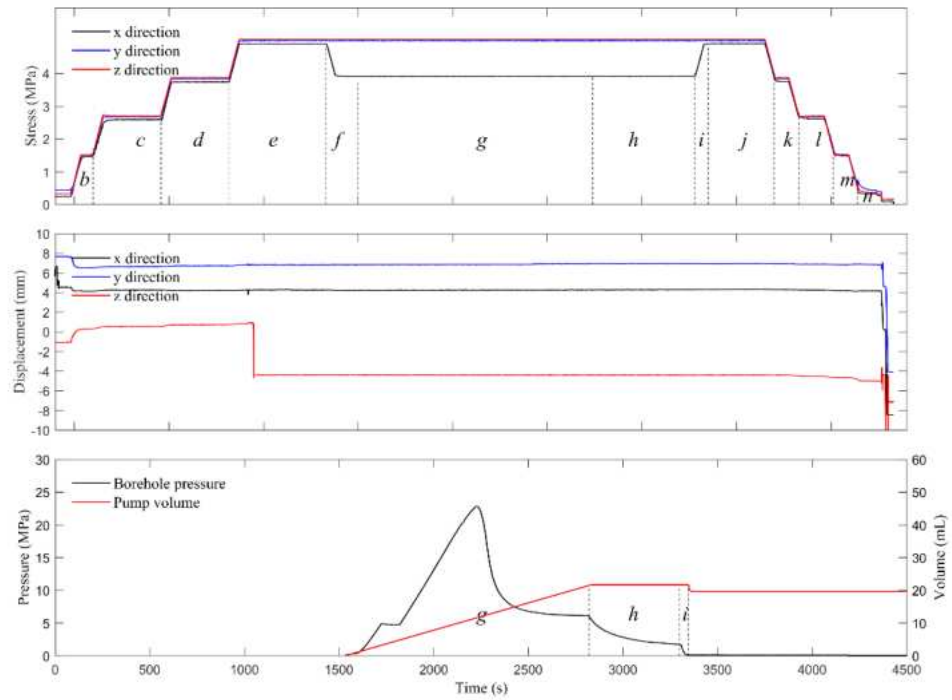


Figure 1.13 Stress, displacement, and borehole pressure and volume responses of rock block-2.

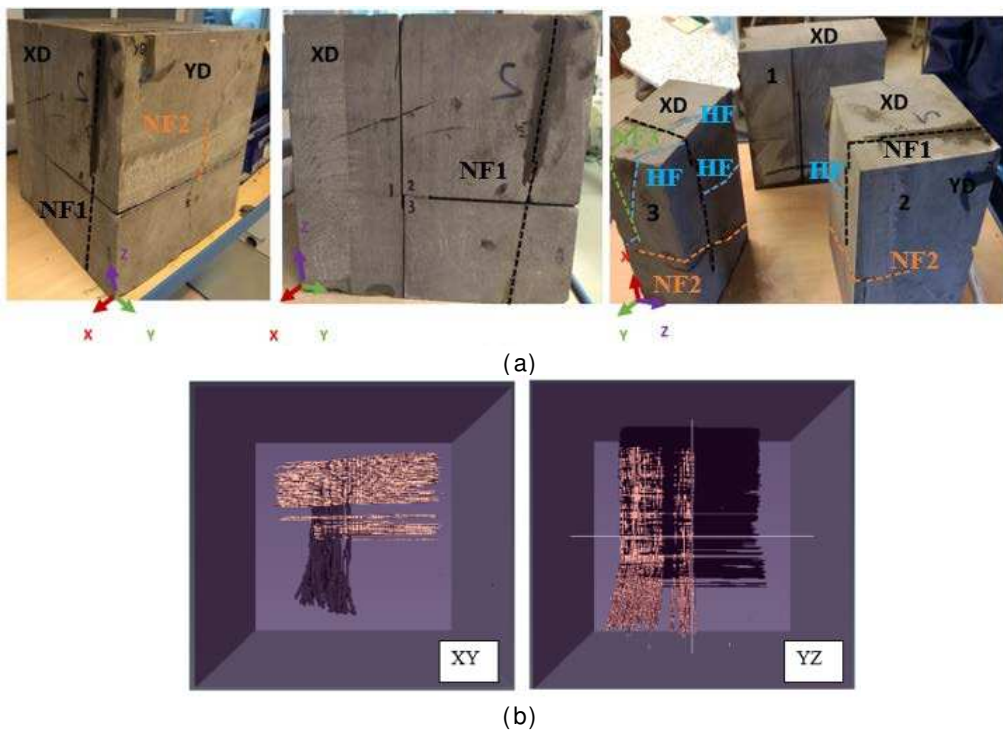


Figure 1.14 (a) Split rock block Sample-2, and (b) its CT scan results.

Figure 1.15 illustrates the influence of hydraulic fracturing on the S-wave velocity tomograms. Seismic velocity tomograms for both rock blocks 1 and 2 did not change significantly after hydraulic fracturing, and they represent the intrinsic properties and mostly the homogenous and intact nature of the rock blocks. Seismic velocity tomography results also confirmed the estimated HF propagations in both rock blocks based on the difference in the seismic wave velocities for the pre- and post-injection stages.

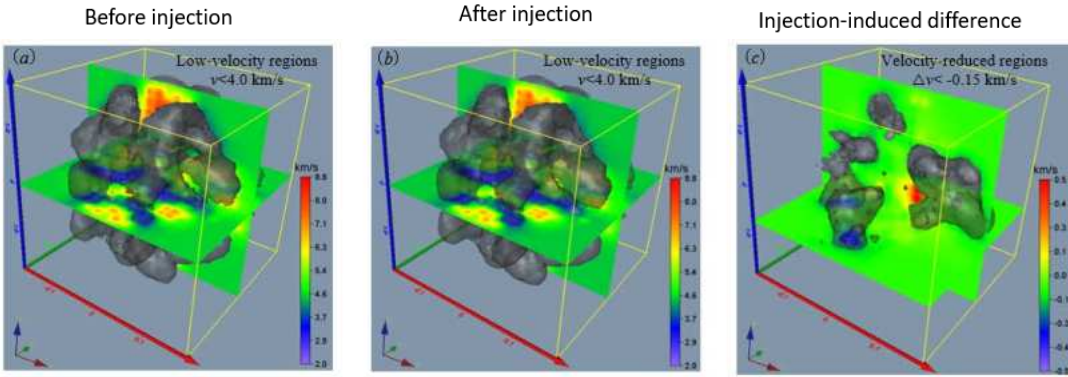


Figure 1.15 S-wave velocity tomograms for Rock block-2 before and after hydrofracturing and injection induced difference.

Conclusions

Results have shown that seismic waves propagating through naturally fractured coal experience multiple reflection and diffraction and become more scattered than that expected in intact rock. The spectrograms of S wave are suitable to reflect the fracture propagation. The analysis of CT images of coal block 2 further revealed the correlation between the fracture propagation, fracturing fluid flow and seismic signals. Analysis of the fluid injection data over the hydraulic fracturing process suggested that a comparatively higher fluid pressure was required for HF initiation in homogenous rock block-1 when compared with that for naturally fractured rock block-2. Visualisation of split post-fractured rock blocks and their corresponding computed tomography analyses provided further information on spatial and geometrical properties of NFs, HFs, and possible NF/HF networks created during fracturing.

Task 1.3 Assessment of in situ stress states and stresses induced around production areas in partner mines (led by IMPERIAL, GIG, CM-VELENJE, JSW, ALTEMIN)

Knowledge of the prevailing in situ stress state at the selected field sites was critical for the design of rock burst and gas outburst prevention methods using large diameter boreholes in WP2, the seismic monitoring layout in WP3 and the modelling of mine scale prevention methods in WP4. Therefore, the main objective of this task was to implement both empirical and numerical methods to define the state and magnitude of stresses around longwall top coal caving (LTCC) panels at CM-Velenje, and working longwall (LW) panels at JSW, and sublevel caving (SLC) coal faces at Spain which is not reported here.

Stress field affected by longwall top coal caving at Coal Mine Velenje

Over 100 years of coal extraction activities at CM-Velenje have created highly stressed “isolated” areas. Excessive stress concentration on coal blocks tend to trigger rock burst events. In order to numerically assess the current stress conditions, using the coal deposit and extraction history data, a three-dimensional geomechanical model was developed in FLAC^{3D}. The physical dimension of the model developed was 1,400×1,100×700m (length×width×height). Three different structures, including coal, clay, and failed clay representing the waste/goaf were used in the model domain.

In order to study the impact of previous mining history on current stress state, initially, all the grids representing extracted coal (waste/goaf) was assigned with the mechanical properties of coal. Initial stress equilibrium was established first to produce an *in situ* stress field. Then the grids representing extracted coal were gradually removed and replaced with the mechanical properties of waste/goaf material. Figure 1.16 presents the vertical stress distribution calculated at CM-Velenje at the start of the project and after considering all the previous coal extraction activities. A high stress concentration zone can be seen at the central coal block left by mining around the area. The average stress (19.8 MPa) on this coal block was more than two times higher than the *in-situ* stress (8.6 MPa).

Throughout the project, the mine has provided Imperial College with monthly updated coal extraction schedule at the microseismic monitoring panels (K.-80/B and K.-80/E) as shown in Figure 1.17a. The extraction period of these two panels span from October 2015 to October 2016. The coal extraction data at these two panels have been regularly updated following the actual mine schedule in the model developed to assess the impact of mining activities on the central coal block (Figure 1.17b).

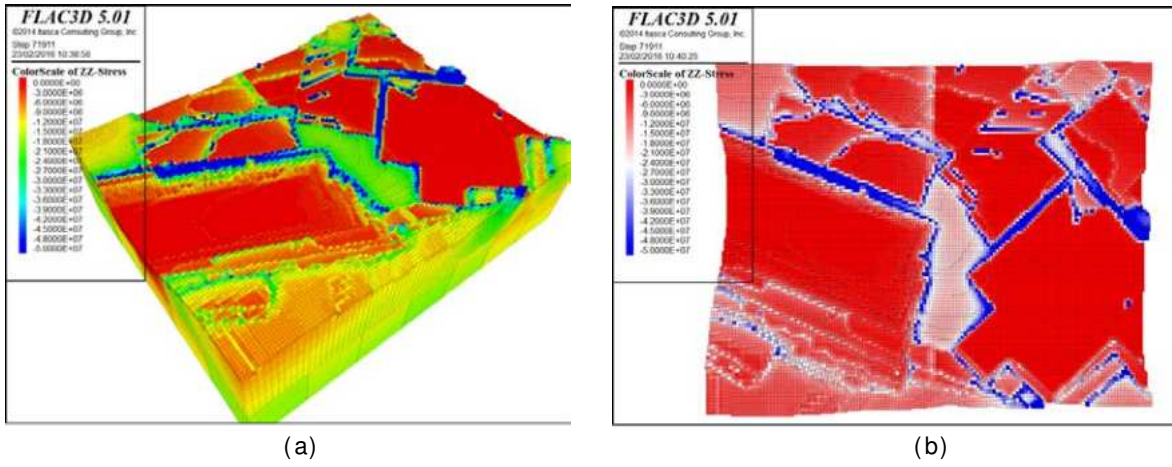


Figure 1.16 Stress field at CM-Velenje at the start of the project (a) 3D view, (b) plan view.

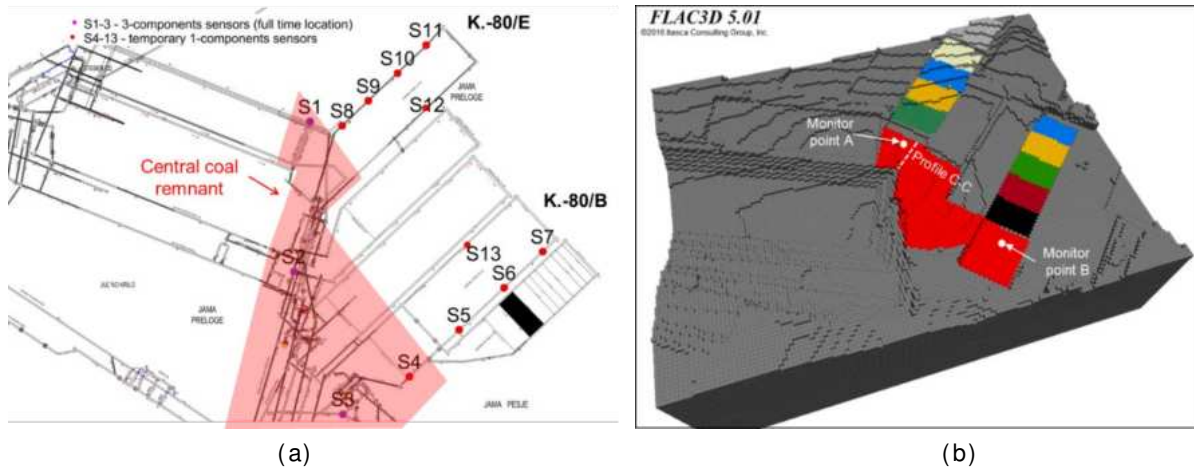


Figure 1.17 (a) Location of the microseismic monitoring stations, (b) numerical model for the K.-80/E and K.-80/B longwall panels at CM-Velenje.

Figure 1.18 presents the contour of stress changes induced by face advance at different time periods. As can be seen, compared with the extraction of K.-80/B panel, the mining of K.-80/E panel has a more significant impact on the stress state at the central coal block. The increment stress can be as high as 0.7 MPa after the extraction of K.-80/E.

Two monitoring points and one monitor profile/line (as marked in Figure 1.17b) have been set within the central coal block close to the active panels. Dynamic stress responses to the coal extraction at K.-80/E and K.-80/B longwall panels were recorded as shown in Figure 1.19.

Modelling results suggested that the extraction of K.-80/E longwall panel can produce a moderate stress increment at the 'upper corner' of the central coal block. This disturbance may induce active seismic events if rock mass is already in critical stress condition. By cross-checking microseismic monitoring results provided by GIG, it was confirmed that, during the completion of K.-80/E longwall panel at the end of June, microseismic events tended to concentrate in this upper corner. One strong seismic event, which had emitted energy over 10^7 J, has also been recorded during the week 30 May to 06 June 2016.

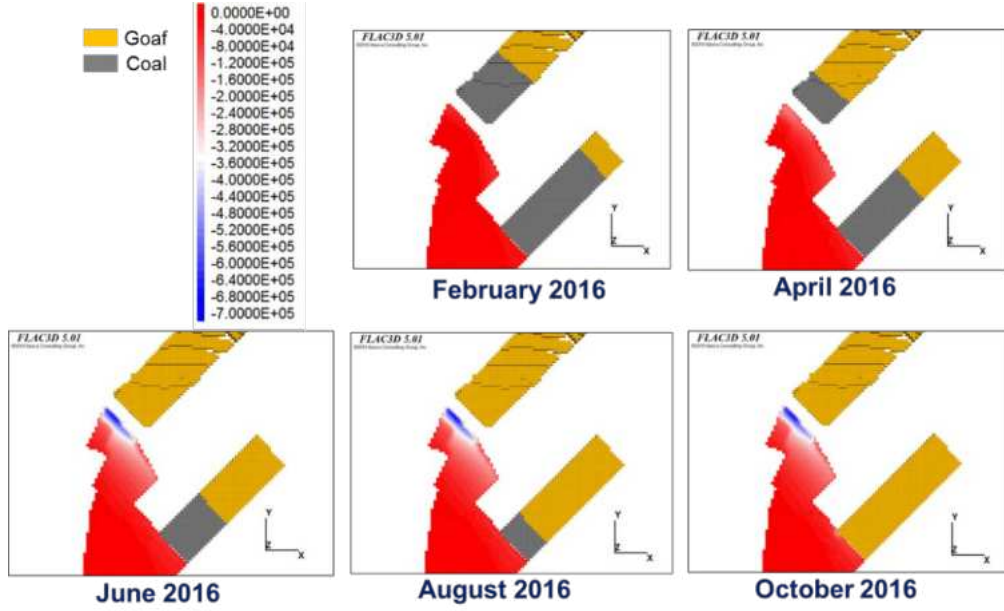


Figure 1.18 Production schedule at K.-80/E and K.-80/B longwall panels at CM-Velenje.

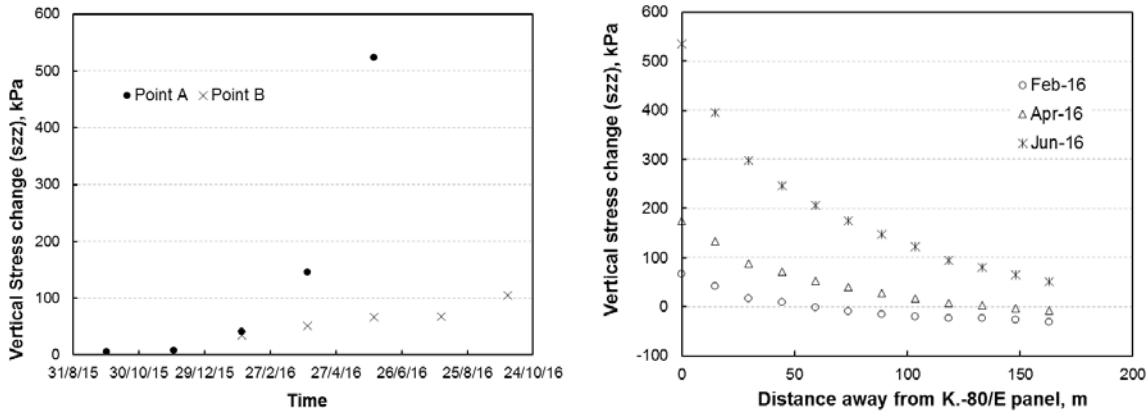


Figure 1.19 Stress changes induced by LTCC face advance (point monitors).

Stress field affected by longwall mining at Pniowek Colliery

Empirical-analytical method

To calculate vertical stress distribution in the plane of seam 404/1 at Coal mine "Pniowek", empirical-analytical method, elaborated in GIG (Kabiesz and Makówka 2009) have been used. The method has been used to calculate vertical component distribution, disturbed by edges of exploitation created in seams: 361, 363 and 404/1. Result of the calculation for Longwalls C-4 and C-5 are presented in Figure 1.20a and b.

Numerical Method

At Imperial, a three dimensional field scale geomechanical model comprising of coal seam 404/1 and 404/2 was constructed using FLAC^{3D} to assess the initial stress field at Pniowek Colliery field site and further assess mining-induced stress changes around the mine openings and surrounding strata at each stage of mine development. The model had the dimensions of 1,500m × 1,500m × 90m in x, y and z directions, respectively. As shown in Figure 1.21, four panels in the coal seam 404/1 and one in the coal seam 404/2 were simulated.

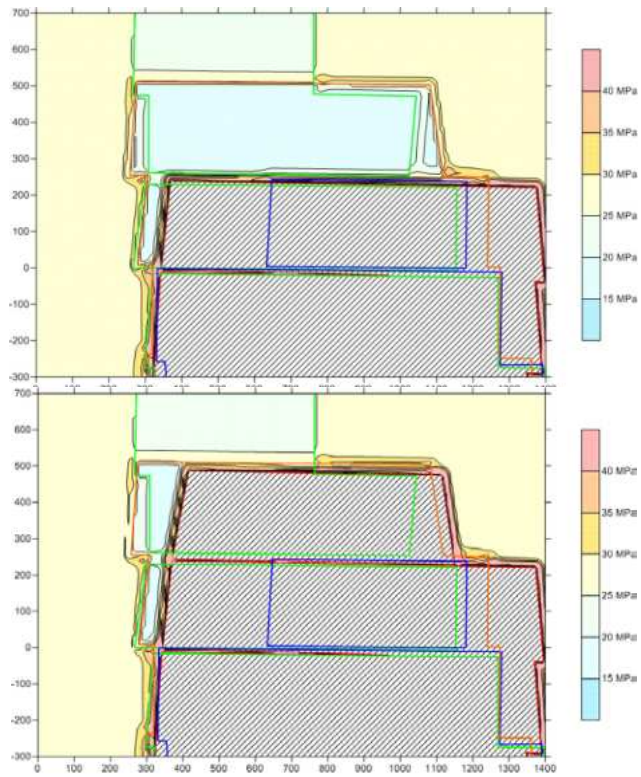


Figure 1.20 Stress state in (a) part C, seam 404/1 – end of longwall C-4 and (b) end of longwall C-5.

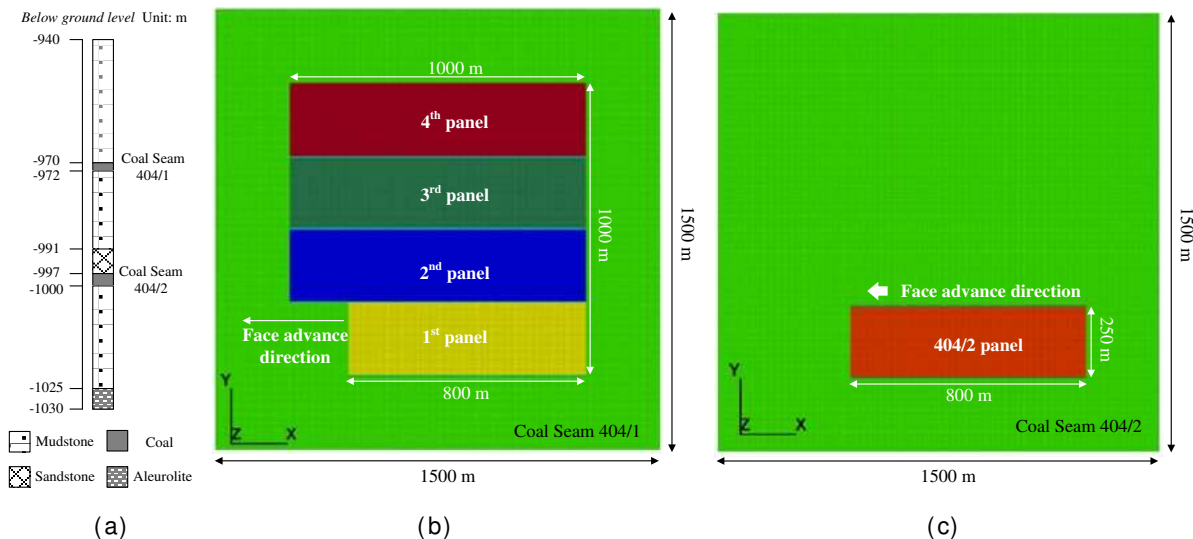


Figure 1.21 (a) General stratigraphy of the 401/1 and 404/2 panels, and model geometry for (b) coal seam 404/1, and (c) coal seam 404/2.

In order to establish the initial stress conditions to account for the effects of previous mining activities in the model, four 5 m-wide roadways were first extracted. After an equilibrium state was achieved, coal extraction at 1st, 2nd, and 3rd longwall panels was conducted sequentially in coal seam 404/1. For each longwall panel, coal was extracted from right to left in excavation steps (Figure 1.21). The advance distance for each excavation step was 20m (~ a week's production). Stress variations in response to each stage of longwall extraction around the 4th panel in seam 404/1 and the seam 404/2 panel were investigated.

Figure 1.22 shows vertical stress contours for the coal seam 404/2 as affected by longwall coal extraction in the coal seam 404/1 at 25m above. It can be observed that the stress relief zone is located under extracted longwall panels and roadways, and the stress concentration zone beneath surrounding strata of mine openings.

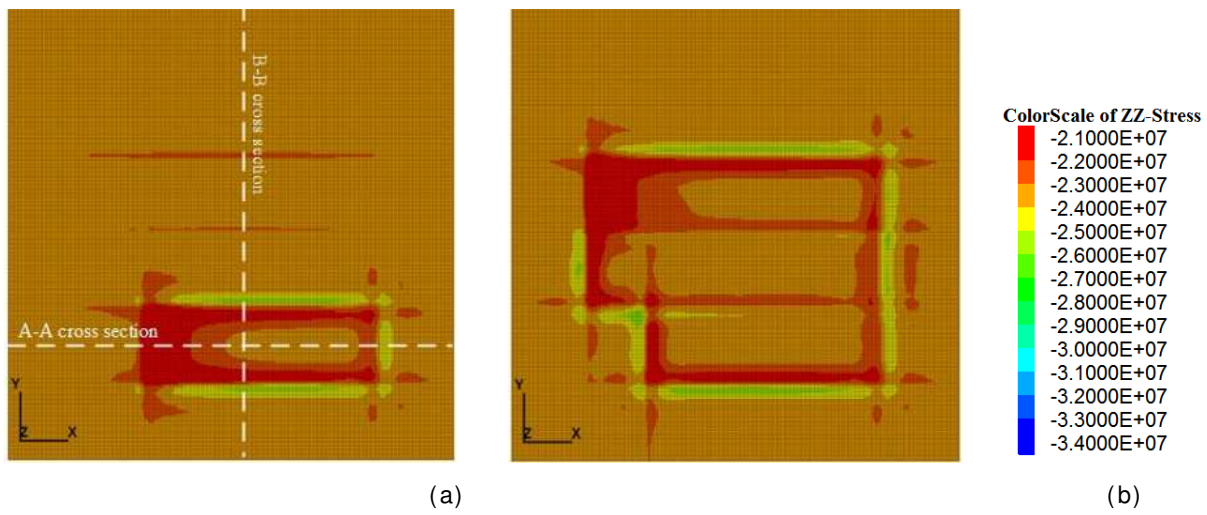


Figure 1.22 Mining-induced vertical stress variations around longwall panels in the coal seam 404/2: (a) 1st panel extraction, (b) 3rd panel extraction.

Figure 1.23 presents the vertical stress profiles along two cross sections taken from Figure 1.22. It can be observed from Figure 1.23a that a zone of stress relaxation is located right beneath the extracted area. Figure 1.23b shows the induced vertical stress variations of the coal seam 404/2 during extraction of the upper coal seam. Vertical stress relaxes at where extraction in the upper coal seam takes place and concentrates at areas beneath the periphery of extracted areas. However, with a stress change less than 3.5MPa from the in situ stress, both stress concentration and relaxation were not as apparent as those in the coal seam 404/1 where mining took place.

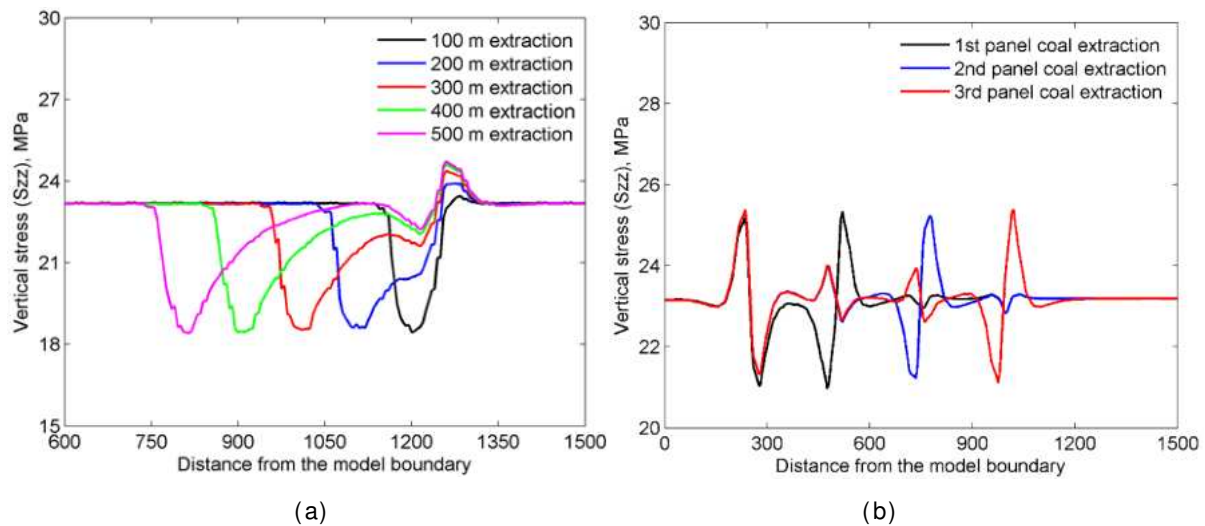


Figure 1.23 Vertical stress profiles for the coal seam 404/2 after the 1st panel extraction: (a) A-A cross section, and (b) B-B cross section.

WORK PACKAGE 2 - DEVELOPMENT AND FIELD TESTING OF TECHNOLOGIES FOR THE PREVENTION OF ROCK BURSTS AND GAS OUTBURSTS

Task 2.1 Field experiments, monitoring and interpretation of the use of large diameter boreholes and blasting for stress relief to prevent rock bursts (led by CM-VELENJE, GIG, IMPERIAL, JSW)

This task aimed at developing and implementing large diameter stress relief boreholes and blast hole drilling to prevent rock bursts at Cole Mine Velenje. Extensive research into zones of increased rock burst activity at the mine was undertaken by analysing the results of mines own seismic monitoring system, the MapROC microseismic monitoring activities and the interpretation of daily mining reports. As an approach to increase both passive and further active rock burst prevention, CMV defined an area where density of seismic events has been relatively higher, compared to other areas of the mine.

Mining reports and analysis have shown major areas of increased stress accumulations and consequent seismic events at around gateroad development or support removal by gateroad closure in the vicinity of barrier pillars which remained unmined after longwall faces were mined out. As shown on Figure 2.1, a kidney-shaped area was defined after monthly revisions of seismic events, mining reports and observations of gateroad support deformations. According to longwall faces advances, this area is continuously revised and its borders are subject to further modification.

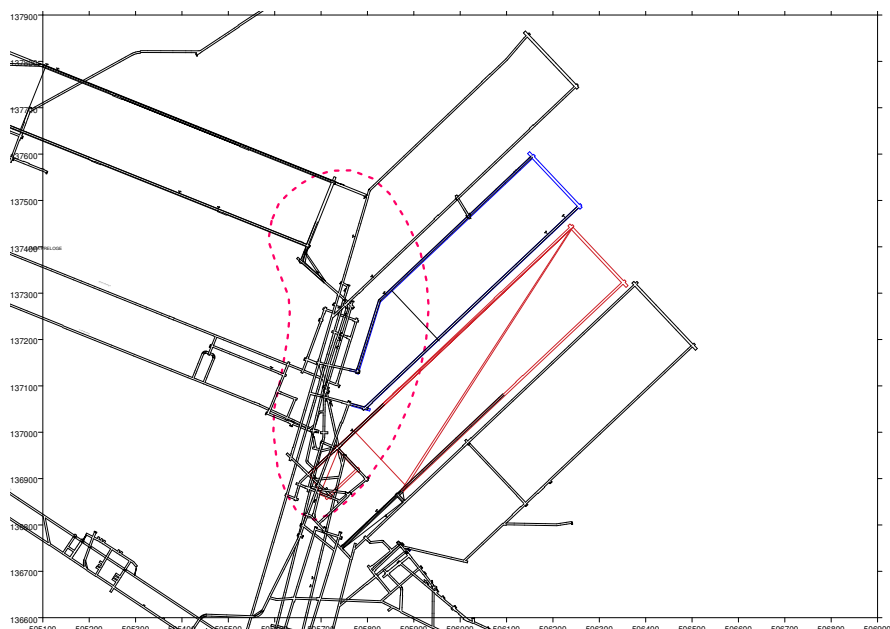


Figure 2.1 CM Velenje mine outline, active and developing longwall faces in 2016. The kidney shaped dashed line marks the area with increased rock burst probability, which was defined after recordings of increased number of seismic events in the region.

Therefore, the planning and design of large diameter stress relief boreholes was introduced as a prevention approach which included guidelines, developed from review of data and experience from rock-seam gas pressure measurements in area in front of longwall face line. Throughout the project each barrier pillar of a new development face (or a group of them affected by development) was selected and a battery of large diameter stress relief boreholes drilled. Gateroad development work was accompanied by stress relief blasting.

Towards the end of the project, the designs and analysis of the results obtained resulted in these procedures becoming part of the mines safety statutes as approved by the National Mines Inspectorate.

Implementation of large diameter stress relief boreholes at Coal Mine Velenje

In the early period of the project in 2016, four zones (L1, L2, L3, L4) were selected for testing large diameter stress relief borehole behaviour. These zones were also equipped with seam gas pressure and composition monitoring boreholes and stress monitoring boreholes in order to help evaluate the performance of these large diameter boreholes. These zones are shown on mine outline in Figure 2.2. A detailed layout of each of these zones are also given in Figure 2.3 and Figure 0.4.

The large diameter stress relief boreholes in zone L1 of Longwall panel D k. -80 were all drilled at 160mm diameter, 50m long and drilled at +5° inclination (Figure 2.3a).

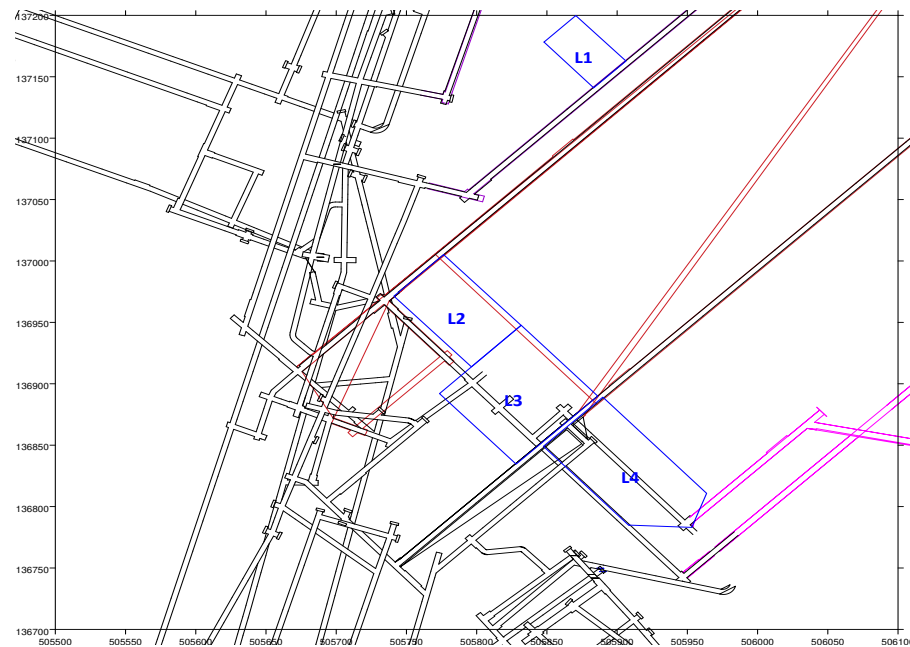


Figure 2.2 CM Velenje detailed mine outline with marked zones for pilot tests of large diameter stress relief boreholes.

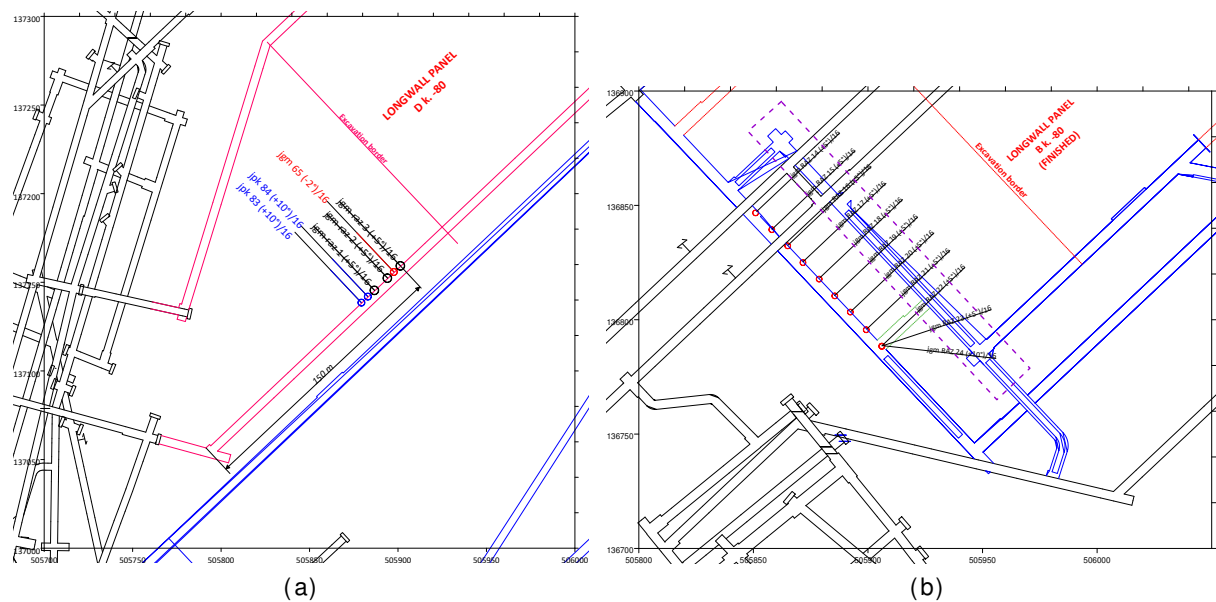


Figure 2.3 (a) Longwall panel D k. -80 with positions of stress relief boreholes, seam gas pressure and composition monitoring boreholes and stress monitoring borehole in Zone L1, (b) Longwall panel A k. -95 development (gateroads in blue), face end line for longwall panel B k.-80, and the locations of stress relief boreholes in Zone L4.

Based on the results obtained from drilling at zone L1 at longwall panel D k. -80, two new zones (L2, L3, Figure 0.4a and b) were chosen, partly in the area of increased rock burst activity (L2). The decision for selecting L3 zone was an attempt to establish a stress relief zone for the total width of longwall panel C k. -80. The longwall face started production in mid-January 2017 but boreholes had to be drilled in advance of mining. Drilling plans in zone L2 included five 160mm diameter stress relief boreholes at a length of 70m and at +5° inclination. Seam gas pressure measurements were designed as an indirect indicator of rock pressure behaviour. Drilling designs in zone L3 were made after promising results in zone L2. Eight large diameter stress relief boreholes at lengths of up to 70m were drilled in order to cover the full width of the barrier pillar in longwall panel C k. -80.

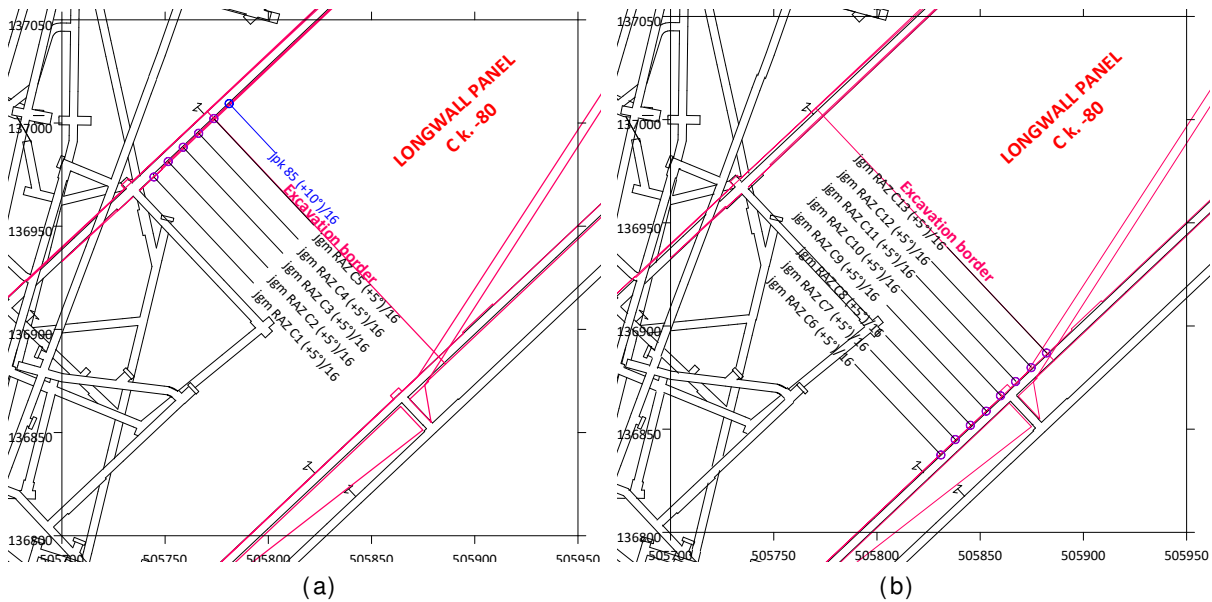


Figure 0.4 (a) Longwall panel C k. -80 with locations of large diameter stress relief boreholes and seam gas pressure monitoring borehole in the intake air gateroad in Zone L2, (b) Longwall panel C k. -80 with locations of stress relief boreholes in the return gate in Zone L3.

Following on the results from drilling in zones L2 and L3 at longwall panel C k. -80, zone L4 (Figure 2.3b) within the barrier pillar of longwall face B k. -80 was selected as the site for large diameter boreholes. Furthermore, this was also identified as an area where the development of a new gateroad for longwall face A k. -95 was planned, and the measures aimed at protecting the development. The boreholes were all drilled at 160mm diameter, 50m length and mostly at +5° inclination.

Post analysis of seismic events over a 2-months period when longwall face B k. -80 was advancing in the vicinity of zones L2 and L3 have shown that the density of recorded seismic events at locations L2 and L3 was relatively low compared to surrounding areas without drilled stress relief boreholes, providing encouragement and further incentive to continue implementing such measures during the rest of the project period.

In parallel with large diameter stress relief boreholes, borehole jpk 85 (+10°)/16 was drilled to monitor seam gas pressure behaviour in the area. As Figure 2.5 indicates, gas pressure in the borehole has shown steady increase as the longwall face approached the monitoring zone, and started declining when the face was around 100 m from the borehole, and then dropped significantly in the stress relief borehole zone confirming the positive effects of the actions taken.

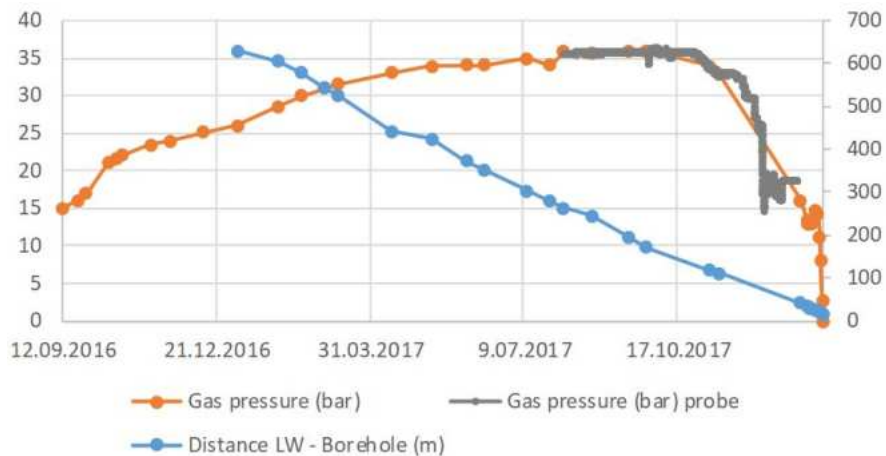


Figure 2.5 Seam gas pressure monitoring at borehole jpk 85 (+10°)/16 (Longwall face C k. -80).

During 2017, Coal Mine Velenje continued drilling long large diameter stress relief boreholes and daily stress relief blasting in developments, and during gateroad support maintenance and longwall

salvaging activities. Figure 2.6 presents the mine outline with generalised locations of activities carried out during 2017. Two new locations Zone L5 and L6 were selected for drilling large diameter stress relief boreholes in areas expected to be affected by two longwall panels E k. -95 and CD3g, which are about to sequentially finish or start production respectively (Figure 2.7).

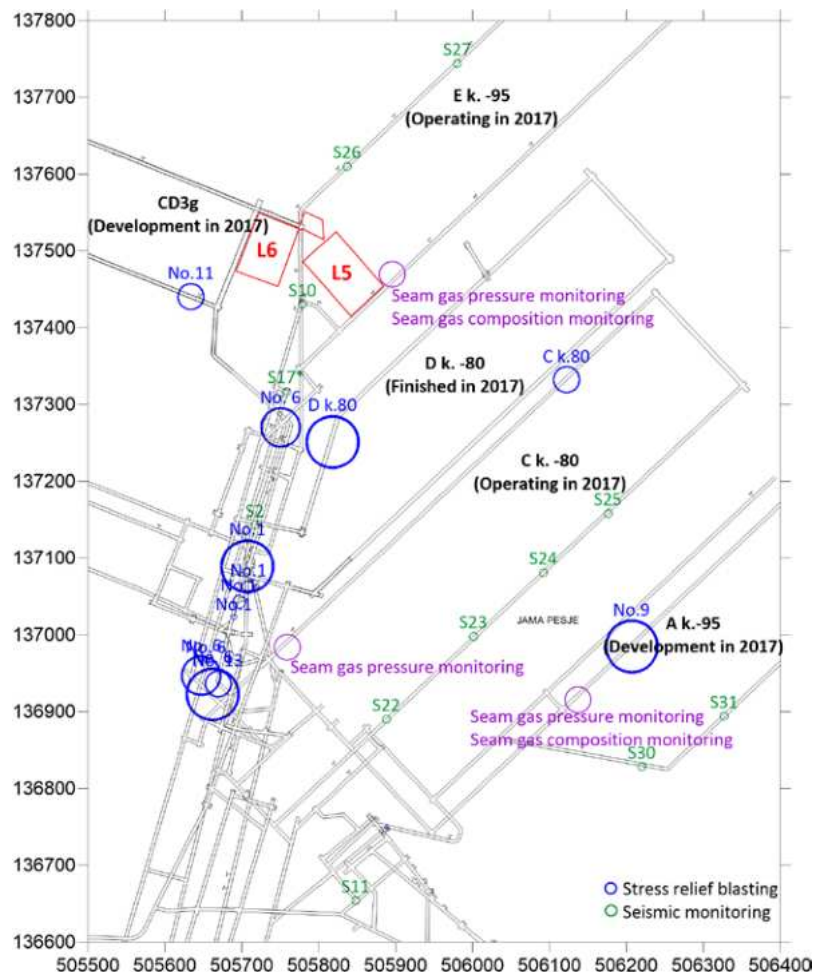


Figure 2.6 Mine outline showing the generalised MapROC activities at Coal Mine Velenje in 2017.

Initially, the large diameter stress relief borehole distribution in E k. -95 was prepared to cover the complete barrier pillar after the completion of production at longwall panel E k. -95. In the case of Zone L6 (Figure 2.7), the focus was not only on large diameter stress relief boreholes as production plans and gateroad developments have indicated possible localised stress concentration. Additional measures were undertaken via low charge daily blasting during gateroad development. In this region, two sets of large diameter stress relief boreholes were drilled, each in the barrier pillars of CD3g and E k. -95 (Figure 2.7). The drilling data have shown significant reduction of boreholes' lengths compared to the planned lengths (down to 40-60m from 80m as planned), however, the results were rather satisfying. Seam gas pressure and composition were also monitored in the area. Further analysis of longwall developments during 2018 and 2019 has shown that the development of gateroads for longwall panel E k. -110 required relatively less stress relief measures (daily blasting, drilling) and the supports installed have not required any maintenance or repairs as a result of these boreholes drilled in Zones L5 and L6 a level above the new developments.

Besides the new areas developed as Zones L5 and L6 in 2017, the performance of large diameter stress relief boreholes in Zones L1, L2, L3 and L4 drilled in 2016 were also continued to be monitored in 2017.

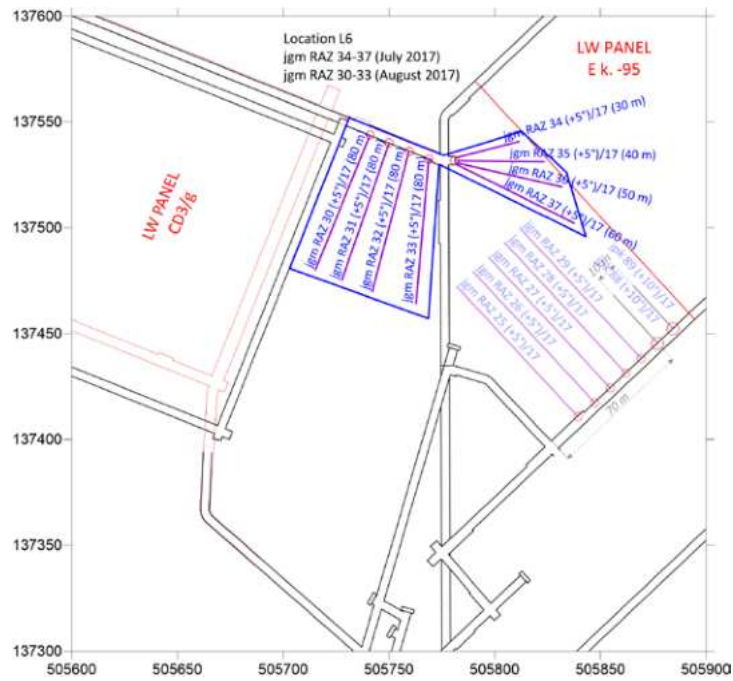


Figure 2.7 Large diameter stress relief boreholes in barrier pillar of LTCC panels CD3g and E k. -95.

Figure 2.8 presents the mine layout during 2018 with the locations of Task 2.1 activities at Coal Mine Velenje. Two new areas where stress relief boreholes are required were identified as the developments for longwall panels Dk. -95 and Ck. -95. At both locations, other research activities besides the large diameter boreholes were also carried out, such as the slotting experiments in Task 2.3 and the Measurement While Drilling (MWD) experiments in Task 2.4. A set of 80m long, 160mm diameter boreholes were drilled at the barrier pillar of Longwall Dk. -95 and monitored together with the slotted boreholes in the area (Figure 2.9).

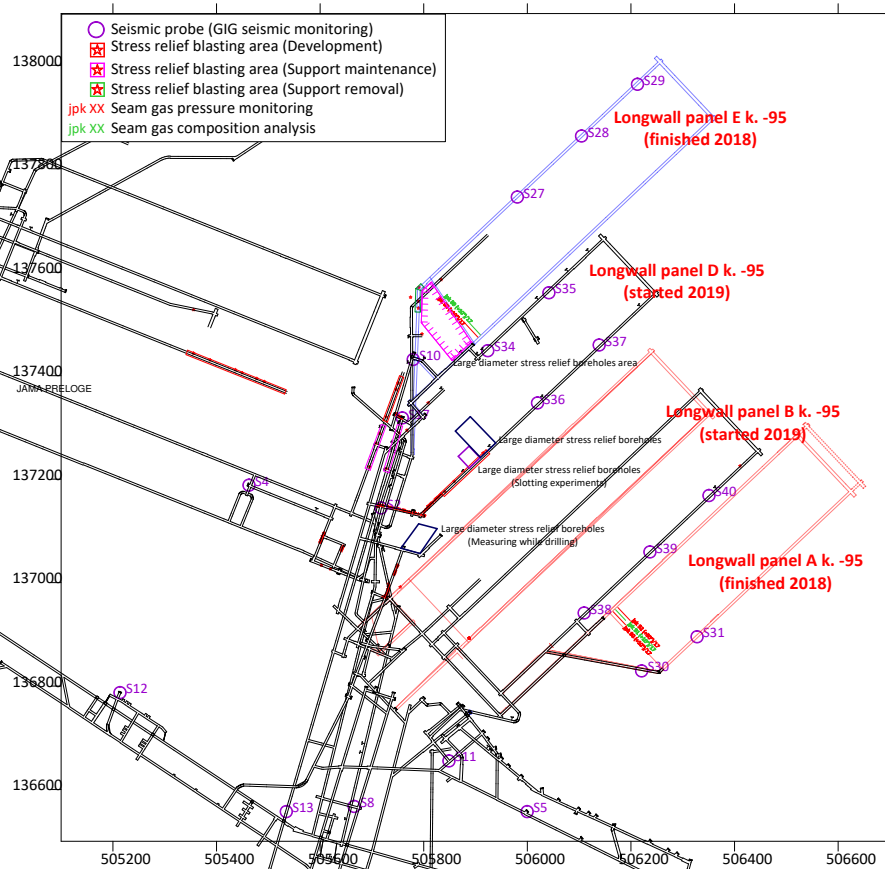


Figure 2.8 Locations of MapROC activities at Coal Mine Velenje in 2018.

Large diameter stress relief drilling at development headings

Based on the success of large diameter stress relief boreholes drilled at barrier pillars, these have also been tested systematically at development headings after the first half of 2018 (Figure 2.10). They were used in many sections after intensity of seismic events increased and coal outbursts or gateroad support damage were observed. As development headings are usually limited in space, the drilling diameters were reduced to 110 mm due to the use of smaller and less powerful drilling rigs. Until MapROC, the National mining regulations in Slovenia lacked guidelines for rock burst prevention measures. These procedures have been since included in a technical documentation which has been submitted to the National mining authorities.

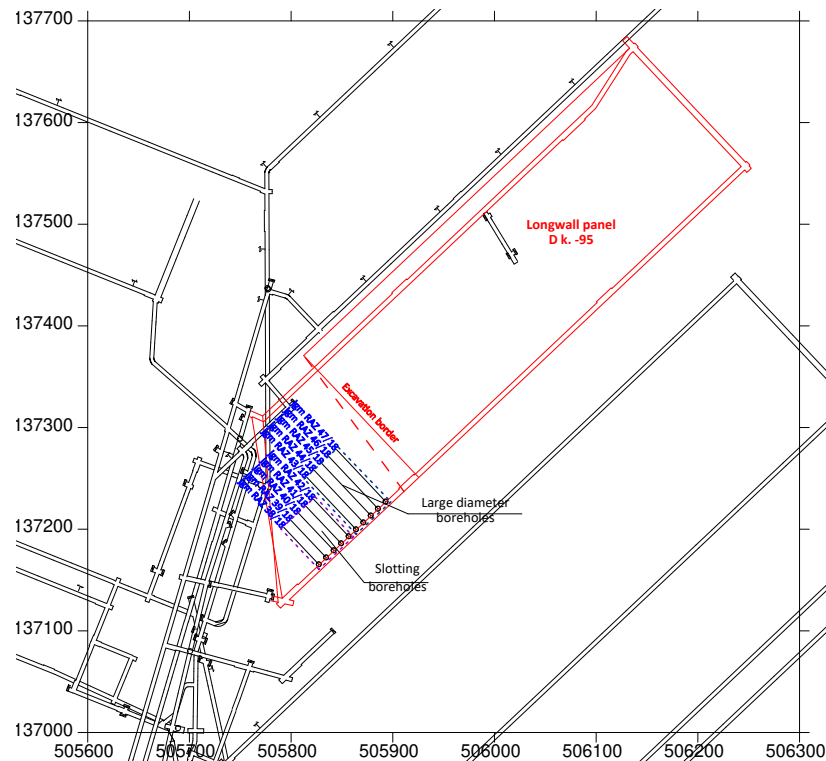


Figure 2.9 Stress relief boreholes in longwall panel D k. -95 (Boreholes jgm RAZ 38 – 42 were drilled for slotting experiments).

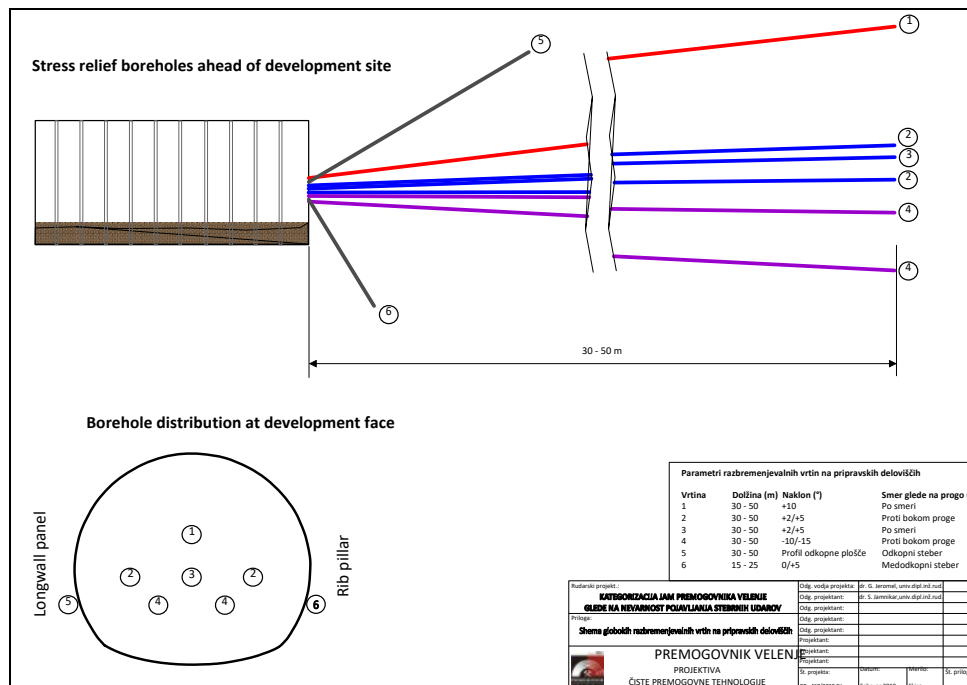


Figure 2.10 Large diameter boreholes in development headings.

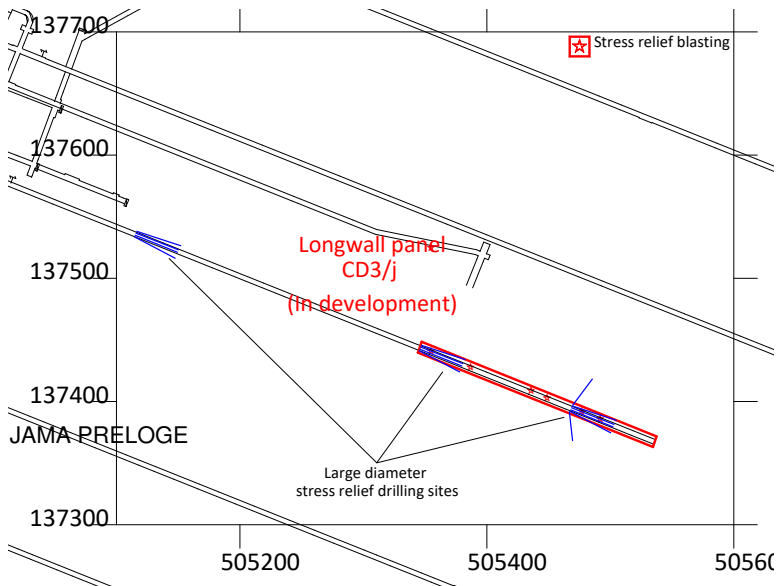


Figure 2.11 Sites of large diameter borehole drilling during the development of the heading for the CD3/j longwall panel. Stress relief drilling was supported by daily blasting along the larger sections.

Figure 2.10 presents Coal Mine Velenje's systematic procedure which is implemented at all development sites against increased rock burst hazards developed as a result of the experience gained in the MapROC project. As shown in Figure 2.11 these measures were introduced during the development of the heading for the CD3/j longwall panel. Usually 3 – 5 boreholes were drilled in the direction of gateroad with low inclinations to the sides of the planned gateroad route.

Implementation of stress relief blasting as a risk mitigation measure at Coal Mine Velenje

During 2016, 33 sites were used for stress relief blasting in multiple blasting boreholes at development headings and during support salvage for gateroad abandonment. Each borehole had four kilograms of permissible explosive charge. Usually, blasting was carried out in multiple boreholes (5 to 12) in order to cover a large area for stress relief effect (Figure 2.12).

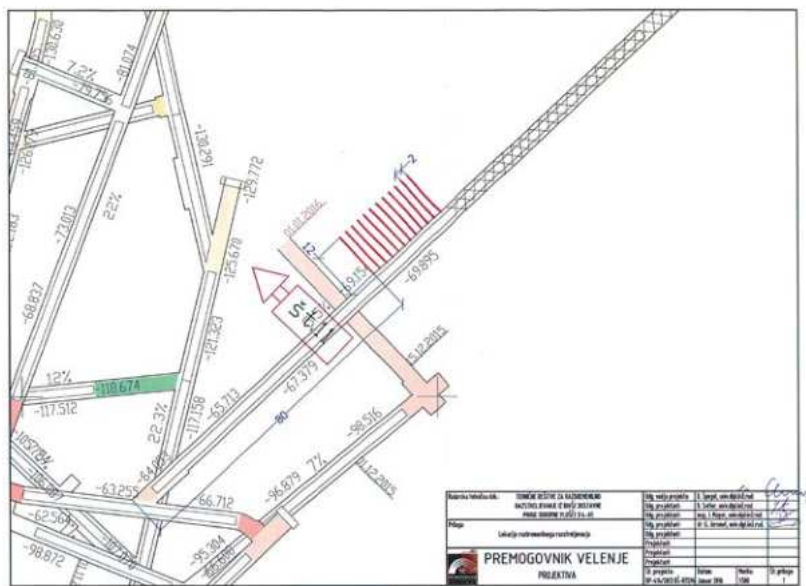


Figure 2.12 Example schematic for blasting location and blasting boreholes positions.

During 2017, Coal Mine Velenje introduced a new system of stress relief blasting as part of daily mining activities, therefore, every development team undertook blasting responsibility when the crew identified increased seismic activity. Figure 2.13 shows the locations and periods of stress relief blasting in given work zones for the purpose of stress relief or to reduce the density and effect of seismic events. Blasthole lengths were generally reduced to 8 meters (overall 5 – 12 m) but preferably used a pair of blastholes. Relatively low charges were prescribed for daily blasts as blasting

was repeated daily for a longer period of time by following the activity location. In total, 13 work sites implemented preventive blasting measures in 2017.

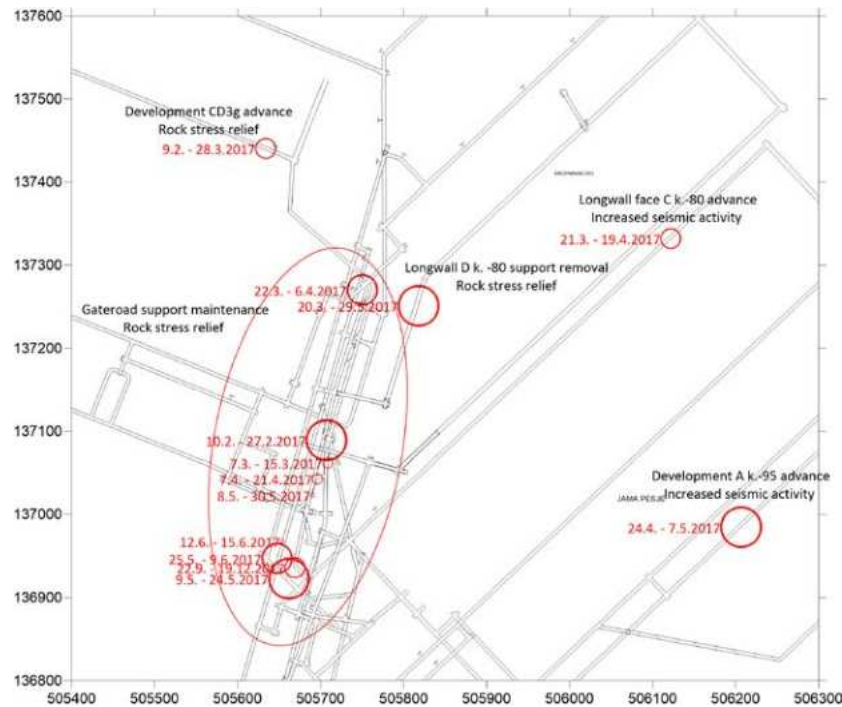


Figure 2.13 Locations and periods of daily stress relief blasting.

In 2018, development and other gateroad heading activities in CM Velenje used daily blasting as a common safety measure. The blasting scheme used up to 6 shot-holes into the face of the development heading with a maximum charge of 3 kg per borehole. In most cases, daily blasting was carried out in 2 shot-holes with a total of up to 6 kg charge. In total, there were 299 blasting campaigns in 2018 which included development headings, gateroad support maintenance sites and gateroad support removal sites. All blasting actions were recorded in a central database.

In conclusion, daily stress relief blasting achieved relatively high level of protection against rock bursts or severe seismic events. The flexibility of the technique allows prompt implementation by different mining crews (certified miner and a supervisor).

Implementation of gas pressure relief blasting as preventive approach at Pniowek Colliery

Under Task 2.1 GIG and JSW performed underground gas pressure relief blasting experiments in development headings at two coal seams, namely Seam 404/1 located in Zone C and Seam 404/2 in Zone N at JSW Pniówek Colliery during 2015, 2016 and 2017.

During 2016, 14 gas pressure relief blasts in coal seam 404/2 were conducted. They were performed in Zone N after methane desorption ratio in coal exceeded 1.2 kPa and its conciseness below 0.5 in Protodiakonov scale. Sixty minutes after the degasifying and gas pressure blast a test borehole was drilled in the coal face and the coal fine samples were collected from depths of 2, 4, 6 and 8 meters. For the coal samples collected from the boreholes methane content was determined in the laboratory. The results obtained were used to calculate degasification ratio of the coal ahead in the coal face being developed.

Gas monitoring at coal seam 404/2 during the development of N4, N5 and N6 inclines have shown variable levels of methane emission, and rock burst and gas outburst potential. After completing the development of the inclines in roadways N-6 and N-5, it was necessary to drive the N-4 incline from the roadway N-5 to create Y-ventilation. During the development of incline N-4 tectonic disturbances (faults) were encountered, which potentially could create gas outburst and rock burst hazards. During the development of incline N-4 in the coal seam 404/2 13 gas pressure blasts were implemented to decrease gas outburst potential when crossing the faults identified as potential risk zones. The increase in recorded methane concentrations after blasting was used to determine additional methane which was released into the workings after gas pressure relief blasts (Figure 2.14). Gas pressure relief blasts implemented in N-4 incline while crossing the fault zone allowed to decrease methane content in the coal ahead of face and mitigated against gas outburst and rock burst hazards.

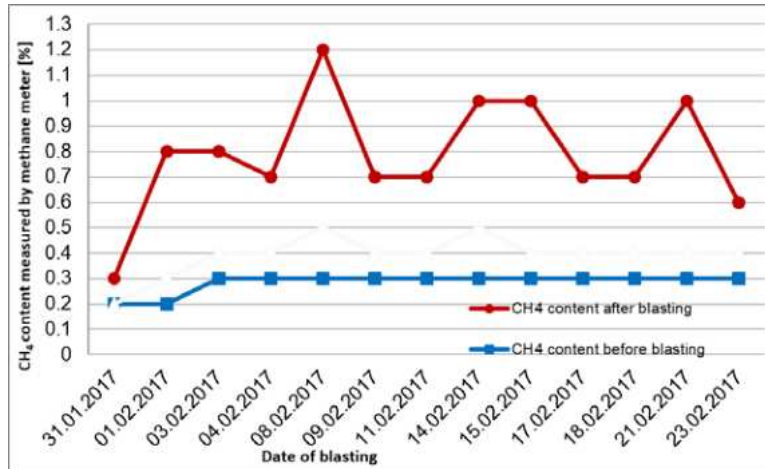


Figure 2.14 Methane emission into the workings 120 minutes after blasting operations in the incline N-4 in coal seam 404/2.

As a result of the observations carried out at the Pniówek Colliery in the early part of the project, and due to lack of microseismic activity experienced during this period, a decision was taken to move the experimental sites to JSW S.A. Budryk Colliery.

Task 2.2 Field experiments, monitoring and interpretation of the use of water injection for gas pressure relief to prevent gas outbursts (led by GIG, AITEMIN, CM-VELENJE, JSW, IMPERIAL)

Due to declining seismic activity in Seam 404/1 at Pniówek Colliery, work in this task was transferred to JSW S.A. Budryk Colliery. Two high pressure water injection tests were performed while roadway B-12 in seam 401 was being developed and the effect of water injection on gas release efficiency from the seam was analysed. The average methane emission rate at previously mined longwall panel B-10 during its production life was determined as $110 \text{ m}^3 \text{ CH}_4/\text{min}$, with the maximum recorded value being $134 \text{ m}^3 \text{ CH}_4/\text{min}$. Therefore, longwall panel B-10 in Seam 401 was classified as one of the gassiest longwall panels exploited in Polish hard coal mines.

The water injection experiments were conducted in development heading B-12 on September 3rd, 2017 and on October 8th, 2017 using the high pressure pump T-100 with a minimum operating pressure of 100 bars. The main difference between above two water injection experiments was the length of boreholes used. In the first test the length of the injection borehole was 30 m and, in case of second-experiment, it was 15 metres.

The water injection tests using borehole #2 with a diameter $\varnothing 85 \text{ mm}$ into the coal bed of 401 coal seam, conducted on September 3rd, 2017 and on October 8th, 2017, were preceded by coal sampling from the borehole #1 with a diameter $\varnothing 42 \text{ mm}$, drilled at distance of about 1.5 m from the borehole #2 (Figure 2.15) in the coal seam in order to determine its methane content. After injecting the water into borehole #2, another borehole #3, with a diameter of $\varnothing 42 \text{ mm}$ was drilled as shown in the figure. This borehole was also used to collect coal samples to determine 401coal seam methane content.

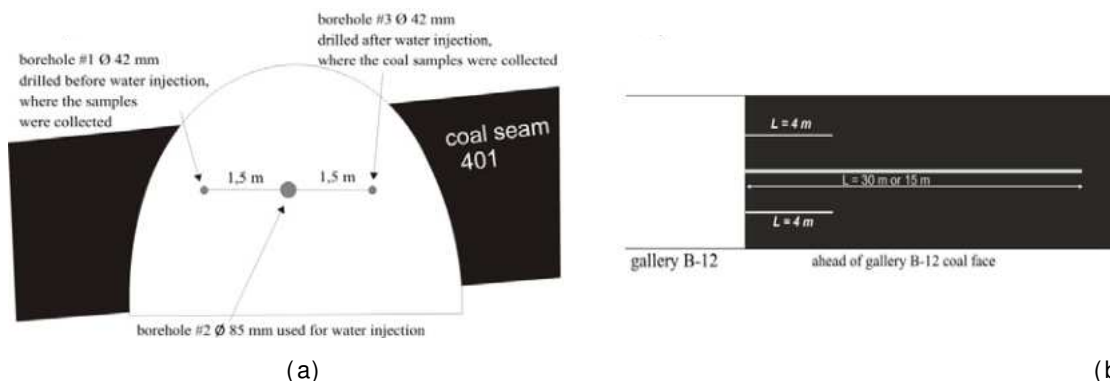


Figure 2.15 Plan and section views of roadway B-12 coal face in Seam 401 and the drilling layout for water injection tests.

An automatic methane detector was installed in Roadway B-12 50 meters from the coal face and data recorded at the control centre on the surface. In addition, air samples were taken at 30 m distance from the face of the roadway before, during and after water injection and analysed by chromatography. The increase of methane concentration during the water injection test into boreholes varied between 0.1 to 0.2%. Total volume of additional methane released in into the roadway B-12 as a result of water injection in 209 minutes was calculated as 52.25 m³.

The methane content of seam 401 before and after water injection at 30 m depth on September 3rd, 2017 was determined from coal samples taken from boreholes #1 and #3 shown in Figure 2.15. It was found that water injection in the seam reduced the gas content by around 20% at 4 m depth. The following conclusions were drawn:

- Water injection into the coal bed resulted in increased methane release from the coal face and decreased, at the same time, the methane content of the coal ahead of working face,
- The gas content of coal at 4 metres depth was reduced by about 20%,
- The methane volume released during the injection period (i.e. within 209 minutes) was 52.5 m³ CH₄,
- Water injection into a borehole at a depth of 30 m did not reduce the gas content of coal seam at greater depths.

On October 8th, 2017 the second water injection test was performed. This time, the water injection borehole was 15 m long. The results have shown that water injection was more effective in reducing gas content at closer distances to the face, which should guide the design of this practice in coal mines. Therefore, the water injection boreholes should not be drilled too deep.

When compared to gas pressure relief blasting described earlier under Task 2.1, it was found that water injection method was not as effective in reducing gas outburst risks. It has been concluded by GIG that this technique has marginal, if any, success in controlling/reducing gas release from the development headings prior to advancing the headings. Therefore, no further work was carried out in 2018.

Task 2.3 Field experiments, monitoring and interpretation of the use of mechanical and/or high pressure slot cutting and hydrofracturing for stress and gas pressure relief to prevent rock bursts and gas outbursts (led by GIG, CM-VELENJE, JSW, IMPERIAL)

The main objective of the use of hydro slotting in Coal Mine Velenje was to test its efficiency in stress relieving and avoiding potential rock bursts or gas outbursts. Initially, the experiments were scheduled to be carried out during April/May 2018. However, CM-Velenje experienced two rock burst events in March and April 2018, which affected roadway development and delayed the slotting trials until October 2018, as the development heading of Dk-95 LTCC panel, where the slotting experiments were planned to be carried out, was damaged and needed to be repaired. The work was completed in October 2018 and the data analysed, Deliverable D2.3 Report completed submitted.

The slotting experiments performed at Coal Mine Velenje were based on the equipment designed and tested during the GasDrain project. The hydro-slotting system developed by the GasDrain project was described earlier in the Mid Term Report and a detailed description of its use at the Zofiowka Colliery of JSW was presented in detail in GasDrain and also in Deliverable D2.3. Here a summary of its implementation at Coal Mine Velenje is presented.

Figure 2.16 shows the area of large diameter borehole hydro-slotting trials as designed after discussions between Coal Mine Velenje and GIG. Five large diameter stress relief boreholes were planned and drilled in preparation for the slotting experiments to be carried out in development heading No. 13 for longwall panel Dk. -95. Actual drilling performance differed slightly from the plan during the preparation of boreholes for slotting experiments. Drilling performance was monitored by manual recordings of parameters and therefore they represent information on coal properties in the area.

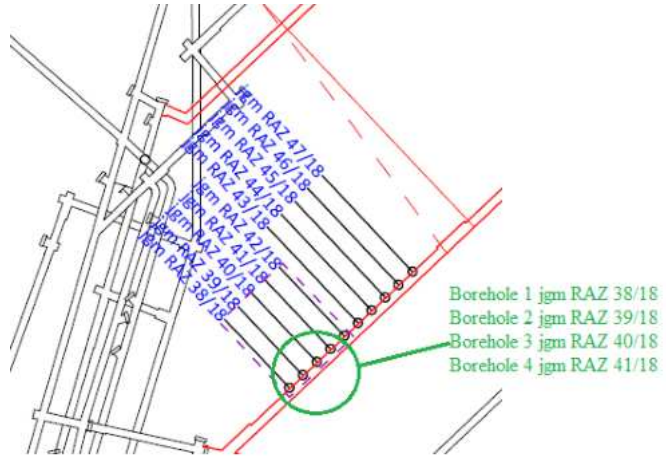


Figure 2.16 Exact location of the 4 boreholes.

According to the designs, the 4 shorter (50m) boreholes illustrated in Figure 2.16 were drilled and slotted first. In the second stage, the next four boreholes (80m) drilled and slotted. As described in detail in the D2.3 report, the dimensions of the boreholes within which the slots were cut, the slotting process, and the observations made during slotting were recorded, accompanied with the relevant schematic of the borehole - see Figure 2.17.

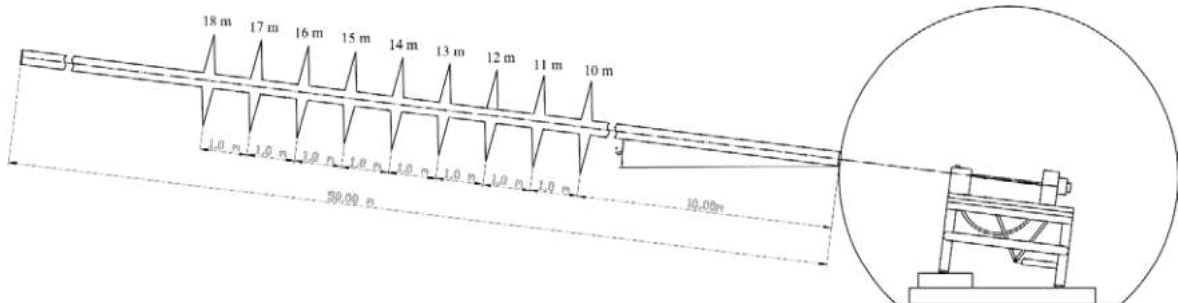


Figure 2.17 Slotting in the borehole 1 jgm RAZ 38/18.



Figure 2.18 Slotting experiments in the development heading of LTCC panel Dk-95.

Performing hydro slotting in a medium subjected to high stress may be associated with the occurrence of dynamic destruction of this medium, which is accompanied by micro-shocks. Therefore, microseismic monitoring during the slotting of the large diameter boreholes was carried out using two geophones installed 3.36m and 6.78 m respectively from the boreholes.

Figure 2.19 presents records of seismoacoustic response of the coal registered during its cutting and performing hydro slotting in one of the slots. In Deliverable Report D2.3 the monitoring of all the slots are presented. In general, the monitored signal from the closer geophone was more than one

order of magnitude weaker than the signal from the farther one. Change of the magnitude of the signal was rather related to the water and drilling outflow than the process of the water jet cutting. No strong acoustic events were observed.

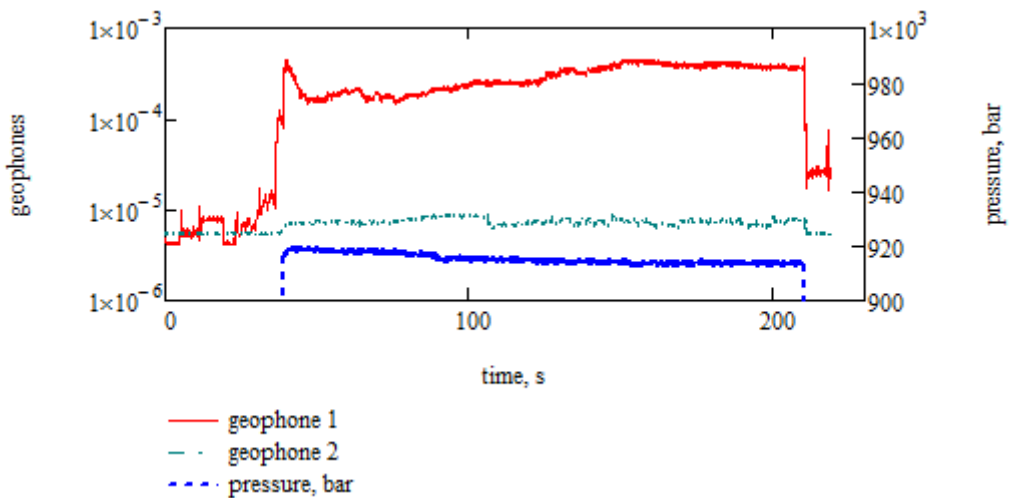


Figure 2.19 Monitoring the cutting of slot no. 2.

In summary, the slotting experiments conducted at Coal Mine Velenje have shown that it is technically possible to safely apply hydro-slotting at LTCC panel developments and enlarge the area of stress relief offered by large diameter boreholes practised at the mine.

As planned, microseismic monitoring continued until the end of the project and Imperial College took over the analysis of the monitored data after January 2019 and carried out risk analysis around panel Dk-95. Figure 2.20 presents the risk assessment carried out based on monitored data during May 2019 indicating a reduced risk around the barrier pillar of longwall panel Dk-95 where the 8 slotted large diameter boreholes were located while the face was approaching to the completion line. This may have an indication that a combination of large diameter boreholes with slotting have been effective, however, it is difficult to generalise from one experiment, if the slots cut added significant value to the already existing large diameter boreholes drilled to enable slotting.

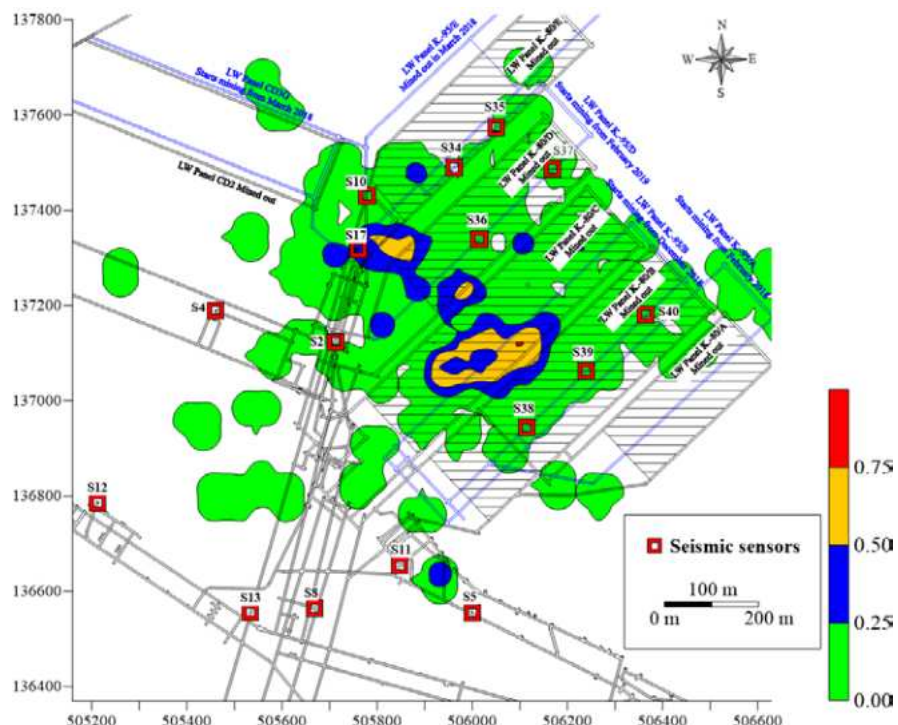


Figure 2.20 Risk assessment in temporal and spatial domains within the period 01/05/2019-31/05/2019 at Coal Mine Velenje.

Task 2.4 Measurement while drilling to characterise coal and rock parameters which influence gas outbursts and rock bursts (led by CM-VELENJE, IMPERIAL, JSW, GIG)

Task 2.4 aimed at investigating the potential use of MWD (Measurement While Drilling), in order to take advantage of routine drilling operations performed, either for pressure/stress relief or for production (blasting), for acquiring data that is helpful to characterise the rock or coal mass from the point of view of risk assessment. The objective was to install sensors in the drilling equipment to monitor performance parameters continuously.

These measurements were planned for Coal Mine Velenje and, initially to be developed and performed by AITEMIN. Upon AITEMIN's departure from the RFCS projects, CM-VELENJE undertook the responsibility for this task and performed the work at one of its large diameter stress relief borehole drilling sites underground. Initial work was carried out using conventional (manual) data acquisition methods, which helped design and develop the digital MWD methodology implemented. Work was completed in December 2018, the data analysed and Deliverable D2.4 Report prepared and submitted.

In the first stage, five long (Figure 2.21), large diameter boreholes with inclinations +2°/-2° were drilled to cover a planned path/area of the development gateroad at longwall panel C k. -95. Additionally, another set of large diameter boreholes (Figure 2.21) were prepared after the first drilling as results were promising.

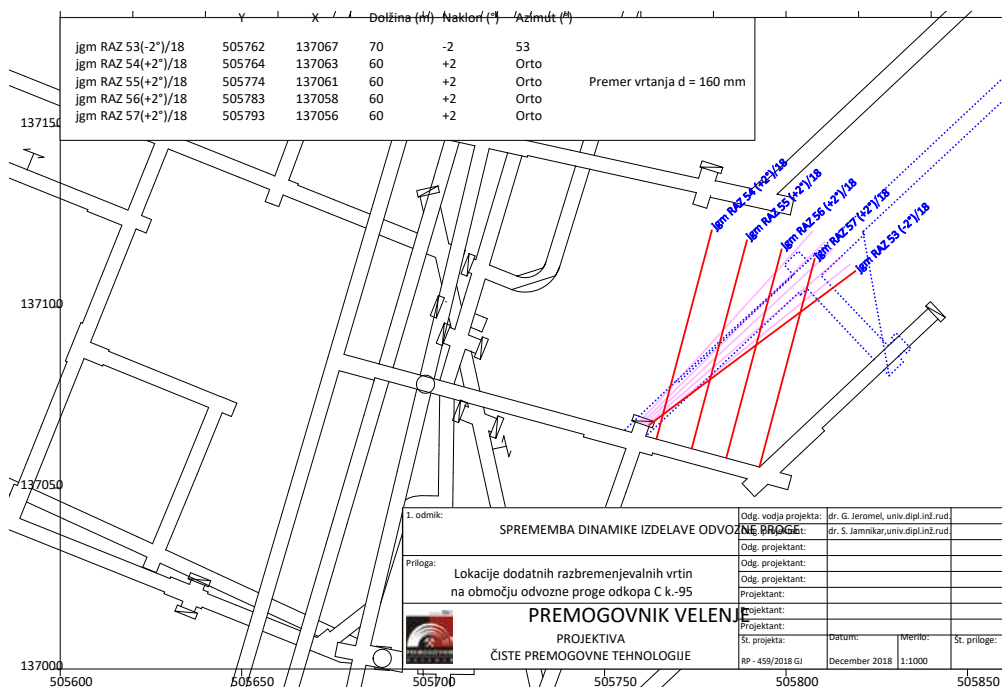


Figure 2.21 Technical plan for the second set of large diameter boreholes (Development C k. -95).

Detailed analysis of monitoring results (MWD) led to several conclusions that were noted during drilling. Observations have shown that exceptionally low thrust force needed to drill in low to moderate fractured zones.

Measurement While Drilling (MWD) of torque and thrust was trialled for the first time at CM Velenje and it showed promising results in combination with detailed material and overall drilling performance recordings. This data is crucial as it was observed that the pressure values observed from the acquired data could be misleading in cases of crushed zones against high strength coal areas, as in both cases torque pressure increases. Overall, the rotation was found to be the most important drilling parameter as it reflects the given conditions in boreholes and a wider area.

In cases of changes in coal strength, the thrust still represents important measure as it follows the heterogeneities of coal and differs for cases of low or high strength coal at a given area. Drilling performance charts for some of the boreholes are presented in Figure 2.22 to Figure 2.24 with comparison between digital (MWD) and manual readings.

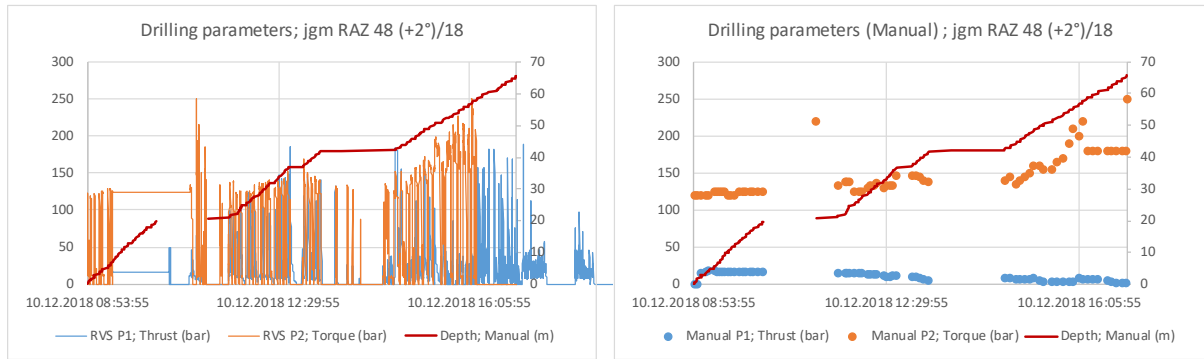


Figure 2.22 Drilling performance for jgm RAZ 48/18. Drilling torque is increased after advancing over fractured zone around 27,5 m, where on contrary thrust is reduced completely. Both parameters gradually increase after approximately 42 m, where drilling team also reported increased material strength and relatively low material output. Given combination of recordings could indicate local zone of stress accumulation.

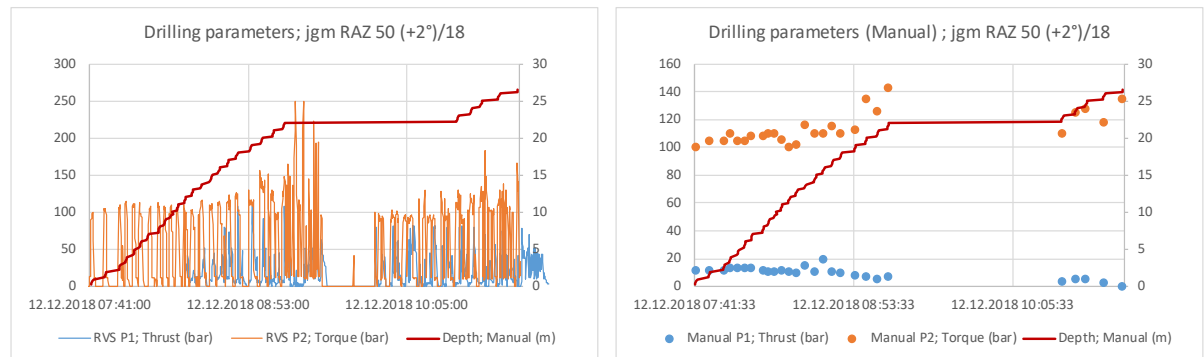


Figure 2.23 Drilling performance for jgm RAZ 50/18. Fractured zone and following increase of borehole material output around the depth of 20 m is shown in rotation pressure chart.

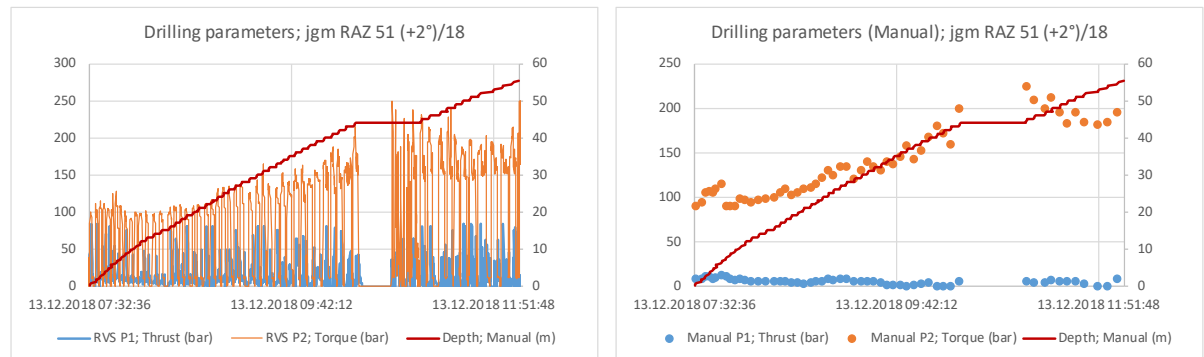


Figure 2.24 Drilling performance for jgm RAZ 51/18. Remarks report continuous fractured zone after the depth of 8,5 m and therefore continuous rise of rotation pressure until nearly final depth. Thrust pressure remained in a range of up to 80 bar along the whole depth of borehole.

WORK PACKAGE 3 - MICROSEISMIC MONITORING AND DEVELOPMENT OF TECHNOLOGIES FOR SHORT-TERM PREDICTION OF ROCK BURSTS AND GAS OUTBURSTS

Task 3.1 Microseismic monitoring of rock burst and gas outburst indicators at JSW and CM-Velenje (led by GIG, JSW, CM-VELENJE)

As prerequisite and part of this task two microseismic systems SOS were built and installed in CM-Velenje and JSW Pniowek coal mines. Each of the two SOS microseismic systems was constructed as a 32 channel data transmission system. The SOS system installed in CM-Velenje mine consisted of 3 tri-axial velocity sensors and 7 uniaxial velocity sensors at the beginning of seismic monitoring in February 2016 and evolved to its final form with increased number of sensors throughout the project (Figure 3.1Error! Reference source not found.). The SOS system installed in Pniowek mine consisted of 6 tri-axial velocity sensors and 9 uniaxial velocity sensors at the whole period of seismic monitoring from February 2016 until December 2016 (Figure 0.2a). The monitoring results from Pniowek Coal Mine have shown that, during mining of coal, there was almost no seismic activity. Therefore, it was decided to move the monitoring system to JSW Budryk Colliery where much higher seismic activity is present. The SOS system installed in Budryk mine consisted of 13 uniaxial velocity sensors and started operation in April 2017 (Figure 0.2bError! Reference source not found.).

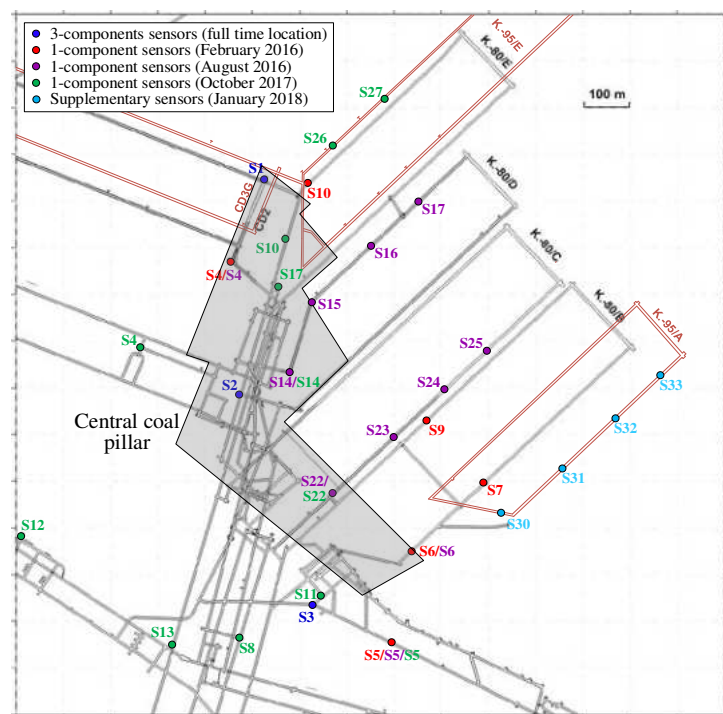


Figure 3.1 Mine production layout at -80 and -95 m production levels during 2016-2019 and the distribution of installed SOS seismic stations of the microseismic monitoring system at Coal Mine Velenje as it evolved throughout the project. The grey zone indicates the approximate shape of the central coal pillar protecting the main mine infrastructure in the production district.

Seismic data analysis was carried out to obtain location and seismic energy for each seismic event. To achieve this objective, the following parameters for each seismic station (channel) and for each recorded seismic event had to be determined: first arrival of seismic P wave, end time of seismic P wave, first arrival of seismic S wave, end time of seismic S wave. These four parameters were picked manually by experienced geophysicists in order to obtain maximum possible accuracy.

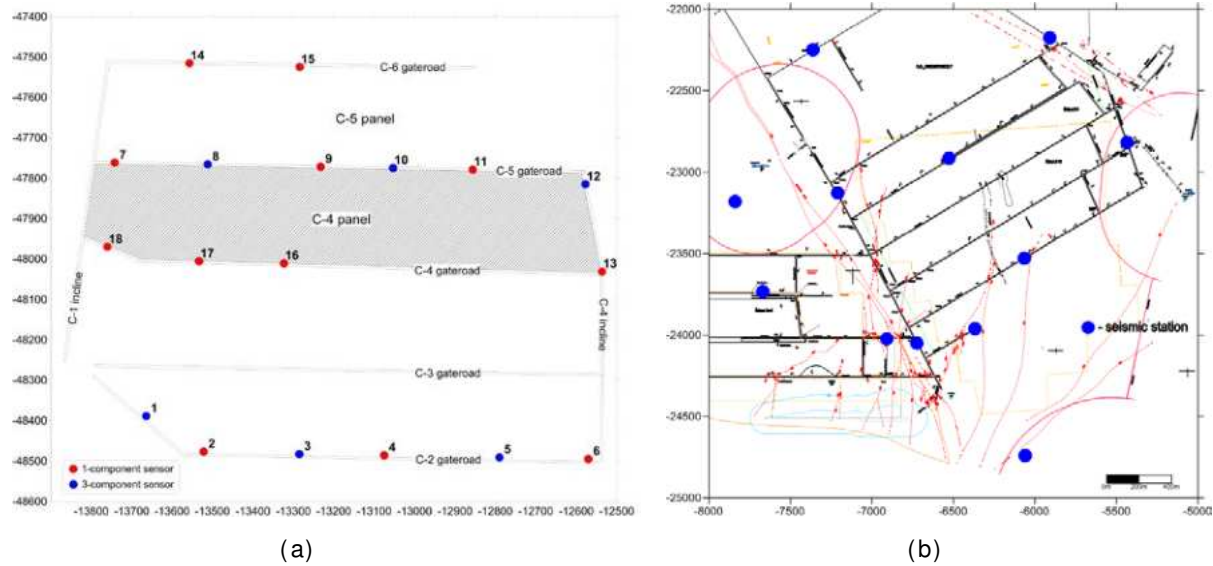


Figure 0.2 Distribution of the seismic stations (a) after completion of SOS microseismic system installation in February 2016 at Coal Mine Pniowek and (b) installation in April 2017 at Coal Mine Budryk.

Analysis of seismic events recorded at Coal Mine Velenje

The analysis of seismic events recorded at Coal Mine CM-Velenje were carried out on a weekly basis and data forwarded to Imperial College and Coal Mine Velenje. Further combined monthly analysis were carried out for the purposes of annual reporting and examples of monthly seismic activity between March 2016 and December 2018 are presented in Figure 0.3 - Figure 3.7.

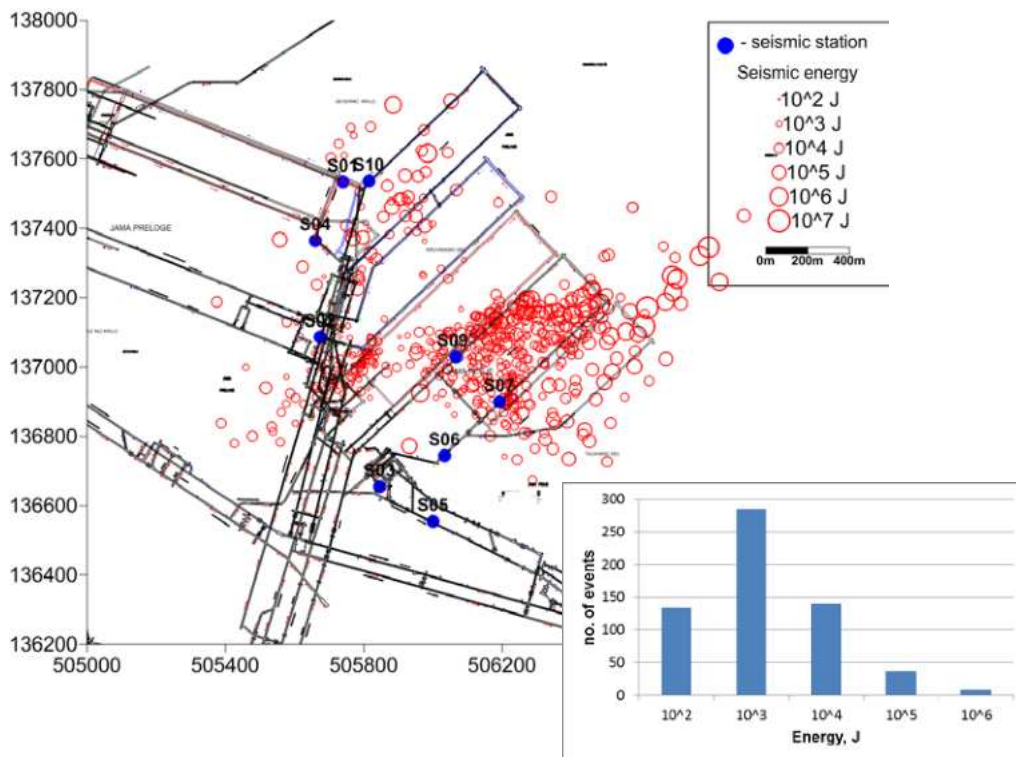


Figure 0.3 Distribution of the seismic events in March 2016 at CM-Velenje mine. Sizes of red circles are proportional to calculated seismic energy. Bottom right – number of seismic events (vertical axis) in seismic energy classes (horizontal axis).

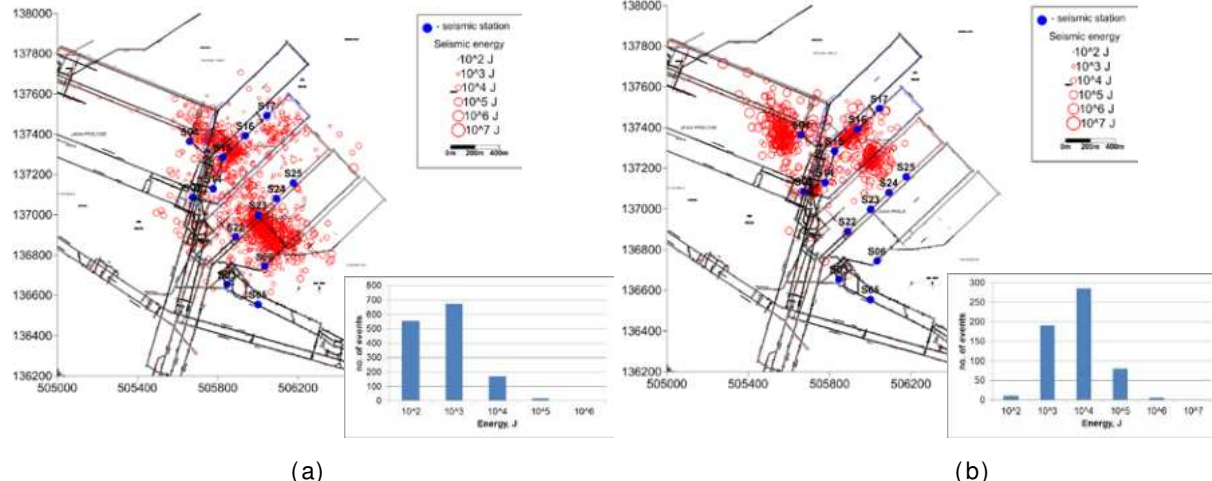


Figure 3.4 Distribution of seismic events in (a) August 2016 and (b) November 2016, and the number of seismic events in seismic energy classes at CM-Velenje mine.

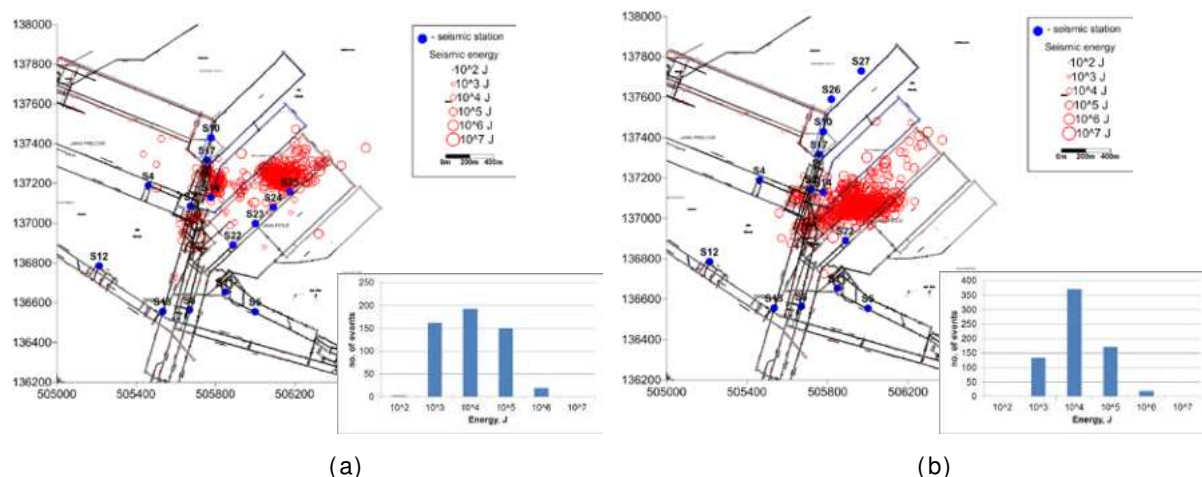


Figure 0.5 Distribution of seismic events in (a) April 2017 and (b) September 2017, and the number of seismic events in seismic energy classes at CM-Velenje mine.

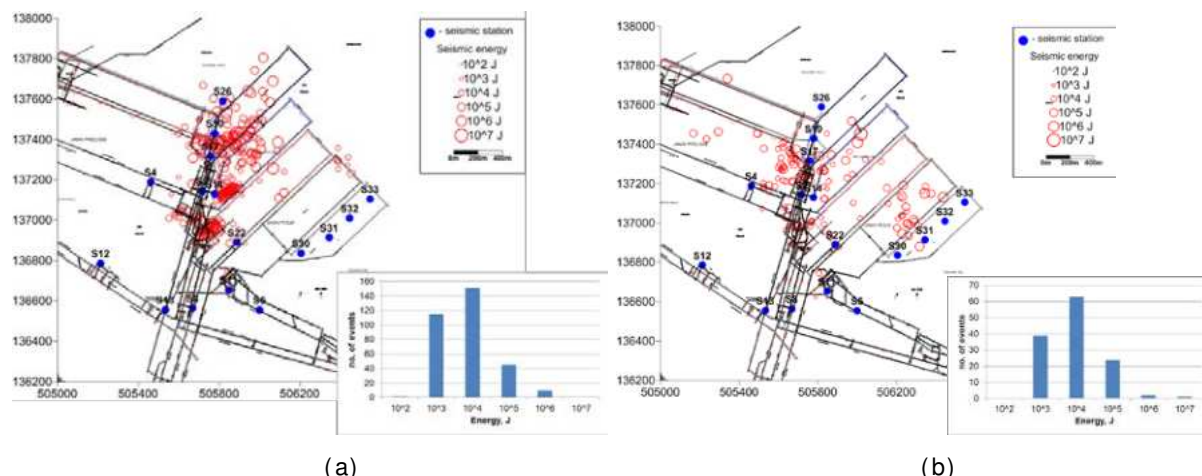


Figure 3.6 Distribution of seismic events in (a) March 2018 and (b) June 2018, and the number of seismic events in seismic energy classes at CM-Velenje mine.

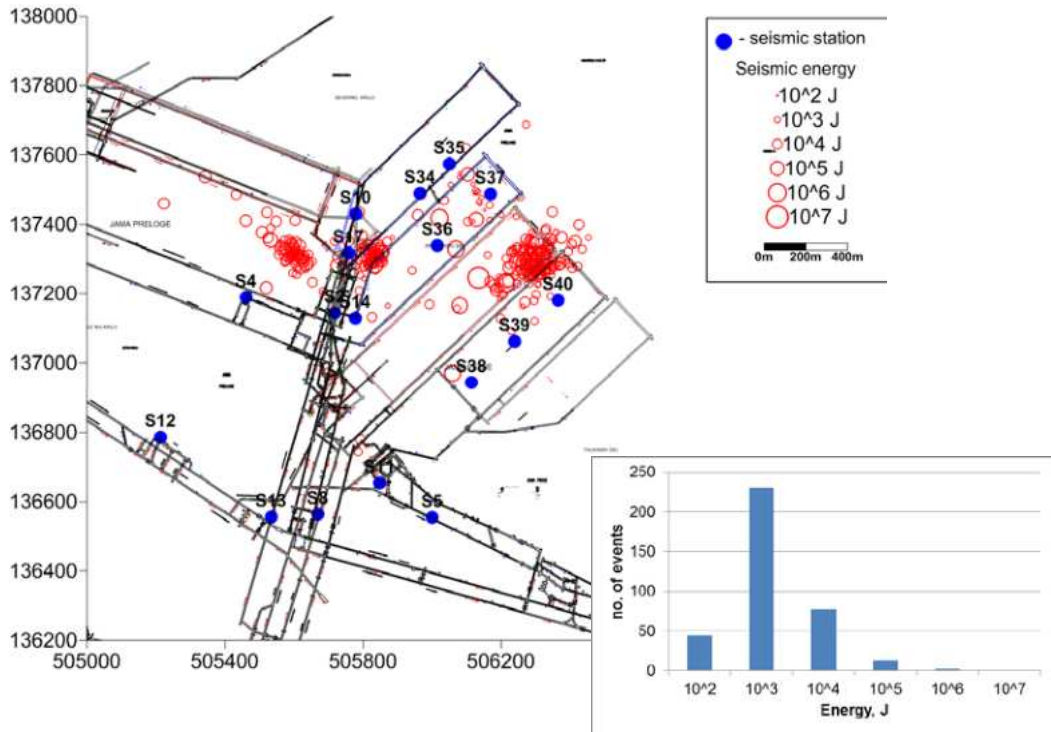


Figure 3.7 Distribution of seismic events (red circles) in December 2018 at CM-Velenje mine. Sizes of red circles are proportional to calculated seismic energy. Bottom right – number of seismic events (vertical axis) in seismic energy classes (horizontal axis).

Seismic monitoring in 2016 included the coal panels: Ak-80, Bk-80, Ck-80, Dk-80, Ek-80, CD2 and CD3. There were about 8119 seismic events recorded and located during 10 months of continuous seismic monitoring. The microseismic monitoring have shown that during mining process, there was high seismic activity in the areas of coal panels Bk-80, Dk-80, Ek-80, C2 and in the area where main galleries are located. The largest seismic events reached seismic energy 10^7 J (local magnitude about 2.7).

Seismic monitoring in 2017 included coal panels: Ak.-95, Ck.-95, Ck. -80, Dk.-95, Dk.-80 and CD3. During the 12 months there were about 6,000 seismic events with seismic energies ranging from 10^2 J to 10^7 J. Most of the seismic activity was related to mining of coal panel Ck.-80. There were two additional clusters of seismic activity observed. The first one was related to mining of coal panel D k.-80 and the second cluster was related to the area of main gate roads position in the central pillar of the mine.

Seismic monitoring in 2018 included coal panels: Ak.-95, Ck.-95, Ck. -80, Dk.- 95, CD3/g and CD3/j. of About 3,000 seismic events with seismic energies ranging from 10^2 J to 10^7 J were recorded in the 12 months period. Most of the seismic activity was related to mining of coal panels Ak.-95, Ck.-80 and CD3/j. There were two additional clusters of seismic activity observed. The first one was related to mining of coal panel Ck.-95 and the second cluster was related to the area of main gate roads position in the central pillar of the mine.

The microseismic monitoring results from CM-Velenje are summarised in Figure 3.8 and Figure 3.9 where distribution of seismic activity and seismic energy between March 2016 and January 2019 is shown. In Figure 3.8 one can find daily and weekly number of seismic events with periods of very low or even no seismic activity and periods with highest number of seismic events. Both of these periods are directly related to mining in Coal Mine Velenje where, in Figure 3.9, one can find lowest and highest seismic energies during the whole period of seismic monitoring using the SOS system.

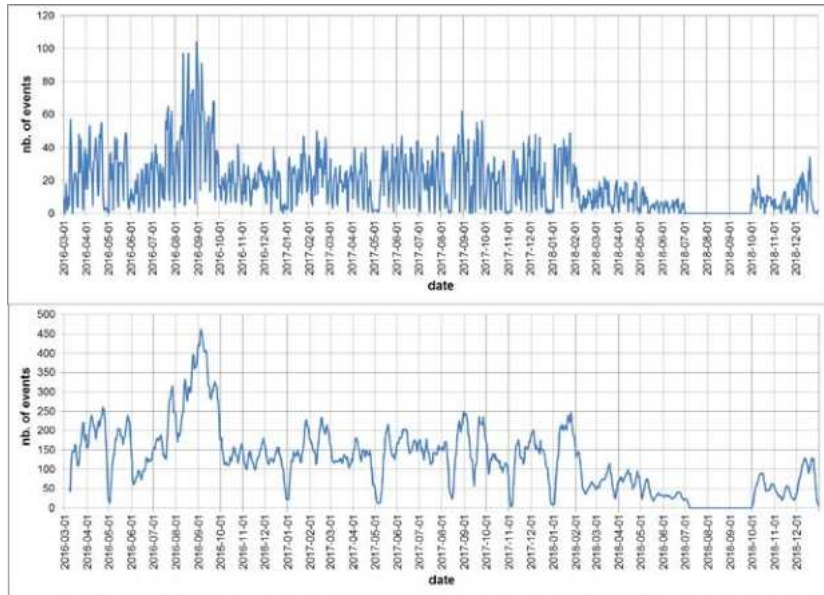


Figure 3.8 Distribution of seismic activity i.e. number of seismic events (vertical axis) in day (top) and week (bottom) time intervals (horizontal axis) between March 2016 and January 2019 at CM-Velenje.

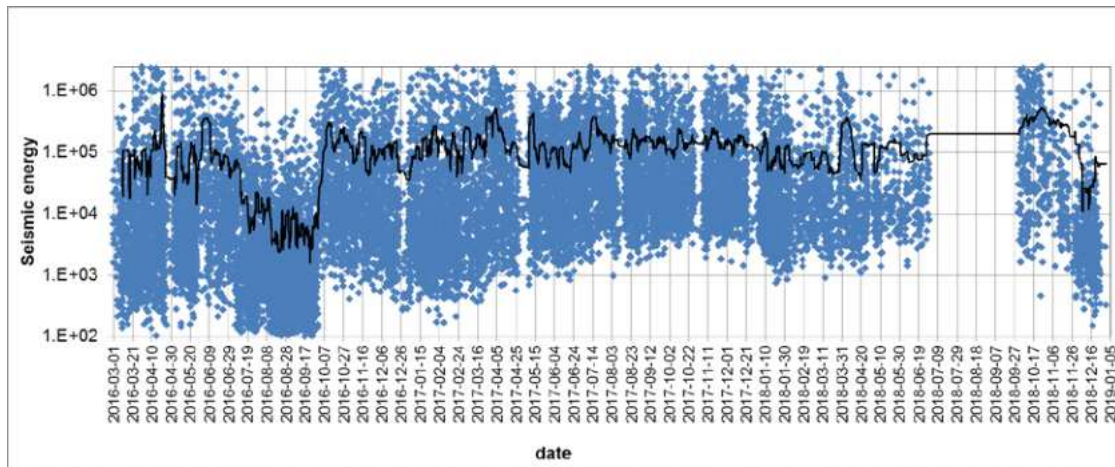


Figure 3.9 Seismic energy distribution for each seismic event (dots) and moving average of seismic energy (thick black line) between March 2016 and January 2019 at CM-Velenje.

Analysis of seismic events recorded at Budryk Coal Mine

Representative examples of the analysis of seismic events recorded at Coal Mine Budryk are presented here. Seismic monitoring in Budryk mine started in April 2017 after moving the system from Phioewek mine and involved coal panels: B-8, B-9, B-10 and B-11. During 9 months, the system recorded about 2,900 seismic events with seismic energies ranging from 10^1J to 10^6J (Figure 3.10 to Figure 3.11). Most of the seismic activity was related to mining of coal panels B-8 and B-11. Seismic events with energies 10^4J were significant in November and December 2017 only.

Seismic monitoring in 2018 involved coal panels: B-8, B-9, B-10 and B-11. During 9 month of continuous seismic monitoring the system recorded about 3,000 seismic events with seismic energies ranging from 10^1J to 10^6J (Figure 3.12 and Figure 3.13). Most of the seismic activity was related to mining of coal panels B-8 and B-11. Seismic events with energies 10^4J were significant in January, February and March only. The microseismic monitoring results from Budryk Coal Mine are summarised in Figure 3.14 where distribution of seismic activity between April 2017 and September 2018 is presented. In Figure 3.14 one can find daily and weekly number of seismic events with periods of very low or even no seismic activity and periods with highest number of seismic events. Both of these periods are directly related to current mining and coal face position in Budryk colliery. Seismic monitoring in Budryk mine was terminated in September in compliance with MapROC schedule.

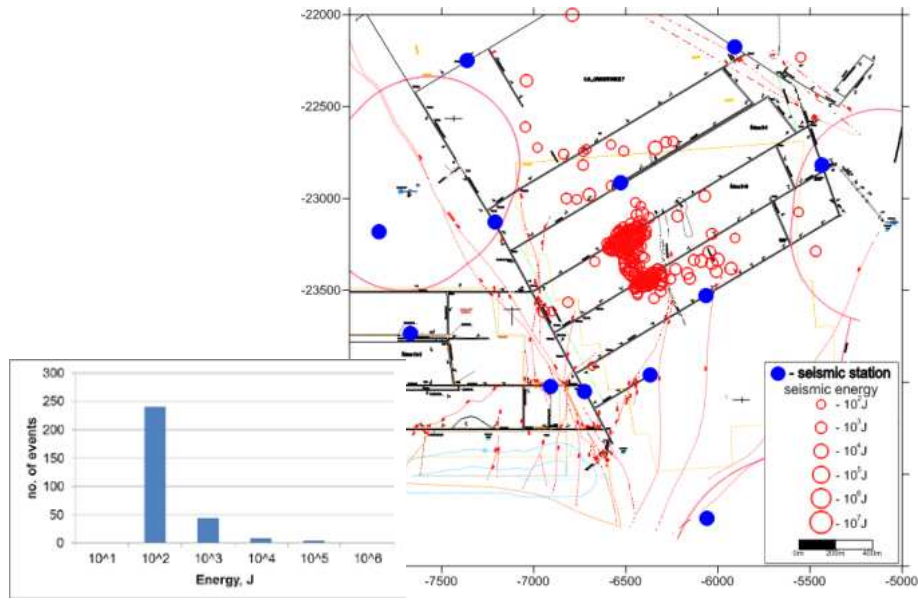


Figure 3.10 Distribution of seismic events in April 2017 at Budryk mine. Sizes of red circles are proportional to calculated seismic energy. Bottom left – number of seismic events (vertical axis) in seismic energy classes (horizontal axis).

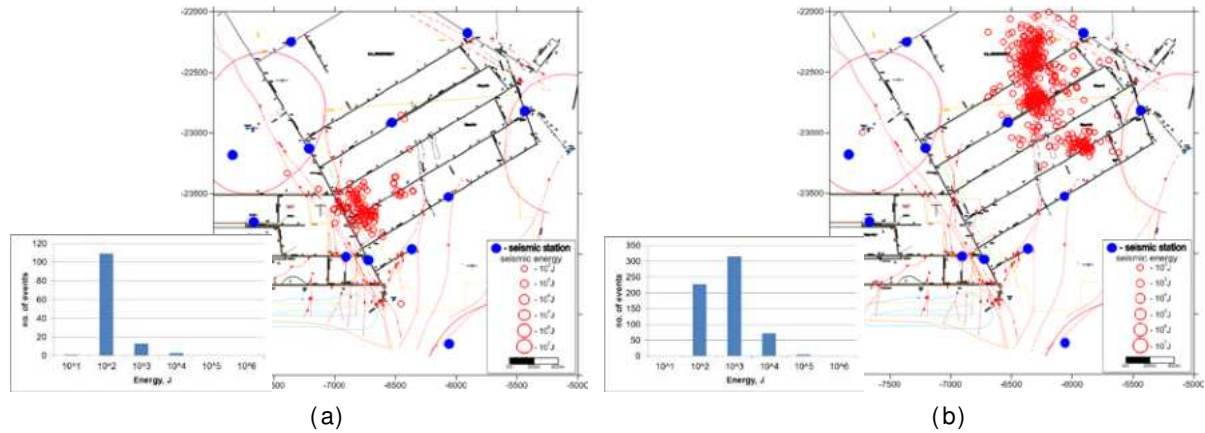


Figure 3.11 Distribution of seismic events in (a) July 2017 and (b) December 2017, and the number of seismic events in seismic energy classes at Budryk mine.

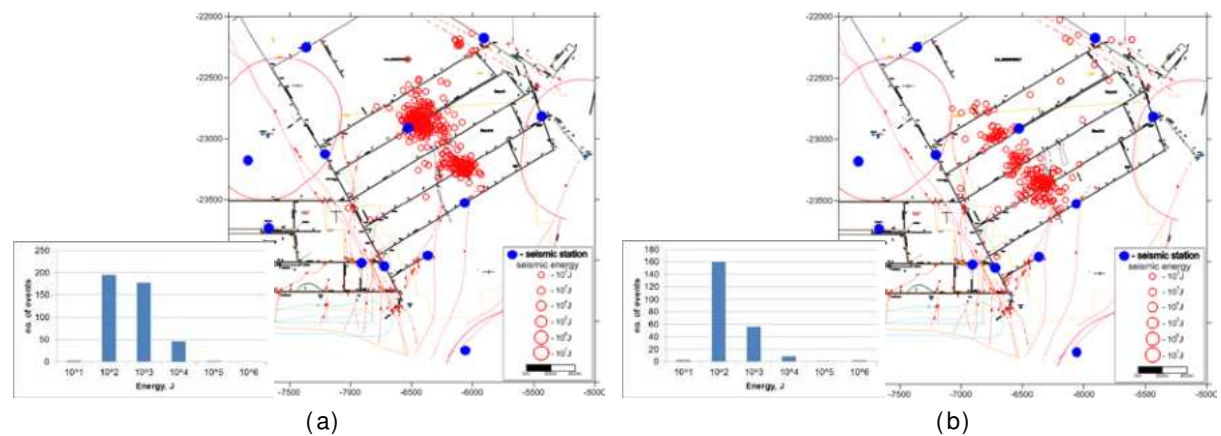


Figure 3.12 Distribution of seismic events in (a) March 2018 and (b) July 2018, and the number of seismic events in seismic energy classes at Budryk mine.

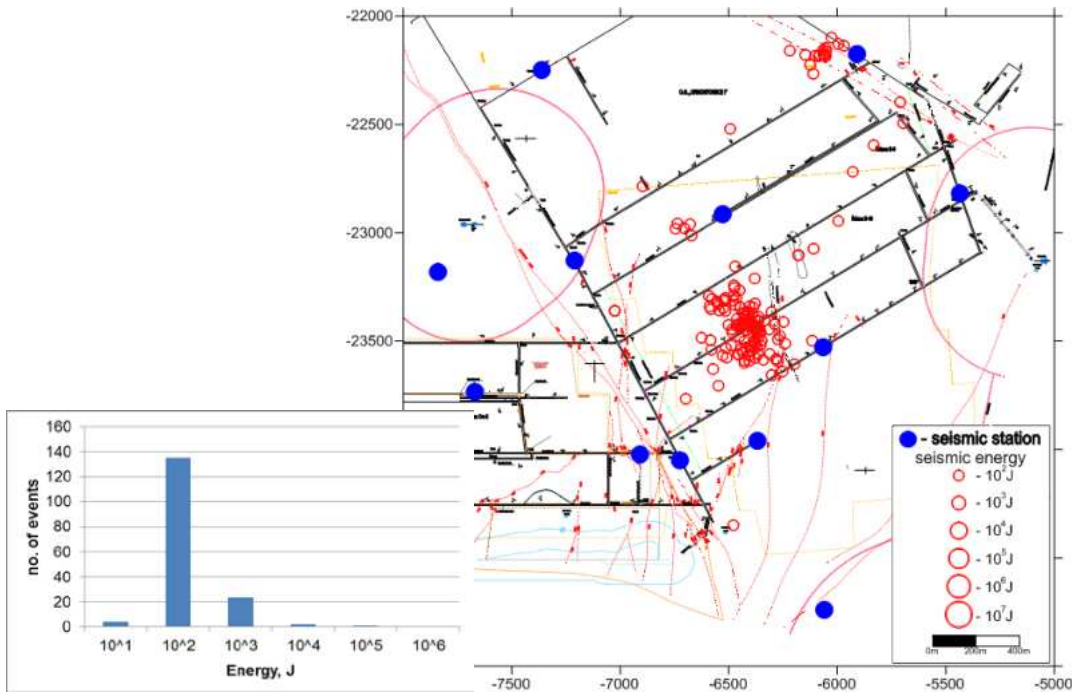


Figure 3.13 Distribution of seismic events in September 2018 at Budryk mine. Sizes of red circles are proportional to calculated seismic energy. Bottom left – number of seismic events (vertical axis) in seismic energy classes (horizontal axis).

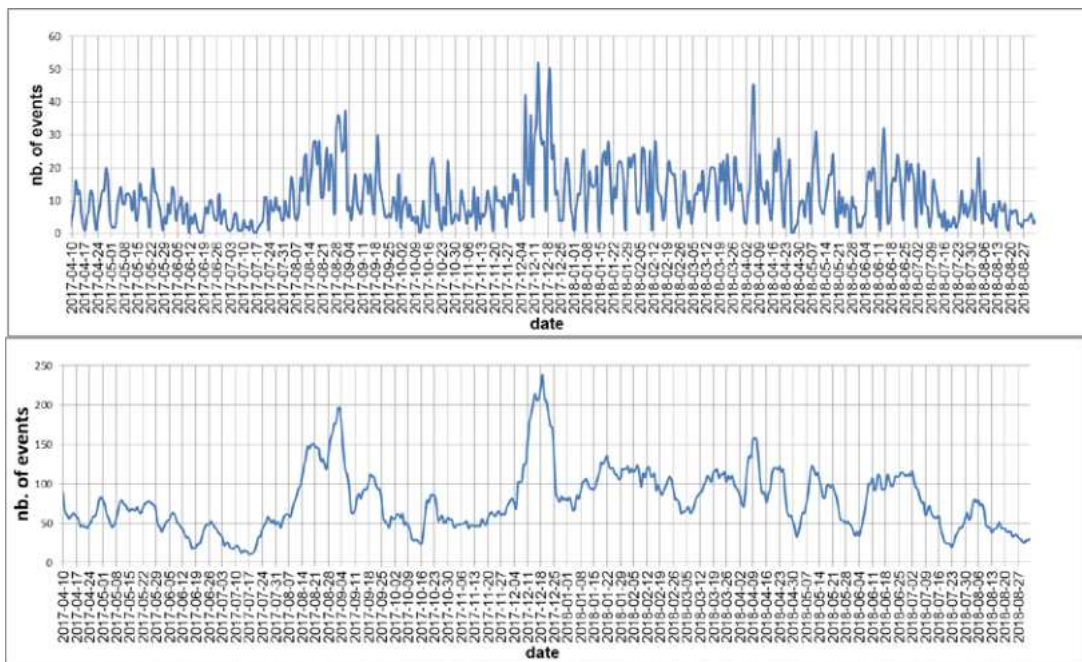


Figure 3.14 Distribution of seismic activity in a day (top) and week (bottom) time intervals between April 2017 and September 2018 at Budryk mine.

Passive Tomography Imaging at Coal Mine Velenje

Passive tomographic calculations and analysis were performed for CM-Velenje covering the area of active coal panels with an area of approximately 1,000 m in X direction and 1,000 m in Y direction. Tomography computation has been conducted every 2 weeks throughout the project. First arrivals of P-wave were used as input data to tomographic algorithm. In each 2 week time interval more than 100 seismic events were used in tomography calculations. The number of picked P wave first arrivals varied from 5 to more than 10 for each seismic event. Constant seismic velocity value equal to 1,450 m/sec was used in the area of investigation as starting velocity model in tomography calculation. This model was also used to locate seismic events. It is believed that high values of seismic velocity on tomographic images are related to increased stress state in the analysed rock mass and tomographic images in the consecutive months show temporal changes of this stress state. Each of the calculated tomographic velocity image indicates several potential areas with high seismic velocity

values in which increased seismic activity can be expected. Those potentially hazardous areas are located in active coal panels and in the area of safety pillar where main galleries of the mine are situated. In the analysed area values of P-wave velocity vary between 1,200 m/sec and 1,700 m/sec. Selected passive tomography velocity images are presented in Figure 3.15 and Figure 3.16.

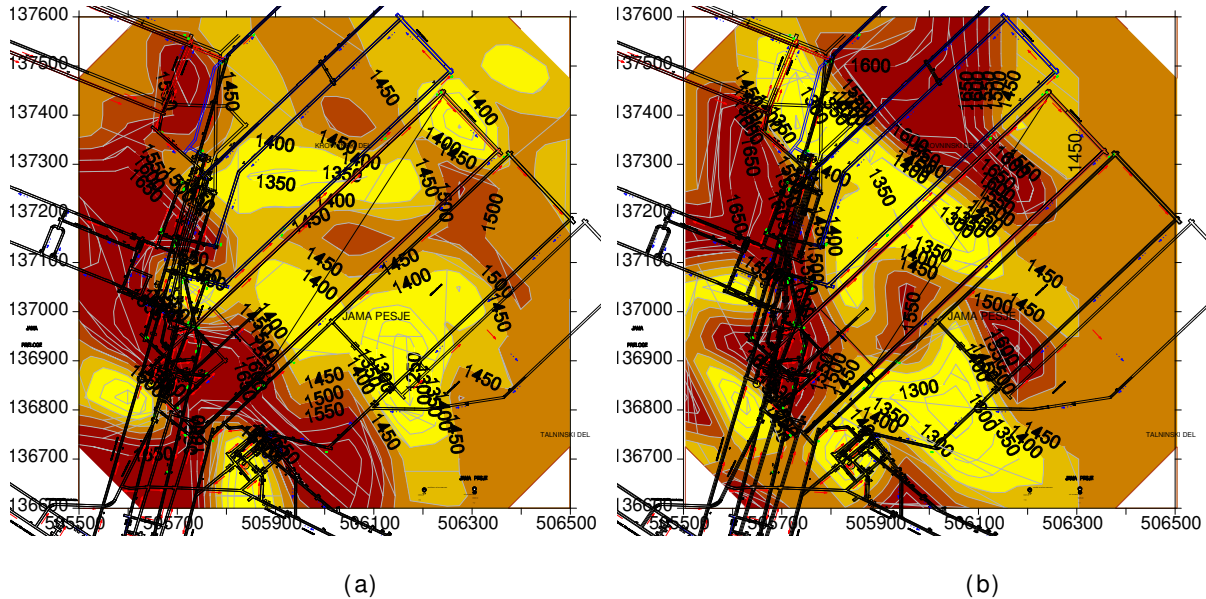


Figure 3.15 Bent-ray tomographic “P” wave velocity image (units m/s) obtained using seismic events recorded (a) between 01st and 15th July 2017 and (b) between 01st and 15th October 2017 at CM-Velenje.

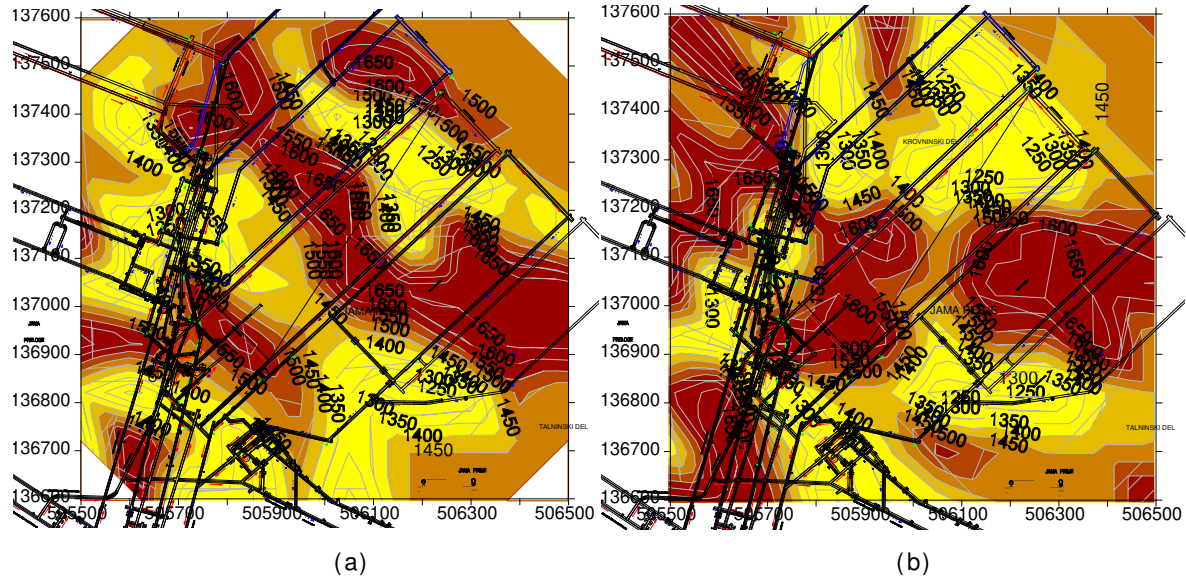


Figure 3.16 Bent-ray tomographic “P” wave velocity image (units m/s) obtained using seismic events recorded (a) between 01st and 15th January 2018 and (b) between 16th and 31st March 2018 at CM-Velenje.

Passive Tomography Imaging at Budryk Coal Mine

Passive tomographic calculations and analysis was also performed in Budryk mine covering an area approx. 2,000 m in X and Y directions. Tomography computation has been made every 2 weeks throughout the project. The number of picked P wave first arrivals varied from 5 to more than 10 for each seismic event. Constant seismic velocity value equal to 4,200 m/sec was used in the area of investigation as starting velocity model. High values of seismic velocity on tomographic images are related to increased stress state in the rock mass and tomographic images. Each of the calculated tomographic velocity image indicates several potential areas with high seismic velocity values in which increased seismic activity can be expected. Many zones with high P-wave velocity values are directly related to current coal face positions of coal panels B-8 and B-11. In the analysed area values

of P-wave velocity vary between 3,800 m/sec and 4,600 m/sec. Selected passive tomography velocity images are presented in Figure 3.17 and Figure 3.18.

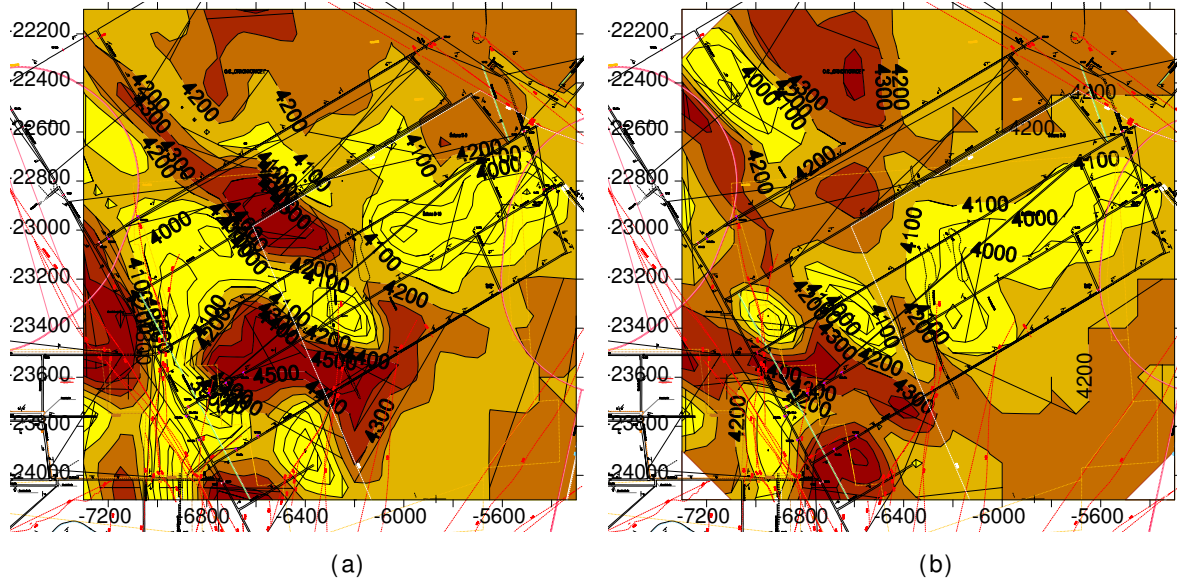


Figure 3.17 Bent-ray tomographic “P” wave velocity image (units m/s) obtained using seismic events recorded (a) between 01st and 15th April 2017 and between 15th and 30th June 2017 at Budryk Coal Mine.

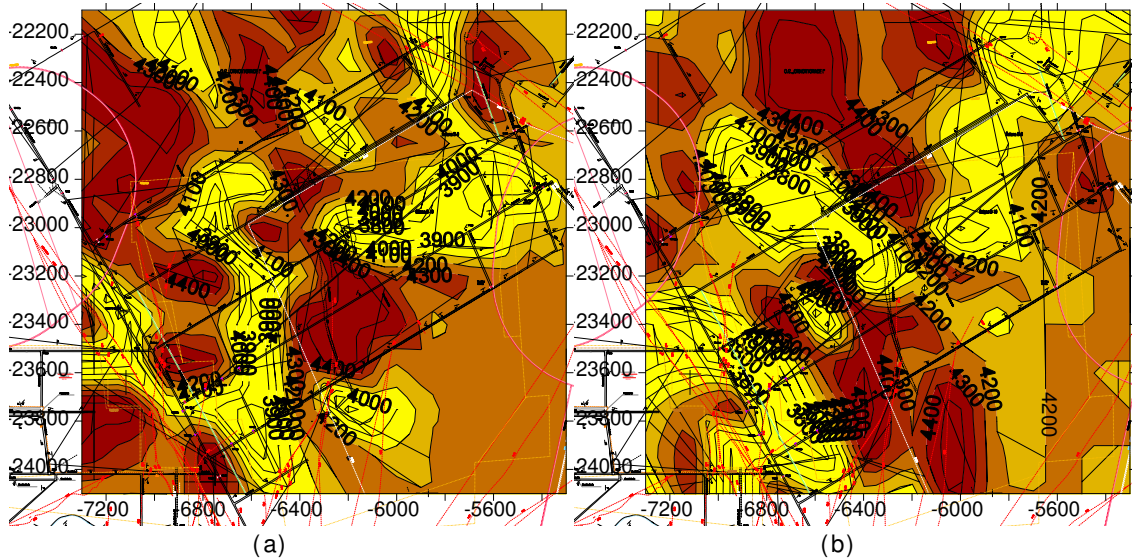


Figure 3.18 Bent-ray tomographic “P” wave velocity image (units m/s) obtained using seismic events recorded (a) between 01st and 15th May 2018 and (b) between 16th and 31st July 2018 at Budryk Coal Mine.

Task 3.2 Development of Artificial Neural Network (ANN) models for the short-term forecasting of rock bursts and gas outbursts (led by IMPERIAL, GIG, CM-VELENJE, JSW).

The main objective of this task is to develop a short-term rock burst and gas outburst forecasting methods using Artificial Neural Network (ANN) models aimed at identifying the field conditions leading to gas outbursts and rock bursts. Utilising the processed microseismic monitoring datasets, feedforward neural networks based on the error back propagation algorithm were adopted to develop and test three different Neural Network models: a Pattern Recognition ANN model, an ANN Fitting model and a Time Series ANN model.

ANN Model Application at Coal Mine Velenje

The ANN Microseismic forecasting model training data covering the period 01/03/2017 to 14/01//2018 were collected from Coal Mine Velenje using the SOS microseismic monitoring system, as shown in Figure 3.19. The data were prepared for use in the ANN models developed.

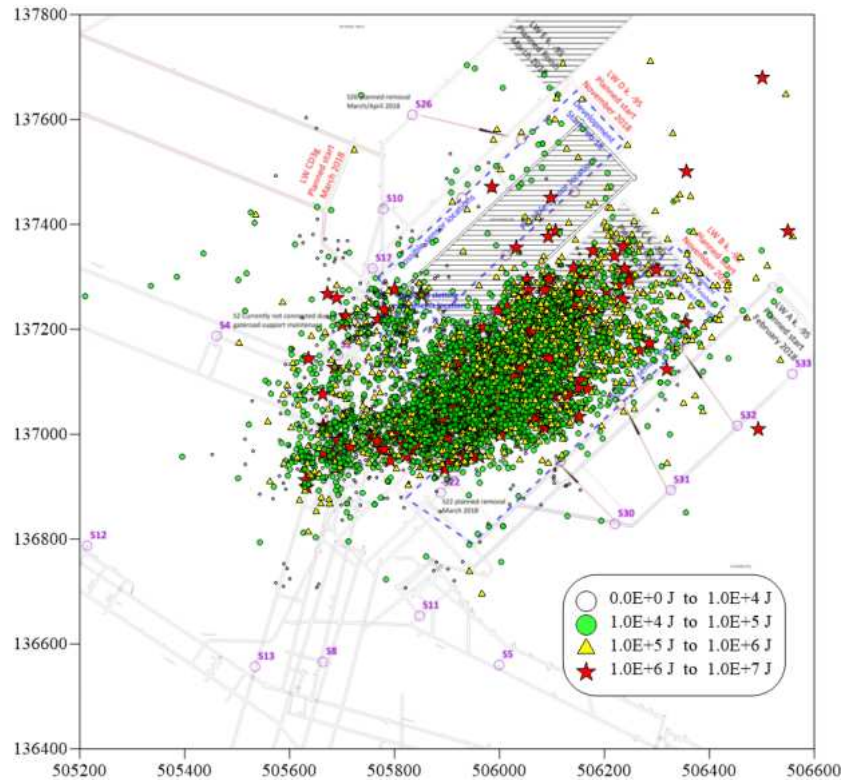


Figure 3.19 Over ten months' microseismic monitoring data at Coal Mine Velenje

As best forecasting ANN model developed, the Time Series Neural Network model was designed to forecast the maximum event energy, the total seismic energy, and the number of seismic events which could occur over the next time period. In the Neural Networks Toolbox for MATLAB, there are three patterns in the Time Series Neural Network model that can be used for the forecast potential for rock bursts and gas outbursts on the basis of microseismic parameters: the nonlinear autoregressive pattern with external inputs, the nonlinear autoregressive pattern without external inputs, and the nonlinear input-output pattern.

A two-layer feed forward network was constructed for the Time Series Neural Network model. All of the training results for the forecast of the number of seismic events are depicted in Figure 3.20, which shows that the correlation coefficients between the output and the target, as a measure of the goodness of fit, are both above 90% for all the training, validation and testing datasets. It is also seen that the errors are very small, compared to the corresponding dimensional unit, which indicates that the models predict the output quite well.

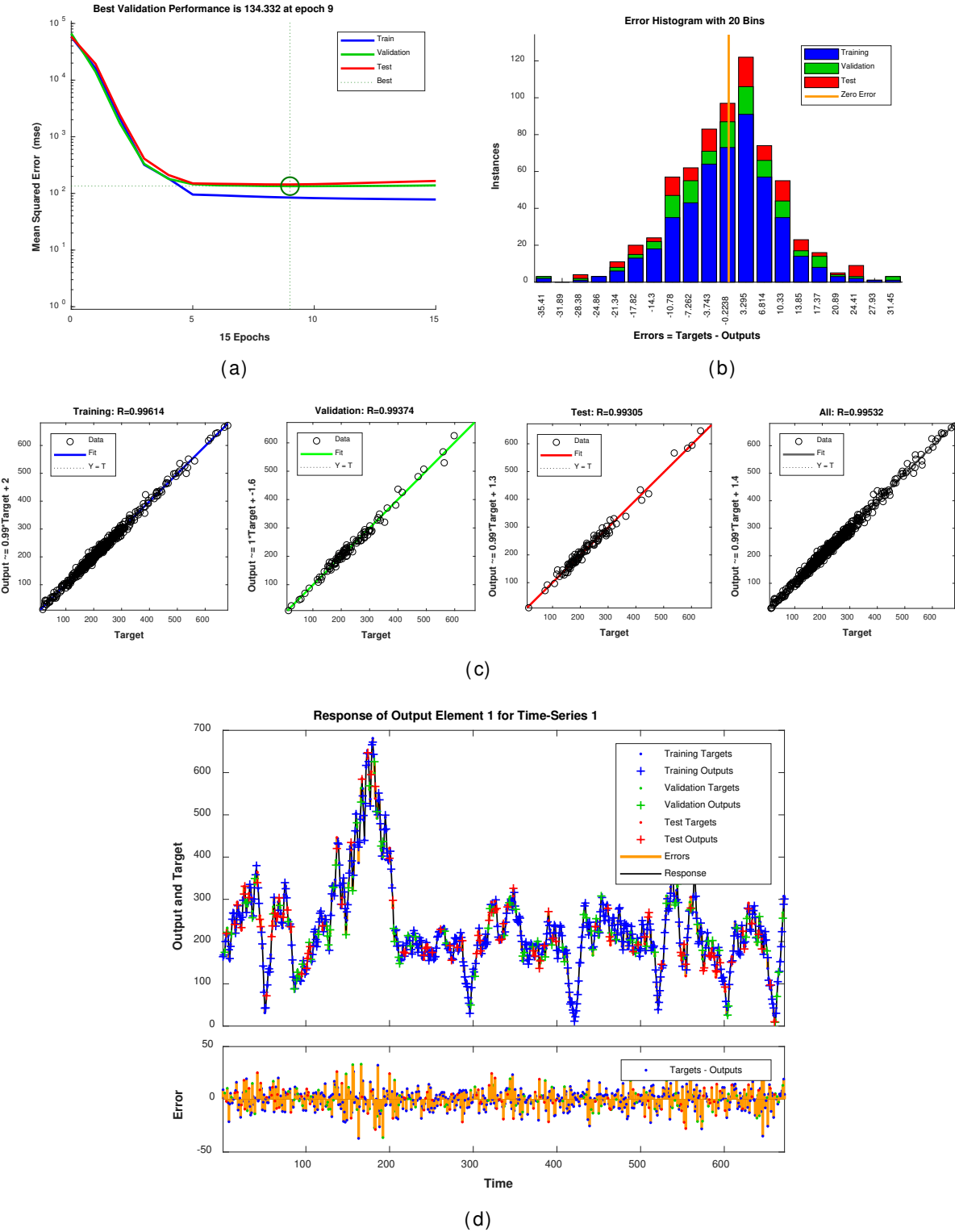


Figure 3.20 Training results for the Time Series Neural Network models for the forecast of the number of seismic events. (a) performance of cross-entropy versus number of iterations (epochs), (b) error histogram for the training, validation and testing data, (c) corresponding regression plots for the target data against the output, and (d) Time series response. This displays the inputs, targets and errors over time. It also indicates which time points were selected for training, testing and validation.

ANN Model Application at Budryk colliery

The ANN Microseismic forecasting model training data covering the period 20/11/2017 to 05/08/2018 were collected from the Budryk colliery using the SOS microseismic monitoring system, as shown in Figure 3.21. The data were prepared for the inputs and outputs in the ANN models.

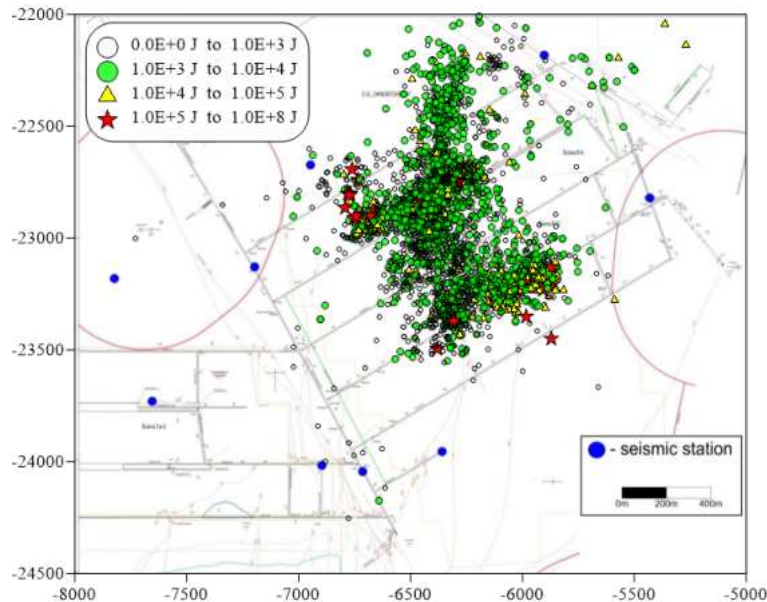


Figure 3.21 Over ten months' microseismic monitoring data from the Budryk colliery.

Figure 3.22 shows training results of the Time Series Neural Network model for the forecast of the maximum seismic event energy. It can be seen that the correlation coefficient between the output and the targets, as a measure of the goodness of fit, is above 90% for all the training, validation and testing datasets. It is also seen that the errors are very small, compared to the corresponding dimensional unit, which indicates that the models predict the output quite well.

Conclusions

Examples of the implementation of the ANN models developed are presented using the processed real time microseismic data from Coal Mine Velenje and Budryk colliery, where both LTCC and the conventional longwall (LW) mining methods are adopted. This allowed the project to develop a universally applicable forecasting models for typical mining scenarios in coal mines. It was observed that, the neural net Pattern Recognition Model could forecast the occurrence probability of strong seismic events; the neural net Fitting Model was good to forecast the magnitude value of maximum seismic event; and the neural net Time Series Model was successful to forecast the total amount of seismic energy and the number of seismic events. Therefore, the set of ANN models developed can be employed to extract precursors of rock bursts and gas outbursts.

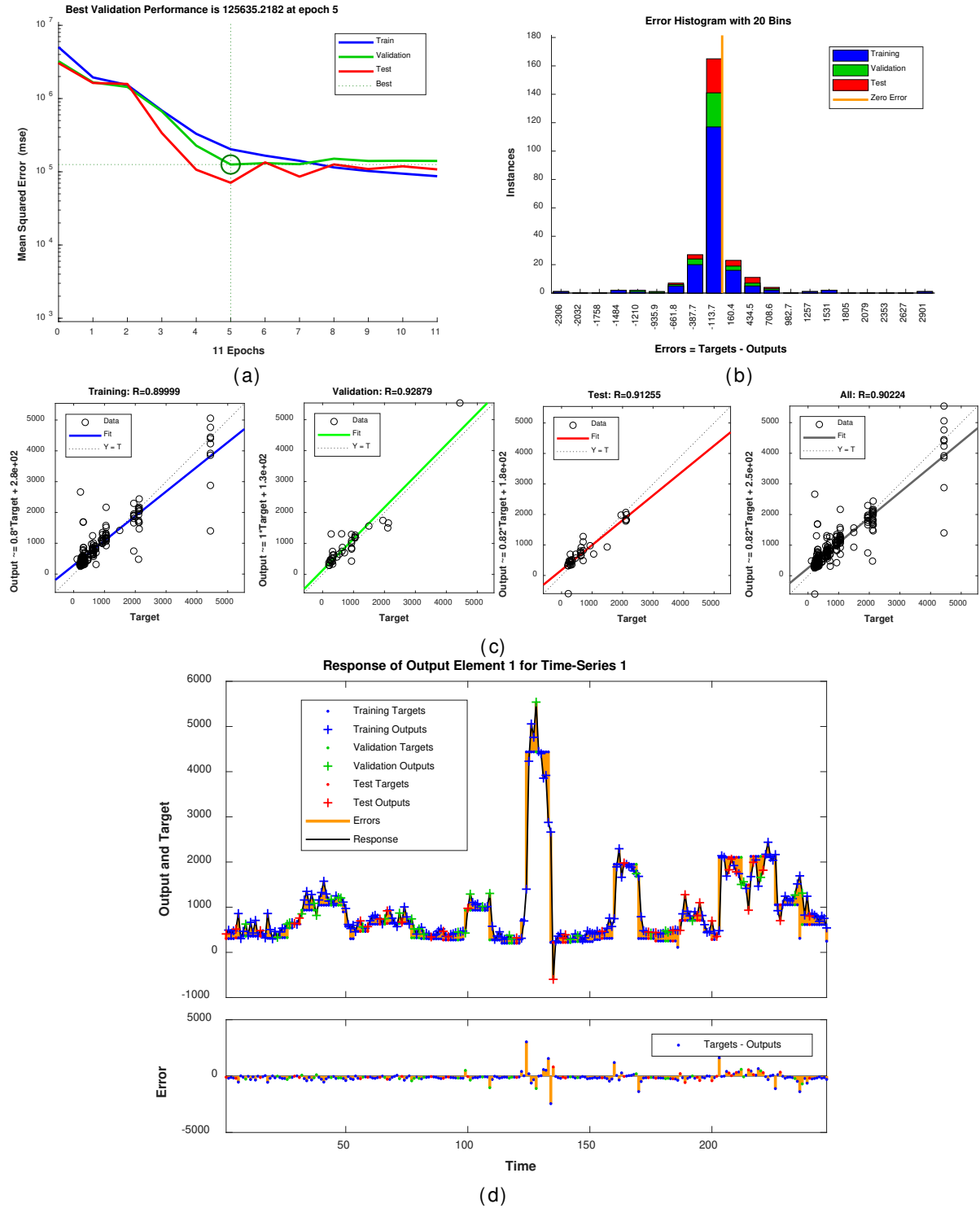


Figure 3.22 Training results for the Time Series Neural Network models for the forecast of the maximum seismic event energy. (a) performance of cross-entropy versus number of iterations (epochs), (b) error histogram for the training, validation and testing data, (c) corresponding regression plots for the target data against the output, and (d) Time series response. This displays the inputs, targets and errors over time. It also indicates which time points were selected for training, testing and validation.

Task 3.3 Development of Fractal Dimension based models for the short-term forecasting of rock bursts and gas outbursts (led by IMPERIAL, GIG, CM-VELENJE, JSW).

The main objective of this task is to develop and validate a predictive methodology based on the fractal theory utilising the processed real time seismic data from partner mines. Six fractal dimension based models were proposed for the short term forecast of rock bursts and gas outbursts utilising

seismic sequences. Multifractal characteristics of microseismicity are expressed in terms of the D_q vs q spectra and $f(a(q))$ vs $a(q)$ spectra. Precursors of rock bursts and gas outbursts identified include the reduction in capacity dimension and information dimension, the steep curve in the multifractal D_q - q spectrum, and the large envelope area of the $f(a)$ - a spectrum.

Application of Fractal Dimension based models for the short-term forecasting of rock bursts and gas outbursts at Coal Mine Velenje

Figure 3.23 shows the spatial and temporal distribution of microseismic events at LW Ck.-80 during the seven months period between 01/03/2017 and 01/10/2017. Clear information on the timing of shift changes, weekends and production periods during the period 05/05/2017 to 13/08/2017 and increased mining intensity from September 2017, after the summer holidays can be found in Figure 3.23b. The fractal methodology adopted in this task is a promising technique for quantifying these microseismic responses associated with mining activities and disturbances.

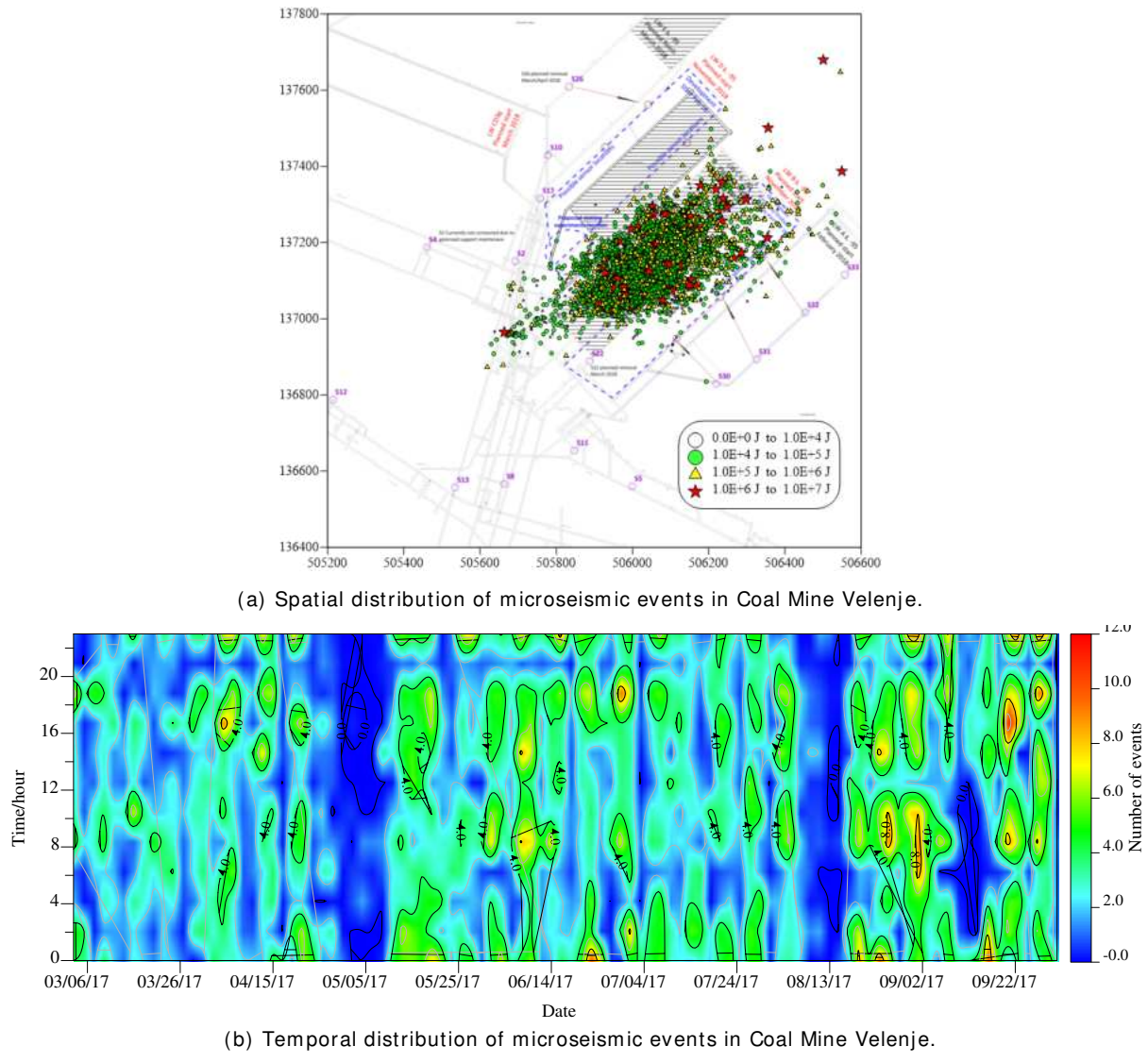


Figure 3.23 Microseismic monitoring in Coal Mine Velenje.

It can be seen in Figure 3.24 that prior to most strong seismic events, there exists a distinct decline in the capacity dimensions and the information dimensions. This decline has been widely known as dimension reduction. As for the multifractal spectra of $f(a)_T$, $f(a)_S$ and $f(a)_E$, their envelop areas become larger, corresponding to the red high value zone in the figure.

Building upon the normalised index, the values of all fractal dimension based models were normalised into 0 to 1, Figure 0.25. According to the assumption of four risk levels (none, weak, moderate, and strong) with respect to the range of risk index values (0 to 0.25, 0.25 to 0.50, 0.50 to 0.75, and 0.75 to 1), the sensitive models (D_{S0} , D_{T1-E} , D_{S1-E} , D_{E1-E} , $f(a)_S$ and $f(a)_E$) indicate that strong seismic events were more likely to occur before the index value reaches the strong grade (or as the values exceed 0.75).

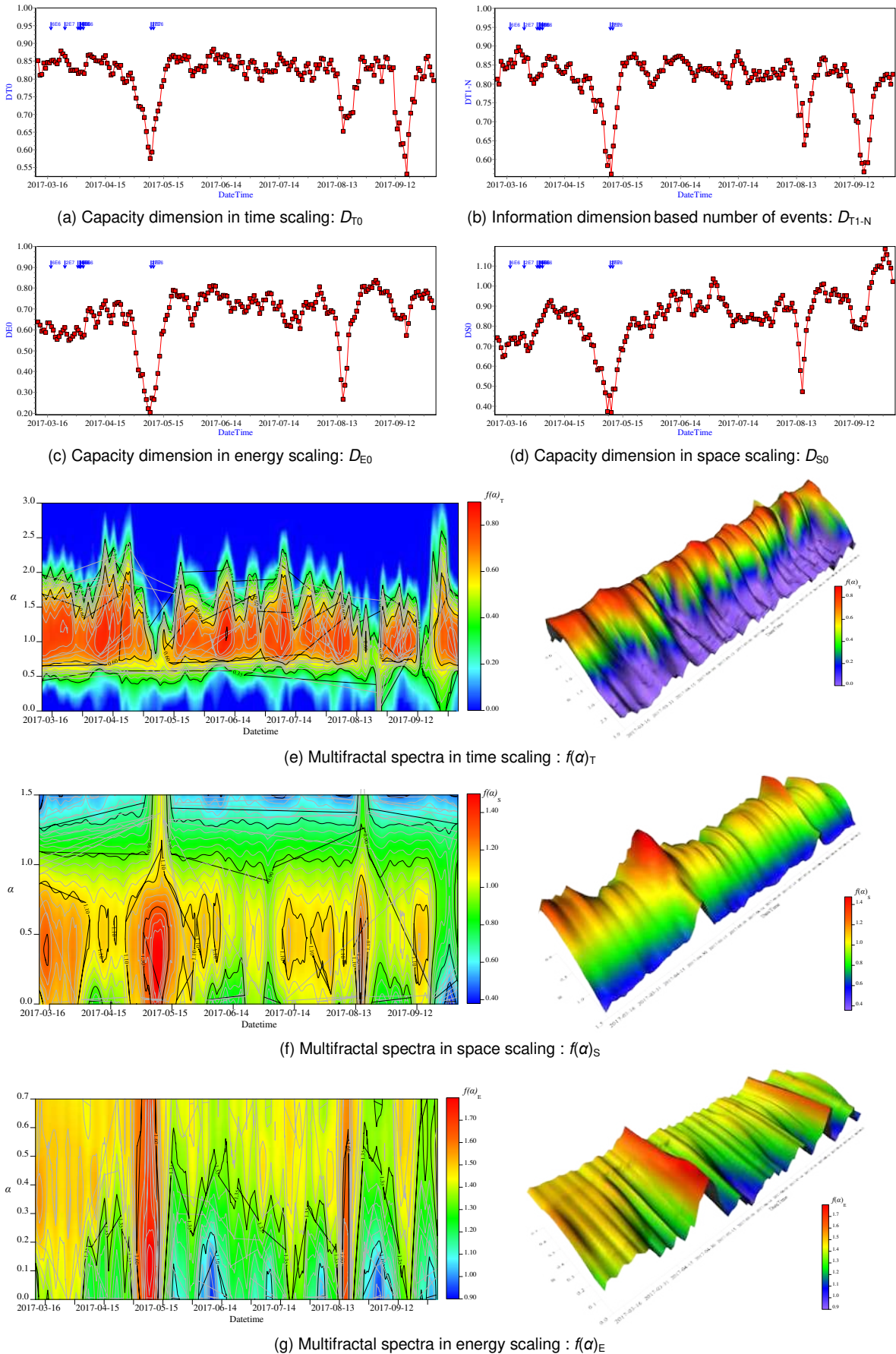


Figure 3.24 Fractal dimension based models applied to microseismic data at Coal Mine Velenje.

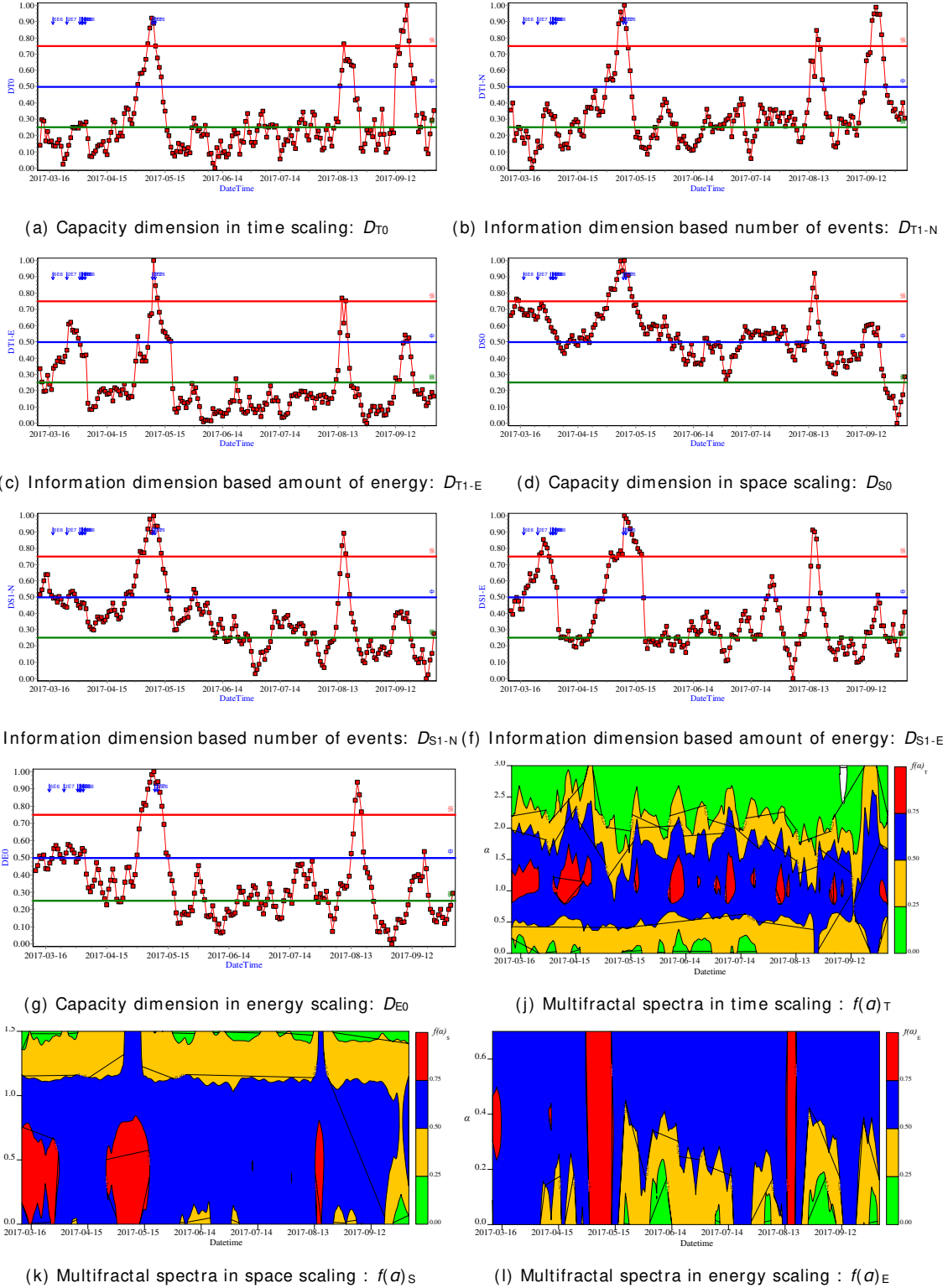


Figure 0.25 Normalisation of fractal dimension based models applied to microseismic data at Coal Mine Velenje.

Application of Fractal Dimension based models for the short-term forecasting of rock bursts and gas outbursts at Budryk Colliery

Figure 3.26 presents the spatial and temporal distribution of microseismic events at Budryk colliery during the ten months mining period between 20/11/2017 and 05/08/2018. Clear indication of the timing of shift changes, production periods during the period 05/05/2018, 03/06/2018 and 20/07/2018, and an increase in mining intensity in December 2017 can be observed from Figure 3.26(b).

Building upon the time sliding window method, the proposed fractal dimension models are plotted for the Budryk Colliery in Figure 3.27. It can be seen that, prior to most strong seismic events, there exists a distinct decline in the capacity dimensions D_{T0} , D_{S0} and D_{E0} , and the information dimensions D_{T1-N} , D_{T1-E} , D_{S1-N} , D_{S1-E} , D_{E1-N} , and D_{E1-E} . This decline has been widely known as dimension reduction. As for the multifractal spectra of $f(\alpha)_T$, $f(\alpha)_S$ and $f(\alpha)_E$, their envelop areas become larger, corresponding to the red high value zone in the figure.

As explained before, different forecasting models are sensitive to different event inducing factors. In the case of Budryk Colliery, D_{T1-N} , D_{T1-E} , D_{S1-N} , D_{S1-E} , D_{E1-N} , $f(\alpha)_T$, $f(\alpha)_S$ and $f(\alpha)_E$ have all shown good performance to extract the precursors of all strong seismic events, but others were not able to identify all of them, especially for the events that occurred in July 2018. It could be concluded that the microseismic time and energy aspects were the sensitive elements in response to the major event inducing factors of rock bursts and gas outbursts at Budryk colliery over this period.

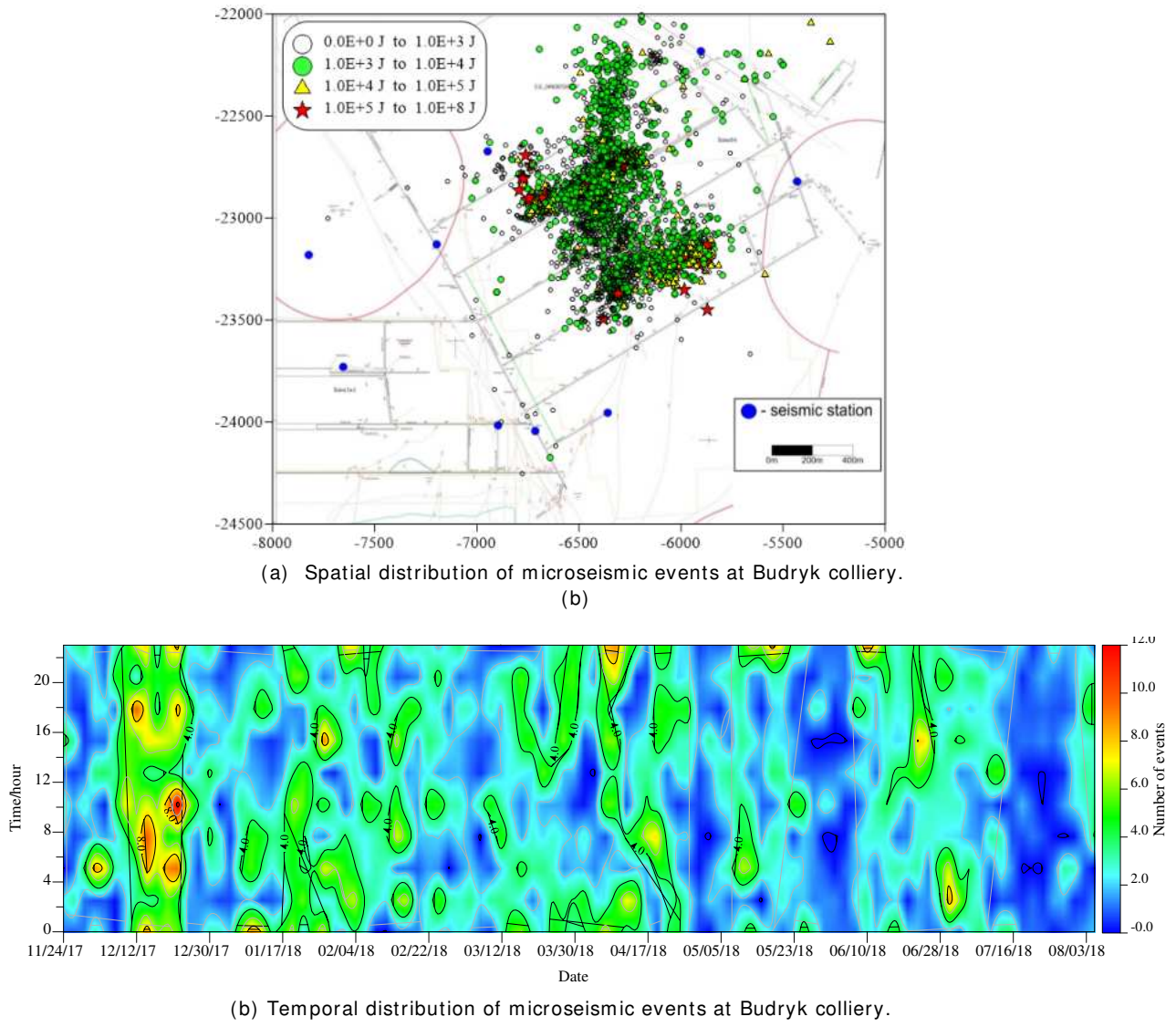


Figure 3.26 Microseismic monitoring at Budryk colliery.

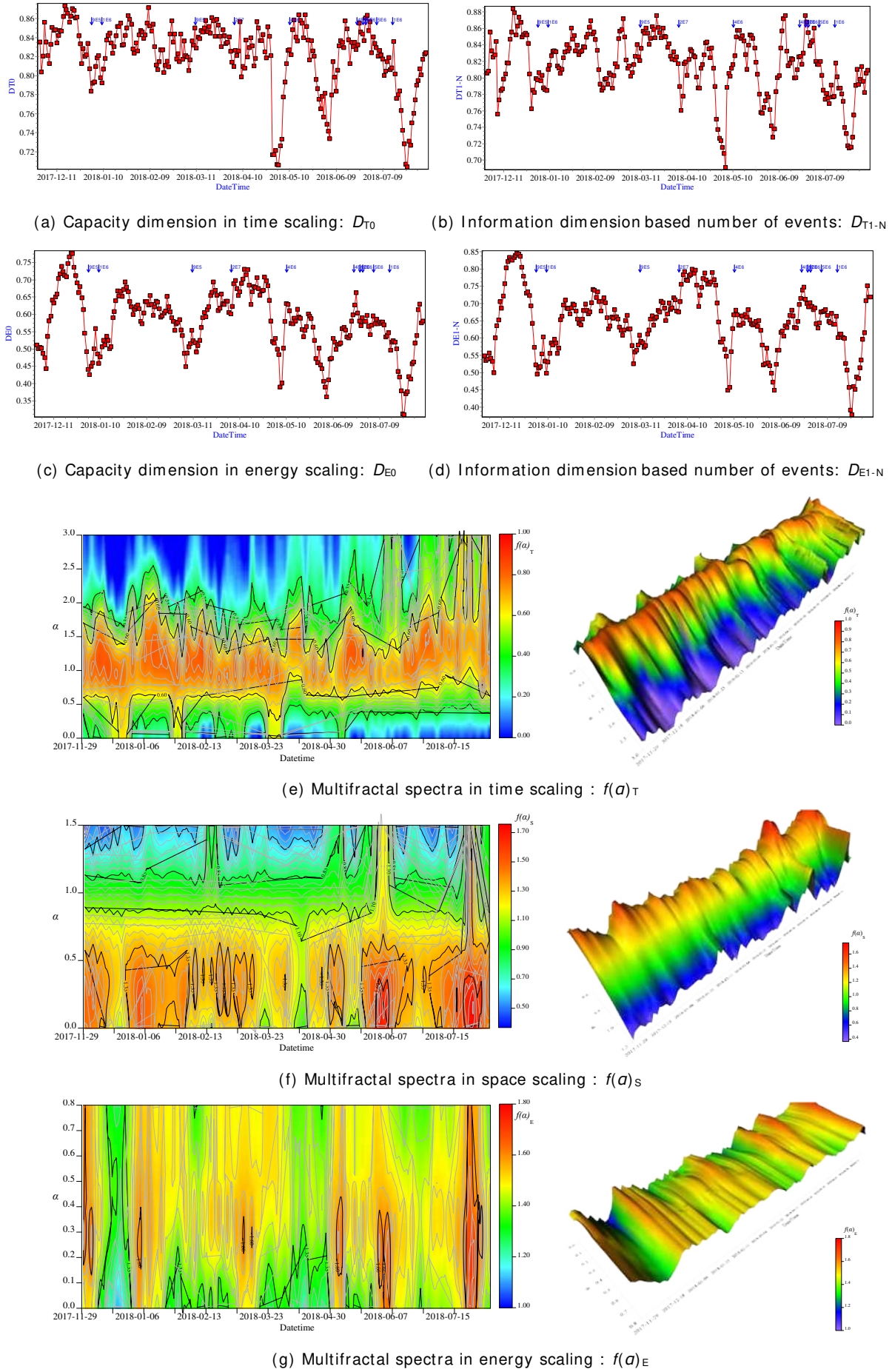


Figure 3.27 Fractal dimension based models applied to the microseismic data at Budryk Colliery.

Based on the normalised index defined in Equations in the detailed Deliverable D3.3 Report, the values of all fractal dimension based models were normalised into 0 to 1, as plotted in Figure 3.28. The sensitive models (D_{T1-N} , D_{T1-E} , D_{S1-E} , D_{E1-E} , $f(a)_T$, $f(a)_S$ and $f(a)_E$) indicate that strong seismic events were more likely to occur before the index reach the higher level.

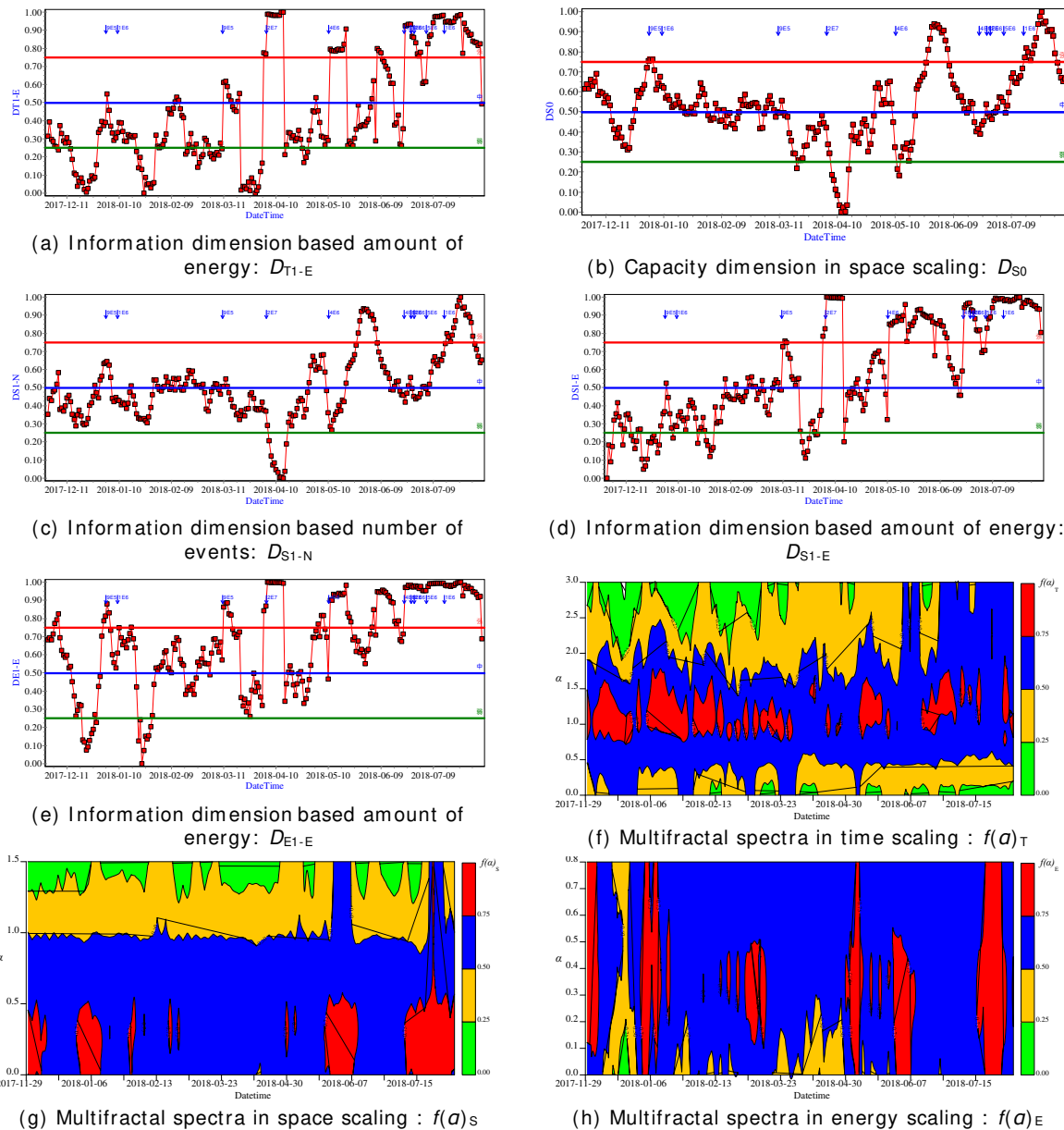


Figure 3.28 Normalisation of fractal dimension based models applied at Budryk Colliery.

Conclusions

Examples of the implementation of the fractal dimension based models developed are presented using the processed real time microseismic data from Coal Mine Velenje and Budryk Colliery, where both LTCC and the conventional longwall (LW) mining methods are adopted. Therefore, this allowed to develop universally applicable forecasting models for typical mining scenarios in coal mines. These models, characterised by the reduction in capacity and information dimensions and the large envelope area of the $f(a)$ - a spectrum without loss of generality, could be employed to provide precursors for rock bursts and gas outbursts.

WORK PACKAGE 4 - NUMERICAL MODELLING OF PERFORMANCE OF ROCK BURST AND GAS OUTBURST PREVENTION METHODS FOR RISK EVALUATION

This WP aimed at numerical modelling of the field application of the borehole stress/gas pressure relief methods as well as modelling stress control and protective mining options in different mine layouts relevant to common coal mining methods implemented in Europe. The main tasks of the WP were:

- Numerical modelling of rock burst and gas outburst prevention techniques using field tested borehole stress and gas pressure relief methods.
- Numerical modelling of rock burst and gas outburst prevention techniques using stress control mining.
- Numerical modelling of rock burst and gas outburst prevention techniques using protective mining.

Task 4.1 Numerical modelling of rock burst and gas outburst prevention techniques using field tested borehole stress and gas pressure relief methods (led by IMPERIAL, GIG, JSW, CM-VELENJE)

This Task aimed at modelling the borehole techniques tested in WP2 and assessing their application and performance for rock burst and gas outbursts control by stress relief in mining layouts commonly used at partner coal mines, mainly the Coal Mine Velenje in Slovenia and JSW Collieries in Poland

As the project progressed and different borehole drilling and stress relief methods were tested at Coal Mine Velenje and JSW Pniowek and Budryk Collieries, it was shown that large diameter boreholes drilled with up to 160 mm diameter at Coal Mine Velenje were very effective when drilled in the barrier pillar of LTCC panels and protect the mine infrastructure and the main central pillar as the longwall face approached the panel completion line.

Drilling and blasting activities were carried out with the use of relatively smaller diameter, shorter boreholes with relatively small charges, mostly in development headings when developing new longwall panels. It was found that blasting in these boreholes were effective within a relatively smaller area around the development headings where they were implemented, and increased permeability and released gas, leading to reduced risk of gas outbursts. On the other hand, high pressure water injection was tested at JSW's Budryk Colliery conclude that, when compared to the gas release achieved from drilling and blasting, the high pressure water injection was not very successful as a measure against gas outburst. Therefore, high pressure water injection was not considered for further modelling in the project.

The large (160 mm) diameter boreholes drilled in the barrier pillars of Coal Mine Velenje throughout the project formed the basis for the field testing and numerical modelling of stress relief boreholes and borehole slotting in this Task. A much detailed description of this work can be found in Deliverable D4.1 Report submitted

As the first step in modelling work under this task the stresses induced with and without using large diameter boreholes were analysed. In order to test the methodology numerically the layout of the large diameter boreholes drilled in the barrier pillar of Longwall Top Coal Caving Panel Bk. -80 at Coal Mine Velenje was used (Figure 4.1).

Model set up

The model geometry used honoured the subsurface dimensions of the area represented with physical dimensions of 90×25×40m (length×width×height) with in situ stress conditions adopted from the large scale long-term stress modelling work carried out under WP1 Task 1.3. The borehole diameters used were 160 mm as in the field applications at Coal Mine Velenje. A borehole spacing of 10 m was used for boreholes of 50 m length. Grid refinement was implemented around the large diameter boreholes to enable detailed analysis of the stresses around the boreholes and numerical modelling carried out in FLAC^{3D} (Figure 4.2). As the model was constructed in coal only due to the ultra-thick seam structure of Coal Mine Velenje, only coal geomechanical properties were used.

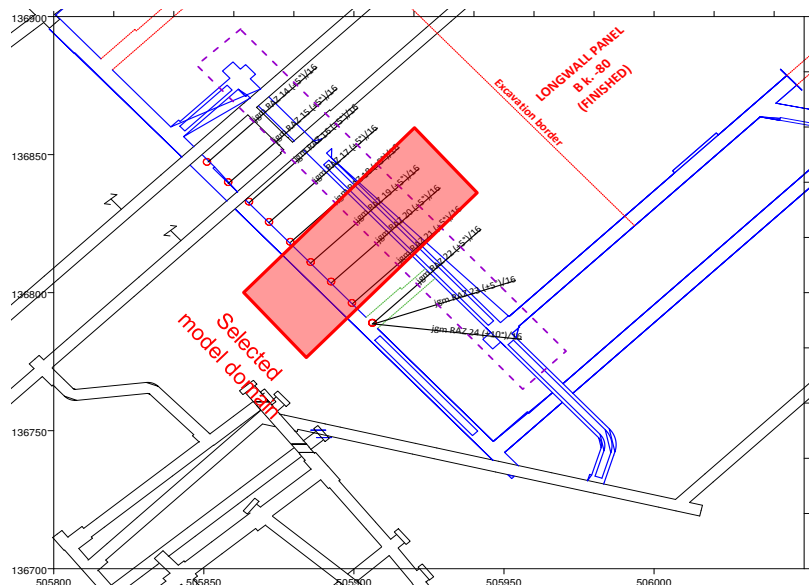


Figure 4.1 Schematic of the large diameter boreholes drilled in the barrier pillar of LTCC Panel B k. -80 at Coal Mine Velenje. The red boxed are represents the model domain.

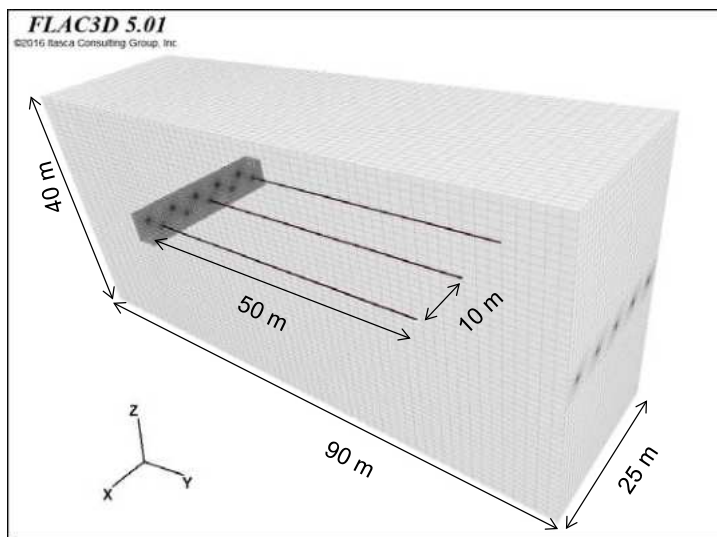


Figure 4.2 Model domain for the large diameter boreholes drilled in the barrier pillar of LTCC Panel B k. -80 at Coal Mine Velenje. The dark grey rectangular prism represents the main gateroad.

Modelling of large diameter boreholes for stress and gas pressure relief

The sequence of modelling included the development of the main gateroad first. The three large diameter boreholes at 10 m spacing were drilled in the model in the scenario with boreholes.

Large-scale modelling of the area in Task 1.3 has suggested that, as a result of previous mining activities, initial vertical stress over the modelled area varied from 22 MPa to 8 MPa along the y-axis reflecting the high stress concentration over the central pillar around the area where the main infrastructure is located (Figure 4.3 and Figure 4.4a). The analysis of the stress alteration induced by the drilling of large diameter boreholes was achieved by comparing the effect of longwall advance towards the barrier pillar with and without the large diameter boreholes. In both cases, a 5 step vertical loading was applied sequentially at the top boundary of the model to simulate the dynamic loading impact of an approaching face in the model (Figure 4.4a and b).

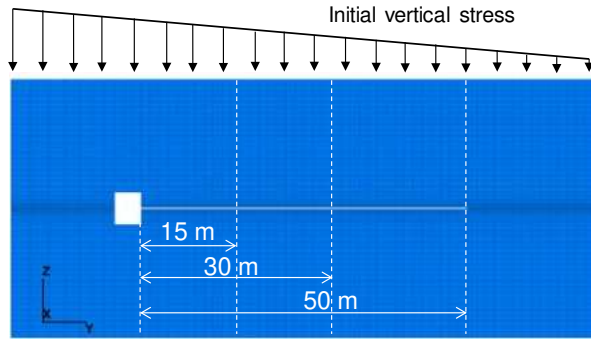


Figure 4.3 Initial stress conditions over the modelled area within the barrier pillar.

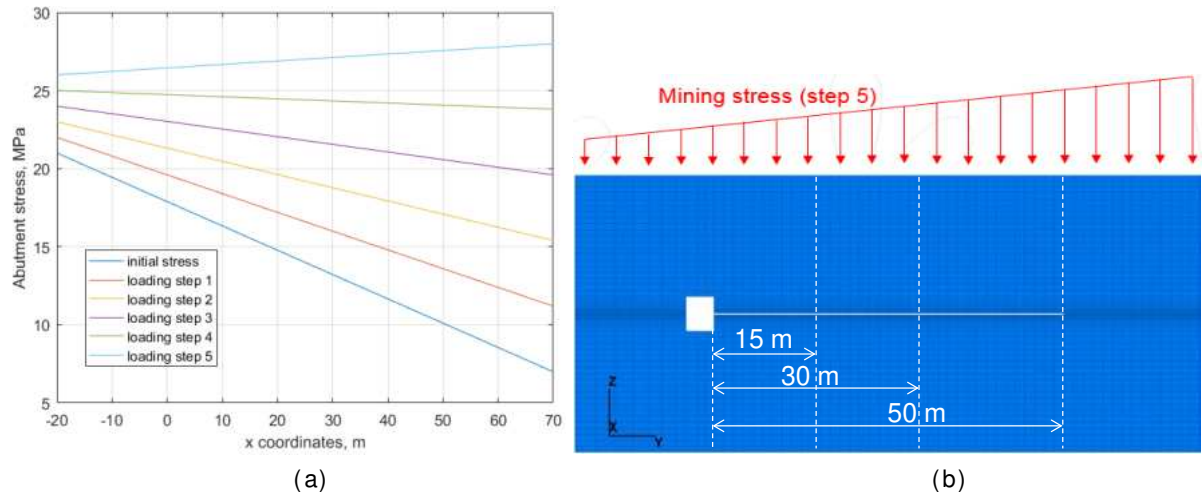


Figure 4.4 Simulation of the abutment stresses conditions within the barrier pillar in the modelled area due to the effects of approaching longwall face.

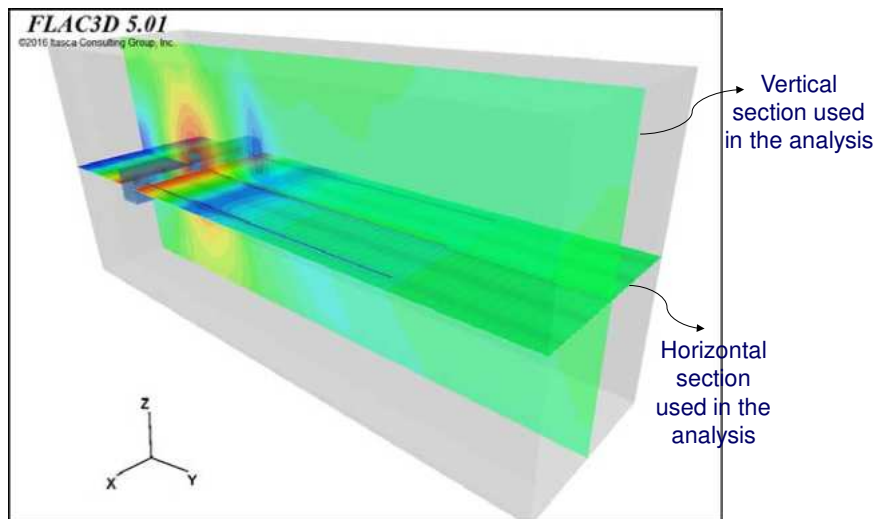


Figure 4.5 Schematic illustration of the position of vertical sections taken through the central borehole and the horizontal sections taken through three boreholes.

Results and discussion

The performance of 50 m long large diameter boreholes was evaluated by analysing the vertical and horizontal stresses over the barrier pillar as the face advanced towards the pillar (Figure 4.5).

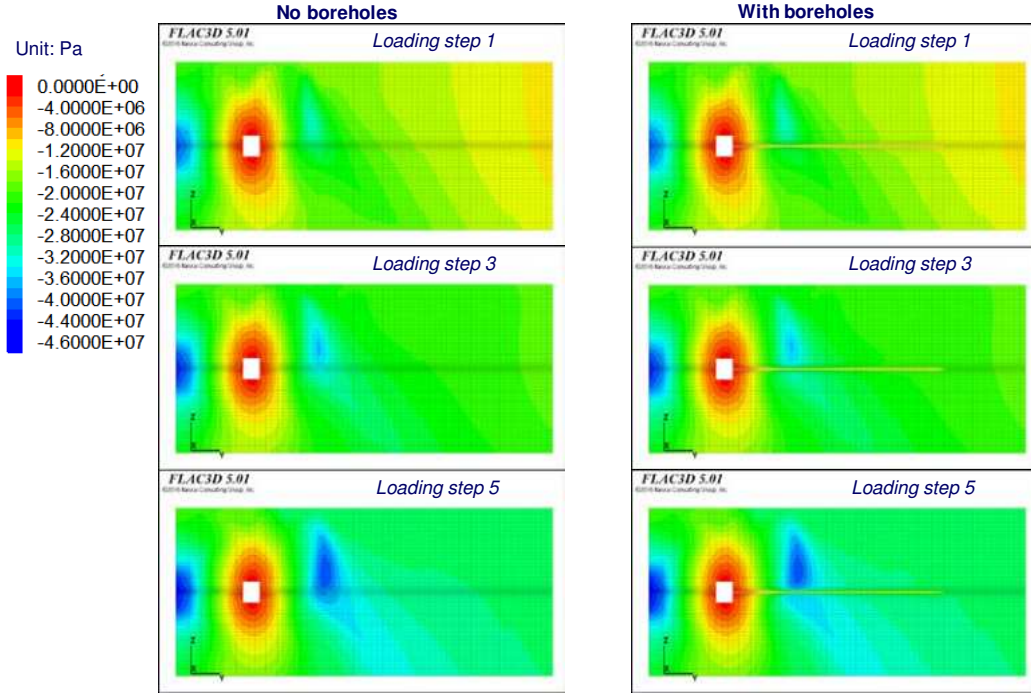


Figure 4.6 Vertical stress contours over the barrier pillar without and with large diameter boreholes as the longwall face approaches the pillar (vertical sections).

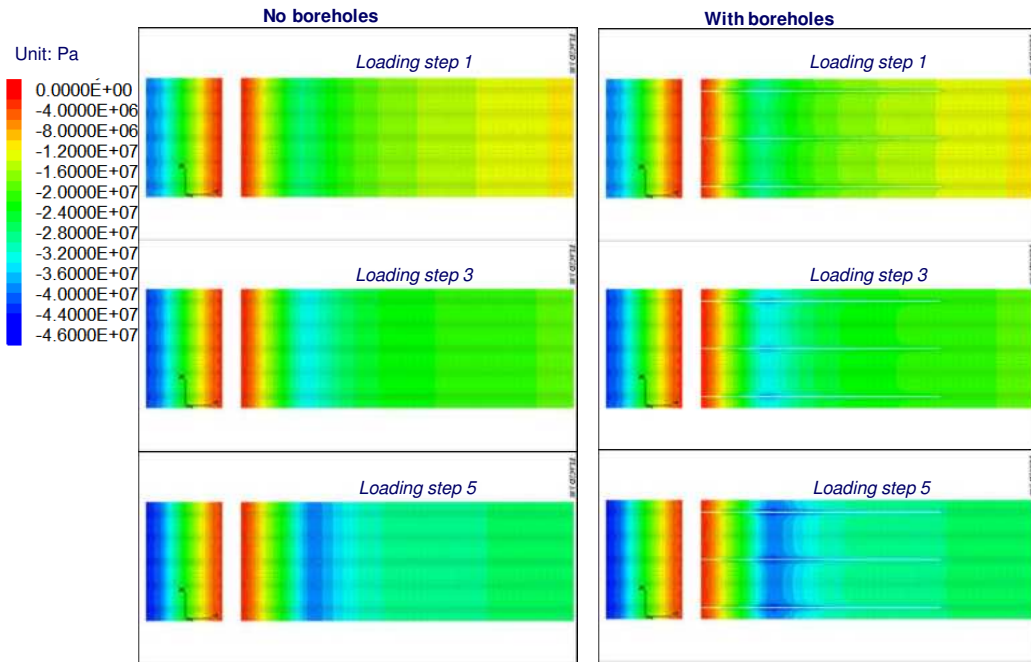
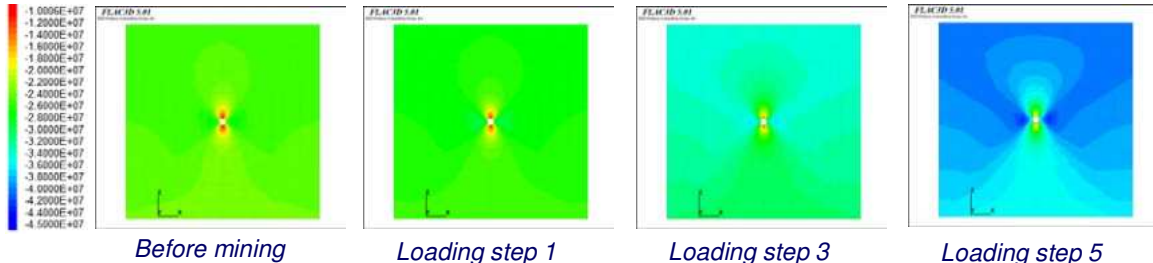


Figure 4.7 Vertical stress contours over the barrier pillar without and with large diameter boreholes as the longwall face approaches the pillar (horizontal sections).

Careful analysis of Figure 4.6 and Figure 4.7 suggest that although the boreholes themselves create a small abutment stress around them a slight stress relief away from the boreholes is also experienced. Furthermore, the analysis of vertical stresses over the boreholes on the vertical sections suggest that the stress abutment due to the approaching longwall face is slightly smaller over the pillar with the large diameter boreholes (Figure 4.6 loading step 5).

Analysis of the vertical stresses in the near wellbore region further demonstrate the development of a localised stress abutment close to the boreholes, particularly when the face is much closer to the boreholes (loading step 5 for vertical section 30m into the barrier pillar in Figure 4.8).

Vertical stress 15 m into the barrier pillar – vertical section



Vertical stress 30 m into the barrier pillar – vertical section

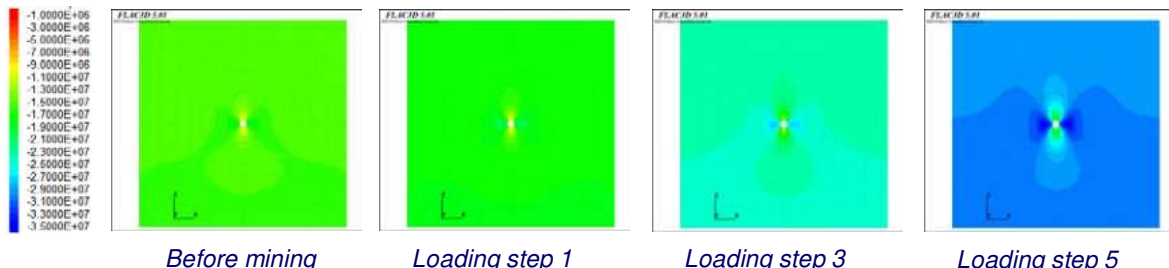


Figure 4.8 Near wellbore region vertical stresses on the barrier pillar illustrated using two vertical planes (vertical sections - please see Figure 4.9 for the position of the plane 30m into the pillar).

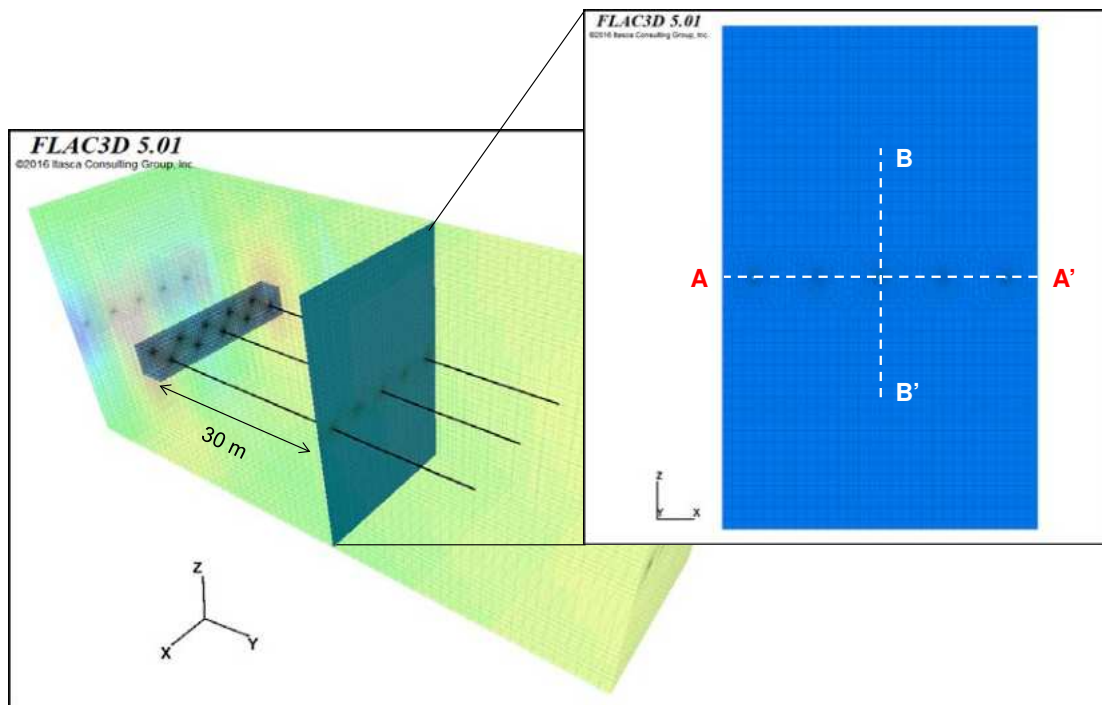
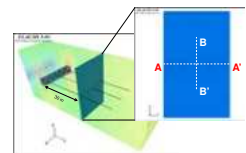


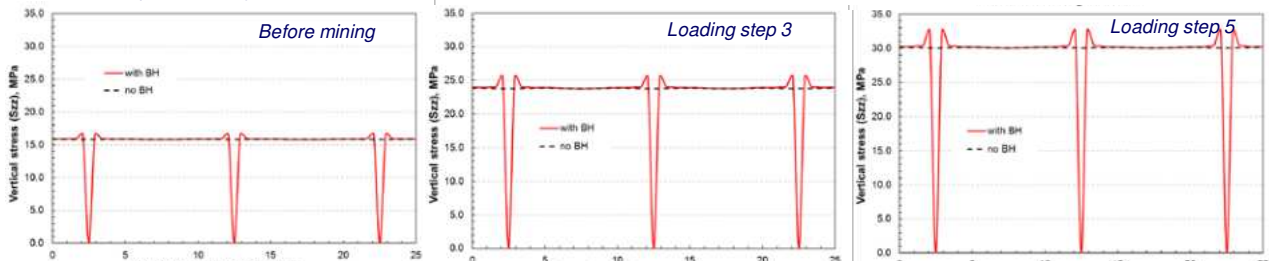
Figure 4.9 Vertical plane 30 m into the barrier pillar along which further stress analysis are carried out.

As Figure 4.10 and Figure 4.11 also illustrate, besides the small local abutment stresses generated by the large diameter boreholes, their stress relief impact is also relatively limited to the near-wellbore region, and the radius of influence is around 1-2 m.

These analyses suggest that, although effective as a stress and gas pressure relief technique, secondary stimulation methods such as blasting, hydraulic fracturing, and slotting may further improve the stress relief achieved if applied together with large diameter boreholes.

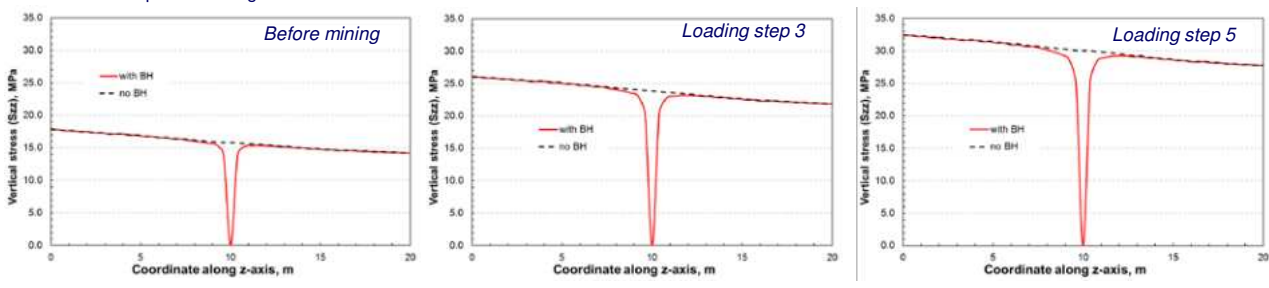


Vertical stress profiles along A-A'



(a)

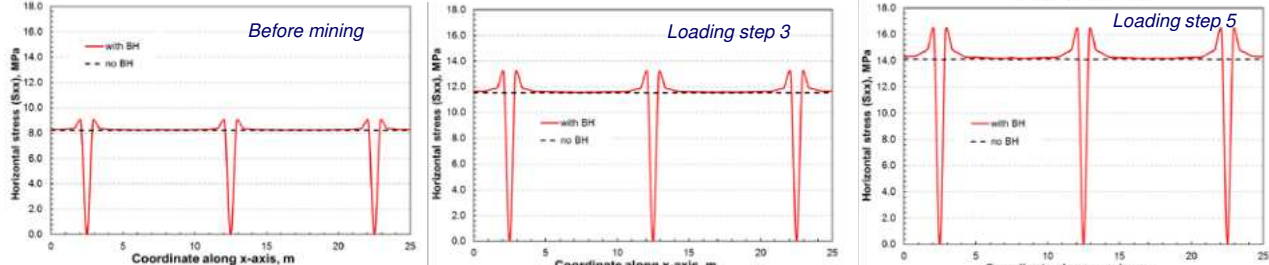
Vertical stress profiles along B-B'



(b)

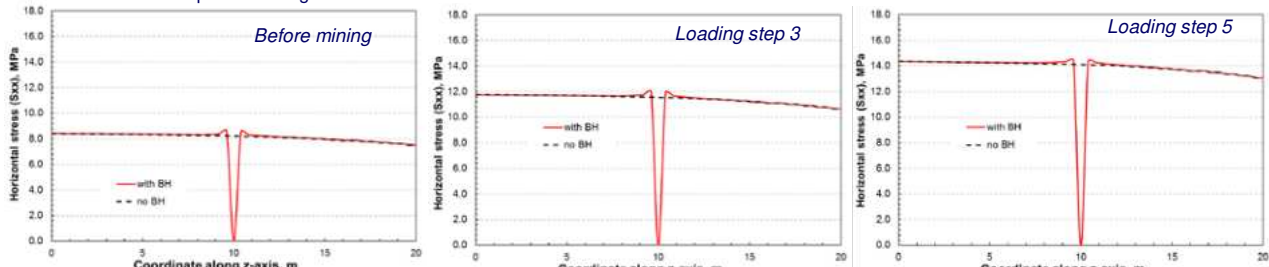
Figure 4.10 Vertical stress profiles over the barrier pillar as the face approaches (a) along A-A' and (b) along B-B' 30 m into the barrier pillar as illustrated in Figure 4.9 (with and without boreholes).

Horizontal stress profiles along A-A'



(a)

Horizontal stress profiles along B-B'



(b)

Figure 4.11 Horizontal stress profiles over the barrier pillar as the face approaches (a) along A-A' and (b) along B-B' 30 m into the barrier pillar as illustrated in Figure 4.9 (with and without boreholes).

Modelling of slot cutting in large diameter boreholes for stress and gas pressure relief

MapROC also investigated the performance of slotting coupled with large diameter boreholes for stress and gas pressure relief using the same Coal Mine Velenje barrier pillar layout that was used in Figure 4.2 for the purposes of comparison.

More recent fieldwork carried out to test slotting in underground boreholes at the Experimental Mine Barbara have shown that slot diameters of up to 1.5m can be achieved. Therefore, in MapROC, multiple slotting of large diameter (160mm) boreholes with 0.1m wide and 1.5m diameter slots with a spacing of 5m were tested to investigate their performance for stress and gas pressure relief.

As illustrated in Figure 4.12, 4 slots were simulated along the three large diameter boreholes in the barrier pillar of LTCC Panel B k. -80 at Coal Mine Velenje. The modelling procedure followed was the same as that followed for large diameter boreholes. The initial stress distribution over the barrier pillar is given in Figures 4.3 and 4.4a. The 5 step loading pattern and the sections used for the stress analysis are the same as those shown in Figures 4.5 and 4.9, as also shown below.

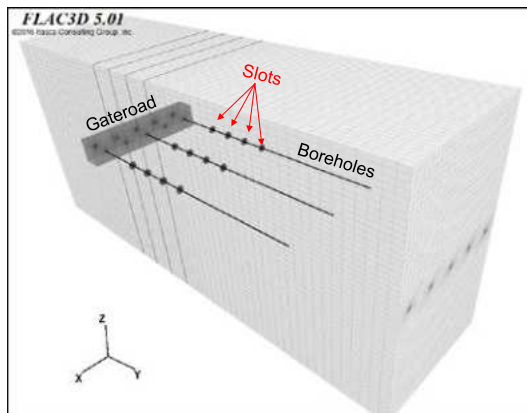


Figure 4.12 Model domain for the large diameter boreholes drilled with 4 slots each in the barrier pillar of LTCC Panel B k. -80 at Coal Mine Velenje.

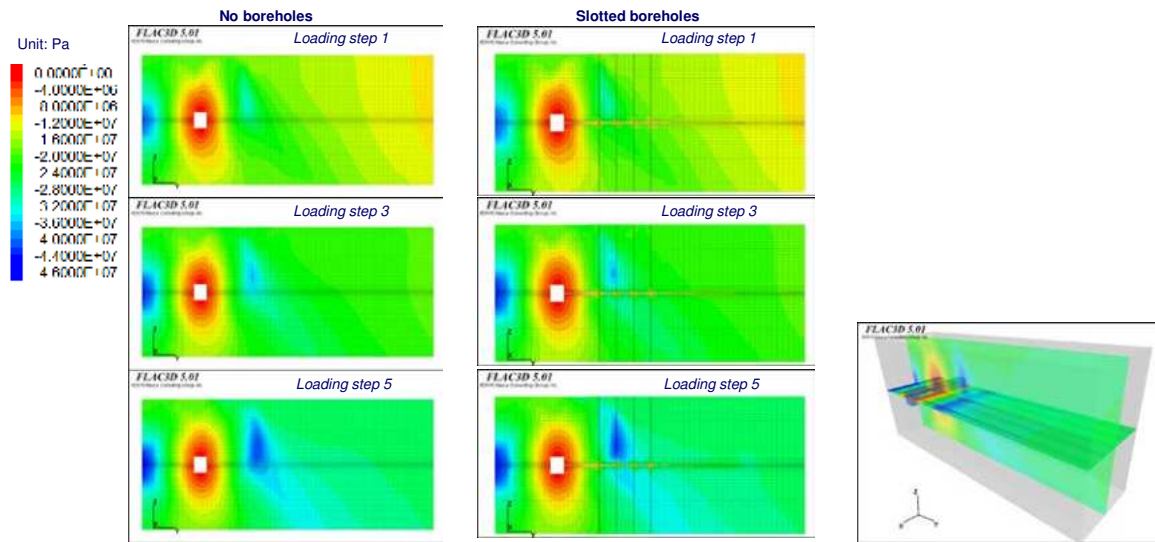


Figure 4.13 Vertical stress contours over the barrier pillar without and with slotted large diameter boreholes as the longwall face approaches the pillar (vertical sections).

As illustrated in Figure 4.13 and Figure 4.14, as the face advances towards the barrier pillar, the front abutment stress over the pillar is reduced further with the use of slotted boreholes (Figure 4.13) and, even with some further local abutment being generated, the stress relief zone widens and extends further between the boreholes as a result of slotting (Figure 4.14).

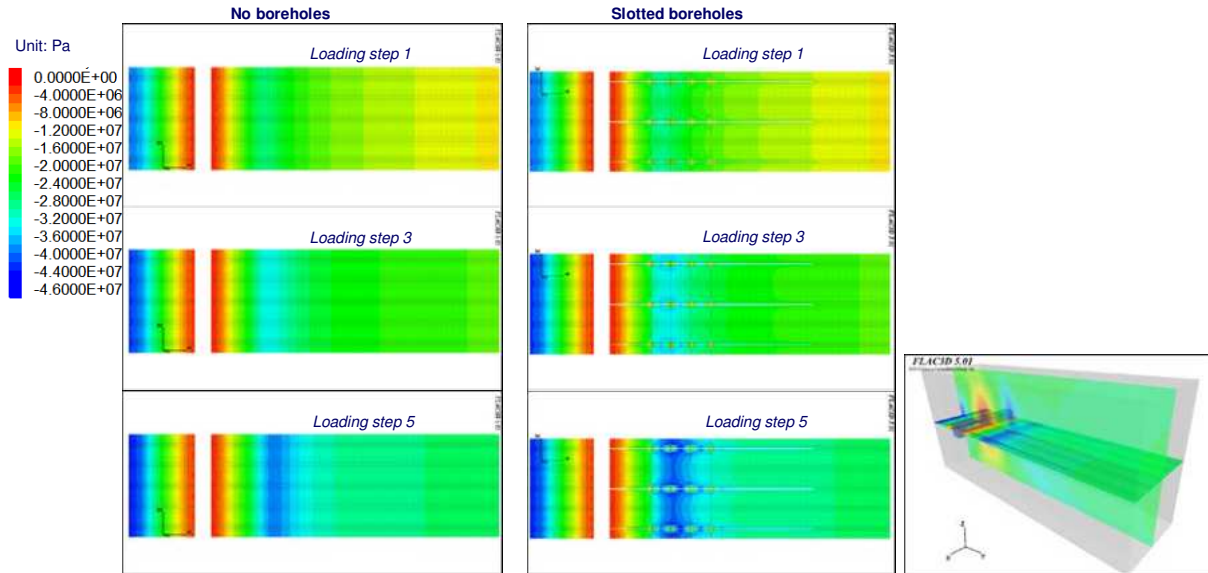


Figure 4.14 Vertical stress contours over the barrier pillar without and with slotted large diameter boreholes as the longwall face approaches the pillar (horizontal sections).

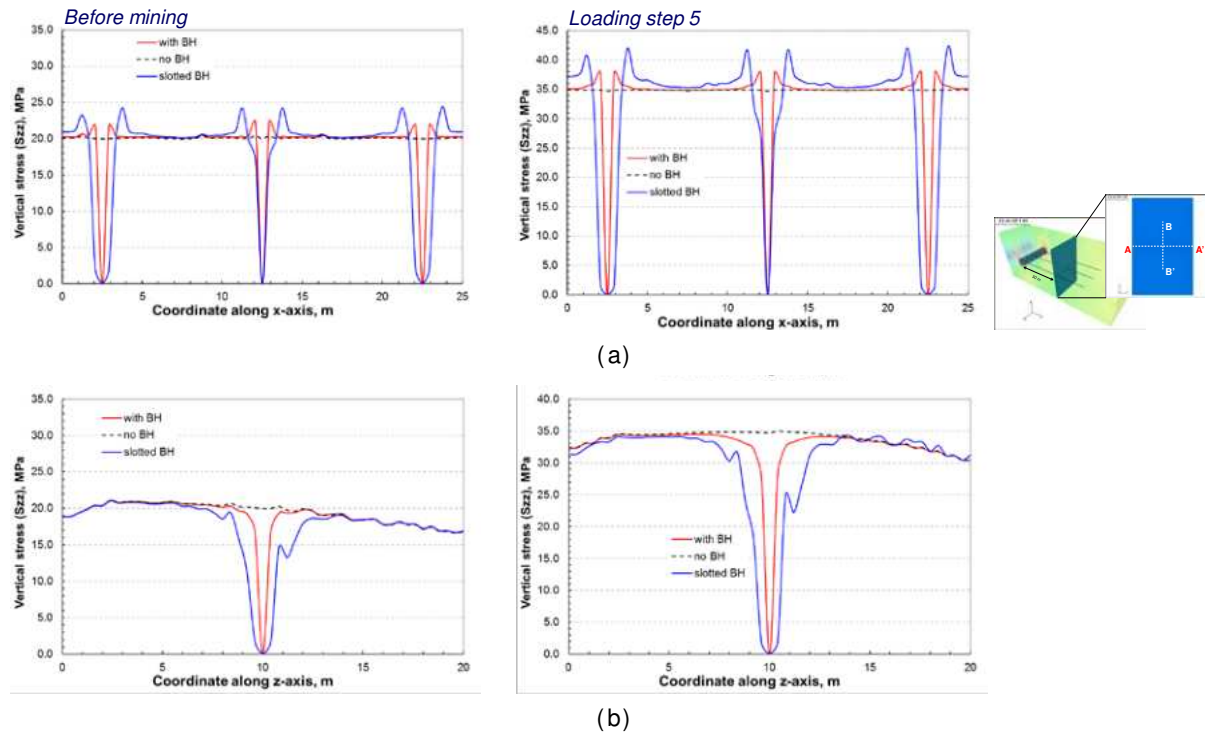


Figure 4.15 Comparison of vertical stress profiles over the barrier pillar as the longwall face approaches (a) along A-A' and (b) along B-B' 30 m into the barrier pillar as illustrated in Figure 4.9 (scenarios with no boreholes, with boreholes and with slotted boreholes).

Figure 4.15 compares the vertical stress profiles over the barrier pillar as the longwall face approaches to it. The scenarios compared include no boreholes, with boreholes and with slotted boreholes with the vertical stress profiles taken along A-A' and B-B' sections 30 m into the barrier pillar as illustrated in Figure 4.9. The localised stress abutment increase around the slotted boreholes is even more evident in this case (Figure 4.15a), however, the vertical stress relief over the slotted boreholes in the vertical plane is also more pronounced, widening the area of influence over the pillar around the slotted boreholes (Figure 4.15b).

Task 4.2 Numerical modelling of rock burst and gas outburst prevention techniques using stress control mining (led by IMPERIAL, GIG, JSW, CM-VELENJE)

Task 4.2 in WP4 aimed at designing mining layouts using sacrificial roadways and/or pillars for stress/gas pressure relief and gas outbursts/rock burst control in coal mining and assess their performance and evaluate risk. To minimise the occurrence of rock bursts and gas outbursts, it is prudent to design the pillars and longwall panels in a manner that the stress acting on these pillars is minimised. This can be achieved by designing the pillars to an optimum geometry which is enough to take the development stress but subsequently yields when the stress increases upon extraction of the longwall panel without accumulating a large amount of vertical stress or elastic strain energy. A detailed analysis of the yield pillar technique is discussed first, and subsequently, optimisation of mining layout is undertaken by laterally shifting the roadway locations in case of multi-seam workings.

Based on the state-of-the-art literature review of previous approaches, and in consideration of the current longwall mining methods implemented at industrial partners CM-VELENJE and JSW, two feasible approaches have been designed. These are:

- I. Design of sacrificial or yielding pillars to make sacrificial roadways
- II. Design of eccentric mine layout in multi-seam workings to strategically locate the roadways.

The designed scenarios were modelled using FLAC3D™ and the resulting stress redistributions in the coal and surrounding coal measures strata were analysed to evaluate performance. The analysis of sacrificial roadways/yield pillar design and eccentric mining layouts are discussed briefly here.

Sacrificial roadways/Yield pillars

To optimise the dimensions of yield pillars, eight different layouts corresponding to yield-abutment (2-entry) and yield-abutment-yield (3-entry) concept of yield pillar designs were analysed in FLAC3D™. Schematic layouts of the 2-entry system are shown in Figure 4.16. Representative schematic layouts of the 3-entry system are shown in Figure 0.17.

Model development

A 3-dimensional numerical model was developed in FLAC3D with a model dimension of $300 \times 300 \times 150$ m, having a grid size of $5 \times 5 \times 2$ m along X-, Y-, and Z- directions, respectively. The geometry of the model was fixed as- a) the length of the longwall panel- 300m, b) the width of the longwall panel- 150m, c) the length of the chain pillars- 70m, d) the width of the chain pillars- 50m e) the width of the yield pillars- 5m and f) the width of the roadways- 5m, for all eight schematic layouts designed to analyse the behaviour of yield pillars in FLAC3D™. Each layout was parametrically varied as per the variations listed in Table 4.1.

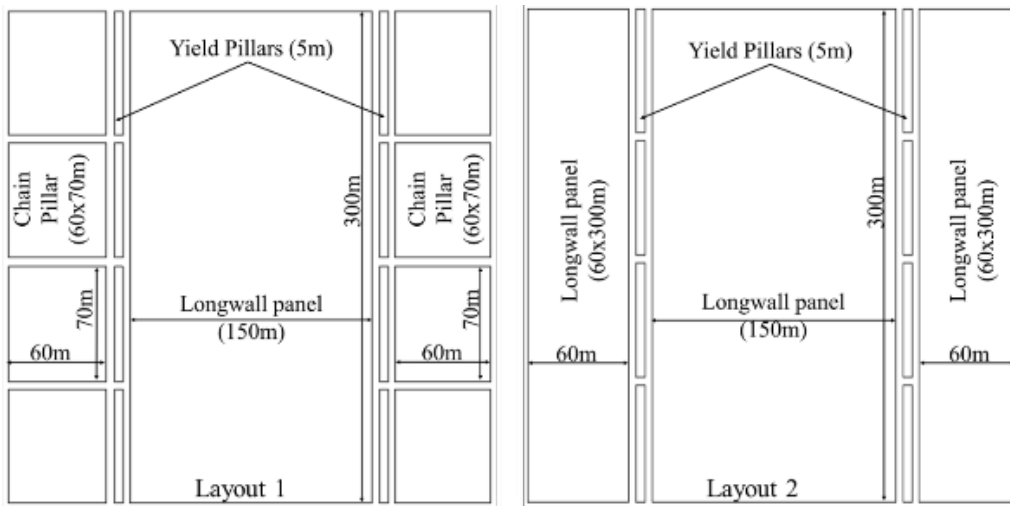


Figure 4.16 Schematic mining layout of a 2-entry (single row) abutment-yield pillar system.

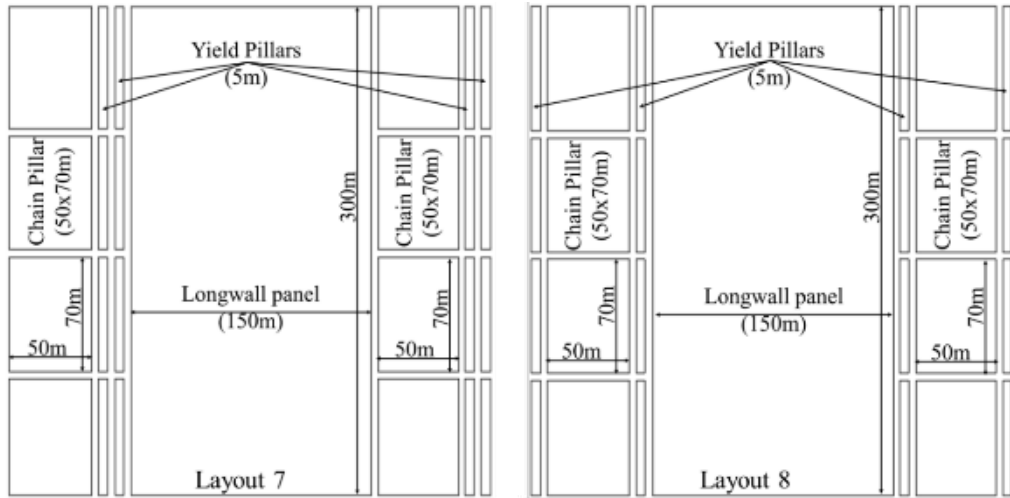


Figure 0.17 Representative schematic mining layout of a 3-entry (two-rows) yield-abutment-yield pillar system.

Table 4.1 Parametric variations in the yield pillar design

Parameters	Variations
Mining depth	600m, 800m, 1000m, 1200m
No. of rows of Yield pillars	1, 2
Yield pillar width	5m, 10m, 15m, 20m
Chain pillar width	50m, 60m
The height of coal extraction	2m, 4m

Analysis of 2-entry abutment-yield pillar layouts

Different layouts were simulated in the developed numerical model as per the designed geometry with a row of yield pillars and a row of chain pillars on either side of the longwall panel as shown in Figure 4.16. The deflection of the roof was evaluated for all the parametric variations to determine the suitable layout. It was observed that the deflection of the roof was around ~16mm for a coal seam thickness of 2m while the deflection was ~80mm for a coal seam thickness of 4m at a mining depth of 1,200m. Similar trends were observed at lower mining depths. It was also observed that yield pillars with the width to height ratio >2, had an inflection in the deflection profile which suggests that such pillars do not yield due to the presence of an insufficient elastic core at the centre of the pillar as shown in Figure 4.18. Error! Reference source not found.

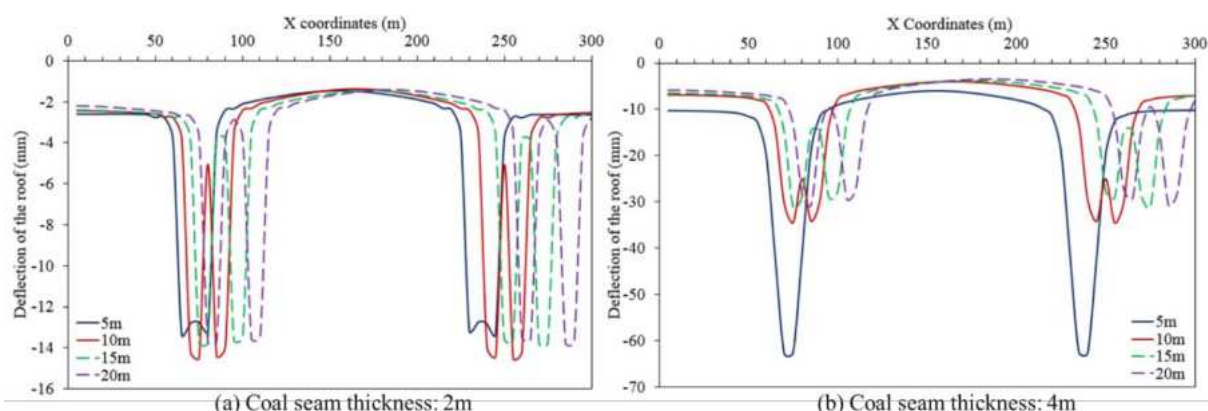


Figure 4.18 Variation in the deflection of the roof with varying yield pillar thickness at a mining depth of 1,000m for a coal seam thickness of (a) 2m and (b) 4m

A representative vertical stress contour developed in the panel for layout 1 is shown in Figure 0.19a. A representative elastic strain energy contour developed in the panel for layout 1 is shown in Figure 0.19b.

It was observed that the vertical stress reaches a peak of around ~50 MPa for a coal seam thickness of 2m at a mining depth of 1,200m. No peak was observed in the vertical stress profile for a coal seam thickness of 4m as shown in Figure 4.20. It was also observed from the figure, that the vertical stress acting on the yield pillar was significantly less than the abutment stress acting on either side of the yield pillar for a coal seam thickness of 4m. Moreover, the maximum vertical stress developed in the yield pillar is equal to the *in-situ* stress state for a coal seam thickness of 4m. This suggests that a lower thickness pillar gradually yields for a coal seam thickness of 4m due to the width-to-height ratio <2. However, a 5m thick yield pillar does not yield for a coal seam thickness of 2m due to the presence of an insufficient elastic core at the centre of the pillar which accumulates more vertical stress resulting in a stress peak. Such dimensions would fall in the critical pillar category and are liable to burst. The magnitude of vertical stress acting on the yield pillar is similar for an increase in the yield pillar thickness.

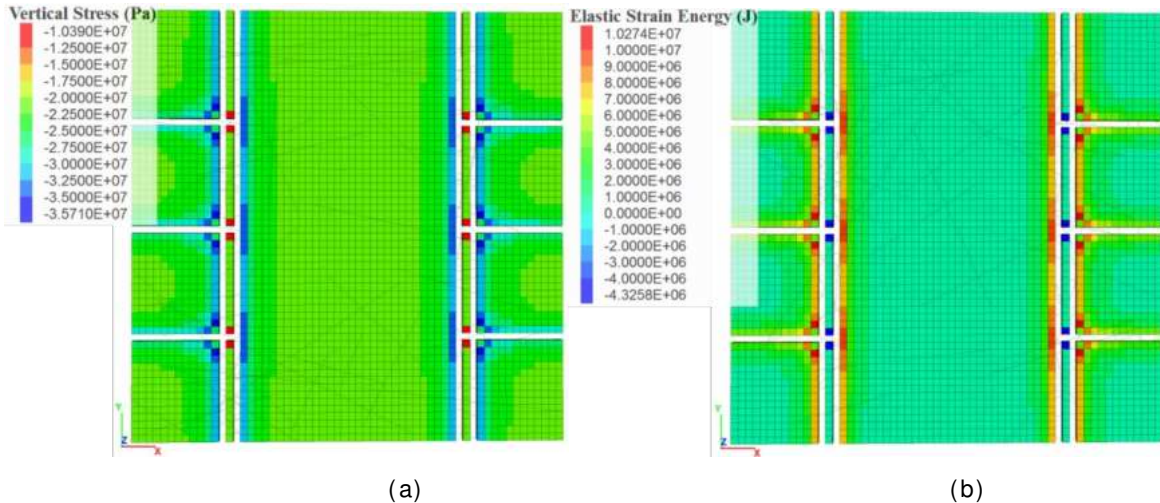


Figure 0.19 Representative layout of (a) Vertical stress contour, (b) Elastic strain energy contour, developed in the panel for Layout 1 for a coal seam thickness of 4m with a yield pillar thickness of 5m.

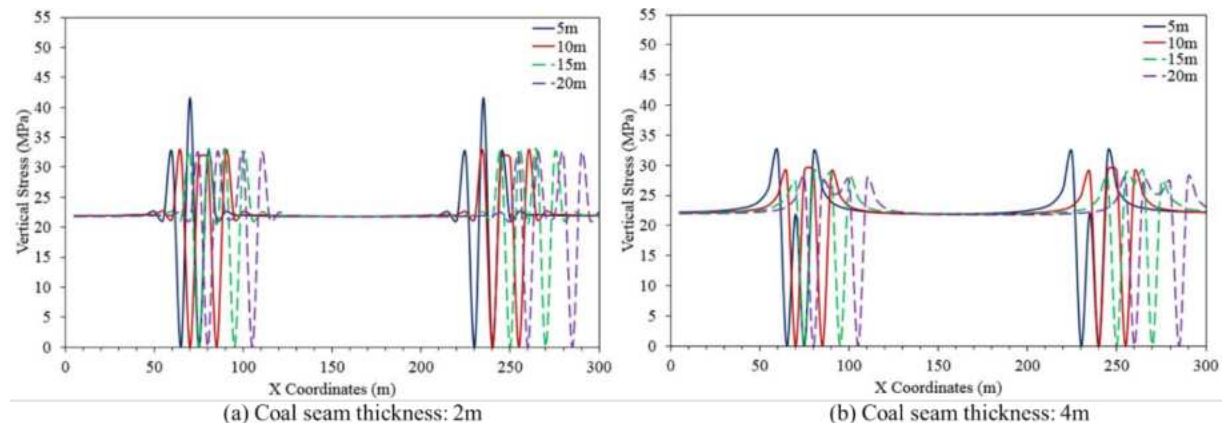


Figure 4.20 Variation in the vertical stress profile with varying yield pillar thickness at a mining depth of 1,000m for a coal seam thickness of (a) 2m and (b) 4m.

The elastic strain energy accumulated in the coal seam for different thickness of yield pillars is shown in Figure 4.21. It was observed from the figure that the elastic strain energy accumulated in the yield pillar reaches a peak for a coal seam thickness of 2m. No such peak was observed in the total elastic strain energy accumulated in the yield pillar for a coal seam thickness of 4m.

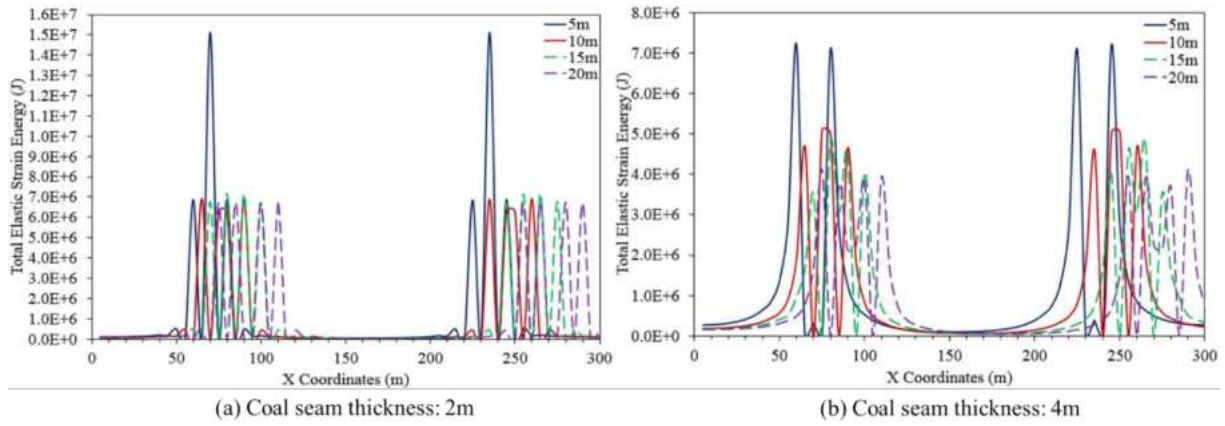


Figure 4.21 Variation in the total elastic strain energy with varying yield pillar thickness at a mining depth of 1,000m for a coal seam thickness of (a) 2m and (b) 4m.

The elastic strain energy accumulated in the yield pillar is significantly less as compared to the elastic strain energy accumulated in the longwall panels for a coal seam thickness of 4m. The trend is similar at all mining depths. Hence, it can be concluded that a yield pillar should have a width to height ratio less than 2, to ensure that the pillars do not fall into the critical pillar category.

Analysis of 3-entry yield-abutment-yield pillar layouts

Six different combinations were considered to determine the optimum layout for a 3-entry yield-abutment-yield pillar system, representative layouts are shown in Figure 0.17. Similar analysis as detailed above for 2-entry abutment-yield pillar system was carried out by varying the input parameters. It was observed that symmetrical layouts offer better ground control conditions in terms of the deflection of the roof, vertical stress acting on the yield pillars and elastic strain energy accumulation in the yield pillars. A detailed analysis is presented in the deliverable D4.2 report. The variation in maximum deflection of the roof, maximum vertical stress acting on the pillars/panels and the maximum elastic strain energy accumulated in the pillars/panels in the coal seam was compared for different layouts as shown in Figure 4.22.

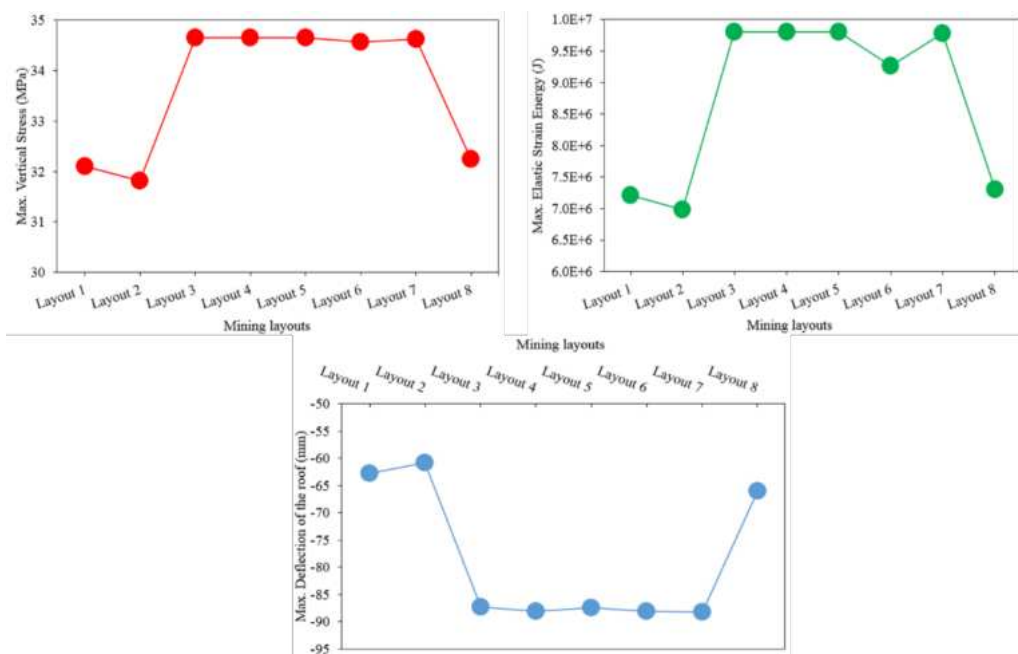


Figure 4.22 Comparative variation in the maximum deflection, maximum vertical stress and maximum elastic strain energy accumulation for different mining layouts for a 5m thick yield pillar having a coal seam thickness of 4m at a mining depth of 1000m.

Based on the parametric analysis of different layouts it was concluded that the symmetrical layouts facilitate uniform stress redistributions around the mining panel, as a result of which, the deflection of the roof and the elastic strain energy accumulated in the seam is relatively less. Hence, the

chances of rock bursts or gas outbursts can be significantly reduced by symmetrically designing the panels.

Eccentric mining layouts

In order to determine the optimum location of roadways in a lower seam for a multi-seam working, several eccentric mining layouts were designed for a 2-entry pillar system with a rib pillar flanked by longwall panels on either side. Layout 2 (2-entry layout with a yield pillar flanked by longwall panels on either side, as shown in Figure 4.16) was found to be the most feasible layout in terms of the deflection of the roof, vertical stress and elastic strain energy accumulation. Layout 2 was modified for this analysis by increasing the width of the yield pillar and by considering it to be a continuous rib pillar on either side of the longwall panel. Several mining layouts were designed by laterally shifting the roadways location in the right side at 10m interval. The designed eccentric mining layout is shown in Figure 4.23.

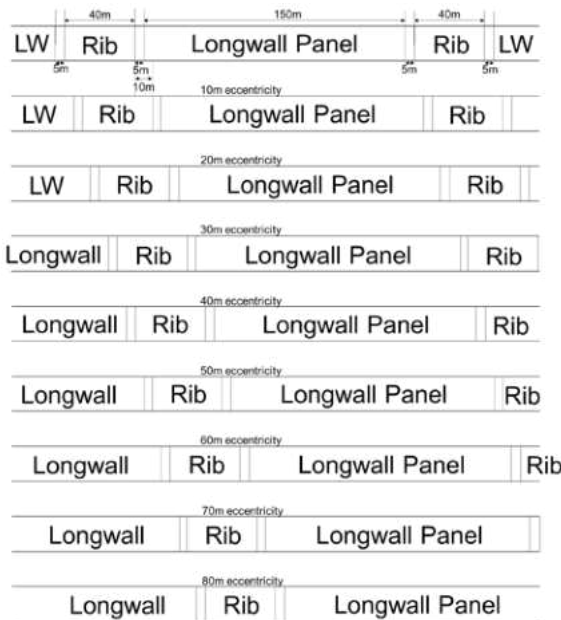


Figure 4.23 Eccentric mining layouts for roadway development in multi-seam workings.

The upper coal seam (Coal 1) was developed as per the dimensions as shown in Figure 4.23 to form roadways, rib pillars and longwall panels. The central longwall panel was then sequentially extracted by removing a volume of $150 \times 5 \times 2$ m along X-, Y- and Z- directions respectively in each excavation step by using the null constitutive model in FLAC3D™. After solving for 500 timesteps, the excavated volume was reinstated using an elastic constitutive model in FLAC3D™ representing recompacted goaf material with significantly low geomechanical properties. A representative model layout for an interbedding thickness of 24m is shown in Figure 4.24.

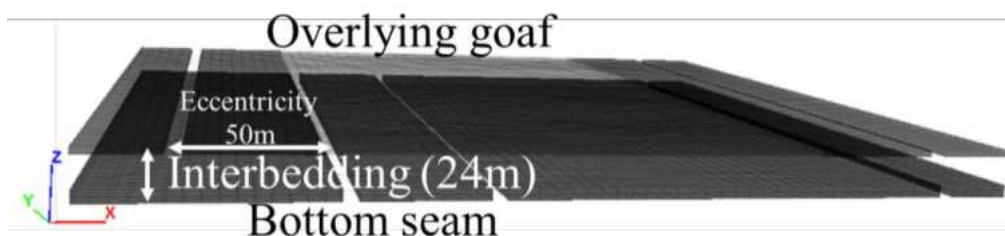


Figure 4.24 A representative mining layout showing an interbedding thickness of 24m for a 50m eccentric roadway development.

The vertical stress profiles in the upper seam and lower seam due to the development and extraction of coal from the longwall panel in the upper seam, and subsequent formation of overlying goaf is shown in Figure 4.25. It is observed that the vertical stress accumulates in the lower seam just beneath the existing roadways in the upper seam, however, the stress decreases towards the centre of the panel. Moreover, the vertical stress is roughly near *in-situ* stress in the middle section of the longwall panel where the caved material is expected to be recompacted.

A comparative analysis of the deflection of the roof in the lower seam for different eccentric layouts is presented in Figure 4.26. The deflection profile of the roof is mostly comparable for the three eccentric values shown in the figure. However, the comparative deflection plot for different eccentric values shows that the maximum deflection is achieved for an eccentricity of 70m.

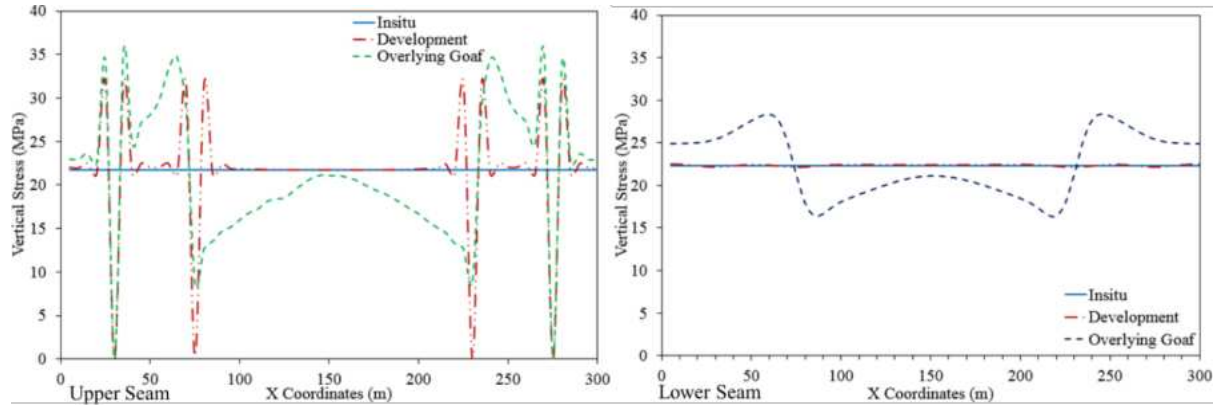


Figure 4.25 Vertical stress profile in the upper and lower seam due to existing overlying goaf.

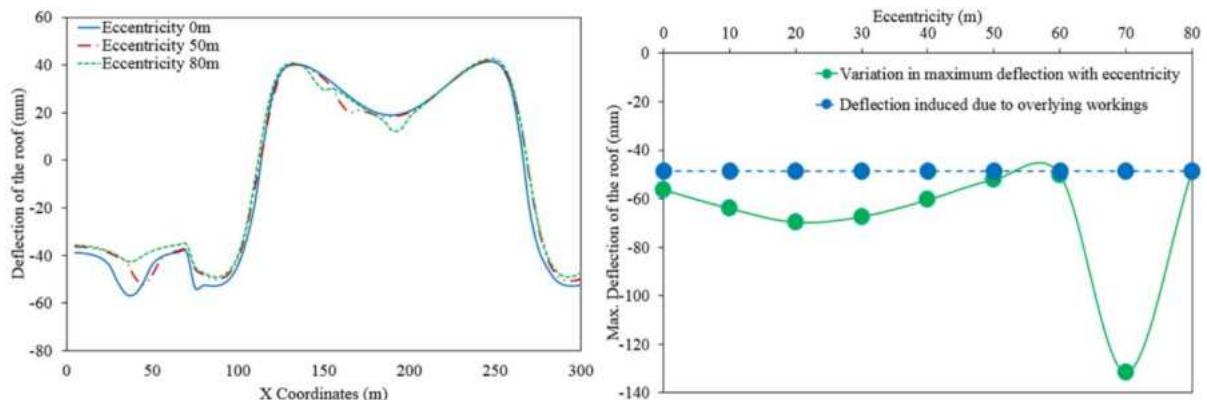


Figure 4.26 Deflection of the roof in the lower seam at different eccentricities.

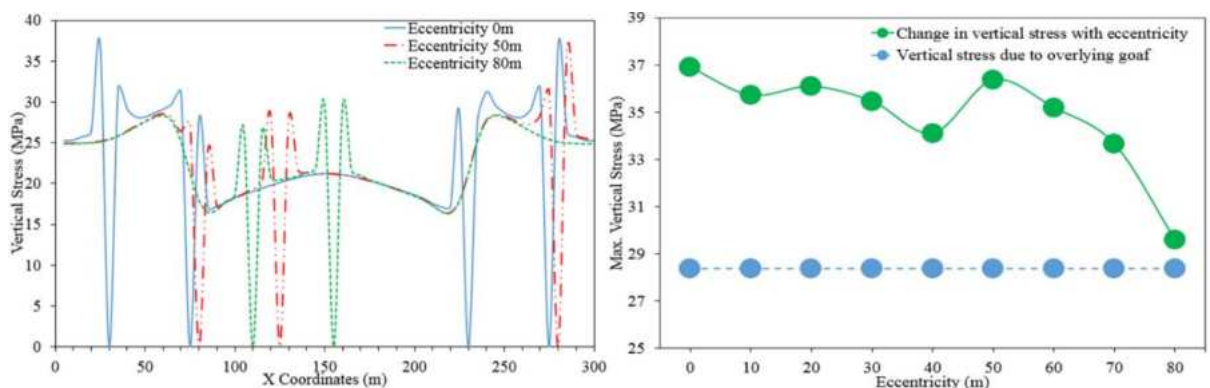


Figure 4.27 Variation in the vertical stress profile in the lower seam at different eccentricities.

A comparative analysis of the vertical stress acting on the rib pillars and longwall panels are shown in Figure 4.27. The vertical stress is more evenly distributed in case of eccentric mining layouts. A comparison of maximum vertical stress acting on the rib pillars and longwall panel suggests that the vertical stress decreases until 40m eccentricity and rises again for 50m eccentricity but subsequently decreases with further increase in eccentricity with a minimum value occurring at 80m eccentricity. Hence, from the comparative analysis, it was concluded that the roadways in the lower seam should be shifted laterally by at least 70m.

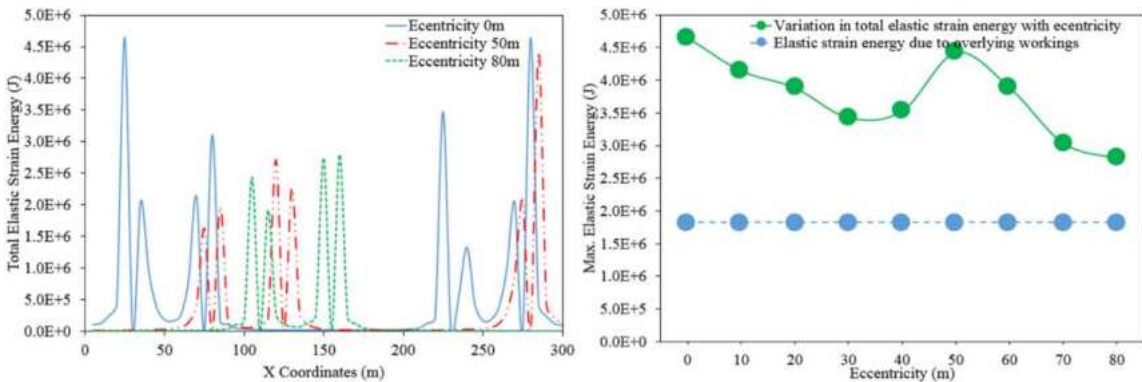


Figure 4.28 Variation in the elastic strain energy in the lower seam at different eccentricities.

Similar observations can be made from the comparative analysis of the elastic strain energy profile as shown in Figure 4.28. The elastic strain energy profile for 50m eccentricity has lesser values around the panel but takes a peak towards the right-hand side which suggests that the tailgate will be vulnerable to rock bursts. From the comparative graph of the maximum elastic strain energy accumulated in the lower seam, it was observed that the elastic strain energy decreases up to 40m eccentricity and then peaks at 50m eccentricity after which it decreases subsequently for an increase in eccentricity.

Conclusions

Based on the analysis of different dimensions of the yield pillar, it was concluded that in case of yield pillars having width to height (w/h) ratio slightly over 2 (e.g. for a yield pillar width of 5m for a coal seam thickness of 2m), a significant amount of vertical stress and elastic strain energy accumulates due to insufficient width of the elastic core. Such pillars fall in the critical pillar category which is vulnerable to rock bursts and gas outbursts. On the basis of the parametric variations considered, it was found that a width to height ratio less than 2 will make an ideal yield pillar.

Eight different mining layouts were analysed with 2-entry (yield-abutment) and 3-entry (yield-abutment-yield) systems. Out of these mining layouts, layout 1, layout 2 and layout 8 showed lesser accumulation of vertical stress and elastic strain energy in the yield pillars as compared to other mining layouts. Hence, it is recommended to use symmetrical mining layouts for 2-entry or 3-entry yield pillar system.

The influence of vertical stress and elastic strain energy in the lower seam was analysed for a multi-seam mining scenario by laterally shifting the location of roadways in the lower seams. The analysis has shown that a lateral shift around half of the width of the longwall panel towards the centre of the longwall panel drastically reduces the vertical stress and elastic strain energy accumulation in the lower seam.

Based on the parametric analysis of yield pillar geometry and mining layouts, it was concluded that the geometry of the yield pillars should have a w/h ratio less than 2. Symmetrical mining layouts should be preferred as the vertical stress and elastic strain energy accumulation is comparatively lesser in symmetrical mining layouts. In case of multi-seam workings, the roadways in the lower seam should be shifted laterally by around half of the width of the longwall panel to minimise the effect of vertical stress and elastic strain energy accumulation in the lower seams.

Hence, a sacrificial roadway having the width to height ratio ($w/h < 2$) in a symmetrical mining layout is most suitable. In the case of multi-seam workings, a minimum shift of half the width of the longwall panel will further reduce the risk of rock bursts and gas outbursts.

Task 4.3 Numerical modelling of rock burst and gas outburst prevention techniques using protective mining (led by IMPERIAL, GIG, JSW, CM-VELENJE)

This Task considered mining layouts which mine upper or lower level coal seams for stress/gas pressure relief and gas outbursts/rock burst control in LW and LTCC layouts and assessed their performance and evaluate risk. The model was expanded in scope to generate a generic model to consider working depths from 600 to 1,200 metres depth with different seam thicknesses and material properties.

Protective mining has been practiced by coal mines as a means to reduce the risk of gas outburst in LW mining of multiple seams (layouts similar to those at JSW mines in Poland) and sublevel caving of steep seams (as practised by Hunosa mines in Spain). Here, a specific application relevant to the JSW Pniowek Colliery is presented and discussed in detail. The numerical modelling of protective

mining scenarios is achieved through IMPERIAL's two-way explicitly coupled geomechanics-reservoir model as described in detail under a number of deliverable reports and will not be repeated here.

Model set up

This model was developed to reproduce protective mining scenarios using the JSW Pniowek colliery Seams 404/1 and 404/2 layouts which are located at ~972 m and ~1000 m depths, respectively. The actual interbedding between the two seams is 28 m of mudstone and 6 m of sandstone, both relatively stronger than the coal seams as shown in Figure 0.29a. In order to demonstrate the technique and the parameters that control its effectiveness a second scenario with an alternative interbedding of 6 m of mudstone and 4 m of sandstone was also set up (Figure 0.29b).

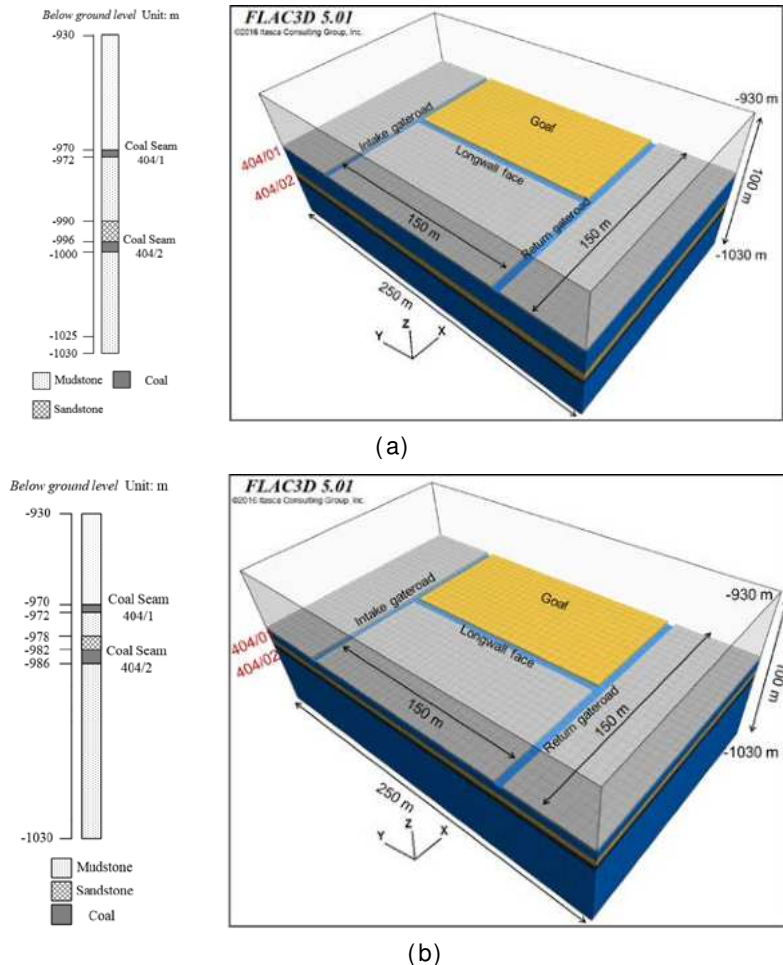


Figure 0.29 Pniowek colliery protective mining scenarios for Seams 404/1 and 404/2.

The physical dimensions of this model were set as $150 \times 250 \times 100\text{m}$ (length \times width \times height) and a uniform size of $5 \times 5 \times 5\text{m}$ (length \times width \times height) was used for each element. It was assumed that Coal Seam 404/1 has a thickness of 2 m and Seam 404/2 has a thickness of 4 m. The development headings and the longwall face are modelled as horizontal boreholes with a bottom-hole pressure as the atmospheric pressure of 0.1MPa. Face advance is modelled by 'remove' and 'reinstate' coal elements. Strain-hardening in the goaf material is represented by:

$$K = \frac{K_0}{1 - \varepsilon_v}$$

Results and discussion

The coupled model simulating the Pniowek colliery layout for the protective mining scenarios was run by retreating the longwall face in Seam 404/1 in twenty steps, each advancing the face by 5 m, and the analysis of stresses and pore pressure in both seams were carried out.

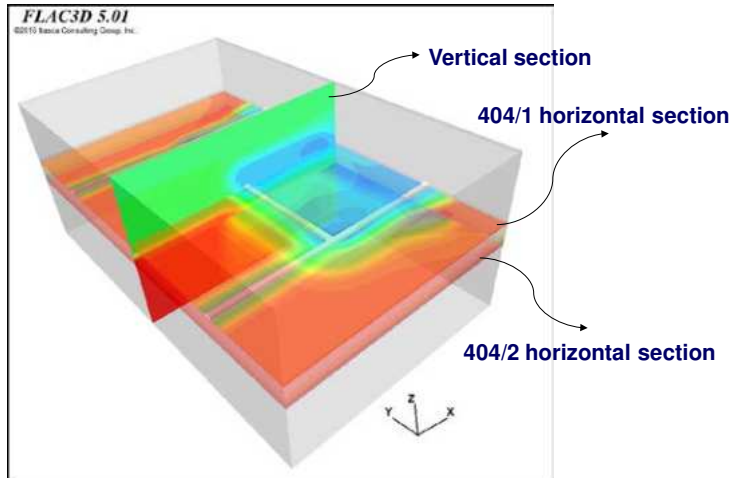


Figure 4.30 Pniowek colliery model showing the positions of horizontal and vertical sections taken from Seams 404/1 and 404/2 for the analysis of stress and pore pressure in each seam during the protective mining scenarios.

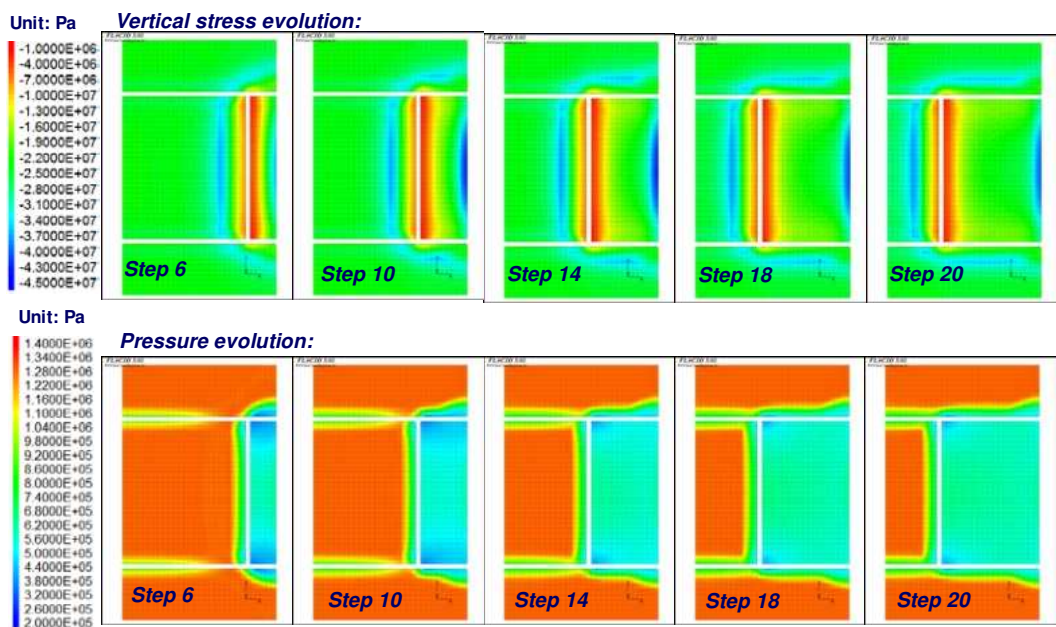


Figure 4.31 Pniowek colliery protective mining scenario: Progressive mining in 404/1 (horizontal section).

Figure 4.30 illustrates the Pniowek colliery model showing the positions of horizontal and vertical sections taken through Seams 404/1 and 404/2 which will be referred to in the analysis of stresses and pore pressures in these seams to evaluate the effect on Seam 404/2 of overmining/protective mining by seam 404/1.

In order to evaluate the changes of stress and pore pressure around the longwall face two different scenarios were run, representing a 34 m interbedding and a 10 m interbedding between Seams 404/1 and 404/2 respectively. Figure 4.31 and Figure 4.32 illustrate the evolution of vertical stress and methane pore pressure around the retreating longwall face in Seam 404/1 over the 20 production steps for the actual layout at Pniowek colliery.

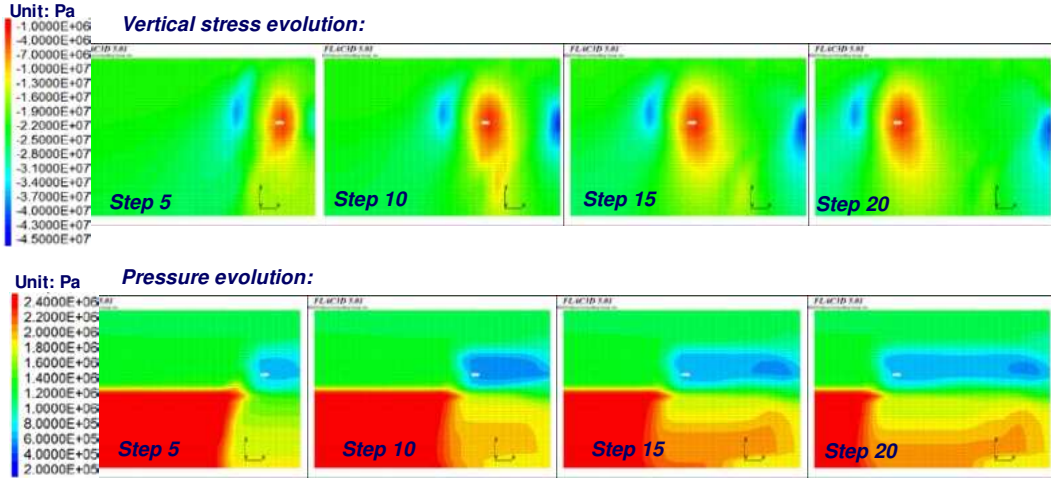


Figure 4.32 Pniowek colliery protective mining scenario: Progressive mining in 404/1(vertical section).

Figure 4.33 illustrates the evolution of methane pore pressure in Seam 404/2 level for the two scenarios (34 m interbedding and 10 m interbedding respectively) in the horizontal plane. It is clear that, while the seam gas pressure in Seam 404/2 remained reasonably close to the in situ pressure for the case with 34 m interbedding, there was a significant pressure relief, therefore gas loss into the Seam 404/1 level for the case with 10 m interbedding due to longwall face operation in the upper seam.

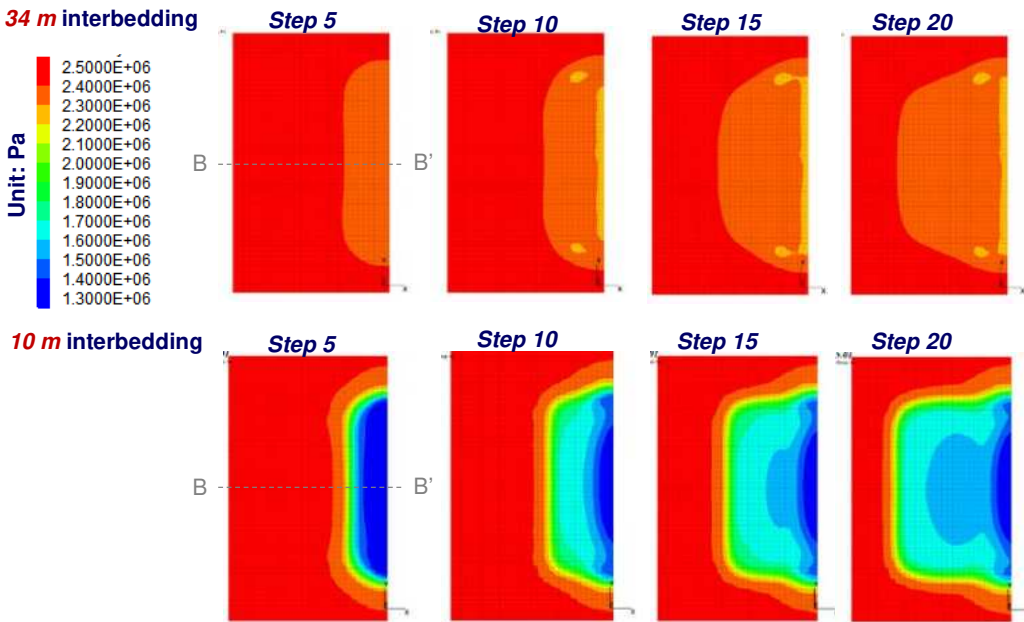


Figure 4.33 Pniowek colliery protective mining scenarios: Pore pressure relief in 404/2 (horizontal section).

Figure 4.34 plots the change in gas pressure in Seam 404/2 level as the longwall face in Seam 404/1 retreats progressively. The low gas pressure front in Seam 404/2 with approximately 1.0 MPa drop (therefore significant gas loss) follows the face advance in the upper level demonstrating the effect of protective mining in controlling floor gas outbursts.

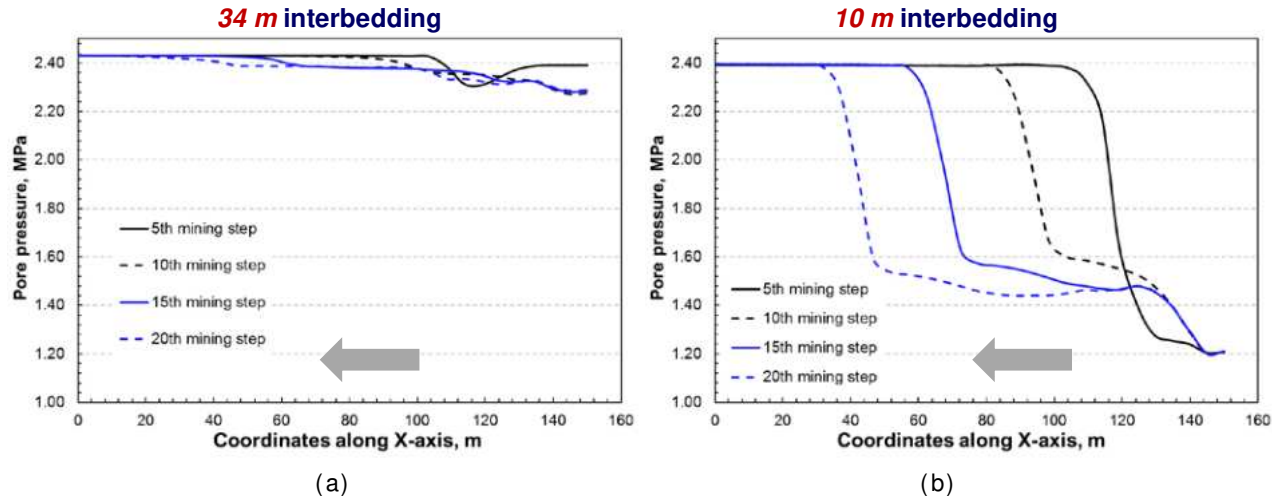


Figure 4.34 Pniowek colliery protective mining scenarios: Pore pressure profiles in Seam 404/2 along B-B' shown in Figure 4.33 for ((a) the 34 m interbedding and (b) 19 m interbedding scenarios.

In these first model runs it was observed that, current layout and the relatively large distance between the two seams at Pniowek colliery creates a limited, if any, stress and pressure relief effect on Seam 404/2 if the mining of Seam 404/1 was considered as a protective mining scenario. Reducing the thickness of the interbedding between the two seams down to 10 m has demonstrated that protective mining can be effective and create stress and pressure relief if the distance between two seams is much smaller.

WORK PACKAGE 5 - DEVELOPMENT AND VALIDATION OF A GENERIC METHODOLOGY FOR THE ASSESSMENT AND MITIGATION OF RISK FROM ROCK BURSTS AND GAS OUTBURSTS

The initial objectives of this WP were:

1. To generalise, test and validate the risk assessment methodology for rock burst and gas outbursts that was previously developed in the COGASOUT project to other mines, and in particular to CM-VELENJE and JSW.
2. To consider the benefit of different gas and pressure relief technologies in terms of risk reduction potential.
3. To consider and evaluate the effect of uncertain geological and mine design related parameters on quantitative risk estimates from numerical modelling.

Following the departure of AITEMIN from the project, IMPERIAL took over the leadership of all the Tasks in this Work Package and extended these objectives towards the development of a more quantitative risk assessment methodology drawing upon the work carried out and progress made in WPs 3 and 4, thus increasing the relevance of the methodologies developed to the work carried out in the project.

Task 5.1 Development of a generic risk assessment methodology for rock bursts and gas outbursts (led by IMPERIAL, GIG, RWTH, CM-VELENJE, JSW)

Initially in the project, it was proposed to develop a conceptual model including geological, coal seam and exploitation method dependent parameters, which can be applicable to different mining conditions utilising site specific parameters. Although this work was extremely useful in structuring the context for the work in this task, as the project progressed, and the preliminary conceptual model was designed, it became clear that the model was limited in quantification and comprehensiveness, and thus may not be applicable to the local conditions in significantly different geological and mining setting. Therefore, it was decided that it will be to the benefit of the project that multiple risk evaluation methods, including field microseismic monitoring data-based risk assessment and numerical modelling of rock burst and gas outburst risk scenarios are added to the concept of risk assessment, which allowed for more quantitative evaluation of both potential and intensity of rock bursts and gas outbursts, and facilitates easy implementation to different geological and mining conditions. Therefore, Task 5.1 made significant use of site specific data and the laboratory and field studies conducted in the project to inform the analysis and develop a generic modelling framework for rock burst and gas outburst risk assessment.

The workflow for the generic risk assessment methodology developed is illustrated in Figure 5.1. A suite of monitoring techniques was employed to monitor geomechanical, microseismic and gas flow behaviour with respect to coal mining. Field microseismic monitoring data, as the primary information source associated with coal/rock fracture and large gas emissions, is fed to a catalogue of risk evaluation methodologies for analysis and forecasting. In addition, numerical modelling of rock burst and gas outburst risk scenarios is performed based on typical mining scenarios in partner mines. Numerical modelling methodologies, focusing respectively on the stress and strain energy accumulation, gas pressure/flow, gas desorption and microseismic behaviour, were developed to meet the demands in modelling specific concerned aspects of rock bursts and gas outbursts. T

Evidence based risk evaluation

Factors affecting rock burst and gas outburst risk

Four significant factors have been shown to account for outburst occurrences: (1) the microstructure and properties of the coal; (2) the content and pressure of the gas retained in the coal seam; (3) geological deformation and depositional structures, and (4) the stress conditions around the coal seam. The major factors are classified into intrinsic factors and extrinsic factors, as summarised in Table 5.1. Historically, this method has been used for many years in the past and is only briefly discussed again here.

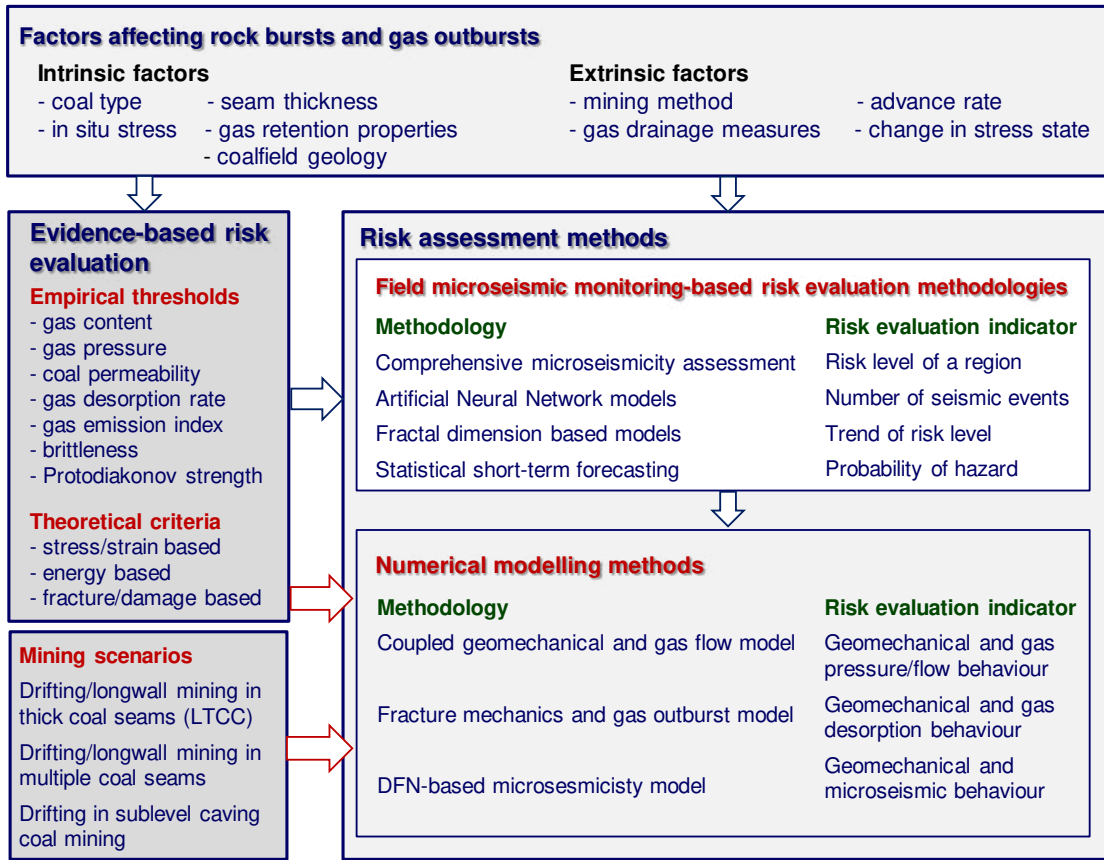


Figure 5.1 Flow diagram of the generic risk assessment methodology.

Table 5.1 Factors affecting rock bursts and gas outburst risk in coal mining.

Categories	Factors	Sub-factors
Intrinsic factors	Coal type	Physical properties: coal rank, grain size, porosity. Mechanical properties: strength, Young's modulus, Poisson's ratio, fracture toughness. Reservoir properties: permeability, Langmuir pressure and volume.
	Seam thickness	Mine depth Seam hardness Seam slope Seam thickness In situ stress
	Geological factors	Tectonic structures and discontinuities (faults, shear bedding zones, etc.) Tectonic activities (igneous intrusions) Gas content Gas composition Gas pressure
	Gas-related factors	Gas pressure gradient Gas adsorption/desorption rate Thick seam longwall coal mining Multi-seam longwall coal mining Sublevel caving coal mining
	Mining methods	
	Stress regime generated Face advance rate	
Extrinsic factors	Gas control measures	Pre-drainage Cross-measure boreholes Protective mining Drainage borehole stimulation

Evaluation criteria for rock bursts and gas outbursts

Evaluation criteria for rock bursts and gas outbursts can be categorised into two types, empirical thresholds and theoretical criteria. Empirical criteria usually utilise a single indicator as the threshold for rock bursts and gas outbursts, and thus are commonly used in the early stages of a project for preliminary design purposes to assess the rock burst and gas outburst risk of mine openings. Table 5.2 summarises some common empirical thresholds used for evaluation of rock burst and gas outburst risk.

Based on different perspectives, a large variety of theoretical criteria were put forward. These theoretical criteria can be categorised into (1) stress/strain failure criteria, (2) energy type failure criteria, and (3) fracture/damage mechanics-based criteria. Stress/strain-based criteria for rock burst risk assessment are based on rock fracture theories under certain circumstances, such as shear rupture along planes of weakness, or failure under coupled static and loads. On the other hand, the effective stress needs to be accounted for in stress/strain-based criteria for gas outburst risk assessment, considering that coal and gas outbursts are of tensile nature. Energy criteria for rock burst risk assessment are based on the relationship between the damage characteristics and strain energy change of surrounding rocks in response to mining activities. Therefore, these criteria reflect not only the capacity to store strain energy in rocks, but also the environment for strain energy accumulation. These energy criteria can be modified for gas outburst risk assessment by taking gas energy into account. Table 5.3 summarises some common theoretical criteria used for evaluation of rock burst and gas outburst risk

Table 5.2 Empirical thresholds for rock bursts and gas outbursts in coal mines.

Categories	Evaluation indices	Remarks/Evaluation criteria
Strength/stress-related	Protodyakonov strength	0.1–0.3 (Wang and Yang, 1980) $(\sigma_0 + \sigma_L)/\sigma_c > 0.8$ (Turchaninov <i>et al.</i> , 1972)
	Ratio of stress over strength	$\sigma_c/\sigma_0 < 2.5$, $\sigma_t/\sigma_0 < 0.16$ (Barton <i>et al.</i> , 1974)
	Drill-cuttings-to-hole volume ratio	$\sigma_0/\sigma_c > 0.55$ (heavy) (Russenes, 1974); $\sigma_0/\sigma_c > 0.7$ (strong) (Hoek & Brown, 1980) $> 3:1 \sim 7:1$ (Hyman, 1987)
Brittleness-related	Brittleness	$B_1 = (\sigma_c - \sigma_t)/(\sigma_c + \sigma_t)$; $B_2 = \sin\varphi$ (Hucka and Das, 1974)
	Gas volume	$> 9 \text{ m}^3/\text{tonne}$ for CH_4 and $6 \text{ m}^3/\text{tonne}$ for CO_2 (Sydney Basin, Australia) (Beamish and Crosdale, 1998); $10 \text{ m}^3/\text{tonne}$ for CH_4 (China) (Zhang, 1992)
	Gas pressure	$> 0.74 \text{ MPa}$ (China) (Chen <i>et al.</i> , 2016)
Gas-related	Gas desorption rate	$3 \text{ cm}^3/35 \text{ s}/10 \text{ g}$
	Gas emission index	5-15 (liable); 15-20 (highly liable) (Ettinger, 1952)
	Permeability	$< 5 \text{ mD}$ (<i>in situ</i>) (Lama and Bodziony, 1998); $< 10^{-3} \text{ mD}$ (core sample) (Gil and Swidzinski, 1988)

Table 5.3 Theoretical criteria for rock bursts and gas outbursts in coal mines.

Categories	Evaluation indices	Remarks/Evaluation criteria
Stress/strain-based	Tensile effective stress (TES)	The stress of a rock/coal element changes from compression to extension.
	Unbalanced pressure driven force (UPDF)	The pressure gradient acting on a rock/coal element overcomes the friction.
	Excess shear stress (ESS) Brittle shear ratio (BSR)	> 15 (Ryder, 1987) > 0.7 (Castro <i>et al.</i> 2012)
Energy-based	Coupled static and dynamic loads	The coupled static and dynamic loads exceed the critical stress limits of coal.
	Strain energy density (SED)	The maximum elastic strain energy per unit volume exceeds a threshold.
	Energy release rate (ERR) Strain energy storage index (W_{et}) Potential energy of elastic strain (PES)	$> 4.7\%$ (Salamon, 1984) > 5.0 (Neyman <i>et al.</i> , 1972) > 150 (Wang and Park, 2001)
Fracture/damage-based	Fracture mechanics-based criteria	The stress intensity factor exceeds the fracture toughness of coal.

Following on from AIITEMIN's initial work during the first reporting period of the project, two former employees of AIITEMIN (on behalf of GIG) further developed an evidence based risk assessment methodology (using factors similar to those listed in Table 5.1 and Table 5.2) and applied this to the sublevel caving mining methods used in steep seams in Spain (Table 0.4). As illustrated in Figure 5.2, gas outburst risk during gateroad/heading development in sublevel caving is reduced if degassing boreholes are used or development advance rate is reduced based on the risk criteria IR developed utilising the influencing factors and their rate of influence from Table 0.4.

Table 0.4 Evidence based empirical methodology developed primarily for sublevel caving coal mining.

	PARAMETER	VALUE	INFLUENCE
COAL SEAM FACTORS	Firedamp concentration	< 5 m³/t 5 – 10 m³/t > 10³/t	Risk (R) = 7% Risk (R) = 22% Risk (R) = 55%
	Desorption rate	< 1,5 cm³/35s/10g 1,5–3 cm³/35s/10g > 3 cm³/35s/10g	0.10R 1.15R 1.60R
	Specific firedamp release	< 20 m³/t 20 – 100 m³/t > 100 m³/t	1.00R 1.20R 1.50R
		CO2 < 10% CO2 > 10%	1.10R 1.50R
		P=P _{isotherm} P>1,2P _{isotherm} P>1,5P _{isotherm}	1.00R 1.10R 1.50R
	Permeability (substantial variation in the value)	Increase Decrease	0.80R 1.55R
	Intrinsic moisture	< 10 % > 10 %	1.00R 0.50R
	Coal rank	Anthracite <8% volatile matter Bituminous 8-40% volatile matter Lignite >40% volatile matter	1.40R 1.20R 0.05R
	PARAMETER	VALUE	INFLUENCE
DRIFT HEADING	Crosscut (Enter the coal seam)	Yes, without drainage boreholes Yes, recognition boreholes Yes, local degassing Yes, total degassing	1.70R 1.20R 0.40R 0.10R
	Influenced area by upper sublevel	YES, distended area YES, overstressed area NO	0.50R 1.20R 1.00R
	Locally faults	YES NO	1.50R 1.00R
	Coal seam thickness variation	< 50% 50% < Variation <100% > 100%	1.00R 1.20R 1.50R
	Local firedamp concentration increase	< 5 m³/t > 5 m³/t	1.00R 1.50R
	Local desorption rate increase	< 1 cm³/35s/10g 1 < increase < 2 cm³/35s/10g > 2 cm³/35s/10g	1.00R 1.20R 1.50R
	Advancing rates	0.8 m/shift 1.6 m/shift 2.4 m/shift >2.4 m/shift	0.80R 1.00R 1.20R 1.40R
	PARAMETER	VALUE	INFLUENCE
MINING METHOD	Advance mining / Retreat mining	Advance mining Retreat mining	1.00R 0.50R
	Advancing rates	0.8 m/shift 1.6 m/shift 2.4 m/shift >2.4 m/shift	0.80R 1.00R 1.20R 1.40R
		NO Yes, inactive shift Yes, degassing boreholes Yes, injection boreholes Yes, partly induced Yes, total induced	1.00R 0.60R 0.50R 0.30R 0.10R 0.05R
	PARAMETER	VALUE	INFLUENCE
SUBLEVEL CAVING	Influenced area by upper level exploitation	YES NO	0.50R 1.00R
	Area influenced by headings in the same level	TOTAL PARTIAL	0.30R 0.70R
	Locally faults	YES NO	1.30R 1.00R
	Firedamp concentration increase	< 5 m³/t > 5 m³/t	1.00R 1.50R
	Desorption rate increase	< 1 cm³/35s/10g 1 < increase < 2 cm³/35s/10g > 2 cm³/35s/10g	1.00R 1.20R 1.50R

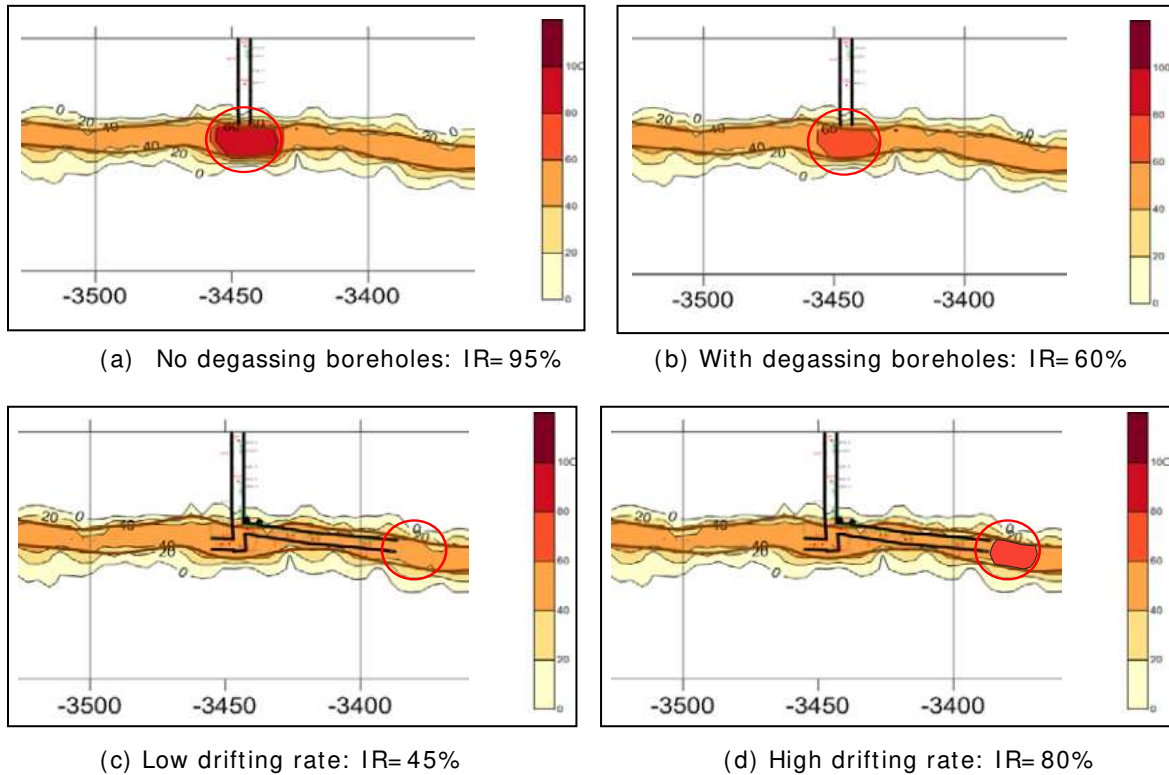


Figure 5.2 Evidence based empirical risk assessment applied to sublevel caving coal mining method.

Field microseismic monitoring based risk evaluation

Field microseismic monitoring data collected in Task 3.1 contain a wealth of information associated with coal/rock fracture and large gas emissions, and are used as the primary information to evaluate rock burst and gas outburst risk. The comprehensive quantitative assessment is first adopted to analyse the monitored microseismic data in terms of temporal, spatial and magnitude characteristics, based on which a comprehensive normalised index is put forward to quantify the risk levels. A series of models aiming at various purposes are then used for the short-term forecast of rock bursts and gas outbursts. Specifically, the Time Series Neural Network model developed in Task 3.2 is adopted to forecast the maximum event energy, the total seismic energy, and the number of seismic events which would take place over the next time period. The fractal dimension based model developed in Task 3.3, characterised by reduction in fractal dimension and multifractal characteristics, is employed to provide precursors for rock bursts and gas outbursts. The statistical short-term forecasting model is developed to estimate the probability of a large microseismic event occurring close to a working face over the next time period, based upon statistical analysis of the microseismic features. The field microseismic monitoring-based risk evaluation methodologies developed are summarised in Table 5.5.

Table 5.5 Field microseismic monitoring-based risk evaluation methodologies.

Risk evaluation methodologies	Purposes	Outputs
Comprehensive quantitative assessment	Forecast the risk levels of mining sites	Risk level
Time series Neural Network model	Forecast the number of microseismic events	Number
Fractal dimension based model	Forecast the risk of microseismicity	Trend
Statistical short-term forecasting model	Forecast the probability of hazards	Probability

As in the case of the development of Artificial Neural Networks and Fractal based models in WP3, the Coal Mine Velenje microseismic monitoring data for the period March-April 2017 as illustrated in Figure 5.3 were used to develop the methodology described here. The comprehensive quantitative assessment methods developed included the use of a number of indices, such as:

- Bursting strain energy index (BSE) in temporal and spatial domains,
- Time-space-magnitude independent information indices,
- Time-space-magnitude compound information indices, and
- Comprehensive index

with a number of indices in each. An example for the use of the BSE index is presented in Figure 5.3. Utilising this methodology, it was seen that the intensity and its corresponding scope of the BSE index increased gradually in front of the face during the longwall panel mining and then up to a strong risk level at Coal Mine Velenje during the period March-April and April-May 2017.

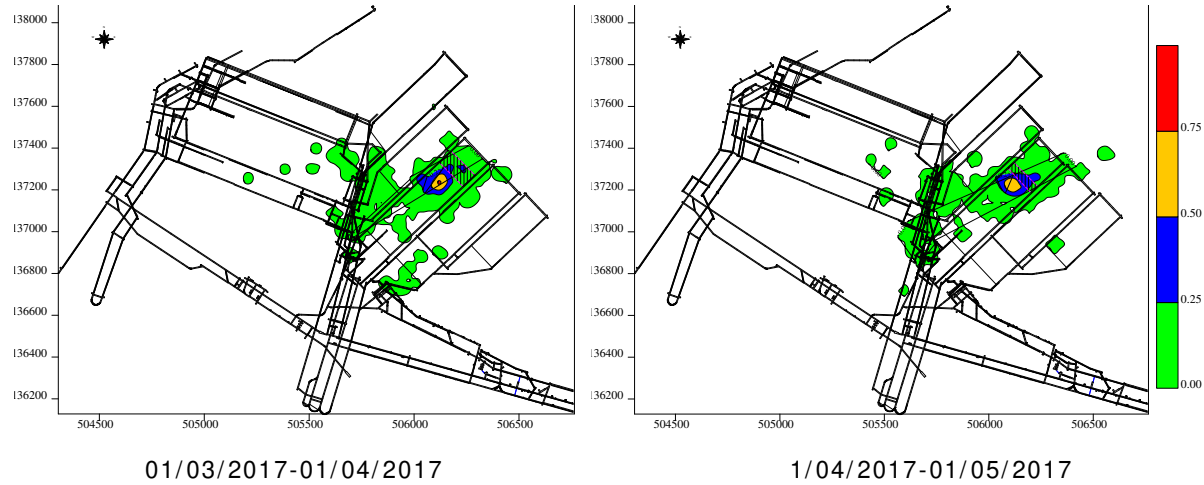


Figure 5.3 Plan views of the BSE index $W_{\varepsilon\text{-spatial}}$ during different mining periods at Coal Mine Velenje.

As illustrated in Figure 5.4 and Figure 5.5 the comprehensive index values increased to a ‘strong’ risk level prior to the strong seismic events at Coal Mine Velenje. Although the development of the above indices is mostly aimed at forecasting rock bursts, their implementation at Coal Mine Velenje, where the seam gas is CO₂ and makes the seam prone to gas outbursts, has shown that the monitored microseismic data can also be utilised in evaluating gas outburst risk.

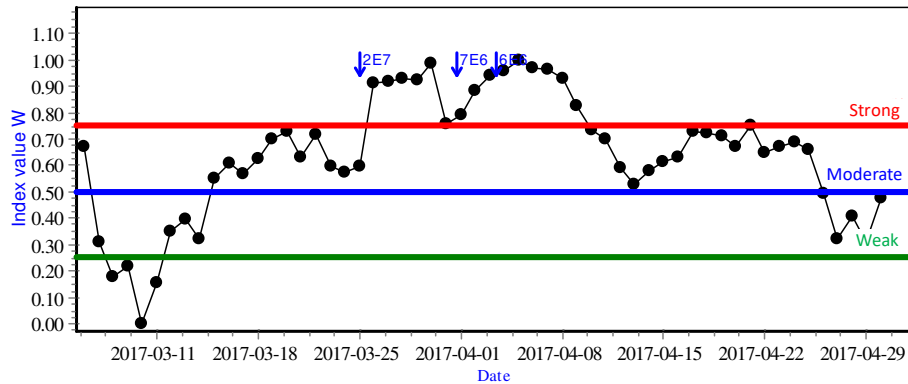


Figure 5.4 The temporal evolution of the comprehensive index integrating with time-space-magnitude independent information indices at Coal Mine Velenje.

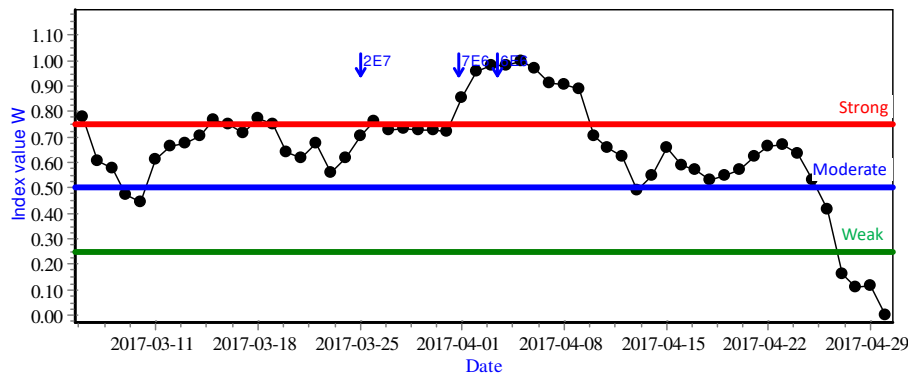


Figure 5.5 The temporal evolution of the comprehensive index integrating with time-space-magnitude compound information indices at Coal Mine Velenje.

Numerical modelling of rock burst and gas outburst modelling

Table 5.6 presents the typical mining scenarios and associated rock bursts/gas outbursts conditions which also are representative of most rock burst and gas outburst cases experienced worldwide, and beyond the partner mines considered in MapROC.

Table 5.6 Typical mining scenarios to be simulated for rock burst and gas outburst risk evaluation.

Mining scenarios	Rock bursts/gas outbursts conditions	Hazards	Modelling methodology
- Drifting/longwall mining in thick coal seams (LTCC)	Strong/weak zones, bedding shear zones	Rock bursts/gas outbursts	Coupled geomechanical and gas flow model,
- Drifting/longwall mining in multiple coal seams	Floor, strong/weak zones, bedding shear zones	Rock bursts/gas outbursts	fracture mechanics-based gas outburst model, DFN-based microseismicity
- Drifting in sublevel caving coal seams	Strong/weak zones, bedding shear zones	Coal and gas outbursts	model.

Three coupled modelling methodologies were developed using a continuum mechanics-based software package FLAC^{3D} and a reservoir simulator ECLIPSE, which is capable of simulating geomechanical behaviour of coal and surrounding rock masses as well as the changes in permeability, gas pressure and gas flow with respect to face advance g during coal mining and/or drifting. Each modelling methodology focuses on specific key influencing factors and addresses a concerned aspect of these hazards.

The fracture mechanics-based gas outburst model simulates the dynamic process of coal and gas outbursts by accounting for gas desorption into fractures around mine openings and subsequent rapid fracture propagation propelled by intra-fracture effective stress. The DFN-based microseismicity model combines deterministic stress and failure analysis and stochastic fracture slip evaluation, based upon the widely accepted fracture slip seismicity-generation mechanism, and simulate microseismic events induced by coal mining/drifting, with the magnitude-frequency distribution reflecting the potential of rock bursts and coal gas outbursts.

Implementation of the criterion for coal and gas outbursts

In developing the coupled geomechanical and gas flow modelling methodology for coal and gas outbursts, a coal element which is adjacent to an open space is deemed to be ejected if the pore pressure gradient towards the opening (at atmospheric pressure) exceeds the coal cohesion (Figure 5.6).

The “ejected” elements are assigned with null properties and the simulation is re-run until a new equilibrium state is reached. This is an iterative process as the ejection of coal elements would create a larger cavity and thus more coal elements would be exposed to the cavity. And this turn may result in the ejection of more elements.

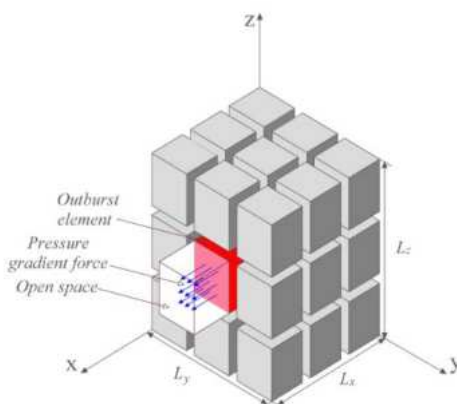


Figure 5.6 A schematic of the criterion for coal element ejection in outburst modelling.

For each ejected coal element with mass m , the volume of released gas is calculated based on the Langmuir isotherm. The post-ejection cavity pressure is then estimated according to Boyle's law assuming that the equilibration of gas pressure is quickly established.

After the start of the outburst post-initiation stage, a distinct pressure difference is established between the solid coal face and the outburst cavity, and this pressure difference provides the driving

force for the domino effect of an outburst. The coal and gas outburst would cease when there are no more elements from solid coal which satisfies the ejection criterion.

Fracture mechanics-based gas outburst model

A theoretical model for dynamic (discrete) fracture behaviour ahead of a working face subjected to the interplay of gas pressure and unloading stress conditions was developed to study the onset and evolution of coal and gas outbursts during coal mining. As a first step, the behaviour of a disk-shaped fracture close to a free face, in terms of its opening, subsequent expansion and rapid propagation, under unloading conditions is considered. Fracture mechanics and gas adsorption kinetics are employed to account for fracture propagation and gas desorption behaviours, respectively.

Figure 5.7 shows a schematic of a coal seam with a working face and an induced failure zone ahead of the face and the resulting stress redistribution. In addition, fractures oriented parallel to the advancing face are also created near the face. Here, the focus is on a newly formed penny-shaped fracture (which is initially closed), and its subsequent opening and propagation as the face advances. The fracture is subjected to an internal gas pressure p as well as the external stress (the minor principal stress σ_{\min}). The dynamic fracture behaviour is controlled by the effective stress ($\sigma_{\text{eff}} = p - \sigma_{\min}$). The intra-fracture gas pressure is affected by the fracture opening (aperture) and inward gas migration. The latter tends to offset the pressure reduction caused by fracture volume increase. As the working face advances, the fracture is likely to experience opening first, then expansion and rapid propagation under the interplay of gas pressure and stress. Different states for a disturbed fracture is summarised in Table 5.7.

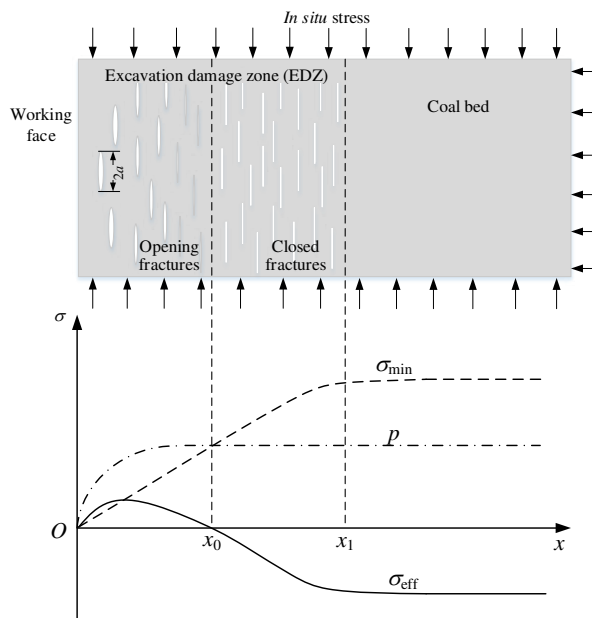


Figure 5.7 Schematic representation of fracture opening in relation to effective stress changes ahead of a working face.

Table 5.7 Different stages of a disturbed fracture.

Stages	Reason	Changes
Fracture opening	Minor principal stress unloading	a constant, V increases, p decreases
Fracture expansion	Gas desorption	a constant, V increases, p increases
Fracture equilibrium	Dynamic adsorption/desorption equilibrium at the pore pressure inside the fracture	a constant, V constant, p constant
Fracture propagation	Effective stress exceeds stress intensity factor (K_{Ic}) at the fracture tip	a increases, p decreases

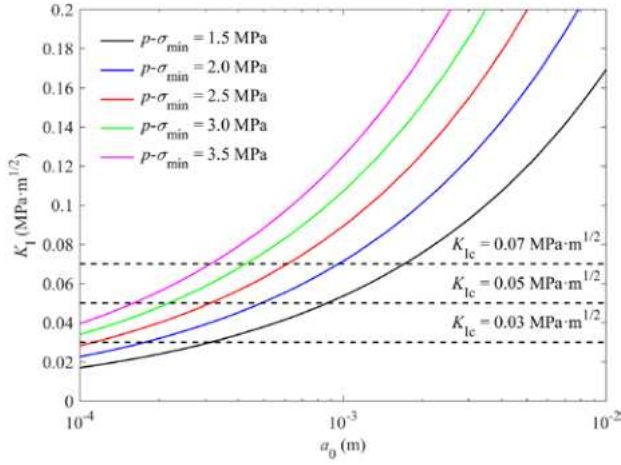


Figure 5.8 Stress intensity factors K_I as a function of fracture radius a_0 and effective stress $p-\sigma_{\min}$. Fractures are deemed to propagate if $K_I \geq K_{Ic}$.

Based on linear elastic fracture mechanics (LEFM), a material is deemed to fail when the stress intensity factor, defined as K_I reaches a critical value K_{Ic} , which is the fracture toughness of coal in this case. Therefore, the threshold limits of coal and gas outbursts can be estimated using practical ranges of the associated model parameters. Figure 5.8 presents critical stress intensity factor K_I for fractures associated with different values of fracture toughness K_{Ic} , fracture radius a_0 , and effective stress $p-\sigma_{\min}$. As can be seen, large fracture radius, high effective stress and low fracture toughness have a favourable effect on the potential of coal and gas outbursts. For typical coal properties and effective stresses faced in coal mining, the minimum fracture radius that can trigger unstable failure spans from below 10^{-4} to over 10^{-3} m.

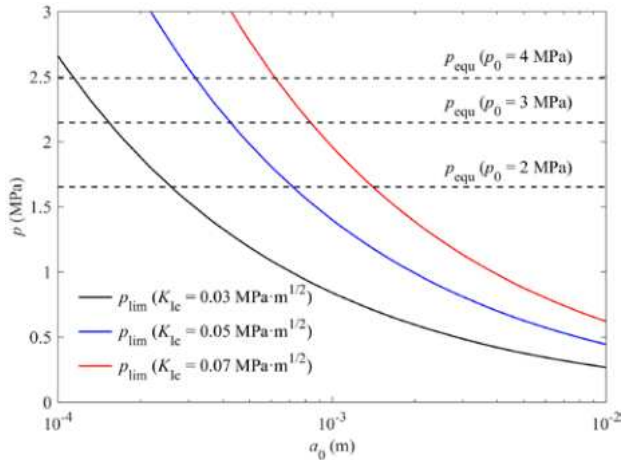


Figure 5.9 Intra-fracture gas pressure p_{lim} as a function of fracture toughness K_{Ic} and fracture radius a_0 for fractures located close to a working face. Fractures are deemed to propagate if $p_{\text{lim}} \leq p_{\text{equ}}$.

The criterion for coal and gas outbursts can equally be expressed in terms of intra-fracture gas pressure, that is, a fracture with continuous inflow of desorbed gas is deemed to propagate if the critical intra-fracture gas pressure p_{lim} to drive fracture propagation is lower than that at adsorption/desorption equilibrium p_{equ} . As illustrated in Figure 5.9, the intra-fracture gas pressure threshold p_{lim} associated with different values of fracture toughness K_{Ic} , fracture radius a_0 and initial gas pressure p_0 for fractures located close to a working face were calculated using coal seam properties from Pniowek Colliery in Poland.

A DFN-based microseismicity model

In order to better understand occurrence of microseismicity in longwall coal mining, a numerical modelling approach which includes stress analysis and fracture slip evaluation sequentially was also developed to model the microseismicity generation in longwall coal mining. The numerical approach incorporates a strain-softening constitutive model to describe the post-failure behaviour of the rock

mass realistically, and implements fractures along which slip can take place to form a microseismic event. The microseismicity modelling procedure involves the following steps:

1. model set-up and initialisation
2. simulation of mining induced stress-redistribution and associated failure analysis
3. microseismic event generation and associated energy release estimation.

Steps 2 and 3 are repeated in each coal excavation step until the completion of longwall mining simulation in one study area. The fracture slip is evaluated at the end of each excavation step, rather than interacting with model elements during the cycling process.

Briefly, using a set of pre-defined attributes, a randomly-distributed network of disc-shaped discrete planar fractures are created in FLAC^{3D} by using various random seeds. The set of attributes includes:

- fracture intensity,
- fracture size range,
- fracture size distribution (power law, Gaussian, uniform and bootstrapped distributions), and
- fracture orientation (random or pre-specified).

Strain-softening post-failure behaviour of coal, based on the experience gained from laboratory triaxial experiments is used in the model. It is assumed that microseismicity is predominantly generated in regions where coal remains intact, and behaves elastically. The Mohr-Coulomb slip condition is used to evaluate if a fracture has slipped or not. The fracture is considered to have slipped if the shear stress along the fracture plane exceeds its resistance τ_{sf} , which is given as:

$$\tau_{sf} = \mu_{sf} \sigma + c_f$$

where σ is the normal stress on the fracture surface, and μ_{sf} and c_f are the static friction coefficient and the cohesion along the fracture, respectively.

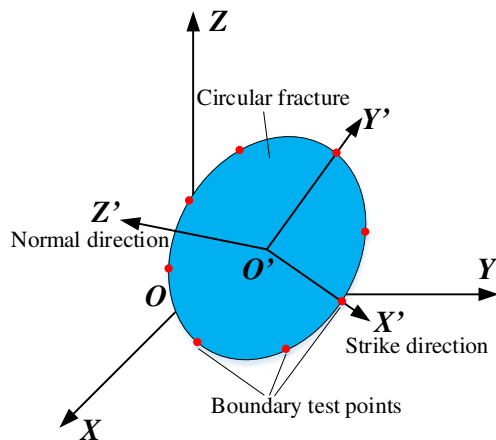


Figure 5.10 Slip test points on the periphery and centre of a circular fracture in local coordinates.

Circular discrete fractures provided in FLAC^{3D} are used and a total of nine test points, eight of them uniformly distributed around the periphery of the circle and one at the centre are checked for slip (Figure 5.10). Slip is deemed to have occurred over the entire fracture face and a microseismic event is generated if the above slip criteria is satisfied at any test point, and the fracture is not considered for slip again in subsequent simulations.

The released energy from a microseismic event is estimated by considering both the fracture size R and stress drop $\Delta\sigma$ along the fracture surface:

$$E_k = \frac{4(1-\nu)\Delta\sigma^2 R^3}{3G(1-\nu/2)}$$

where ν and G are the Poisson's ratio and shear modulus of the host rock, respectively. The energy release equation shows that the released kinetic energy is proportional to the cube of fracture size (radius) and square of the stress drop, suggesting that it is strongly affected by the fracture size and to a less extent by the rock strength and mechanical properties.

Conclusions

The work carried out in Task 5.1 aimed at developing methodologies to estimate the rock burst and gas outburst risk utilising site specific data and the laboratory and field studies conducted in the MapROC project. A generic risk assessment methodology, which is comprised of a conceptual model, field microseismic monitoring-based risk evaluation and numerical simulation of r risk scenarios.

Microseismicity associated with coal mining is monitored and fed to a catalogue of risk evaluation models aimed at forecasting the risk levels of rock bursts and coal and gas outbursts in terms of different evaluation indices. A comprehensive quantitative assessment model performs analysis on the temporal, spatial and magnitude characteristics of microseismicity, with a comprehensive normalised index put forward to classify risk levels. The Time Series Neural Network model developed in Task 3.2 is adopted to forecast the maximum event energy, the total seismic energy, and the number of seismic events which would happen over the next time period. The fractal dimension based model developed in Task 3.3, characterised by reduction in fractal dimension and multifractal characteristics, was employed to provide precursors for rock bursts and gas outbursts. The statistical short-term forecasting model is developed to estimate the probability of a large microseismic event occurring close to a working face over the next time period, based upon statistical analysis of the microseismic features.

Three numerical modelling methodologies, the coupled geomechanical and gas flow model, the fracture mechanics-based gas outburst model, and the DFN-based microseismicity model, were developed aimed at simulating gas pressure/flow, gas desorption, and microseismic response, in addition to geomechanical behaviour in response to coal mining. Field-scale numerical models under different geological and mining conditions can be constructed using any of these modelling methodologies, whichever is appropriate for the specific purpose. A variety of rock burst and gas outburst prone conditions can be designated and simulated for risk assessment.

Task 5.2 Testing and validation of the developed generic risk assessment methodology at partner mines using the field and laboratory data collected (led by IMPERIAL, CM-VELENJE, JSW)

The main objective of this task was to implement and validate the generic risk assessment methodology developed in Task 5.1 for a representative number of scenarios that may be encountered at Coal Mine Velenje and JSW, based on a suite of site specific parameters monitored in the field and the laboratory. Work focused on the implementation of four field microseismic monitoring-based risk assessment methodologies developed, as Artificial Neural Network (ANN) models, Fractal Dimension based models, comprehensive microseismicity assessment and statistical short-term forecasting, to microseismicity recorded at Coal Mine Velenje and Budryk Colliery based on the data available as appropriate. Example application of the ANN and Fractal Dimension based models to Coal Mine Velenje and Budryk Colliery data is already described in detail under WP3 Tasks 3.2 and 3.3 of this report. Therefore, these will not be repeated again here, rather, focus will be on the relevant applications comprehensive microseismicity assessment and statistical short-term forecasting methodologies, as well as the numerical modelling methodologies applications of which have not been reported earlier in this document.

The numerical modelling approaches developed were applied to field production designs common to most European longwall coal mining layouts as well as LTCC mining layouts taken from Coal Mine Velenje.

Comprehensive microseismicity assessment model application at Coal Mine Velenje

As developed and reported earlier, there are three first-class indices and 16 second-class indices in the comprehensive microseismicity assessment methodology, as summarised in Figure 5.11. All these indices are categorised into bursting strain energy indices (BSE) in temporal and spatial domains, time-space-magnitude independent information indices, and time-space-magnitude compound information indices. Both of them can be normalised by a comprehensive index, which allows for a more quantitative evaluation of the likelihood for the occurrence of rock bursts and gas outbursts.

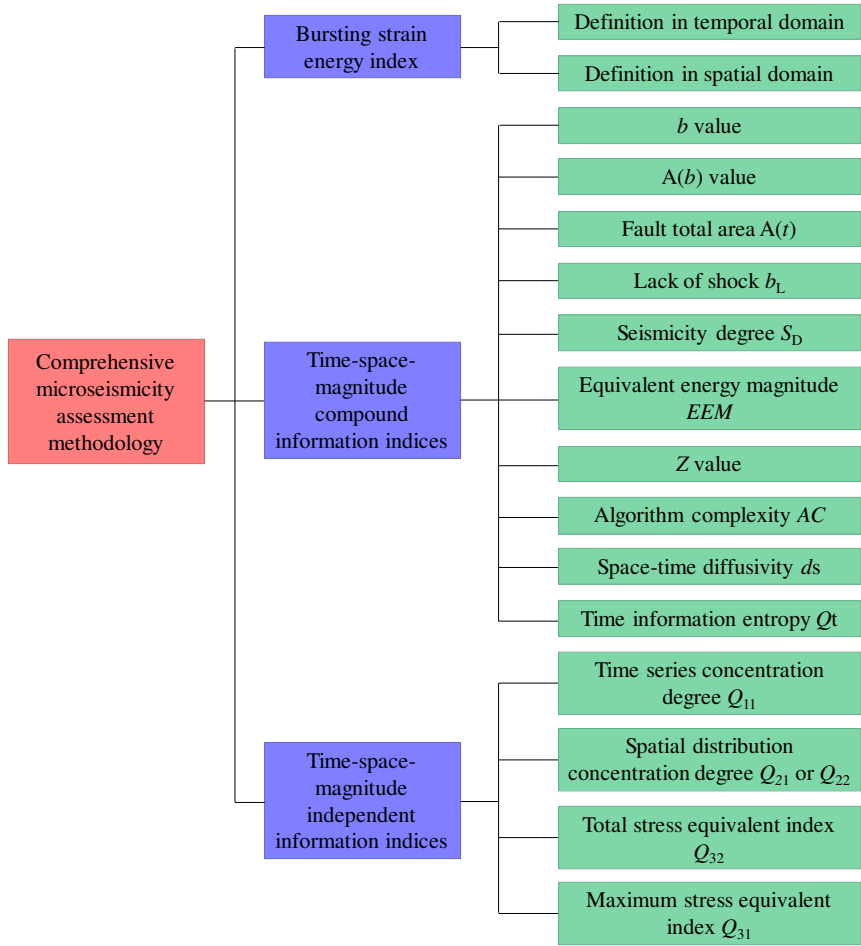


Figure 5.11 Framework of the comprehensive microseismicity assessment methodology.

The longwall panel K.-80/C at Coal Mine Velenje, whose whole mining activities have been monitored by the SOS microseismic system was used for the model testing and calibration. During the period from 01/03/2017 to 01/10/2017, 4,404 seismic events induced by mining activities were recorded, as presented in Figure 5.12.

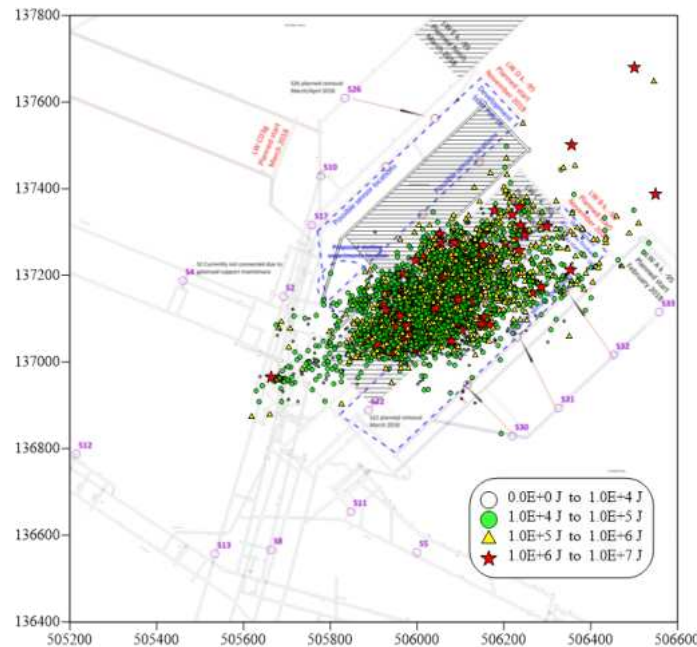


Figure 5.12 Spatial distribution of microseismic events around longwall panel K.-80/C in Coal Mine Velenje.

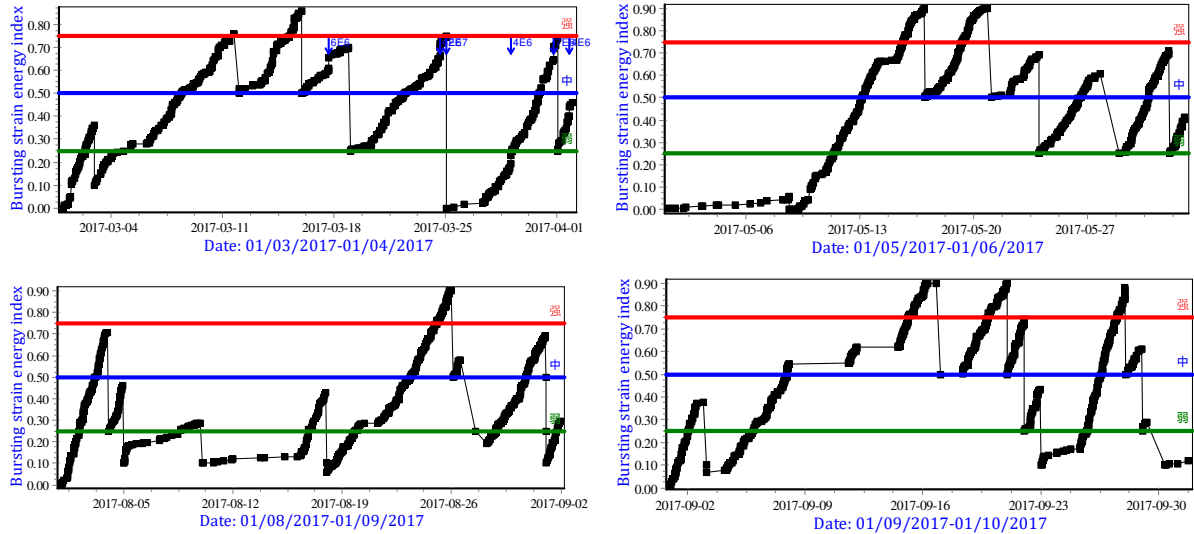


Figure 5.13 Temporal evolution of the bursting strain energy index for longwall panel K.-80/C.

Figure 5.13 and Figure 50.14 show the temporal and spatial evolutions of the bursting strain energy index (BSE), which allows us to conclude that the BSE index, can be used for short term spatial-temporal forecasting of rock bursts. The corresponding temporal sequence curves and spatial contour maps calculated based on the BSE index suggested that it can quantitatively evaluate rock burst tendency within the monitored area in short time and actively track the evolution of such hazardous areas and the level of rock burst risk therein.

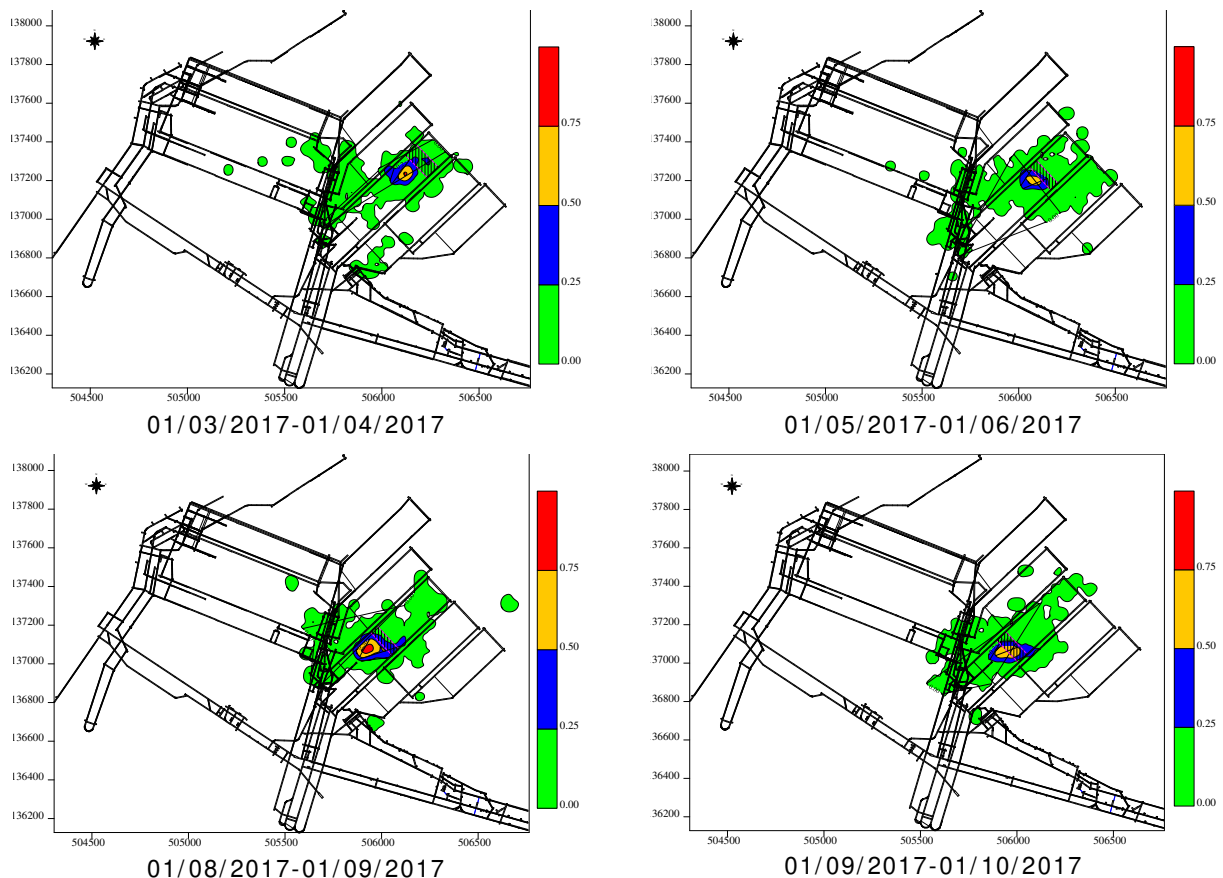


Figure 50.14 Spatial evolution of the bursting strain energy index around longwall panel K.-80/C.

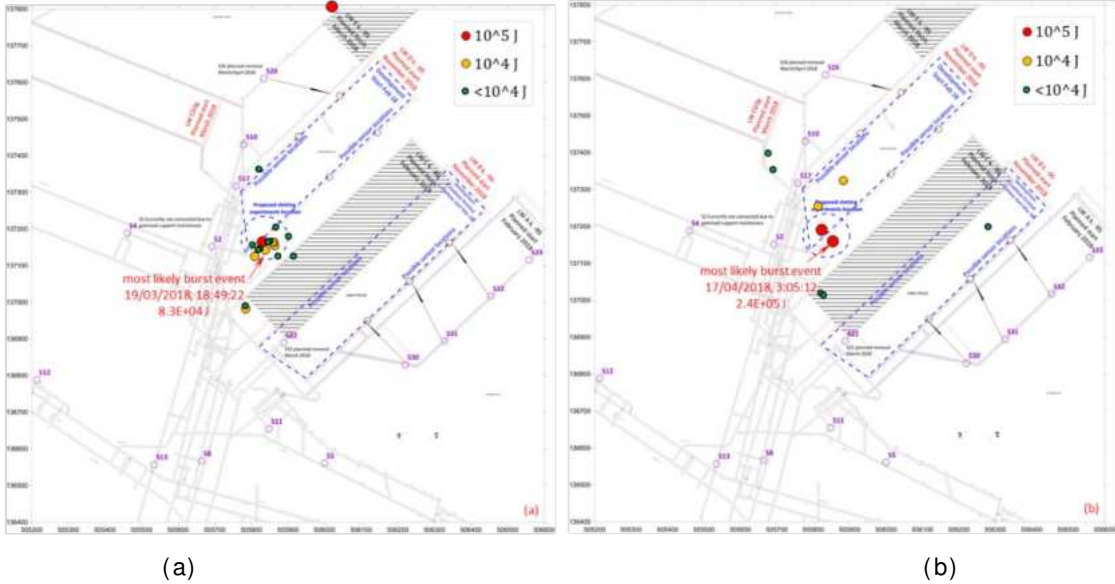


Figure 5.15 Microseismic response to rock burst events: (a) Microseismic events related to the rock burst event “18:49:22 19/03/2018”; (b) Microseismic events related to the rock burst event “3:05:12 17/04/2018” at development heading for longwall panel K. -95/D.

As discussed earlier, the comprehensive microseismicity assessment methodology developed can be conducted on a daily basis. In order to apply this model further to a real case at Coal Mine Velenje, the seismic events recorded at 18:53:50 on 19/03/2018 and 3:05:12 on 17/04/2018 during the heading development for longwall K. -95/D were used examples (Figure 5.15(a) and (b)).

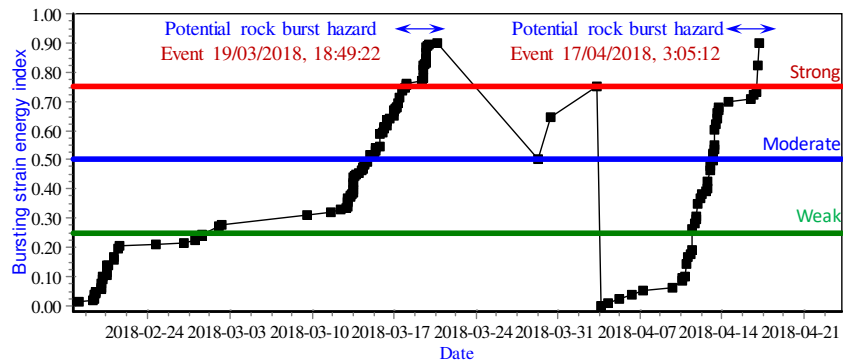


Figure 5.16 The temporal evolution of the BSE index $W_{\varepsilon\text{-temporal}}$ prior to the seismic events experienced at Coal Mine Velenje development heading for longwall panel K. -95/D.

Figure 5.16 and Figure 5.17 show the temporal and spatial evolutions of the bursting strain energy index (BSE). The results indicate that the values of the BSE indices in spatial and temporal domains normally increase gradually to the strong risk level prior to the rock burst events occurred. Further analysis of the same set of recorded data utilising time-space-magnitude information indices, such as fault total area, seismic diffusivity, degree of seismicity, total stress equivalent, time series concentration degree and Z value, confirms an obvious tendency in these indices for the precursor of rock burst hazard (Figure 5.18).

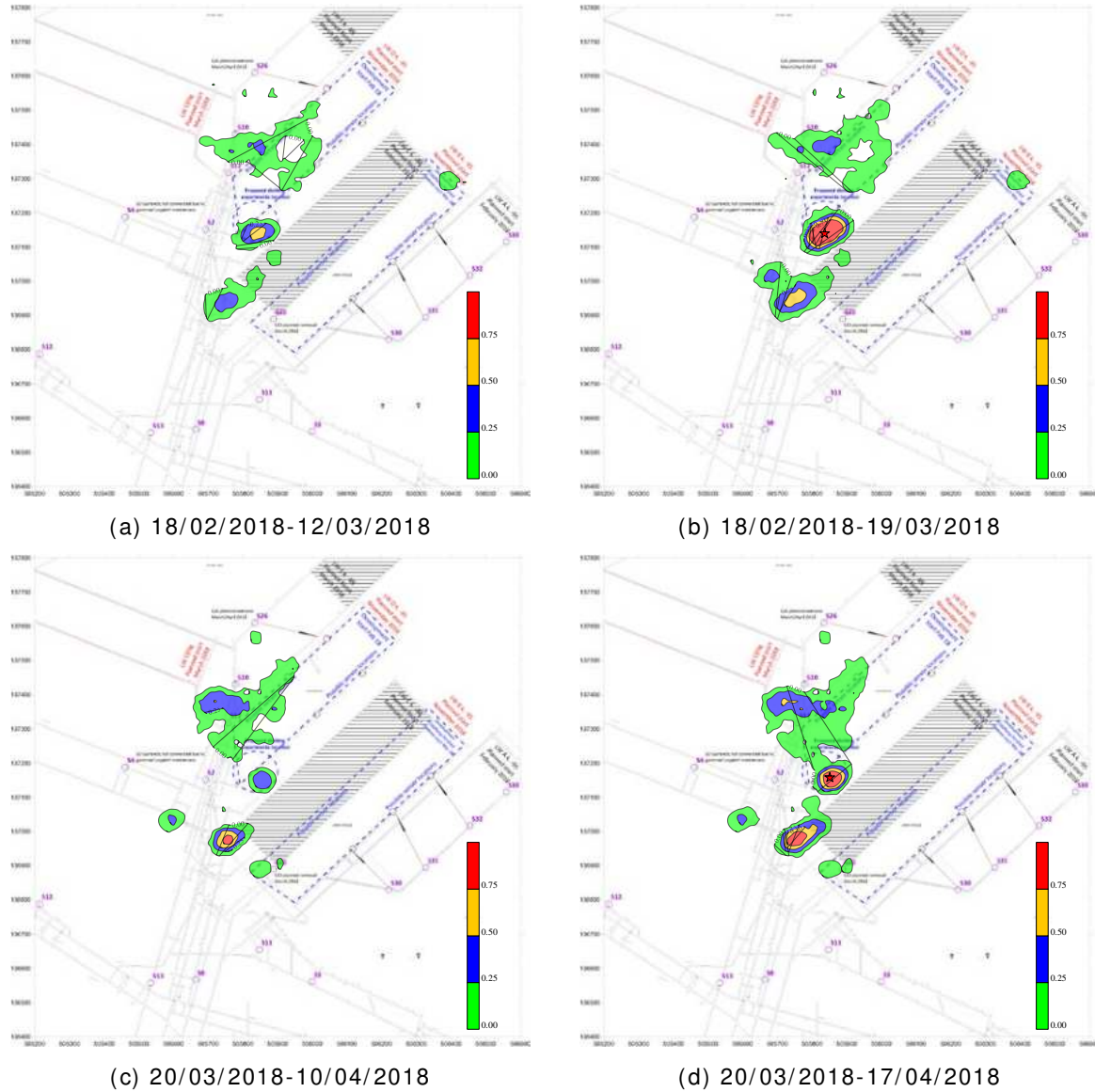


Figure 5.17 Plan views of the BSE index $W_{\epsilon\text{-spatial}}$ before the rock burst events which were experienced at 18:49:22 on 19/03/2018 and at 3:05:12 on 17/04/2018 at heading for panel K. -95/D.

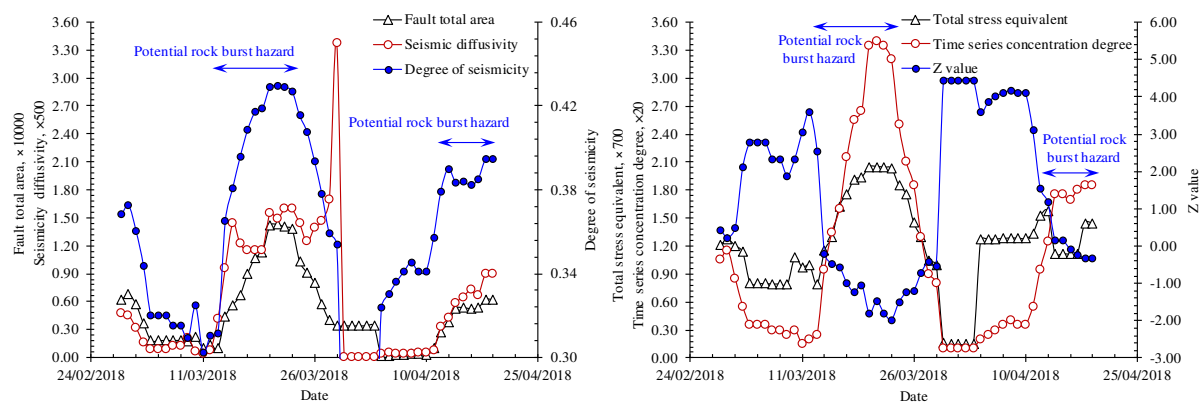


Figure 5.18 Temporal risk assessment based on the sequential evolution of seismic indicators at development heading for longwall panel K. -95/D.

In order to compare the results from the comprehensive risk assessment methodology for the seismic events that took place at development heading for longwall panel K. -95/D the risk analysis based on temporal evolution of fractal dimension based indices developed in WP3 (Figure 5.19a) are also

presented here. The figure illustrates that there are two periods of dramatic drop to a low value and then an initial increase, suggesting potential seismic hazards. By further processing of these fractal indices utilising the fractal-fuzzy model, a probabilistic assessment for each seismic hazard level and its comprehensive assessment was also achieved (Figure 5.19b). Such analysis can be conducted on a daily basis and help plan safety measures.

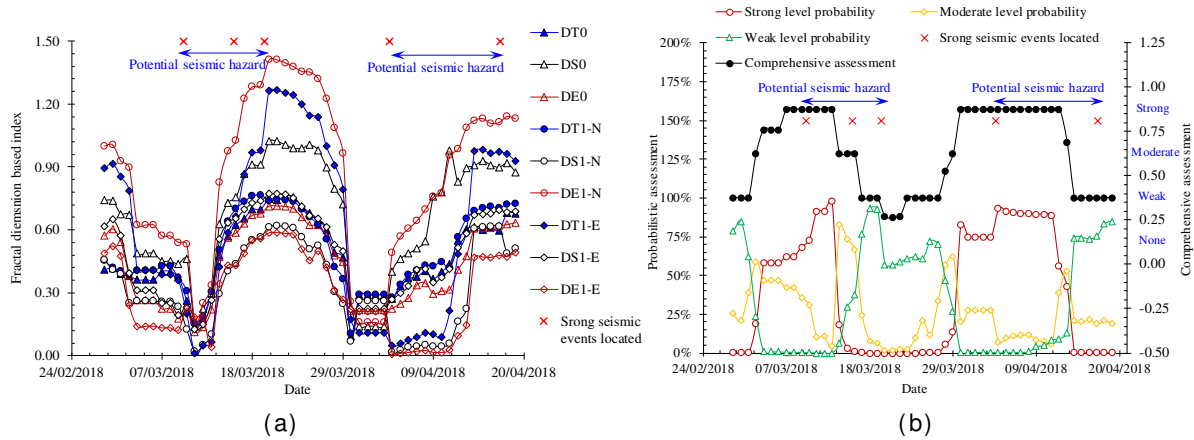


Figure 5.19 (a) Sequential evolution of fractal indices, (b) Probabilistic and comprehensive assessment of seismic hazards at development heading for longwall panel K.-95/D.

Application of the statistical short-term forecasting model at Coal Mine Velenje

The forecasting methodology developed was applied to longwall coal mining-induced microseismicity recorded during 2016-2018 at each of three completed LTCC panels (panels K.-80/B, K.-80/D and K.-80/C) at Coal Mine Velenje, which were considered to have a complete record of mining-induced microseismicity and consist of a relatively large number of events (> 2,500 events each).

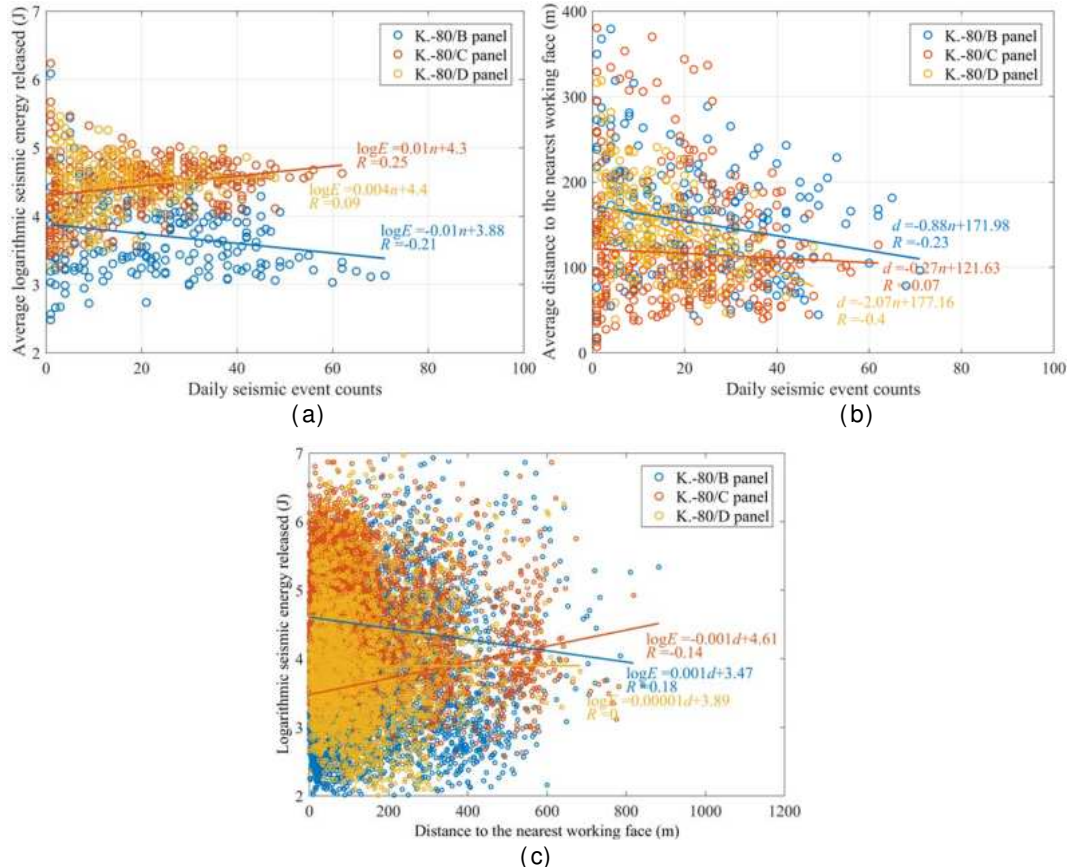


Figure 5.20 Relationship between the daily seismic event rate, average seismic energy released, and spatial distribution of recorded microseismicity around three longwall panels at CM-Velenje.

The length of time window ΔT needs to be determined based on the event rate and mining schedule. Considering the long-term monitored data analysis from Coal Mine Velenje, and the literature a ΔT of 14 days was used in the project. The forecasted probability of hazardous microseismic events was updated on a daily basis ($\Delta t = 1$ day) as a reference in order for a timely evaluation of the hazard potential. The probability of hazardous microseismicity and recommended face advance upper limits were updated each day from 14 days after the start of coal production until abandonment at each panel.

The very low correlation coefficient obtained for each variable pair in Figure 5.20 suggests that each variable is barely influenced by, or at least very weakly correlated with the other two variables. Therefore, the density, size and scaling, and spatial distribution of fractures around the three longwall panels are verified to be mutually independent, and it is practically feasible to employ the joint probability for hazardous microseismicity forecasting.

Figure 5.21 presents an example time-varying scaled daily event count, the probability of a single microseismic event being a large event, and the probability of a single microseismic event being close to the face-line, based on fitted distributions for microseismicity within the moving time window around longwall panel K.-80/D. Here $F(M)$ is the cumulative distribution function (CDF) of the energy magnitude distribution and $F(d)$ is the cumulative distribution function (CDF) of spatial distribution of microseismicity. This figure represents the dynamic evolution of abundance, magnitude and spatial distribution of fractures around the panels as longwall faces advance. The curves are fairly continuous, which verifies that attributes of fractures around longwall panels reflected from the recorded microseismicity are spatially continuous.

The abundance of fractures around K.-80/D panel is steady in the first three months of coal production, but then gradually increases around fivefold by the completion of the panel. The fracture size distribution was found to be mostly stable for all three longwall panels, with reduced risks of large events in some periods, such as 30/08-15/10/2016 for K.-80/D panel. It was interesting to note that the probability of a single microseismic event being close to the face-line showed a general increasing trend for all three panels during coal production. This change indicates elevated levels of spatial clustering of fractures, since all the three longwall faces were advancing towards the central coal pillar with high stress concentration.

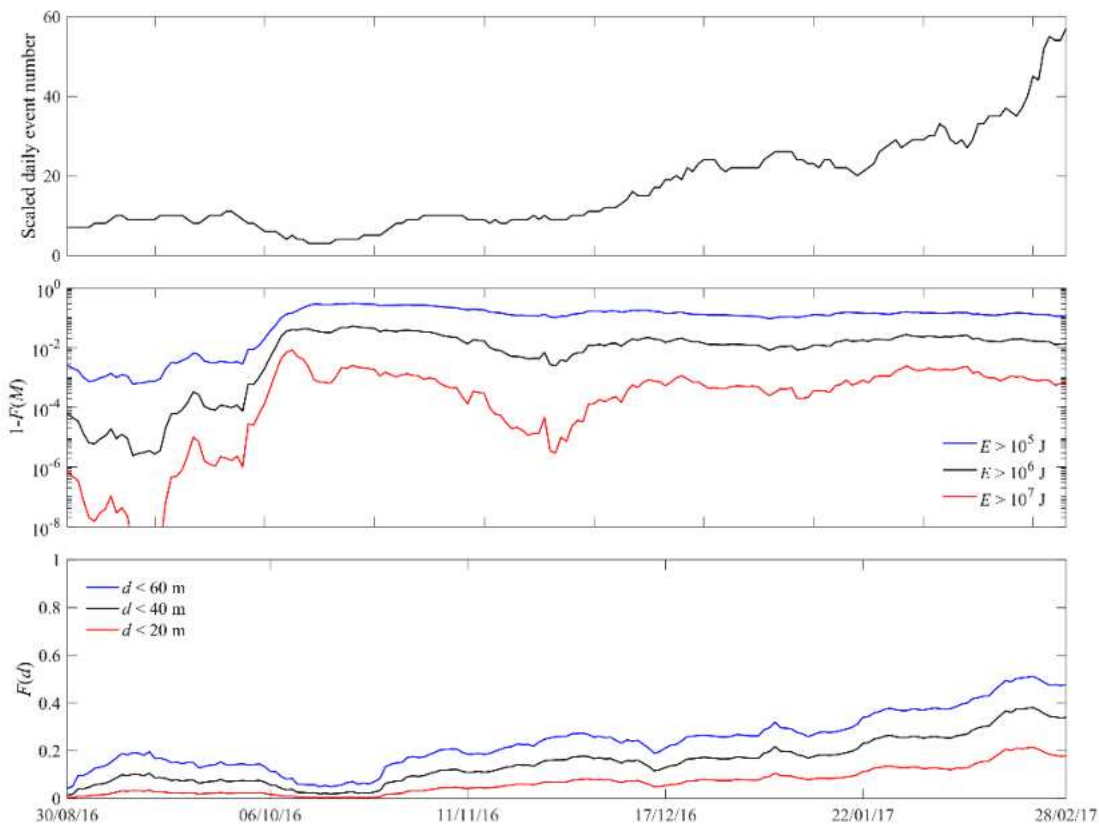


Figure 5.21 Time-varying temporal, magnitude and spatial seismic indicators decoupled from mining activities for microseismicity around panel K.-80/D. (Scaled daily event number under the average face advance rate represents the density of underlying fractures; the probability of a single microseismic event being a large event reflects the size distribution of underlying fractures; the probability of a single microseismic event being close to the longwall face reveals the spatial distribution of underlying fractures.)

Figure 0.22 presents an example time-varying forecasted daily event number, and probability that large microseismicity, microseismicity close to the working face, and hazardous microseismicity occur on the day of forecasting for LTCC panel K.-80/B. Recorded daily numbers of total microseismic events, large events, events close to the working face, and hazardous events are plotted, respectively. The forecasted daily event counts from the statistical model show excellent agreement with recorded numbers of microseismicity, with large event counts being forecasted at high face advance rates, and no events being forecasted when the coal production ceases. Here P_M is the probability that at least one event with a magnitude greater than M occurs over the next time interval Δt , P_d is the probability that at least one event with a distance less than d to the face-line occurs over the next time interval Δt and P is the probability that at least one hazardous event occurs over the next time interval Δt .

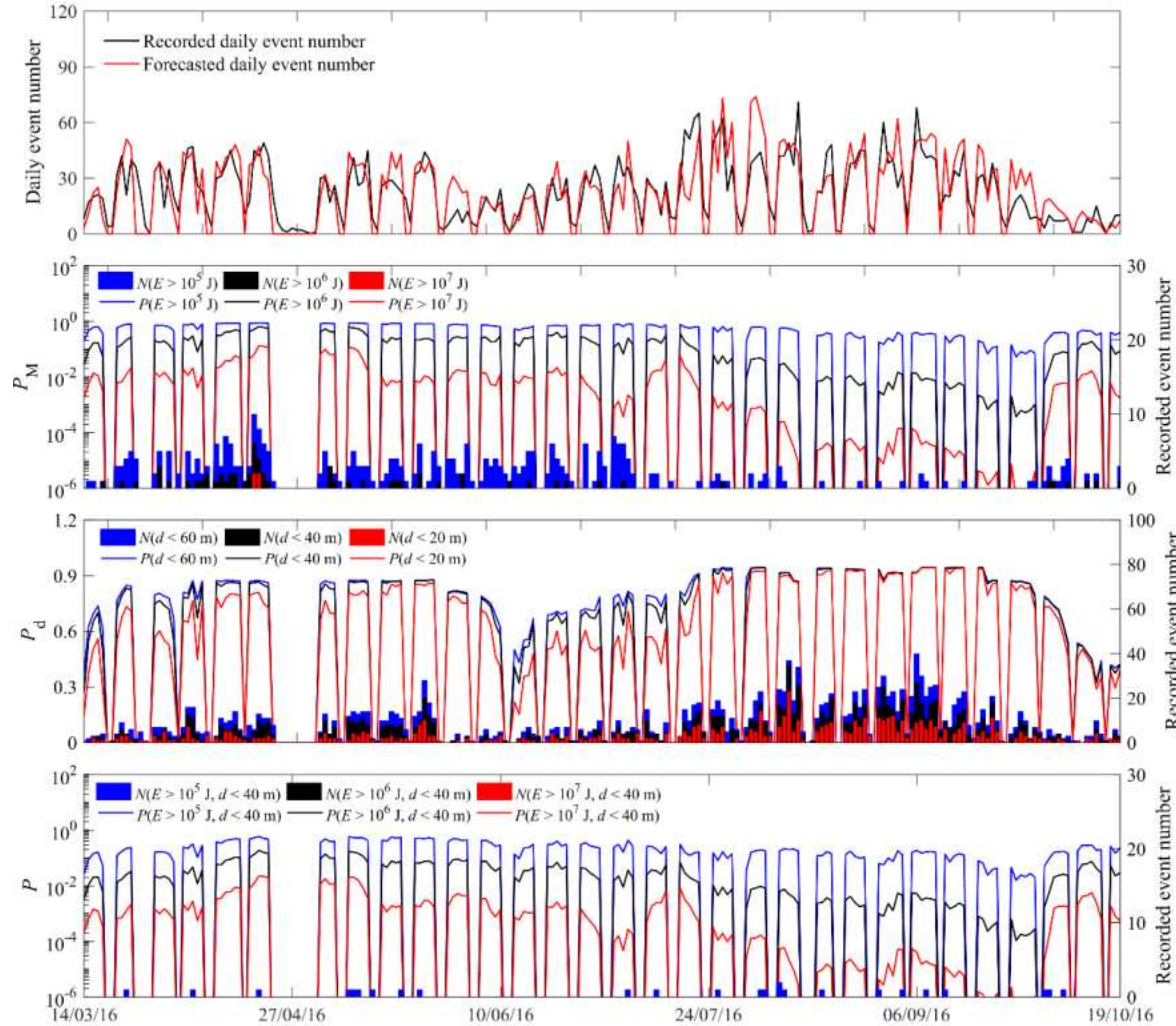


Figure 0.22 Time-varying forecasted daily event number, and forecasted probability that at least a large microseismic event, a microseismic event close to the face-line, and a hazardous microseismic event occurs on the day of forecasting around panel K.-80/B.

The forecasted probability of large microseismicity P_M approximately follows the general trend of $1-F(M)$ in Figure 5.21. When the coal production ceases at weekends or during holidays, the probability of large microseismicity is forecasted as 0 since the forecasted event count is 0. The forecasted probability for microseismicity with an energy released greater than 10^5 J mostly stays at a high level above 70% on working days for all three longwall panels analysed in the project, and it can be seen that these events are quite common. By contrast, the forecasted probabilities for microseismicity at energy levels of 10^6 and 10^7 J show a tremendous decrease of several orders of magnitude, and such events are much less frequent. As can be seen from Figure 0.22, when the forecasted probability of microseismicity with $E > 10^7$ J around the K.-80/B panel reaches a peak of 6.5% and 12.9% on 19 and 20 April 2016, four such large microseismic events occurred around the same panel, two on each of those two days, respectively.

The forecasted probability of microseismicity close to the working face approximately follows the general trend of $F(d)$ in Figure 5.21. For all three longwall panels, more microseismicity were recorded close to the working face when the model estimates a higher probability of such events. As an example, the statistical model estimates the probability that at least a microseismic event occurs close to the working face to be above 90% on working days between 25/07-23/09/2016 at K.-80/B panel. This is verified by recording a large number of microseismicity within 20 m distance to the K.-80/B face during these dates.

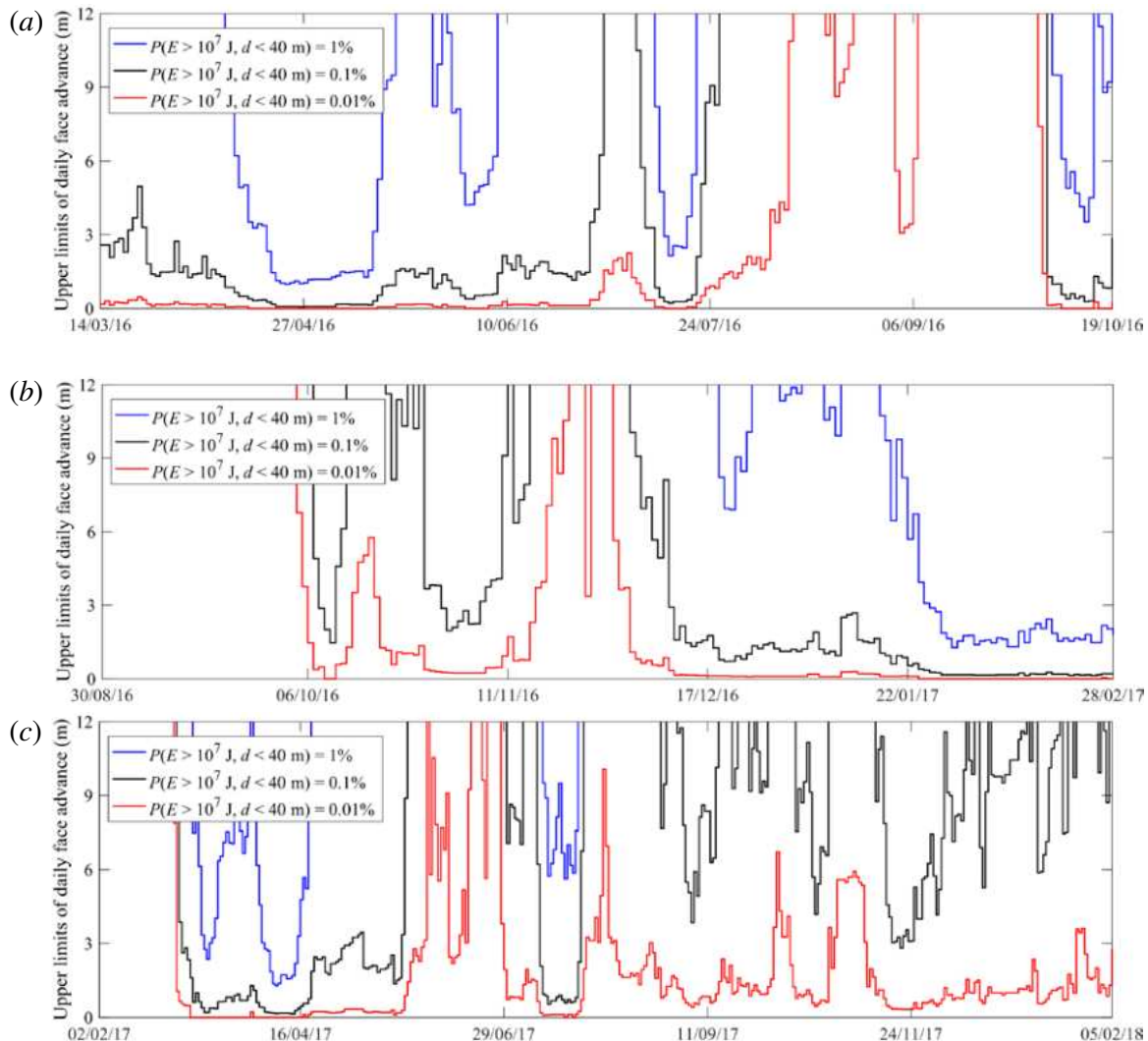


Figure 5.23 Recommended upper limits of daily face advance given probability thresholds of hazardous events for (a) panel K.-80/B, (b) panel K.-80/D, and (c) panel K.-80/C.

It was also shown that the methodology can be used for real-time control of face advance rates based on the probability forecasting. The recommended face advance rates for the three longwall panels modelled in the project were estimated over the coal production period using three probability limits (1%, 0.1% and 0.01%) for hazardous microseismicity ($E > 10^7 \text{ J}$ and $d < 40 \text{ m}$), as shown in Figure 5.23. While a probability limit of 0.01% prohibits longwall mining over a considerable portion of the production period, probability limits of 0.1% and 1% allow higher face advance rates over the period of high hazard risk for the three longwall panels.

Application of the numerical models developed to forecast rock bursts and gas outbursts at partner mines and/or similar mining layouts

The suite of numerical modelling methodologies developed for rock burst and gas outburst risk assessment were also implemented at Coal Mine Velenje and JSW, as well as being representative of mining applications similar to the layouts used by these companies. Table 5.8 presents the modelling methodologies developed applicable to typical mining scenarios and associated rock bursts/gas outbursts conditions, which are also representative of most rock burst and gas outburst cases experienced at partner mines considered in MapROC.

Table 5.8 Modelling methodologies applicable for typical mining scenarios simulated in rock burst and gas outburst risk evaluation.

Modelling methodologies	Mining scenarios	Rock bursts/gas outbursts conditions	Hazards
- Coupled geomechanical and gas flow model	Drifting/longwall mining, stress control mining and protective mining in multiple coal seams	Floor, strong/weak zones, bedding shear zones	Rock bursts/gas outbursts
- Fracture mechanics-based gas outburst model	Drifting mining in thick coal seams (LTCC)	Strong/weak zones, bedding shear zones	Coal and gas outbursts
- DFN-based microseismicity model	Longwall mining in thick coal seams (LTCC)	Strong/weak zones, bedding shear zones	Seismic hazards

The theory and development of all these models were presented in detail in the relevant Deliverable reports. The application of the coupled geomechanical and gas flow modelling for protecting mining in multiple seam layouts such as those at JSW and the modelling of stress control mining were described in detail under WP4 earlier, therefore these are not repeated here.

Modelling of floor outbursts in multiple coal seams

The coupled geomechanical and gas flow model was also utilised to model the initiation of a floor outburst at the upper seam when longwall mining in multiple coal seams in multi-seam layouts similar to those in Pniowek and Budryk colliery type layouts. A 2D model capturing the cross section of an advancing longwall face was constructed (Figure 5.24a). The model domain measures 100 × 150 m (length × height) with finer grids (1 × 1 m) placed at the model centre. Figure 0.24b illustrates the general stratigraphy considered in the model.

Strain-softening model has been used to represent the non-linear post failure behaviour of coal and rock. Coupled geomechanical and gas flow modelling was carried out to simulate face advance at a rate of 2 m per day for 10 days. The vertical stress was determined by computing the overburden weight using an average rock density of 2,260 kg/m³. The two horizontal stresses were assumed to be equal and are a result of the rock Poisson's Ratio response to gravity loading. The initial stress equilibrium was established prior to coal extraction. The rock elastic and strength properties as well as reservoir properties were obtained from the laboratory tests on samples taken from exploration boreholes and field measurements. Reservoir temperature was set as 23 °C. The initial seam gas pressure in coal Seam B was assumed to be the double of that in the coal Seam A. To generate the condition for a floor outburst the mudstone and sandstone structures were assumed to be impermeable.

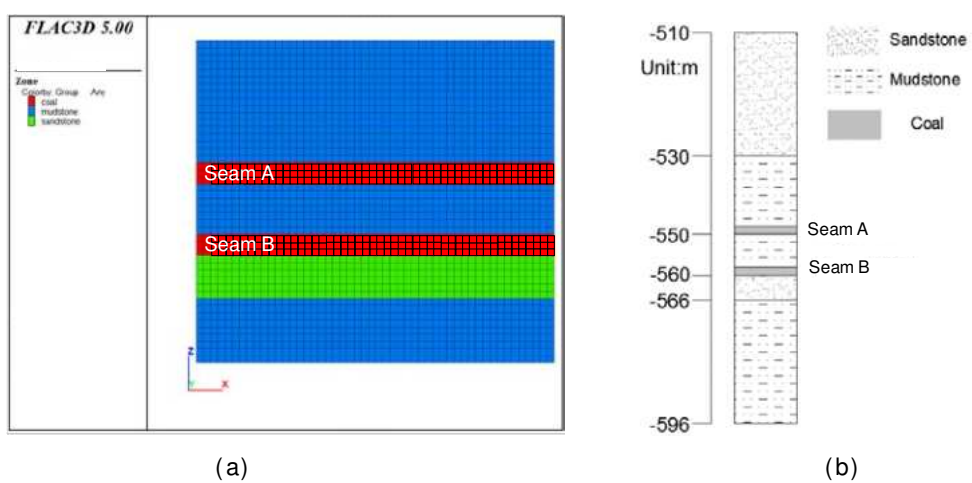


Figure 0.24 (a) Development of a 2D floor outburst model (a close-up view of the central area), (b) General stratigraphy of the floor outburst model.

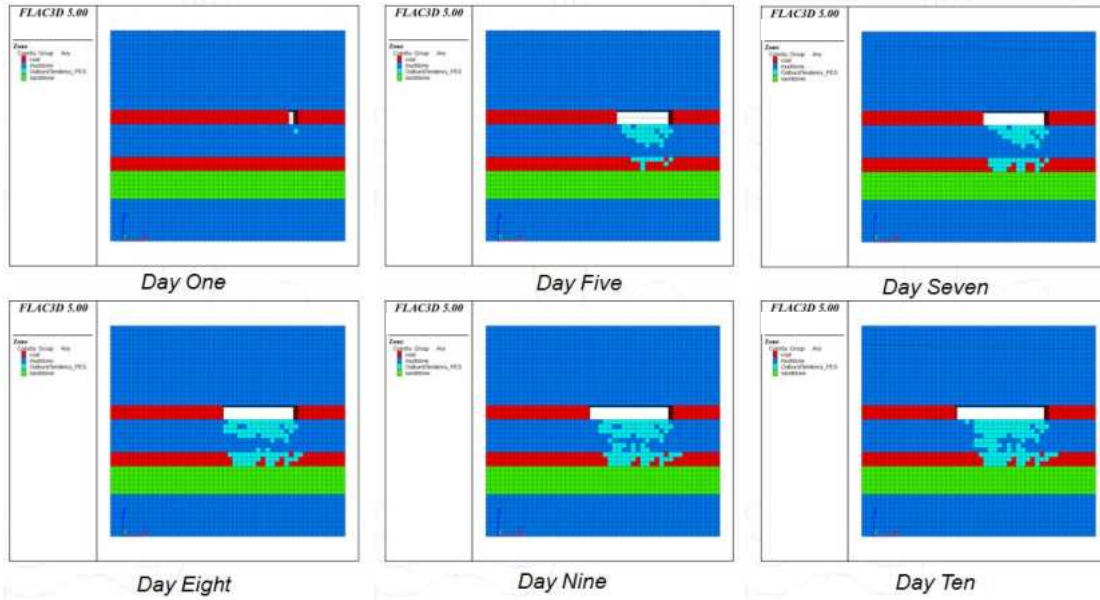


Figure 5.25 Failure of floor coal/rock elements with the advance of the longwall face.

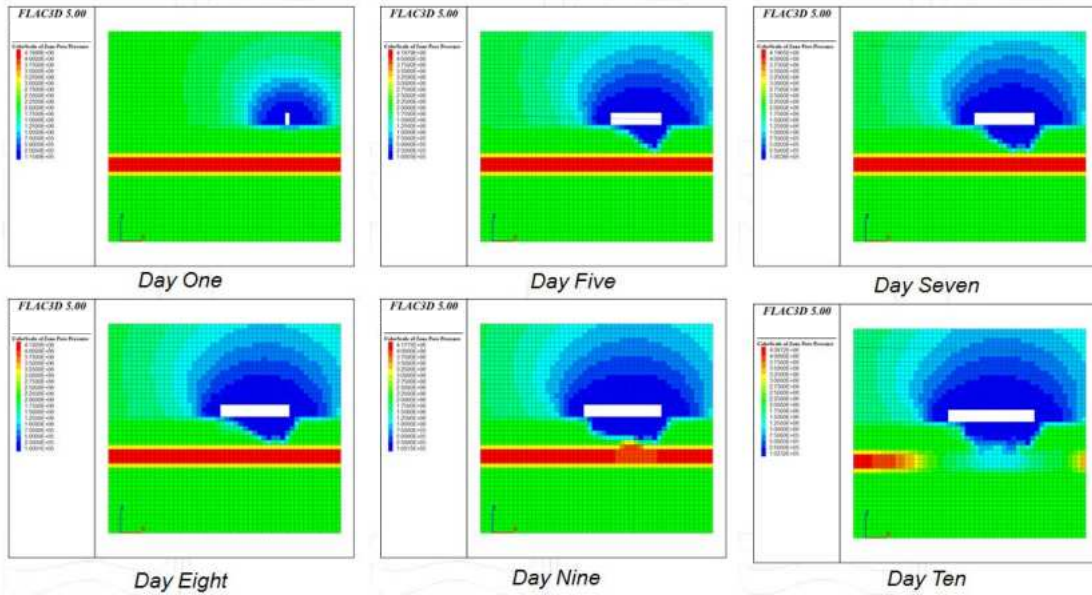


Figure 5.26 Simulated pressure evolution in a floor outburst condition.

Figure 5.25 presents the simulated sequence of floor coal failure as the coal face advances. The corresponding pressure evolution is plotted in Figure 5.26. A notable pressure relief occurs on the 10th day, with the establishment of a flow conduit between coal Seams A and B.

Fracture mechanics-based gas outburst modelling for drifting in thick coal seams

The fracture mechanics-based gas outburst model was adopted to simulate the dynamic process of coal and gas outbursts triggered by roadway development, followed by a parametric analysis on the influence of various factors including fracture toughness of coal, fracture radius, initial gas pressure and in situ stress state. The model developed was applied to model development headings in thick seams, using one of the LTCC layouts at Coal Mine Velenje as illustrated in Figure 5.27. A 6 m × 11 m × 3 m outburst prone zone, represented by a much lower coal fracture toughness, was placed in the coal seam 10 m ahead of the roadway, which was developed by excavation steps. The elements in the outburst prone zone were refined down to 0.2 m in each direction to better represent the gas pressure evolution and mechanical behaviour in response to roadway development.

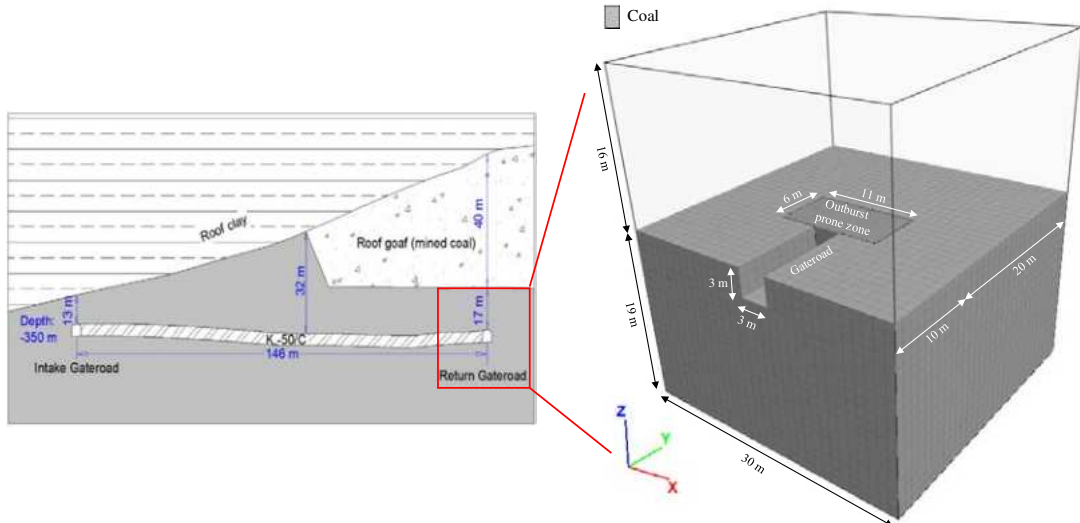


Figure 5.27 General stratigraphy and model geometry of roadway development in the modelled coal seam around LTCC panel K. -50/C.

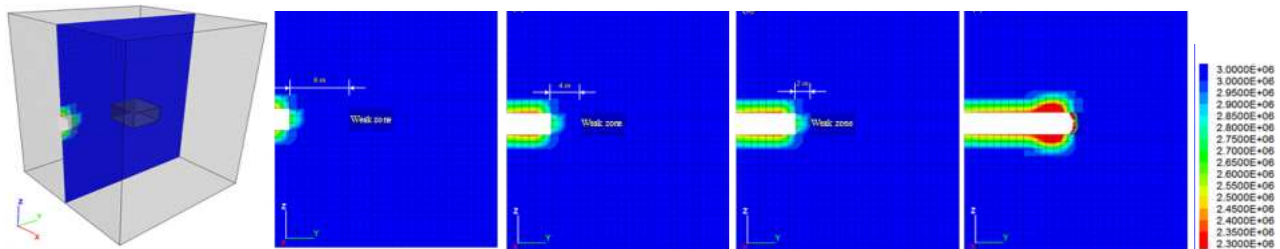


Figure 5.28 Intra-fracture gas pressure distribution caused by gas desorption after each roadway development step (Unit: Pa).

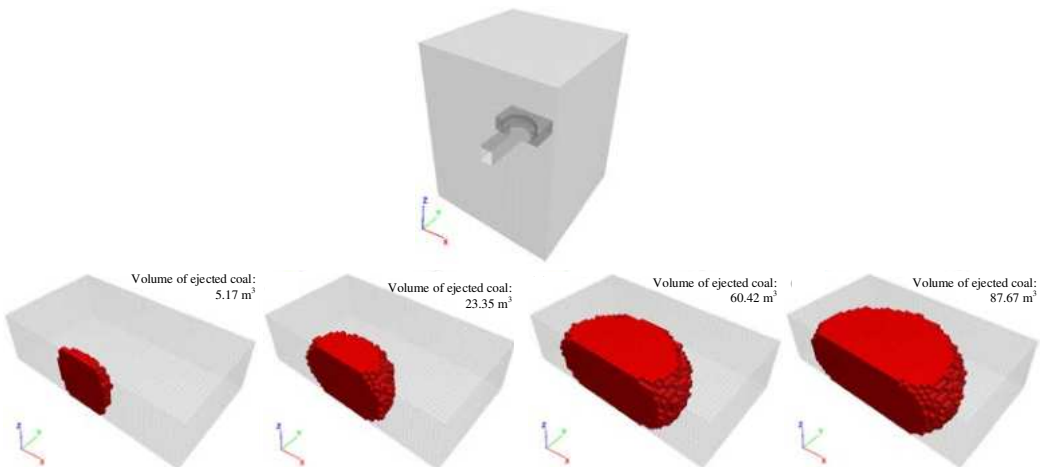


Figure 5.29 Extension of the coal outburst zone over time: 60 s, 180 s, 300 s and 360 s after reaching the outburst prone zone.

Figure 5.28 presents a plan view of the evolution of intra-fracture gas pressure distribution 360 s after each roadway development step. The intra-fracture gas pressure is relieved within a 2 m wide zone ahead of the development face due to mining-induced stresses, but no coal failure is induced during the first three roadway development steps shown. As the development heading reaches the outburst prone zone, a coal and gas outburst is initiated. Figure 5.29 illustrates how the coal outburst progresses from the exposed working face into the outburst prone zone. Expulsion of coal at the working face causes the subsequent ejection of neighbouring coal elements by aggravating the release of in situ stress and facilitating gas desorption-driven fracture opening and propagation. This results in an accelerated growth of the ejected volume of coal over time.

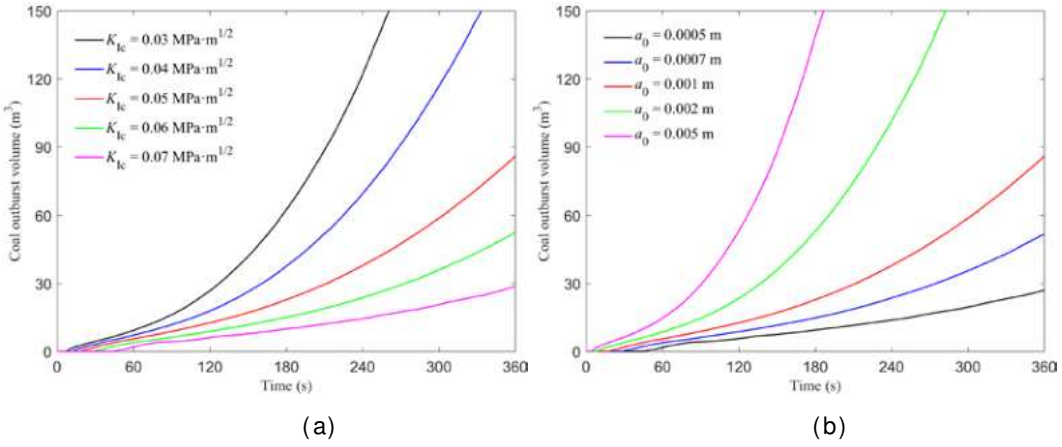


Figure 5.30 Influences of (a) K_{lc} , (b) a_0 on the ejected volume of coal over time.

Based on the model findings, evolution of intra-fracture gas pressure and associated fracture behaviour before and after the onset of gas outbursts were analysed and the effects of different influencing factors on the intensity of coal and gas outbursts evaluated. Figure 5.30 illustrates the effects of different influencing factors on the intensity of coal and gas outbursts, represented by ejected volume of coal over time. The time delay before the onset of a coal and gas outburst is dominated by fracture toughness K_{lc} and fracture radius a_0 . Large fracture toughness, fracture radius and initial gas pressure and low minor principal stress have favourable effects on the intensity of coal and gas outbursts. It was clear that the outburst intensity is very sensitive to fracture toughness and fracture radius.

DFN-based microseismicity modelling in longwall top coal caving mining

By combining deterministic stress and failure analysis and stochastic fracture slip evaluation, a DFN-based microseismicity model was developed and used simulate the field observed microseismic events induced by the progressive advance of the LTCC face towards a heterogeneous xylite-rich zone at Coal Mine Velenje. A 3D model was constructed to represent the LTCC panel K. -50/C, the floor coal and the overlying strata shown in Figure 5.27 above. Figure 5.31(a) presents the 3D model constructed to represent the LTCC panel K. -50/C. The geometry of the xylite-rich zone inferred from the active seis-mic tomography measurements was digitised and implemented into the FLAC3D model, assuming full penetration within the coal panel. Two sets of fractures were employed in the model: one set for the xylite-rich zone (Set 1), and the other for the remaining zones (Set 2). For both fracture sets, the fracture positions and orientations were set to be random, and the fracture radii ranged from 0.9 m to 6.5 m. A fracture number of 44,707 and scaling exponent $a_c = 2.7$ were applied for the Set 2 to calibrate the synthetic microseismic intensity and size distribution to the recorded ones. In order to account for the stochastic nature of DFN, a total of five series of DFN realisations were generated for each modelling scenario.

The elastic properties (bulk modulus and shear modulus) of the xylite were set to be the same as those of coal, and strength properties (compressive and tensile strength) of xylite were set to be one to two times those of coal. A total of twelve extraction steps were simulated (from right to left in Figure 5.31(a), from 23rd May to 28th August. Each excavation step represented coal extraction for one week. The fracture distribution for the modelling scenario is presented in Figure 5.31(b). Multiple runs were carried out with various rock strengths for xylite and fracture attributes within the xylite-rich zone, respectively:

- (1) The geometry parameters for fractures in the heterogeneous zone remained the same as those in the coal seam, and four scenarios were considered by varying compressive and tensile rock strength of elements within the heterogeneous zone: (a) $\sigma_{ch} = \sigma_{cc}$, $\sigma_{th} = \sigma_{tc}$; (b) $\sigma_{ch} = 1.5\sigma_{cc}$, $\sigma_{th} = 1.5\sigma_{tc}$; (c) $\sigma_{ch} = 2\sigma_{cc}$, $\sigma_{th} = 2\sigma_{tc}$, and (d) $\sigma_{ch} = 2.5\sigma_{cc}$, $\sigma_{th} = 2.5\sigma_{tc}$.

where σ_{cc} and σ_{tc} are respectively the compressive and tensile strengths of the coal seam, and σ_{ch} and σ_{th} are those of the heterogeneous zone.

- (2) The rock strength of the heterogeneous zone remained the same as that of the coal seam, and four scenarios were considered by varying the fracture intensity term and size distribution exponent of fractures hosted by the heterogeneous zone: (a) $a_h = 2.7$, $a_h = a_c$; (b) $a_h = 2.4$, $a_h = 0.9a_c$; (c) $a_h = 2.1$, $a_h = 0.8a_c$, and (d) $a_h = 1.8$, $a_h = 0.7a_c$.

where a_h is the power law distribution exponent for the heterogeneous zone, and a_c and a_h are the fracture intensity terms for the coal seam and heterogeneous zone, respectively. Since the fracture density term α is proportional to the fracture number in a certain volume, a_h is controlled by changing

the total number of fractures assigned to the heterogeneous zone. The fracture distribution for the scenario (d) is presented in Figure 5.31b.

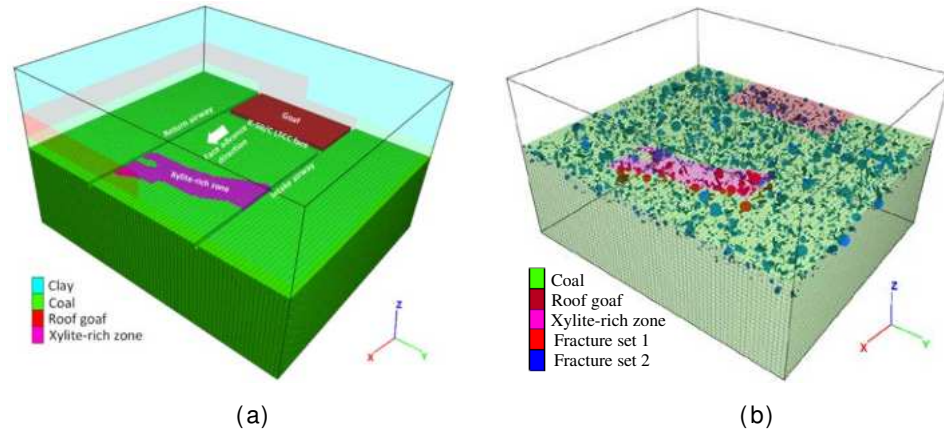


Figure 5.31 Mining geometry and geological implementation of the xylite-rich zone: (a) 3D model geometry, and (b) Distribution of DFNs located at the panel level [-330 m, -350 m] following power law relationship with $a_c = 2.7$, $a_h = 1.8$, $\alpha_h = 0.7\alpha_c$.

Based on the numerical modelling results, the frequency-magnitude distribution, logarithmic released energy, stress drop and the effects of fracture attributes on seismic response were evaluated. Figure 5.32a presents the variation of fitted b values from frequency-magnitude distribution of recorded and simulated microseismicity over the monitoring period. When the rock strength of elements within the xylite-rich zone is the same as that of coal, b values of microseismicity are quite consistent. When the rock strength of elements within the xylite-rich zone is stronger than that of coal, there is a notable reduction in b values several weeks before the xylite-rich zone is reached. An average b value of 0.67 can be fitted when approaching the xylite-rich zone for the modelling scenario $\sigma_{ch} = 2.5\sigma_{cc}$, $\sigma_{th} = 2.5\sigma_{tc}$.

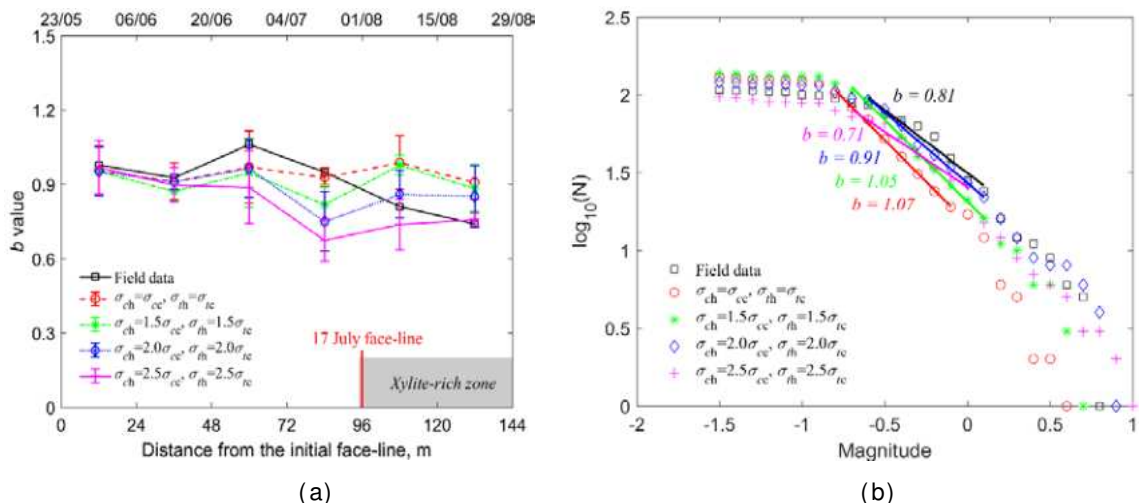


Figure 5.32 (a) The bi-weekly b values for frequency-magnitude distribution of the recorded and simulated microseismic events over the monitoring period, (b) Examples of b values obtained through regression fitting for the recorded and simulated microseismic events during 1 to 14 August 2011.

Figure 5.32b shows an example of the frequency-magnitude distribution of recorded and simulated microseismicity during a two-week period after reaching the xylite-rich zone. The frequency-magnitude distribution for different modelling scenarios approximately follows a power law relationship, but the fitted curve becomes less steep with increasing rock strength of elements within the xylite-rich zone, i.e. the b value decreases. When the rock strength of elements within the xylite-rich zone is 2.0-2.5 times of that of coal, the fitted b values match well with that of recorded microseismicity.

Note that, following the Gutenberg and Richter law, the magnitude-frequency plot of microseismic events follows a power-law relationship:

$$\log_{10} N = a - bM$$

Where N is the number of events with a magnitude larger than magnitude M , and a and b are constants. Results from DFN-based microseismicity modelling in longwall top coal caving mining suggested that both the high rock strength and low scaling exponent of fractures contribute to deviations of microseismic characteristics such as the decrease of b value. Such deviations in recorded microseismicity are believed to result from the combined effects of increased stress drops and slipped fracture sizes when the heterogenous xylite-rich zone is approached. The results can provide implications for a precursory detection of abnormal geological strata and fracture attributes.

Conclusions

Results have suggested that both field microseismic monitoring-based risk evaluation methodologies and numerical modelling methodologies were able to represent mining induced microseismicity. Results obtained also provide insights on mechanisms of seismic hazards, such as the fracture-slip mechanism of microseismicity associated with longwall top coal caving mining, and gas-desorption driven fracture propagation in coal and gas outbursts.

The successful application of the risk assessment methodology developed leads to the confidence to extend its application to risk assessment for a wide variety of rock burst and gas outburst prone conditions, including but not limited to strong/weak zones, bedding shear zones, fracture zones, stress concentration districts, gas-rich coal seams and unfavourable mining layouts, as indicated in the proposed generic model and field measurements. The generic methodology is believed to be applicable to most European coal mines with different geological and mining conditions.

As each risk assessment method was developed aiming at a specific forecasting purpose and addresses a certain concerned feature associated with rock burst and coal and gas outburst hazards in coal mines, it is recommended to apply an appropriate risk assessment method depending on the local geological and mining conditions, interested key indicators, monitoring techniques available and specific forecasting requirements.

Task 5.3 Modelling and probabilistic assessment of risk for rock bursts and gas outburst in coal mines (led by IMPERIAL, JSW, CM-VELENJE)

This Task follows on from Tasks 5.1 and 5.2 where a generic risk assessment methodology was developed in Task 5.1 and the different elements of the methodology, developed based on the research findings of WPs 2, 3, and 4 were applied using mining layouts relevant to the partner mines operated by JSW and Coal Mine Velenje in Task 5.2 in a deterministic way. However, there are a number influencing parameters which interact with each other within the mining system in a complex manner and affect liability to rock bursts and gas outburst in coal mines. In this task, the numerical models developed in Work Package 4, Task 4.2 were generalised by implementing a parametric assessment approach to the model runs to understand the interaction between several of these influencing parameters. Stochastic models were simulated and analysed by varying the major influencing parameters leading to rock bursts and gas outbursts as identified in the project.

Rock engineering system (RES) is used to list all the causative factors in a coherent way integrating the knowledge in a field into a coherent whole. RES enables recognition of various interconnections within a system which may not be apparent from the behaviour of individual sub-systems. It enables understanding of the whole system as an integration of several parts and their interdependencies and synthesising. Since rock bursts and gas outbursts have a complex mechanism, a detailed interaction matrix of the rock engineering system was developed for the analysis of the occurrence of rock bursts and gas outbursts in underground coal mines.

Furthermore, the numerical modelling methodologies developed were implemented towards testing of a probabilistic risk assessment methodology to evaluate the effect of lithological heterogeneity on rock bursts and gas outbursts in longwall coal mining. Mechanical, elastic and reservoir properties of a heterogeneous coal seam were attributed consistently for several realisations to analyse their influence on rock burst and gas outburst potential. To demonstrate the probabilistic risk assessment methodology, several scenarios were developed by varying the degree of lithological heterogeneity caused by xylite within a mostly detritic lignite coal seam in the modelled heterogeneous zone using the Velenje deposit example which was introduced under the last section of Task 5.2 in this report (Figure 5.31).

Interaction matrix and Rock Engineering System based approach to risk assessment

In this part of the project, the coupled numerical models developed and applied to sacrificial roadways/yield pillars and eccentric mining layouts in Task 4.2 were combined with the Rock

Engineering System (RES) methodology to consider various interconnections within a system which may not be apparent from the behaviour of individual sub-systems. An interaction matrix was created for a comprehensive assessment of all the mining, geomechanical and reservoir engineering factors for risk evaluation.

Models developed in Task 4.2 were used to understand the relative dominance of each influencing factor on the rock engineering system. In order to carry out the numerical analysis, a 3D generic base model was developed as illustrated in Figure 5.33 and used in all the parametric analysis.

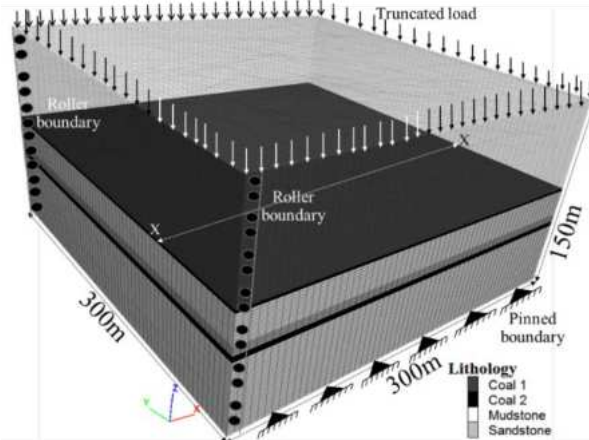


Figure 5.33 Base model developed in FLAC3D™ with boundary conditions.

Parametric analysis of sacrificial roadways/yield pillar layouts

To optimise the dimensions of yield pillars, two different layouts corresponding to yield-abutment pillars (2-entry and 3-entry) were analysed. A schematic layout of the 2-entry system is shown in Figure 4.16 and the 3-entry system is shown in Figure 0.17 presented under WP4 were used to analyse eError! Reference source not found.ight different layouts in FLAC3D™. The parametric variations undertaken in the analysis are listed in Table 5.9. The elastic and mechanical properties of coal, rock and floor were varied at different mining depths.

Table 5.9 Parametric variations in the yield pillar design

Parameters	Variations
Mining height	2m, 4m
Mining depth	600m, 800m, 1000m, 1200m
No. of rows of Yield pillars	1, 2
Yield pillar width	5m, 10m, 15m, 20m
Chain pillar width	50m, 60m

Based on the analysis presented in Task 4.2, yield pillars with a width to height ratio over 2 were accumulating large amount of vertical stress and elastic strain energy leading to situations of rock bursts and gas outbursts. The deflection of the roof was analysed for eight different mining layouts as compared for different seam thicknesses at different depths in Figure 5.34a (mining layouts 1to 8 are shown in detail in D4.2 report), indicating that the deflection of the roof is much smaller for a coal seam thickness of 2m at all depths, where the magnitude of deflection increases with an increase in mining depth. This was attributed to stiffer yield pillars with a width to height ratio > 2 for a coal seam thickness of 2m. A comparative graph analysing the vertical stress accumulation for a coal seam thickness of 2m and 4m at all mining depths is shown in Figure 5.34b. It can be observed that the vertical stress acting on 2m pillars/panel is higher at all mining depths as compared to those acting for a coal seam thickness of 4m.

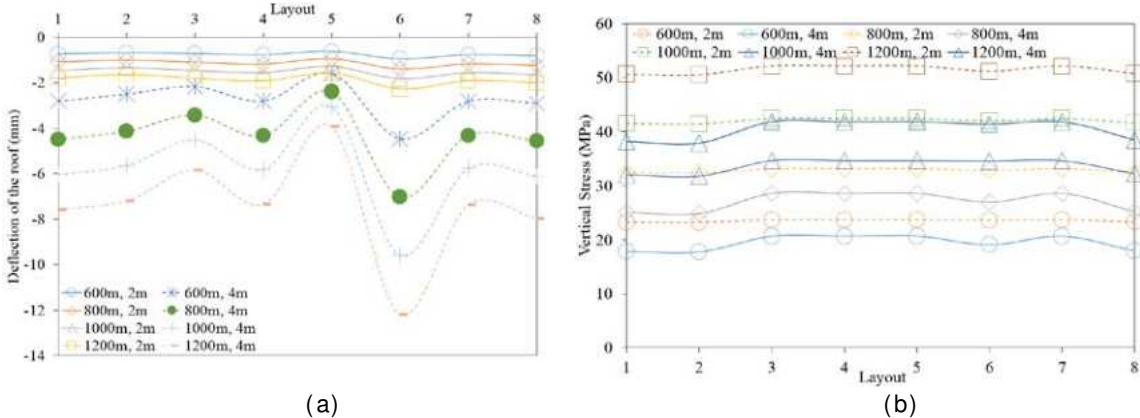


Figure 5.34 Comparative analysis of (a) the deflection of the roof and (b) the vertical stress accumulation for a coal seam thickness of 2m and 4m at all mining depths.

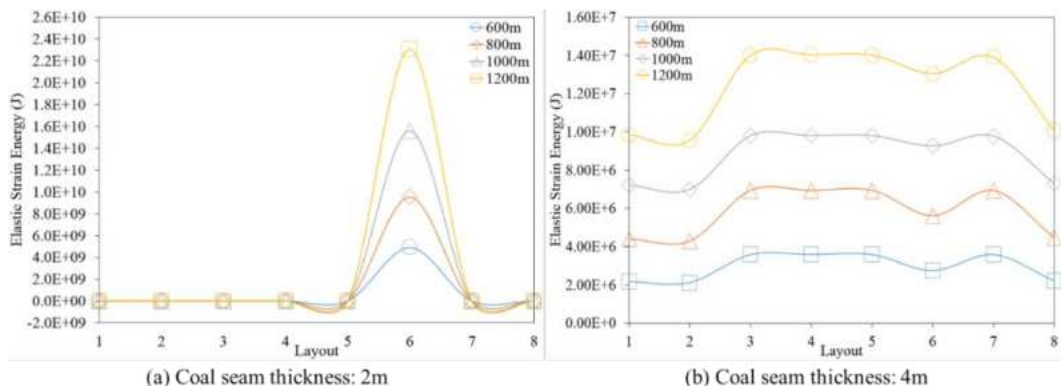


Figure 5.35 Variation in elastic strain energy accumulation in the coal seam for different mining depths.

Figure 5.35 shows that the elastic strain energy accumulated in the coal seam with a thickness of 2m is three orders higher than the elastic strain energy accumulated for a coal seam thickness of 4m. It was also found that the elastic energy accumulation in 3-entry layouts with 5 m yield pillars is significantly higher as compared to all other mining layouts, and make them prone to rock bursts and gas outbursts and hence should be avoided. It was concluded that, symmetric mining layouts (as in layout 1, layout 2 and layout 8 in Figures 4.16 and 4.17 presented earlier) offered relatively better ground control conditions as compared to asymmetrical mining layouts.

Parametric analysis of eccentric mining layouts

Different eccentric mining layouts as detailed in Task 4.2 Figures 4.23 and 4.24 were designed to analyse the vertical stress and elastic strain energy relief in the lower seam in multi-seam workings at JSW and many other similar mining conditions in Europe. The mining layouts were parametrically varied to assess the influence of an overlying goaf on working in the lower seam. The parameters were varied as listed in Table 5.10.

Table 5.10 Parametric variations in the eccentric mining layouts

Parameters	Variations
Mining height	2m, 4m, 6m
Mining depth	600m, 800m, 1000m, 1200m
Interbedding thickness	10m, 25m, 40m

Figure 5.36a illustrates that the maximum deflection of the roof in the lower seam is the largest for an interbedding thickness of 10m and a thicker upper seam induces relatively less deflection of the roof in the lower seam. The maximum vertical stress acting on the lower seam varies non-linearly with the change in coal seam thickness in the upper seam for the same interbedding thickness and, with an increase in the interbedding thickness, the induced vertical stress in the lower seam decreases (Figure 5.36b). Figure 5.36c illustrates that the maximum elastic strain energy accumulated in the lower seam decreases with an increase in the interbedding thickness. Similar trends were observed at other mining depths. It was therefore concluded that an eccentricity of around 80m or half the width of the longwall panel would significantly reduce the ground control problems leading to rock bursts and gas outbursts in the lower seam in multi-seam workings.

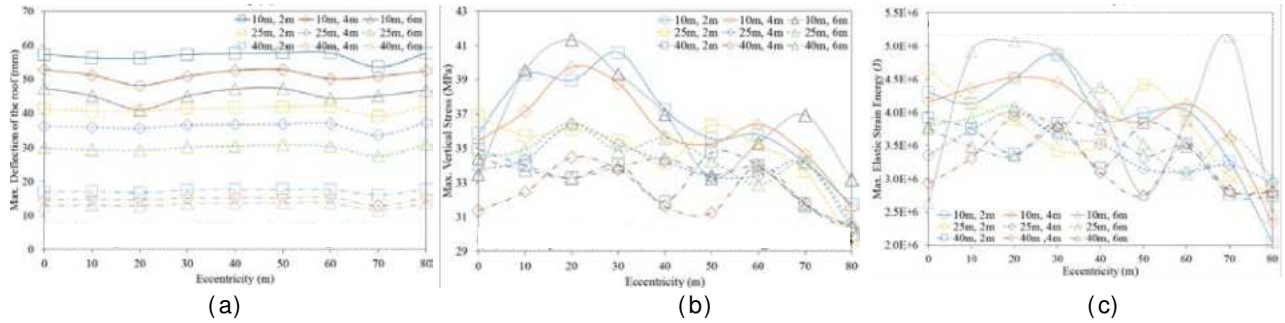


Figure 5.36 Comparison of the variation (a) in the deflection of the roof in the lower seam, (b) in the vertical stress acting on the lower seam and (c) in the elastic strain energy accumulated in the lower seam for different interbedding thicknesses in a multi-seam working at 1,000m mining depth.

Parametric analysis of protective mining layouts

The two-way coupled geomechanical and gas flow model developed was used to analyse the effect of different mining geometries and seam gas content to investigate the nature of stress and gas pressure relief achieved in protective mining scenarios. Using the base model (Figure 5.33) and the layout in Figure 5.37 a parametric analysis was undertaken by varying different influencing parameters as listed in

Table 5.11.

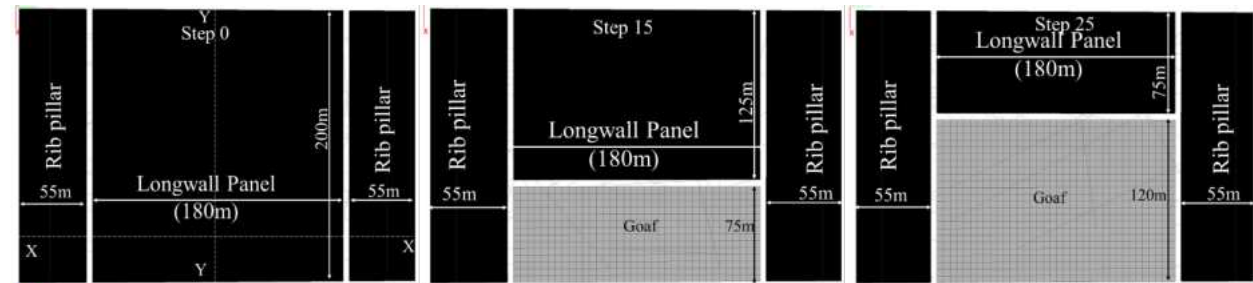


Figure 5.37 Numerical modelling layouts at different excavation steps for the protective seam.

Table 5.11 Parametric variations in the protective mining layouts

Parameters	Variations
Mining height (m)	2m, 4m
Mining depth (m)	600m, 800m, 1000m, 1200m
Interbedding thickness (m)	10m, 25m, 40m
Gas content (m ³ /tonne)	5, 10, 15

Besides the deflection of the roof and the vertical stress concentration in the upper seam which is mined as the protective seam and the protected seam below, the elastic strain accumulation in the two seams and the gas pressure variation in the protected seam were studied for the scenarios set up. It was observed that, along section XX (Figure 5.37) of the longwall face, the elastic strain energy accumulation increases towards the centre of the panel and with mining depth. It was also found that there is a corresponding energy relief in the protected seam due to an overlying goaf (Figure 5.38). Figure 5.39 shows that there is around 1MPa gas pressure relief in the protected seam due to mining in the protective seam with a thickness of 2m for an interbedding thickness of 25m.

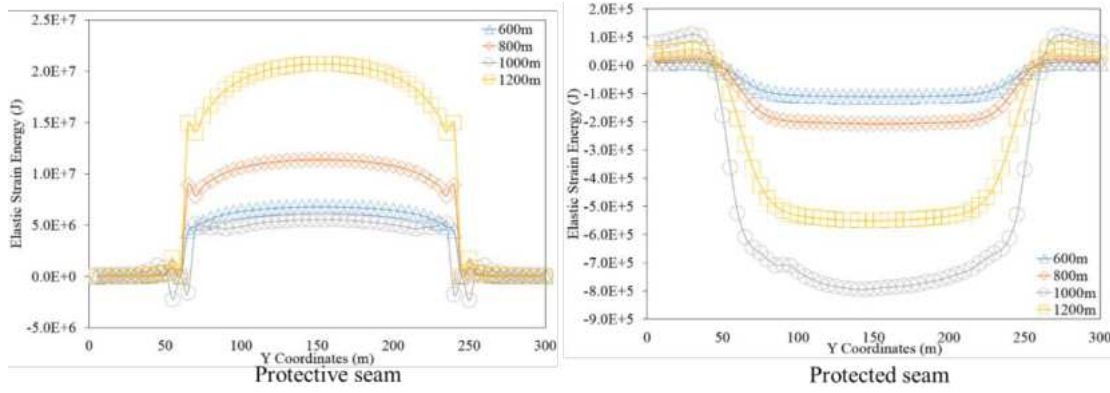


Figure 5.38 Elastic strain energy accumulation in the protective seam and the protected seam for an interbedding thickness of 25m for a seam thickness of 2m (along section XX in Figure 5.37).

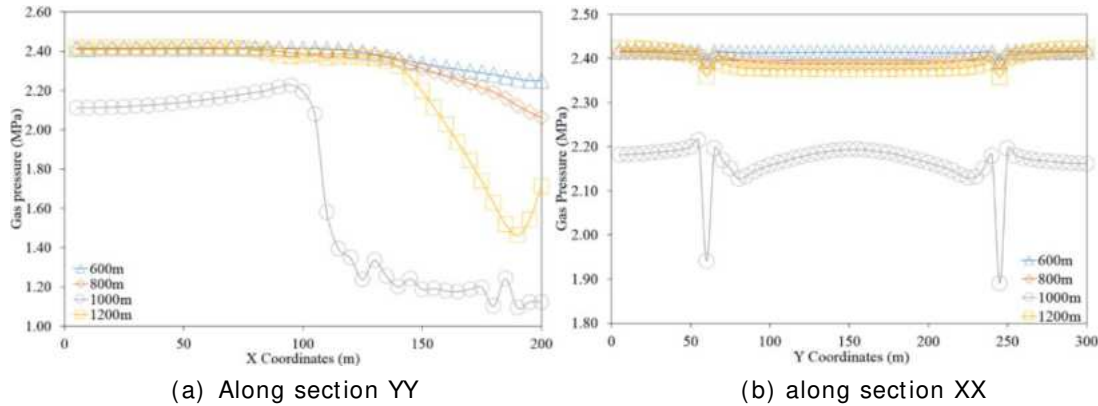


Figure 5.39 Gas pressure variation in the protected seam (along section XX and section YY in Figure 5.37).

Probabilistic risk assessment methodology to evaluate the effects of lithological heterogeneity
The parameters that influence the occurrence of rock bursts and gas outbursts include:

- a) mine design parameters, such as depth, the geometry, seam thickness and overburden,
- b) geomechanical characteristics of the seam, the immediate roof and the floor, and
- c) reservoir parameters, like gas pressure, gas composition, sorption properties, porosity and permeability of the coal seam.

Most of the previous research considered an underground mining scenario with a homogeneous distribution of rock and coal lithotypes and isotropic rock properties within the mining area. However, coal seams formed in different coal accumulation environments are inherently heterogeneous. Such heterogeneity in the coal seam induced during coal formation may adversely affect the safety of mining operations by inducing rock bursts and gas outbursts.

Previous research by Imperial College in MapROC and other RFCS projects found that lithological heterogeneity can contribute to the occurrence of microseismicity associated with rock bursts and gas outbursts. As the last step in this project, and in order to assess the rock burst and gas outburst potential associated with heterogeneous coal deposits, a systematic probabilistic investigation was conducted by varying the degree of heterogeneity and associated geomechanical and reservoir properties of the heterogeneous lignite seam. Rock burst and gas outburst risk in the heterogeneous lignite seam representing Coal Mine Velenje conditions was assessed in terms of stress and gas flow behaviour.

A geostatistical non-conditional simulation method was used to distribute lithological properties within a heterogeneous zone in the lignite coal seam to be mined in the model. The coupled gas flow and geomechanical model was developed to model the retreating longwall top coal caving face towards the heterogeneous zone using ECLIPSE 300 and FLAC3D.

Previous seismic monitoring research conducted at Coal Mine Velenje led to the identification of areas of xylitic dominance contributing to the potential for rock burst and gas outburst risk at the mine. Taking analogy from the field cases, a three-dimensional fork-shaped solid was created with varying extent along the X-, Y- and Z- axes, and a lateral offset in the vertical plane, considering the burial of trees by river streams over a long period of time to represent a xylite-dominated area. A 500 m

$\times 500 \text{ m} \times 150 \text{ m}$ model grid was developed in FLAC3D along the X-, Y- and Z- axes, respectively. The grid size was maintained as $5 \text{ m} \times 5 \text{ m} \times 3 \text{ m}$ along the X-, Y- and Z- axes. The fork-shaped solid, assuming full penetration in the coal seam, comprised a total of 10,703 heterogeneous coal grid cells (Figure 5.40a).

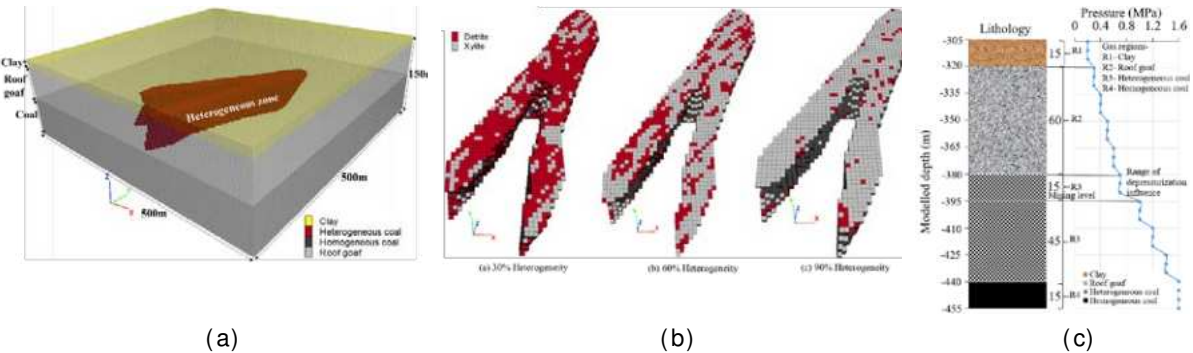


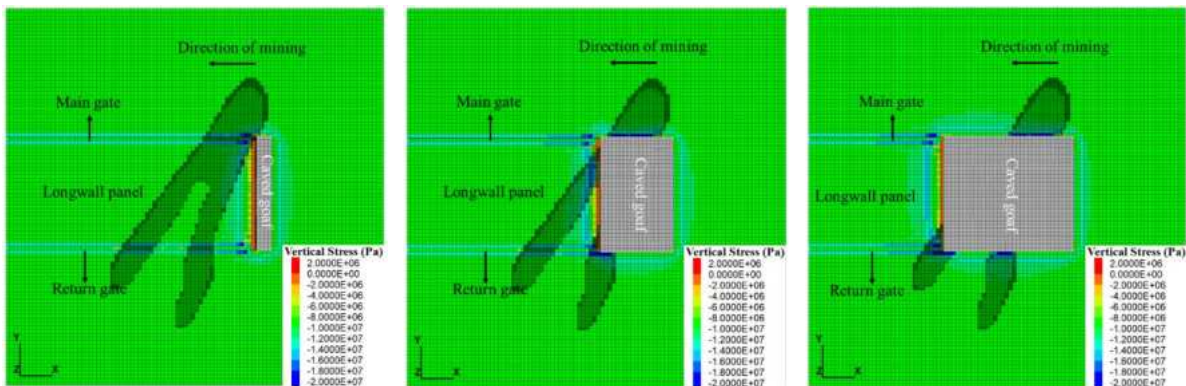
Figure 5.40 (a) The fork-shaped solid imported as a heterogeneous zone in the model grid developed in FLAC3D, (b) Example distributions of xylitic and detritic coal in the heterogeneous model zone, (c) lithology and gas pressure gradient used in constructing the coupled model.

An identical resolution grid in the geostatistical software Isatis was used to generate lithological distributions of xylite throughout the model domain. The ratio among the semi-major axes of xylite ellipsoids was maintained as 4:2:1. Several distributions with a different number of Poisson points were simulated to vary the proportion of heterogeneity and were only retained for the fork shaped heterogeneous zone in FLAC3D. All grid elements with a heterogeneity value above '0' (xylite ellipsoid assignment) were re-grouped as xylite, while all other values were considered as detritic coal. Several distributions, as illustrated in Figure 5.40b, were considered for the analysis, out of which the two examples (30% and 90% heterogeneity) discussed here.

The lithology used in the numerical model along with different rock layers, including heterogeneous and homogeneous coal zones is shown in Figure 5.40c. The elastic, mechanical, porosity and permeability properties and pure gas Langmuir adsorption isotherms for carbon dioxide and methane determined in the laboratory representative of samples obtained from Coal Mine Velenje were used. The fluid pressure in the model was assigned as shown in Figure 5.40c.

To simulate a depth of -305 m, an overburden load was applied on the top surface considering a density of $2,360 \text{ kg/m}^3$ and the model was gravity loaded. A model was developed in ECLIPSE with the same model dimension as in FLAC3D to facilitate seamless assignment of heterogeneous values to the zones in ECLIPSE. The coalbed methane module in ECLIPSE was used with two different coal regions to represent different desorption behaviour for detrite and xylite.

A longwall panel with a face width of 140 m was developed and, after preliminary runs to stabilise fluid pressure, the model was run for 40 excavation steps of 5 m face retreat, simulating the process followed in LTCC for a 15 m thick excavation. This process continued during which the longwall face passed from the non-heterogeneous zone into heterogeneous zone and beyond (Figure 5.41) to record the variation in vertical stress, gas pressure build-up and gas emission rate at the longwall face and the different heterogeneity scenarios modelled analysed.



(a) After five excavation steps. (b) After twenty excavation steps. (c) After thirty-five excavation steps.

Figure 5.41 Different stages of development and longwall top coal caving mining sequence.

The coupled model developed with the xylite heterogeneity scenarios was sequentially extracted to represent a retreating longwall top coal caving mining panel. To analyse the effect of heterogeneity on the vertical stress redistribution and gas pressure build-up, two cross-sections- one along XX and another along YY (Figure 5.42) were so chosen that they intersect the heterogeneous zone. The green intersections in the cross-section represent the zones where the cross-section cuts through the heterogeneous zone.

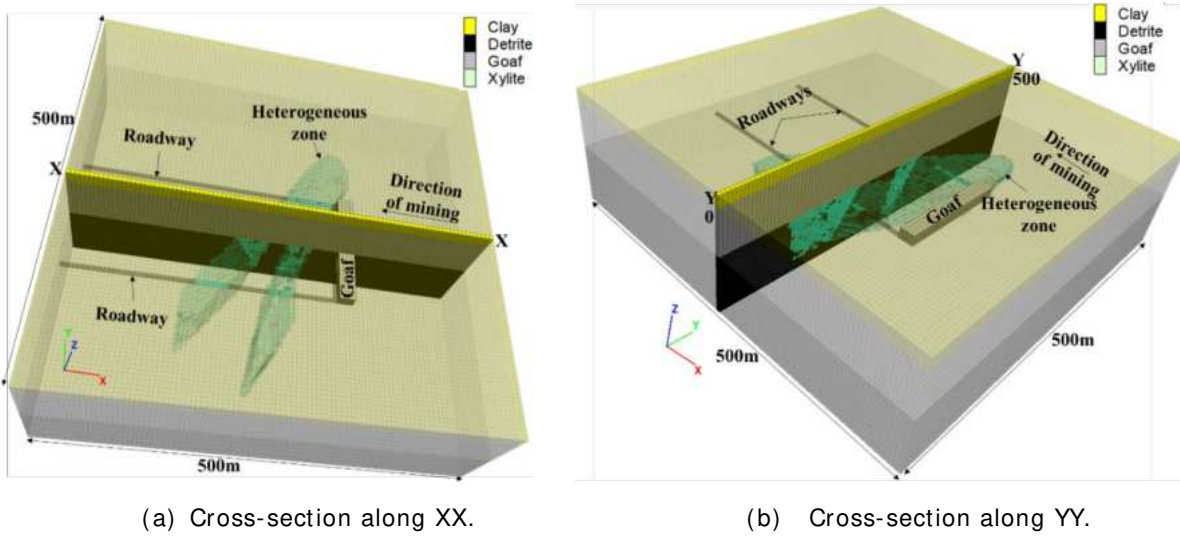


Figure 5.42 Cross-sections along which the vertical stress and gas pressure build-up are analysed.

As Figure 5.43a illustrates, pore pressure was relatively lower over the main heterogeneous zone and does not change significantly as the face advances towards this zone.

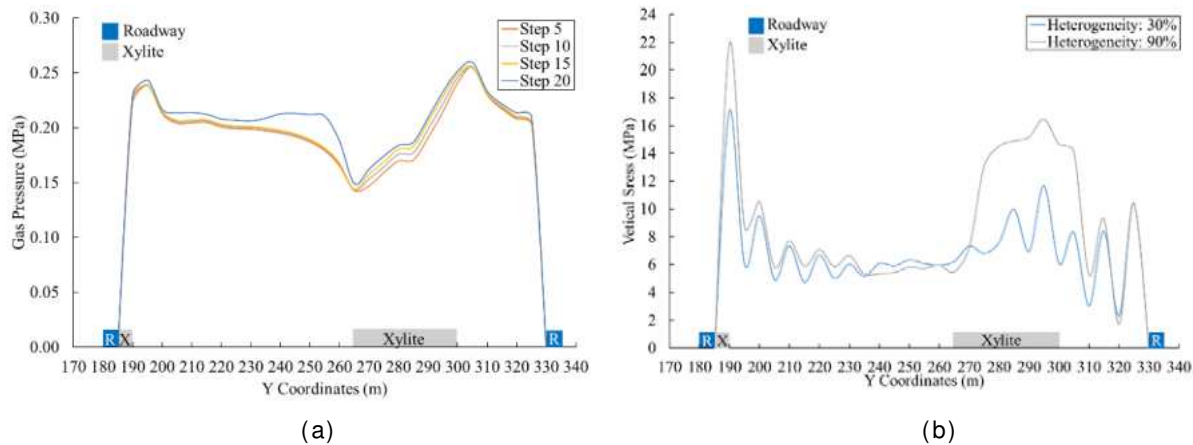


Figure 5.43 (a) Variation in pore pressure along the longwall face and the panel edges for 90% xylite heterogeneity (YY section), (b) comparison of vertical stresses acting on the longwall face and the panel edges for 90% and 30% xylite heterogeneity cases at excavation step 20 (YY section).

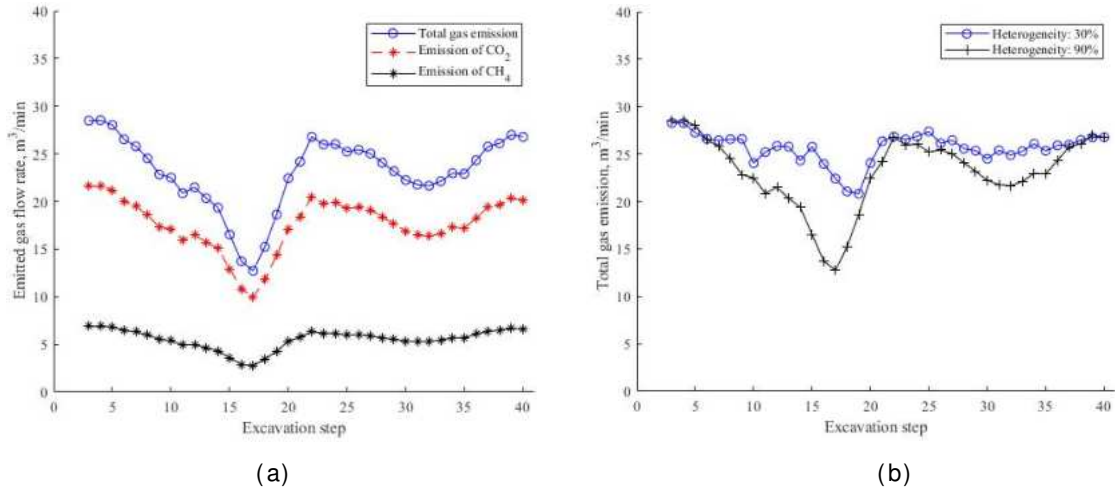


Figure 5.44 (a) Gas emission rate from the longwall face at 90% xylite heterogeneity (b) Total gas emission rates from the longwall face for two different heterogeneity scenarios.

Different degrees of heterogeneity assigned to the heterogeneous zone were used to assess the effect of heterogeneity on stress, gas pressure build-up and gas emission rate at and around the longwall faces. Figure 5.43b presents a comparison between the findings for 30% and 90% xylite heterogeneity for vertical stresses acting on the longwall face and the panel edges

As presented in Figure 5.44a, for 30% and 90% xylite heterogeneity, the total gas emission rate decreases steadily from ~30 m³/min to less than ~15 m³/min as the face approaches the heterogeneous zone, and then builds up rapidly as the heterogeneous zone is cut through by the advancing longwall face, releasing the gas accumulated behind this zone. Figure 5.44b illustrates the total gas emission rates for 30% and 90% xylite heterogeneity cases. While the gas emission rate at 30% heterogeneity case is relatively steady, the sharp decline towards the heterogeneous zone and a rapid increase in the gas emission rate as the face cuts through this zone for 90% heterogeneity case suggests that the presence of a high strength and low permeability xylite zone may create a potential gas outburst risk. This suggests that, depending on the degree of lithological heterogeneity, excessive gas emission or gas outburst conditions may be present at the face.

This work has shown that there is significant benefit in extending the probabilistic approach to implement a more comprehensive set of research with much varied heterogeneity representations in the future.

WORK PACKAGE 6 - CONCLUSIONS, RECOMMENDATIONS AND DISSEMINATION

The main objectives of this WP were:

- To compile the background state of the art knowledge in rock bursts and gas outbursts together with the MapROC project related research findings, field practice and experience gained from the research outcomes and present these at a project Workshop to disseminate this knowledge to a wide audience within the European coal mining community.
- To compile a project “lessons learnt and recommendations document” in the form of best-practice document upon completion of all the project tasks, and issue to assist industrial stakeholders and the scientific community towards achieving the general objectives of controlling and preventing rock bursts and gas outburst in coal mines

This WP was led by GIG.

Task 6.1 Dissemination Workshop (led by GIG, ALL PARTNERS)

Organised by GIG and the Coordinator, the MapROC dissemination workshop was held in Katowice on May 30th 2019 in order to achieve widest possible attendance by the coal mining community in Europe.

Task 6.2 Lessons learnt document (led by IMPERIAL, ALL PARTNERS)

This task aimed at summarising the state-of-the-art best technologies developed towards monitoring, assessment, prevention and mitigation of rock burst and gas outburst hazards in coal mines during the MapROC project.

Mining induced high stress and gas pressure concentrations often result in rock bursts and/or coal/gas outbursts (or sudden/uncontrolled emissions of gas). These events not only form a serious safety risk, but also represent a problem for coal production. Rock bursts and gas outbursts have also been the main hazards experienced by the industry partners in Slovenia, Poland and Spain.

Considering the partner mining industries, while rock bursts at Coal Mine Velenje are mostly induced on large coal blocks while development, gas outbursts have been recorded in and around production longwalls, mostly initiated by lithological heterogeneities or tectonic disturbances in the seam. The effect of tectonic disturbances and/or lithological heterogeneities on gas outbursts was already observed during the CoGasOUT project during the analysis of active seismic tomography and passive microseismic monitoring at Coal Mine Velenje. Therefore, besides rock burst which occur while driving headings, and predominantly due to stress concentrations were also targeted gas outbursts which mostly occur at longwall faces during coal production. A number of coal mines operated by JSW, such as the mining districts H, D and G in the Zofiówka coal mine have been identified as the area most prone to rock bursts as well as coal and gas outburst hazards. In general, the longwall exploitations often experience 1st, 2nd or 3rd degree rock bursts but not coal or gas outbursts. On the other hand, roadway drivages often experience coal and gas outbursts as well as rock bursts. As initially considered as a project partner in the proposal, S.A. Hullera Vasco-Leonesa also experienced gas outburst and sudden emissions often during roadway development in Spain, which also guided the research carried out in the project.

The development and use of advance warning or short term prediction methods based on field monitored hazard indicators, such as monitored microseismic data analysis was seen as one of the key aspects to achieving such objective in MapROC. Based on the learnings from field monitoring and/or implementation of risk mitigation measures, laboratory experiments and theoretical development work and model applications, a state-of-the-art best practice document was written up as Deliverable D6.2 Report. This report presented the details of the achievements of the project as best-practice, which the reader is referred to. Here a summary of the achievements will be presented.

The true-triaxial testing of large, naturally fractured coal and coal measures rock samples and comparing their seismic response to stress and fracturing helps characterise the seismic wave velocities in different geological media under different mining environments and aid the analysis of underground microseismic monitoring data.

The large diameter stress and gas pressure relief boreholes used at barrier pillars and the borehole blasting practices extensively tested at Coal Mine Velenje over 40 months proved to be very effective in limiting and avoiding rock bursts and gas outbursts while driving headings. The response of the rock and coal structures to driving development headings and/or longwall advance, where these measures were taken, was assessed against the microseismic monitoring data, which demonstrated the effectiveness of these measures. Please refer to Figures 2.3 to 2.13 as examples of the implementation of this technique at Coal Mine Velenje. Comparison of the use of blasting and high pressure water injection against gas outbursts in development headings at JSW have shown that

high pressure water injection was not as effective as blasting. Please refer to Figure 2.14 and relevant section of this report for the details.

As a result of the experience gained in MapROC, the systematic use of large diameter stress and gas pressure relief boreholes in rib pillars, and the implementation of a combination of large diameter boreholes and blasting in development headings, have now entered in Coal Mine Velenje's statutes (Figure 6.1 presents the an example for the blasting guidelines) and will be implemented at all development sites against increased rock burst hazards as best-practice.

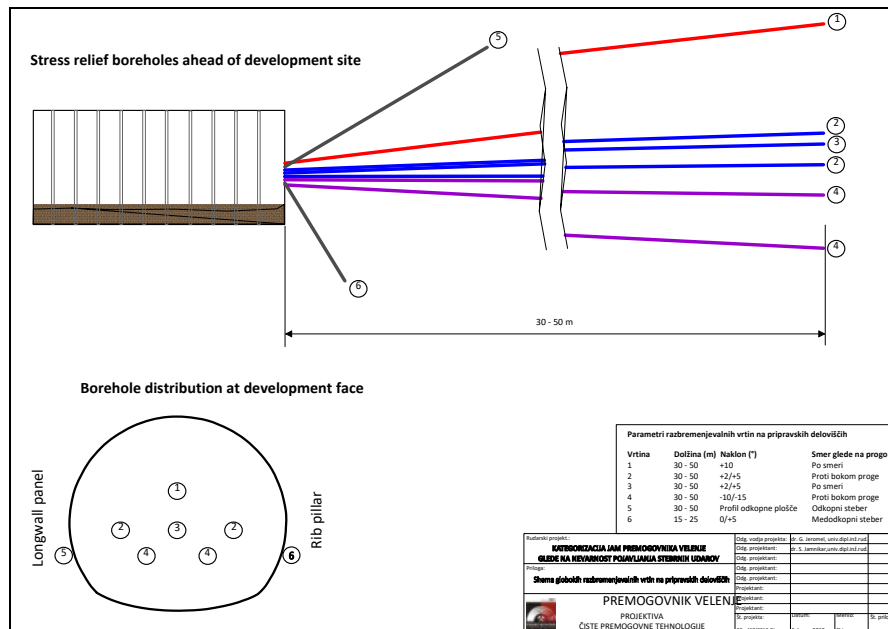


Figure 6.1 Guidelines for the use of large diameter boreholes in development headings.

Extensive field microseismic monitoring carried out over nearly 36 months at two mines and near-real-time assessment of this data on a weekly basis led to the development of a number of risk assessment techniques, which were validated for their future use by the industry. The use and interpretation of these long-term recorded microseismicity data led to the development of a catalogue of short term risk evaluation models aiming at forecasting the risk levels of rock bursts and coal and gas outbursts in terms of different evaluation indices:

- The comprehensive quantitative assessment model performed analysis on the temporal, spatial and magnitude characteristics of recorded microseismicity, with the risk levels being classified by a comprehensive normalised index. The model was validated using both the long-term microseismic monitoring data obtained at Coal Mine Velenje and the Budryk colliery at JSW.
- The Time Series Neural Network model developed was adopted to forecast the maximum event energy, the total seismic energy, and the number of seismic events which would happen over the next production day. The model was validated using both the long-term microseismic monitoring data obtained at Coal Mine Velenje and the Budryk colliery at JSW.
- The fractal dimension based model, characterised by reduction in fractal dimension and multifractal characteristics, was employed to provide precursors for rock bursts and gas outbursts. The model was validated using both the long-term microseismic monitoring data obtained at Coal Mine Velenje and the Budryk colliery at JSW.
- The statistical short-term forecasting model was utilised to estimate the probability of a large microseismic event occurring close to a working face over the next time period, and led to the optimisation of longwall face advance rates. The model was validated using the long-term microseismic monitoring data obtained at Coal Mine Velenje.

Some of the examples of these model applications are already presented in relevant Sections of this Final Report earlier, and these short term microseismicity forecasting models can now be implemented at other European and international coalfields.

Utilising all the learnings from MapROC, a generic risk assessment methodology was developed and validated using to a representative number of mining scenarios utilising site-specific data and the laboratory and field studies conducted in the MapROC project. Besides the field microseismic

monitoring-based risk evaluation methods referred to above, a catalogue of numerical modelling methods were also developed and validated. These include:

- the coupled geomechanical and gas flow model, which was applied to two mining scenarios, the floor outburst caused by drifting/longwall mining in multiple coal seams, and protective mining,
- the fracture mechanics-based gas outburst model, which was employed to model the dynamic process of coal and gas outburst triggered by drifting in thick coal seams, and
- the DFN-based microseismicity model, which was applied to model the microseismic response to longwall coal mining in thick coal seams where lithological heterogeneity leads to excessive gas emissions and potential coal and gas outbursts.

As described in the previous section, all these MapROC project based developments were combined under a generic risk assessment methodology to guide the industry in their measures against rock bursts and coal and gas outbursts. The successful application of the risk assessment methodologies builds the confidence to extend its application to risk assessment for a wide variety of rock burst and gas outburst prone conditions, including but not limited to strong/weak zones, bedding shear zones, fracture zones, stress concentration districts, gas-rich coal seams and unfavourable mining layouts, as indicated in the proposed generic model and field measurements. The generic methodology is believed to be applicable to most European coal mines with different geological and mining conditions.

Task 6.3 Scientific journal and conference publications (led by RWTH, ALL PARTNERS)

Publications so far from the project are as follows:

- Krause E., Skiba J., Przybylski M. "Methane release after tremors in the neighbourhood of incline C-1 in the coal seam 404/1", XXIII International Technical and Scientific Conference from the cycle of NATURAL MINING HAZARDS 2016 entitled: "Natural Mining Hazards in XXI century", Szczyrk (Poland), October 8th, 2016.
- Cao W., Shi J-Q., Durucan S., Si G. and Korre. "Modelling the influence of heterogeneity on microseismic characteristics in longwall coal mining", ARMA 2017, presented in June 2017 in San Francisco, US.
- Cao, W., Shi, J.Q., Si, G., Durucan, S., and Korre, A. "Numerical modelling of microseismicity associated with longwall coal mining", Int. J Coal Geology, Elsevier, Volume 193, 1 June 2018, Pages 30-45.
- Cao, W., Shi, J.Q., Durucan, S., Si, G. and Korre, A. "Gas-driven rapid fracture propagation and gas outbursts under unloading conditions in coal seams", presented at the American Rock Mechanics Association Conference, ARMA 2018, presented in June 2018 in Seattle, US.
- Yildirim, B., Cao, W., Durucan, S., Korre, A., Wolf, K.H., Bakker, R., Barnhoorn, A. "The effect of natural fracture heterogeneity on hydraulic fracture performance and seismic response in shale and coal formations, presented at the American Rock Mechanics Association, ARMA 2018, presented in June 2018 in Seattle, US.
- Agrawal. H., Durucan, S., Cao, W., Cai, W., "Evaluation of Parameters Affecting the Energy Accumulation in Longwall Mining", presented at the American Rock Mechanics Association Conference (ARMA 2019) in June 2019 in New York, US.
- Cai, W., Durucan, S., Shi, J.Q., Cao, W., Agrawal, H., Korre, A., Jamnikar, S., Rošer J., "Development of fractal-fuzzy evaluation methodology and its application for seismic hazards assessment using microseismic monitoring in coal mining", presented at the American Rock Mechanics Association Conference, ARMA 2019, presented in June 2019 in New York, US.
- Cao, W., Durucan, S., Cai, W., Shi, J.Q., Korre, A., "Multiple-panel Longwall Top Coal Caving Induced Microseismicity: Monitoring and Development of a Statistical Forecasting Model for Hazardous Microseismicity", presented at the American Rock Mechanics Association, ARMA 2019, presented in June 2019 in New York, US.
- Yildirim, B., Durucan, S., Cao, W., Cai, W., Shi, J., Korre, A. "Experimental and Numerical Investigation into Hydraulic Fracture and Natural Fracture Interaction in Shale Formations", presented at the American Rock Mechanics Association Conference, ARMA 2019, presented in June 2019 in New York, US.
- Cao, W., Shi, J.Q., Durucan, S., Si, G., Korre, A. "Numerical modelling of anomalous microseismicity characteristics influenced by geological heterogeneity in longwall coal mining", International Journal of Coal Geology, Elsevier, Volume 216, December 2019, Article 103305.
- Cao, W., Shi, J.Q., Durucan, S., Si, G., Korre, A. "Gas-driven rapid fracture propagation under unloading conditions in coal and gas outbursts", International Journal of Rock Mechanics and Mining Sciences, Elsevier, Volume 130, June 2020, Article 104325.
- Cao, W., Durucan, S., Si, G., Cai, W., Shi, J.Q., Korre, A., Jamnikar, S., Rošer, J., Lurka, A., Siata R., "The role of mining intensity and pre-existing fracture attributes on spatial, temporal and magnitude characteristics of

microseismicity in longwall coal mining”, paper in print at Rock Mechanics and Rock Engineering, Springer, 2020, **53**, PP.4139–4162.

Yildirim, B., Durucan, S., Cao, W., Cai, W., Shi, J., Korre, A. “Experimental and Numerical Investigation into Hydraulic Fracture and Natural Fracture Interaction in Shale Formations”, paper invited for publication in the Special Issue of Rock Mechanics and Rock Engineering, Springer, 2020.

Cao, W., Yildirim, B., Durucan, S., Wolf, K.H., Cai, W., Agrawal, H., Korre., “Active acoustic monitoring of hydraulic fracturing in naturally fractured coal under true triaxial stresses”, Fuel, Elsevier, **288**, March 2021, 119618.

Cao, W., Durucan, S., Cai, W., Shi, J.Q., Korre, A. “physics-based probabilistic forecasting methodology for hazardous microseismicity associated with longwall coal mining”, International Journal of Coal Geology, Elsevier, **232**, 1 December 2020, 103627.

Agrawal, H., Cao, W., Durucan, S., and Korre, A., “Development of a probabilistic risk assessment methodology to evaluate the effect of lithological heterogeneity on rock bursts and gas outbursts in longwall coal mining”, American Rock Mechanics Association Conference (ARMA 2020), June 2020 in Golden, Colorado, US, ARMA 20-A-2116.

A few other publications from the final years' work are also being written up for further publications.

EXPLOITATION AND IMPACT OF THE RESEARCH FINDINGS

Actual Applications

Work Package 1: Laboratory and Field Characterisation of Coal Seams and Surrounding Rocks as Indicators for Rock Burst and Gas Outbursts

The data generated in WP1 were utilised in the design of risk mitigation measures implemented underground in WP2; in the analysis of field monitored microseismicity data in WP3; in the development and implementation of numerical models in WP4 and WP5.

Work package 2: Development and Field Testing of Technologies for the Prevention of Rock Bursts and Gas Outbursts

The systematic use of large diameter stress and gas pressure relief boreholes in rib pillars, and the implementation of a combination of large diameter boreholes and blasting in development headings, have now entered in Coal Mine Velenje's statutes and will be implemented at all development sites against increased rock burst hazards as best-practice.

These technologies are available for application at all European and international coal mines and both Coal Mine Velenje and Imperial College would be prepared to provide the necessary support and service where necessary.

Work package 3: Microseismic Monitoring and Development of Technologies for Short-term Prediction of Rock Bursts and Gas Outbursts

Long-term underground monitoring of microseismicity data in the project and their near-real-time processing demonstrated that this methodology can effectively be used for the purposes of industrial measures taken against rock bursts and gas outbursts in coal mining. Nevertheless, due to operational reasons, the layout of the sensors used for microseismic monitoring were, in the main, on the horizontal plane. This led to the current uncertainties in the location of the events in the vertical plane. Monitoring technologies have evolved significantly since the start of CoGasOUT and MapROC and new tools have been developed. There are opportunities for these techniques to be introduced in underground coal mining for increasing the accuracy of the interpretations further and eliminate these uncertainties.

The Artificial Neural Network and Fractal Dimension based models and the short-term statistical microseismicity forecasting models developed were demonstrated for their applicability at CM-Velenje and JSW mines and can be further applied to other European coal mines.

Work package 4: Numerical Modelling of Performance of Rock Burst and Gas Outburst Prevention Methods for Risk Evaluation

The numerical models developed in this WP were used in their applications to mining layouts representing both Longwall Top Coal Caving of thick coal seams and conventional longwall mining in multi seam horizons in demonstrating their use in risk assessment in WP5.

Work package 5: Development and validation of a generic methodology for the assessment and mitigation of risk from rock bursts and gas outbursts.

WP 5 Developed and implemented a generic risk assessment methodology drawing upon the work carried out in WPs 1, 2, 3 and 4 in the project, utilising the field monitored microseismicity data and the forecasting models developed. The risk assessment methodology and the models developed were applied to the relevant project mining layouts.

Work package 6: Conclusions, recommendations and dissemination.

The project workshop was held, a state-of-the-art best practice document was written, which can be used by the industry, a significant number of journal publications and conference presentations were made.

TECHNICAL AND ECONOMIC POTENTIAL, POSSIBLE APPLICATION AT OTHER COALFIELDS

The rock burst and gas outburst mitigation measures developed and proven have the potential to eliminate future seismic events and improve safety in underground mines, reduce stoppages and loss of production which occurs at least once a year and last at least one week, costing over €1 Million worth of revenue at coal mines. As described in the project deliverables and the reports, these techniques developed are generic in nature and are applicable in Europe and internationally.

OTHER ASPECTS CONCERNING THE DISSEMINATION OF RESULTS

Attended by European coal mining industry and actively contribute to by researchers from Europe, China and India, the objective of the MapROC project and the final Workshop strengthened the reputation of the RFCS programme and disseminated information on related research activities and achievements in a number of consecutive American Rock Mechanics Association (ARMA) conferences throughout the project. The last dissemination activity in these conference series will be during 2020 ARMA Conference.

PATENTS

So far, no patent applications were made.

LIST OF ACRONYMS AND ABBREVIATIONS

ANN - Artificial Neural Networks
BSE - Bursting Strain Energy
CMI - Central Mining Institute
ECLIPSE – Reservoir Simulation Software by Schlumberger
ECSC – European Coal and Steel Community
EEM – Equivalent Energy Magnitude
FLAC^{3D} – Geomechanics Simulation Software by ITASCA
GRSS - Upper Silesian Regional Seismological Network
LTCC - Longwall Top Coal Caving
LVDT - Voltage Displacement Transducers
LW Longwall
MWD – Measurement While Drilling
OKCB - Ostrava-Karviná Coal Basin
PPV - Peak Particle Velocity
RFCS – Research Fund for Coal and Steel
USCB - Upper Silesia Coal Basin
SLC – Sublevel Caving
SOS GIG - Seismic Observation System

REFERENCES

- Cai, W., Dou, L., Cao, A., Gong, S., Li, Z., 2014. Application of seismic velocity tomography in underground coal mines: A case study of Yima mining area, Henan, China. *J. Appl. Geophys.* 109, 140–149. doi:10.1016/j.jappgeo.2014.07.021.
- Gensterblum, Y., van Hemert, P., Billemont, P., Battistutta, E., Busch, A., Krooss, B.M., De Weireweld, G., Wolf, K.-H.A.A., 2010. European inter-laboratory comparison of high pressure CO₂ sorption isotherms II: Natural coals. *International Journal of Coal Geology* 84, 115-124.
- Gilbert, P., 1972. Iterative methods for the three-dimensional reconstruction of an object from projections. *J. Theor. Biol.* 36, 105–117.
- Kabiesz J., Makówka J. (2009) Empirical-analytical method for evaluating the pressure distribution in the hard coal seams. *Mining Science and Technology* 19, pp. 556-562
- Jeromel, G., 2010. Constitutive model of multiple hanging wall caving in underground coal mining. (Doctoral dissertation).
- McKavanagh, B.M., Enever, J.R., 1980. Developing a microseismic outburst warning system, in: In Proceedings of the Second Conference on Acoustic Emission/Microseismic Activity in Geologic Structures and Materials. pp. 211–225.
- Styles, P., Emsley, S.J., Jowitt, T., 1988. Microseismic monitoring for the prediction of outbursts at Cynheidre Colliery, Dyfed, S. Wales. *Geol. Soc. London, Eng. Geol. Spec. Publ.* 5, 423–433. doi:10.1144/GSL.ENG.1988.005.01.47.
- Weniger, P., Francù, J., Hemza, P., Kross, B.M., 2012. Investigations on the methane and carbon dioxide sorption capacity of coals from the SW Upper Silesian Coal Basin, Czech Republic. *International Journal of Coal Geology* 93, 23-39.

BIBLIOGRAPHY

- Aki K., Lee W.H.K. (1976).: „Determination of three-dimensional velocity anomalies under a seismic array using first P arrival times from local earthquakes”, J. Geophys. Res. 81, 4381-4399.
- Aki K., Richards P.G. (1980), “Quantitative Seismology. Theory and Methods”. W.H. Freeman, San Francisco.
- Andrews D. J., (1986): Objective determination of source parameters and seismicity of earthquakes of different size. In Earthquake Source Mechanics (S. Das. J. Boutwright and C. H. Sholz, eds) Maurice Ewing, Vol. 6, Am. Geophys. Union. Washington D.C., 259-267
- Ben-Menachem A., Singh S.J. 1981: Seismic waves and sources. Springer-Verlag, New York.
- Bjork A., Dahlquist G. (1987), Metody numeryczne - Numerical methods, PWN, Warszawa – in Polish
- Brady B.G. and Brown E.T. 1985: Rock Mechanics for Underground Mining. George Allen and Unwin
- Dubiński J., Kabiesz J., Lurka A., (2011), Review of present-day methods of rockburst hazard prevention in Polish mining industry. In proceedings: World Mining Congress. Istanbul, pp413-423
- Dubiński J., Mutke G. (2005). „Study of temporal changes of P-Wave velocity in Polish copper mines in high seismic activity zones”. The 6th International Symposium on Rockburst and Seismicity in Mines (RaSiM6). Australia – Perth. 2005.
- Dubinski, J. (1989): A seismic method for the monitoring of mine tremors hazard in hard coal mines. Scientific works of the Central Mining Institute, Katowice. (in Polish)
- Dubiński, J. and Dworak, J. (1989): Recognition of the zones of seismic hazard in Polish coal mines by using a seismic method, PAGEOPH vol. 123, No. 3.
- Gibowicz J., Kijko A. (1994), “An Introduction to Mining Seismology”, Academic Press, San Diego, New York, Boston, London, Tokyo, Toronto.
- Glazer S.N., Lurka A., Application of passive seismic tomography to cave mining operations based on experience at Palabora Mining Company, South Africa, 1st International Symposium on Block and Sub-level Caving, 2007, Cape Town, South Africa, 369-388
- Lurka A. (2000), Analysis of errors of mining tremors using implicit function, PhD thesis, GIG, Katowice – in Polish
- Lurka A., (1996), “A certain new method for seismic network optimization and its consequences”, Acta Montana, 10, Praha.
- Lurka A., (2002): „Seismic hazard assessment in the Bielszowice coal mine using the passive tomography”, in: Seismogenic Process Monitoring (eds. H. Ogasawara, T. Yanagidani & M. Ando), A.A. Balkema Publishers.
- Lurka A., (2011) Theoretical Travel-Time Calculation of Seismic Waves Using Lie Group Theory of Conformal Transformations, Bulletin of the Seismological Society of America, vol. 101 no. 4 pp. 1959-1964
- Jeromel, G., Medved M., Likar, J., 2010. An analysis of the geomechanical processes in coal mining using the Velenje mining method. Acta Geotechnica Slovenica.vol.7 no. 1, pp. 31 – 45.
- Maxwell S.C. & Young R.P. (1994):” Application of seismic tomography to induced seismicity investigations”, in: Proceedings of Eurock ‘94, Balkema, Rotterdam.
- Mc. Garr A., (1991): „Observation constraining near-source ground motion estimated from locally recorded seismograms”. J. Geophys. Res., 96, pp. 16.495-16.508.
- Mendecki A.J. (ed), (1997): „Seismic monitoring in Mines”. Chapman & Hall, London.
- Mutke G., Dubiński J., Lurka A., (2015), New Criteria To Assess Seismic And Rock Burst Hazard In Coal Mines, Archive of Mining Sciences, Vol. 60/3, pp. 743-760
- Mutke G., Lurka A., Dubiński J., (2009), Seismic Monitoring and Rock Burst Hazard Assessment in Deep Polish Coal Mines – Case Study of Rock Burst on April 16, 2008 in Wujek-Slask Coal Mine. Proc. 7th Int. Conf. on Rockbursts and Seismicity in Mines, Rinton Press., New York, pp. 1413-1424.
- Mutke G., Lurka A., Mirek A., Bargieł K., Wróbel J. (2001): „ Temporal changes in seismicity and passive tomography images: a case study of Rudna copper ore mine-Poland” . V International Symposium Rockbursts and Seismicity in Mines (RaSiM5), The South African Institute of Mining and Metallurgy.

Press, W. H., Flannery, B. P., Teukolsky, S. A., and Vetterling, W. T. (1990), Numerical Recipes: The Art of Scientific Computing", Cambridge University Press, New York.

Schwefel H.P. (1995): „Evolution and optimum seeking”, John Wiley&Sons

Tarantola A. (1986): „Inverse Problem Theory”, Elsevier

LIST OF FIGURES

Figure 1.1	Large (600x600x400 mm) coal sample from the Pniowek Colliery Seam 404/1 and the 38mm diameter core samples prepared for testing.	11
Figure 1.2	External views of the four-column ESH rock testing unit and digital control hardware.	12
Figure 1.3	Stress-strain and permeability-strain behaviour seam 404/1 coal sample from the Pniowek Colliery.....	12
Figure 1.4	High pressure Langmuir isotherms for Seam # 8 samples from the HUNOSA Sueros Colliery measured at 45°C.	15
Figure 1.5	(a) True triaxial rock testing set-up equipped with loading, injection and acoustic systems, and (b) experiment control, recording, and monitoring units.	15
Figure 1.6	(a) Cubic coal block from partner coal mine in Poland, and (b) fracture outcrops on each face of the coal block.....	16
Figure 1.7	(a) Homogeneous rock block-1, and (b) Natural fractures on ZC, YD, YC, and XC surfaces of block-2.	16
Figure 1.8	Stress, displacement and injection histories for coal block 2 during the true triaxial experiments.	17
Figure 1.9	CT-scanned images before and after hydraulic fracturing for coal block 2: (a) surfaces, and (b) slice views (ONF: oil-intruded natural fractures; NNF: non-intruded natural fractures).	18
Figure 1.10	Reconstructed natural and hydraulic fracture networks from CT scan images: (a) 3D view for coal block 2, and (b) side view for coal block 2 (HF: hydraulic fractures; ONF: oil-intruded natural fractures; NNF: non-intruded natural fractures).	18
Figure 1.11	S wave velocity as a function of hydrostatic confining stress.	19
Figure 1.12	S-wave velocity tomograms for coal block 2: (a) before hydraulic fracturing, (b) after hydraulic fracturing, and (c) the difference induced by hydraulic fracturing.....	19
Figure 1.13	Stress, displacement, and borehole pressure and volume responses of rock block-2.	20
Figure 1.14	(a) Split rock block Sample-2, and (b) its CT scan results.	20
Figure 1.15	S-wave velocity tomograms for Rock block-2 before and after hydrofracturing and injection induced difference.	21
Figure 1.16	Stress field at CM-Velenje at the start of the project (a) 3D view, (b) plan view.	22
Figure 1.17	(a) Location of the microseismic monitoring stations, (b) numerical model for the K.-80/E and K.-80/B longwall panels at CM-Velenje.	22
Figure 1.18	Production schedule at K.-80/E and K.-80/B longwall panels at CM-Velenje.	23
Figure 1.19	Stress changes induced by LTCC face advance (point monitors).	23
Figure 1.20	Stress state in (a) part C, seam 404/1 – end of longwall C-4 and (b) end of longwall C-5.	24
Figure 1.21	(a) General stratigraphy of the 401/1 and 404/2 panels, and model geometry for (b) coal seam 404/1, and (c) coal seam 404/2.	24
Figure 1.22	Mining-induced vertical stress variations around longwall panels in the coal seam 404/2: (a) 1 st panel extraction, (b) 3 rd panel extraction.....	25
Figure 1.23	Vertical stress profiles for the coal seam 404/2 after the 1 st panel extraction: (a) A-A cross section, and (b) B-B cross section.	25
Figure 2.1	CM Velenje mine outline, active and developing longwall faces in 2016. The kidney shaped dashed line marks the area with increased rock burst probability, which was defined after recordings of increased number of seismic events in the region.	27
Figure 2.2	CM Velenje detailed mine outline with marked zones for pilot tests of large diameter stress relief boreholes.	28
Figure 2.3	(a) Longwall panel D k. -80 with positions of stress relief boreholes, seam gas pressure and composition monitoring boreholes and stress monitoring borehole in Zone L1, (b) Longwall panel A k. -95 development (gateroads in blue), face end line for longwall panel B k.-80, and the locations of stress relief boreholes in Zone L4.28	

Figure 2.4 (a) Longwall panel C k. -80 with locations of large diameter stress relief boreholes and seam gas pressure monitoring borehole in the intake air gateroad in Zone L2, (b) Longwall panel C k. -80 with locations of stress relief boreholes in the return gate in Zone L3.	29
Figure 2.5 Seam gas pressure monitoring at borehole jpk 85 (+10°)/16 (Longwall face C k. -80).29	
Figure 2.6 Mine outline showing the generalised MapROC activities at Coal Mine Velenje in 2017.....	30
Figure 2.7 Large diameter stress relief boreholes in barrier pillar of LTCC panels CD3g and E k. -95.	31
Figure 2.8 Locations of MapROC activities at Coal Mine Velenje in 2018.....	31
Figure 2.9 Stress relief boreholes in longwall panel D k. -95 (Boreholes jgm RAZ 38 – 42 were drilled for slotting experiments).	32
Figure 2.10 Large diameter boreholes in development headings.	32
Figure 2.11 Sites of large diameter borehole drilling during the development of the heading for the CD3/j longwall panel. Stress relief drilling was supported by daily blasting along the larger sections.....	33
Figure 2.12 Example schematic for blasting location and blasting boreholes positions.	33
Figure 2.13 Locations and periods of daily stress relief blasting.....	34
Figure 2.14 Methane emission into the workings 120 minutes after blasting operations in the incline N-4 in coal seam 404/2.	35
Figure 2.15 Plan and section views of roadway B-12 coal face in Seam 401 and the drilling layout for water injection tests.	35
Figure 2.16 Exact location of the 4 boreholes.	37
Figure 2.17 Slotting in the borehole 1 jgm RAZ 38/18.	37
Figure 2.18 Slotting experiments in the development heading of LTCC panel Dk-95.	37
Figure 2.19 Monitoring the cutting of slot no. 2.	38
Figure 2.20 Risk assessment in temporal and spatial domains within the period 01/05/2019-31/05/2019 at Coal Mine Velenje.....	38
Figure 2.21 Technical plan for the second set of large diameter boreholes (Development C k. -95).....	39
Figure 2.22 Drilling performance for jgm RAZ 48/18. Drilling torque is increased after advancing over fractured zone around 27,5 m, where on contrary thrust is reduced completely. Both parameters gradually increase after approximately 42 m, where drilling team also reported increased material strength and relatively low material output. Given combination of recordings could indicate local zone of stress accumulation.	40
Figure 2.23 Drilling performance for jgm RAZ 50/18. Fractured zone and following increase of borehole material output around the depth of 20 m is shown in rotation pressure chart....	40
Figure 2.24 Drilling performance for jgm RAZ 51/18. Remarks report continuous fractured zone after the depth of 8,5 m and therefore continuous rise of rotation pressure until nearly final depth. Thrust pressure remained in a range of up to 80 bar along the whole depth of borehole.	40
Figure 3.1 Mine production layout at -80 and -95 m production levels during 2016-2019 and the distribution of installed SOS seismic stations of the microseismic monitoring system at Coal Mine Velenje as it evolved throughout the project. The grey zone indicates the approximate shape of the central coal pillar protecting the main mine infrastructure in the production district.	41
Figure 3.2 Distribution of the seismic stations (a) after completion of SOS microseismic system installation in February 2016 at Coal Mine Pniowek and (b) installation in April 2017 at Coal Mine Budryk.....	42
Figure 3.3 Distribution of the seismic events in March 2016 at CM-Velenje mine. Sizes of red circles are proportional to calculated seismic energy. Bottom right – number of seismic events (vertical axis) in seismic energy classes (horizontal axis).	42

Figure 3.4	Distribution of seismic events in (a) August 2016 and (b) November 2016, and the number of seismic events in seismic energy classes at CM-Velenje mine.	43
Figure 3.5	Distribution of seismic events in (a) April 2017 and (b) September 2017, and the number of seismic events in seismic energy classes at CM-Velenje mine.	43
Figure 3.6	Distribution of seismic events in (a) March 2018 and (b) June 2018, and the number of seismic events in seismic energy classes at CM-Velenje mine.	43
Figure 3.7	Distribution of seismic events (red circles) in December 2018 at CM-Velenje mine. Sizes of red circles are proportional to calculated seismic energy. Bottom right – number of seismic events (vertical axis) in seismic energy classes (horizontal axis).	44
Figure 3.8	Distribution of seismic activity i.e. number of seismic events (vertical axis) in day (top) and week (bottom) time intervals (horizontal axis) between March 2016 and January 2019 at CM-Velenje.	45
Figure 3.9	Seismic energy distribution for each seismic event (dots) and moving average of seismic energy (thick black line) between March 2016 and January 2019 at CM-Velenje.	45
Figure 3.10	Distribution of seismic events in April 2017 at Budryk mine. Sizes of red circles are proportional to calculated seismic energy. Bottom left – number of seismic events (vertical axis) in seismic energy classes (horizontal axis).	46
Figure 3.11	Distribution of seismic events in (a) July 2017 and (b) December 2017, and the number of seismic events in seismic energy classes at Budryk mine.	46
Figure 3.12	Distribution of seismic events in (a) March 2018 and (b) July 2018, and the number of seismic events in seismic energy classes at Budryk mine.	46
Figure 3.13	Distribution of seismic events in September 2018 at Budryk mine. Sizes of red circles are proportional to calculated seismic energy. Bottom left – number of seismic events (vertical axis) in seismic energy classes (horizontal axis).	47
Figure 3.14	Distribution of seismic activity in a day (top) and week (bottom) time intervals between April 2017 and September 2018 at Budryk mine.	47
Figure 3.15	Bent-ray tomographic “P” wave velocity image (units m/s) obtained using seismic events recorded (a) between 01st and 15th July 2017 and (b) between 01st and 15th October 2017 at CM-Velenje.	48
Figure 3.16	Bent-ray tomographic “P” wave velocity image (units m/s) obtained using seismic events recorded (a) between 01st and 15th January 2018 and (b) between 16th and 31th March 2018 at CM-Velenje.	48
Figure 3.17	Bent-ray tomographic “P” wave velocity image (units m/s) obtained using seismic events recorded (a) between 01st and 15th April 2017 and between 15th and 30th June 2017at Budryk Coal Mine.	49
Figure 3.18	Bent-ray tomographic “P” wave velocity image (units m/s) obtained using seismic events recorded (a) between 01st and 15th May 2018 and (b) between 16th and 31th July 2018 at Budryk Coal Mine.	49
Figure 3.19	Over ten months' microseismic monitoring data at Coal Mine Velenje.	50
Figure 3.20	Training results for the Time Series Neural Network models for the forecast of the number of seismic events. (a) performance of cross-entropy versus number of iterations (epochs), (b) error histogram for the training, validation and testing data, (c) corresponding regression plots for the target data against the output, and (d) Time series response. This displays the inputs, targets and errors over time. It also indicates which time points were selected for training, testing and validation.	51
Figure 3.21	Over ten months' microseismic monitoring data from the Budryk colliery.	52
Figure 3.22	Training results for the Time Series Neural Network models for the forecast of the maximum seismic event energy. (a) performance of cross-entropy versus number of iterations (epochs), (b) error histogram for the training, validation and testing data, (c) corresponding regression plots for the target data against the output, and (d) Time series response. This displays the inputs, targets and errors over time. It also indicates which time points were selected for training, testing and validation.	53
Figure 3.23	Microseismic monitoring in Coal Mine Velenje.	54

Figure 3.24	Fractal dimension based models applied to microseismic data at Coal Mine Velenje.....	55
Figure 3.25	Normalisation of fractal dimension based models applied to microseismic data at Coal Mine Velenje.....	56
Figure 3.26	Microseismic monitoring at Budryk colliery.....	57
Figure 3.27	Fractal dimension based models applied to the microseismic data at Budryk Colliery.....	58
Figure 3.28	Normalisation of fractal dimension based models applied at Budryk Colliery.....	59
Figure 4.1	Schematic of the large diameter boreholes drilled in the barrier pillar of LTCC Panel B k. -80 at Coal Mine Velenje. The red boxed area represents the model domain... ..	62
Figure 4.2	Model domain for the large diameter boreholes drilled in the barrier pillar of LTCC Panel B k. -80 at Coal Mine Velenje. The dark grey rectangular prism represents the main gateroad.	62
Figure 4.3	Initial stress conditions over the modelled area within the barrier pillar.....	63
Figure 4.4	Simulation of the abutment stresses conditions within the barrier pillar in the modelled area due to the effects of approaching longwall face.	63
Figure 4.5	Schematic illustration of the position of vertical sections taken through the central borehole and the horizontal sections taken through three boreholes.	63
Figure 4.6	Vertical stress contours over the barrier pillar without and with large diameter boreholes as the longwall face approaches the pillar (vertical sections).....	64
Figure 4.7	Vertical stress contours over the barrier pillar without and with large diameter boreholes as the longwall face approaches the pillar (horizontal sections).....	64
Figure 4.8	Near wellbore region vertical stresses on the barrier pillar illustrated using two vertical planes (vertical sections - please see Figure 4.9 for the position of the plane 30m into the pillar).....	65
Figure 4.9	Vertical plane 30 m into the barrier pillar along which further stress analysis are carried out.....	65
Figure 4.10	Vertical stress profiles over the barrier pillar as the face approaches (a) along A-A' and (b) along B-B' 30 m into the barrier pillar as illustrated in Figure 4.9 (with and without boreholes).	66
Figure 4.11	Horizontal stress profiles over the barrier pillar as the face approaches (a) along A-A' and (b) along B-B' 30 m into the barrier pillar as illustrated in Figure 4.9 (with and without boreholes).	66
Figure 4.12	Model domain for the large diameter boreholes drilled with 4 slots each in the barrier pillar of LTCC Panel B k. -80 at Coal Mine Velenje.....	67
Figure 4.13	Vertical stress contours over the barrier pillar without and with slotted large diameter boreholes as the longwall face approaches the pillar (vertical sections).....	67
Figure 4.14	Vertical stress contours over the barrier pillar without and with slotted large diameter boreholes as the longwall face approaches the pillar (horizontal sections).....	68
Figure 4.15	Comparison of vertical stress profiles over the barrier pillar as the longwall face approaches (a) along A-A' and (b) along B-B' 30 m into the barrier pillar as illustrated in Figure 4.9 (scenarios with no boreholes, with boreholes and with slotted boreholes).....	68
Figure 4.16	Schematic mining layout of a 2-entry (single row) abutment-yield pillar system... ..	69
Figure 4.17	Representative schematic mining layout of a 3-entry (two- rows) yield-abutment-yield pillar system.. ..	70
Figure 4.18	Variation in the deflection of the roof with varying yield pillar thickness at a mining depth of 1,000m for a coal seam thickness of (a) 2m and (b) 4m	70
Figure 4.19	Representative layout of (a) Vertical stress contour, (b) Elastic strain energy contour, developed in the panel for Layout 1 for a coal seam thickness of 4m with a yield pillar thickness of 5m.....	71
Figure 4.20	Variation in the vertical stress profile with varying yield pillar thickness at a mining depth of 1,000m for a coal seam thickness of (a) 2m and (b) 4m.....	71

Figure 4.21	Variation in the total elastic strain energy with varying yield pillar thickness at a mining depth of 1,000m for a coal seam thickness of (a) 2m and (b) 4m	72
Figure 4.22	Comparative variation in the maximum deflection, maximum vertical stress and maximum elastic strain energy accumulation for different mining layouts for a 5m thick yield pillar having a coal seam thickness of 4m at a mining depth of 1000m.	72
Figure 4.23	Eccentric mining layouts for roadway development in multi-seam workings.	73
Figure 4.24	A representative mining layout showing an interbedding thickness of 24m for a 50m eccentric roadway development.	73
Figure 4.25	Vertical stress profile in the upper and lower seam due to existing overlying goaf.	74
Figure 4.26	Deflection of the roof in the lower seam at different eccentricities.....	74
Figure 4.27	Variation in the vertical stress profile in the lower seam at different eccentricities.	74
Figure 4.28	Variation in the elastic strain energy in the lower seam at different eccentricities.	75
Figure 4.29	Pniowek colliery protective mining scenarios for Seams 404/1 and 404/2.....	76
Figure 4.30	Pniowek colliery model showing the positions of horizontal and vertical sections taken from Seams 404/1 and 404/2 for the analysis of stress and pore pressure in each seam during the protective mining scenarios.	77
Figure 4.31	Pniowek colliery protective mining scenario: Progressive mining in 404/1 (horizontal section).....	77
Figure 4.32	Pniowek colliery protective mining scenario: Progressive mining in 404/1(vertical section).....	78
Figure 4.33	Pniowek colliery protective mining scenarios: Pore pressure relief in 404/2 (horizontal section).....	78
Figure 4.34	Pniowek colliery protective mining scenarios: Pore pressure profiles in Seam 404/2 along B-B' shown in Figure 3.5.24 for ((a) the 34 m interbedding and (b) 19 m interbedding scenarios.	79
Figure 5.1	Flow diagram of the generic risk assessment methodology.....	82
Figure 5.2	Evidence based empirical risk assessment applied to sublevel caving coal mining method.	85
Figure 5.3	Plan views of the BSE index $W_{\varepsilon-spatial}$ during different mining periods at Coal Mine Velenje.....	86
Figure 5.4	The temporal evolution of the comprehensive index integrating with time-space-magnitude independent information indices at Coal Mine Velenje.	86
Figure 5.5	The temporal evolution of the comprehensive index integrating with time-space-magnitude compound information indices at Coal Mine Velenje.	86
Figure 5.6	A schematic of the criterion for coal element ejection in outburst modelling.....	87
Figure 5.7	Schematic representation of fracture opening in relation to effective stress changes ahead of a working face.	88
Figure 5.8	Stress intensity factors K_I as a function of fracture radius a_0 and effective stress $p_{\sigma_{min}}$. Fractures are deemed to propagate if $K_I \geq K_{Ic}$	89
Figure 5.9	Intra-fracture gas pressure p_{lim} as a function of fracture toughness K_{Ic} and fracture radius a_0 for fractures located close to a working face. Fractures are deemed to propagate if $p_{lim} \leq p_{equ}$	89
Figure 5.10	Slip test points on the periphery and centre of a circular fracture in local coordinates.....	90
Figure 5.11	Framework of the comprehensive microseismicity assessment methodology.	92
Figure 5.12	Spatial distribution of microseismic events around longwall panel K.-80/C in Coal Mine Velenje.	92
Figure 5.13	Temporal evolution of the bursting strain energy index for longwall panel K.-80/C....	93
Figure 5.14	Spatial evolution of the bursting strain energy index around longwall panel K.-80/C .	93
Figure 5.15	Microseismic response to rock burst events: (a) Microseismic events related to the rock burst event "18:49:22 19/03/2018"; (b) Microseismic events related to the rock	

	burst event "3:05:12 17/04/2018" at development heading for longwall panel K. -95/D.....	94
Figure 5.16	The temporal evolution of the BSE index $W_{\varepsilon\text{-temporal}}$. prior to the seismic events experienced at Coal Mine Velenje development heading for longwall panel K. -95/D.	94
Figure 5.17	Plan views of the BSE index $W_{\varepsilon\text{-spatial}}$ before the rock burst events which were experienced at 18:49:22 on 19/03/2018 and at 3:05:12 on 17/04/2018 at heading for panel K. -95/D.	95
Figure 5.18	Temporal risk assessment based on the sequential evolution of seismic indicators at development heading for longwall panel K. -95/D.....	95
Figure 5.19	(a) Sequential evolution of fractal indices, (b) Probabilistic and comprehensive assessment of seismic hazards at development heading for longwall panel K. -95/D.....	96
Figure 5.20	Relationship between the daily seismic event rate, average seismic energy released, and spatial distribution of recorded microseismicity around three longwall panels at CM-Velenje.....	96
Figure 5.21	Time-varying temporal, magnitude and spatial seismic indicators decoupled from mining activities for microseismicity around panel K.-80/D. (Scaled daily event number under the average face advance rate represents the density of underlying fractures; the probability of a single microseismic event being a large event reflects the size distribution of underlying fractures; the probability of a single microseismic event being close to the longwall face reveals the spatial distribution of underlying fractures.)	97
Figure 5.22	Time-varying forecasted daily event number, and forecasted probability that at least a large microseismic event, a microseismic event close to the face-line, and a hazardous microseismic event occurs on the day of forecasting around panel K.-80/B.	98
Figure 5.23	Recommended upper limits of daily face advance given probability thresholds of hazardous events for (a) panel K.-80/B, (b) panel K.-80/D, and (c) panel K.-80/C.	99
Figure 5.24	(a) Development of a 2D floor outburst model (a close-up view of the central area), (b) General stratigraphy of the floor outburst model.....	100
Figure 5.25	Failure of floor coal/rock elements with the advance of the longwall face.....	101
Figure 5.26	Simulated pressure evolution in a floor outburst condition.....	101
Figure 5.27	General stratigraphy and model geometry of roadway development in the modelled coal seam around LTCC panel K. -50/C.	102
Figure 5.28	Intra-fracture gas pressure distribution caused by gas desorption after each roadway development step (Unit: Pa).	102
Figure 5.29	Extension of the coal outburst zone over time: 60 s, 180 s, 300 s and 360 s after reaching the outburst prone zone.	102
Figure 5.30	Influences of (a) K_{lc} , (b) a_0 on the ejected volume of coal over time.	103
Figure 5.31	Mining geometry and geological implementation of the xylite-rich zone: (a) 3D model geometry, and (b) Distribution of DFNs located at the panel level [-330 m, -350 m] following power law relationship with $a_c = 2.7$, $a_h = 1.8$, $\square_h = 0.7 \square_c$	104
Figure 5.32	(a) The bi-weekly b values for frequency-magnitude distribution of the recorded and simulated microseismic events over the monitoring period, (b) Examples of b values obtained through regression fitting for the recorded and simulated microseismic events during 1 to 14 August 2011.....	104
Figure 5.33	Base model developed in FLAC3D™ with boundary conditions.	106
Figure 5.34	Comparative analysis of (a) the deflection of the roof and (b) the vertical stress accumulation for a coal seam thickness of 2m and 4m at all mining depths.	107
Figure 5.35	Variation in elastic strain energy accumulation in the coal seam for different mining depths.	107

Figure 5.36	Comparison of the variation (a) in the deflection of the roof in the lower seam, (b) in the vertical stress acting on the lower seam and (c) in the elastic strain energy accumulated in the lower seam for different interbedding thicknesses in a multi-seam working at 1,000m mining depth.....	108
Figure 5.37	Numerical modelling layouts at different excavation steps for the protective seam... ..	108
Figure 5.38	Elastic strain energy accumulation in the protective seam and the protected seam for an interbedding thickness of 25m for a seam thickness of 2m (along section XX in Figure 5.37).	109
Figure 5.39	Gas pressure variation in the protected seam (along section XX and section YY in Figure 5.37).	109
Figure 5.40	(a) The fork-shaped solid imported as a heterogeneous zone in the model grid developed in FLAC3D, (b) Example distributions of xylitic and detritic coal in the heterogeneous model zone, (c) lithology and gas pressure gradient used in constructing the coupled model.....	110
Figure 5.41	Different stages of development and longwall top coal caving mining sequence..	110
Figure 5.42	Cross-sections along which the vertical stress and gas pressure build-up are analysed.	111
Figure 5.43	(a) Variation in pore pressure along the longwall face and the panel edges for 90% xylite heterogeneity (YY section), (b) comparison of vertical stresses acting on the longwall face and the panel edges for 90% and 30% xylite heterogeneity cases at excavation step 20 (YY section).....	111
Figure 5.44	(a) Gas emission rate from the longwall face at 90% xylite heterogeneity (b) Total gas emission rates from the longwall face for two different heterogeneity scenarios.	112
Figure 6.1	Guidelines for the use of large diameter boreholes in development headings.....	114

LIST OF TABLES

Table 1.1	He-Pycnometry results on dry coal from the Pniówek Colliery.	11
Table 1.2	Gas slippage factors and intrinsic permeabilities at 30 MPa confining pressure for constant downstream and uptake experiments for samples from the Pniówek Colliery.....	11
Table 1.3	Example results of methane content experiments on coal and outburst indexes in the seam 404/1, Zone C at Pniówek Colliery.....	13
Table 1.4	Results of Pniówek Colliery methane sorption experiments.	13
Table 1.5	Geomechanical properties of coal and over/underburden at Coal Mine Velenje (Jeromel, 2010).	14
Table 1.6	Uniaxial compression test results for lithologies from Coal Mine Velenje.	14
Table 1.7	Triaxial compression test results for lithologies from Coal Mine Velenje.	14
Table 5.1	Factors affecting rock bursts and gas outburst risk in coal mining.....	82
Table 5.2	Empirical thresholds for rock bursts and gas outbursts in coal mines.....	83
Table 5.3	Theoretical criteria for rock bursts and gas outbursts in coal mines.....	83
Table 5.4	Evidence based empirical methodology developed primarily for sublevel caving coal mining.	84
Table 5.5	Field microseismic monitoring-based risk evaluation methodologies.....	85
Table 5.6	Typical mining scenarios to be simulated for rock burst and gas outburst risk evaluation..	87
Table 5.7	Different stages of a disturbed fracture.	88
Table 5.8	Modelling methodologies applicable for typical mining scenarios simulated in rock burst and gas outburst risk evaluation.	100
Table 5.9	Parametric variations in the yield pillar design.....	106
Table 5.10	Parametric variations in the eccentric mining layouts	107
Table 5.11	Parametric variations in the protective mining layouts.....	108

Getting in touch with the EU

In person

All over the European Union there are hundreds of Europe Direct information centres. You can find the address of the centre nearest you at:

https://europa.eu/european-union/contact_en

On the phone or by email

Europe Direct is a service that answers your questions about the European Union. You can contact this service:

- by freephone: 00 800 6 7 8 9 10 11 (certain operators may charge for these calls),
- at the following standard number: +32 22999696 or
- by email via: https://europa.eu/european-union/contact_en

Finding information about the EU

Online

Information about the European Union in all the official languages of the EU is available on the Europa website at: https://europa.eu/european-union/index_en

EU publications

You can download or order free and priced EU publications at: <https://publications.europa.eu/en/publications>. Multiple copies of free publications may be obtained by contacting Europe Direct or your local information centre (see https://europa.eu/european-union/contact_en).

EU law and related documents

For access to legal information from the EU, including all EU law since 1952 in all the official language versions, go to EUR-Lex at: <https://eur-lex.europa.eu>

Open data from the EU

The EU Open Data Portal (<https://data.europa.eu/euodp/en/home>) provides access to datasets from the EU. Data can be downloaded and reused for free, for both commercial and non-commercial purposes.

The main objective of MapROC project has been to field test and develop a number of rock burst and gas outburst prevention techniques based on stress and pressure relief principles and evaluate their performance through continuous microseismic monitoring at mine sites.

It was established that large diameter stress and gas pressure relief boreholes used at barrier pillars, and the borehole blasting practices extensively tested at Coal Mine Velenje were very effective. As a result, these measures have now entered in Coal Mine Velenje's statutes and will be implemented at all development sites against increased rock burst hazards.

Extensive field microseismic monitoring carried out at two mines and near-real-time assessment of this data on a weekly basis led to the development of a number of risk assessment techniques which were validated for their future use by the industry. A catalogue of short term risk evaluation models aiming at forecasting the risk levels of rock bursts and coal and gas outbursts in terms of different evaluation indices. Furthermore, a number of numerical modelling methods were also developed and validated.

Utilising all the learnings from MapROC, a generic risk assessment methodology was developed and validated using to a representative number of mining scenarios utilising site-specific data and the laboratory and field studies conducted in the MapROC project. The generic methodology is believed to be applicable to most European coal mines with different geological and mining conditions.

The state-of-the-art best technologies report describing the monitoring, assessment, prevention and mitigation of rock burst and gas outburst hazards in coal mines can be used by the industry in Europe and internationally.

